Compréhension de l'expression génique à travers l'étude des bases structurales de la traduction ribosomique eucaryote

Muminjon Djumagulov

UNIVERSITÉ DE STRASBOURG

ÉCOLE DOCTORALE des sciences de la vie et de la santé

IGBMC – CNRS UMR 7101 – Inserm U 964

THÈSE présentée par :

Muminjon DJUMAGULOV

soutenue le : **23 novembre 2018**

pour obtenir le grade de : **Docteur de l'université de Strasbourg**

Discipline/ Spécialité : Biophysique et Biologie Structurale

(Biophysic and Structural Biology)

Accuracy of gene expression through understanding structural basis of a translation cycle on the eukaryotic ribosomes

THÈSE dirigée par :

Mme. YUSUPOVA Gulnara	Directeur de recherche, Université de Strasbourg

RAPPORTEURS :

M. CONDON Ciarán	Directeur de recherche, Université Paris Diderot (Paris)
M. MECHULAM Yves	Directeur de recherche, Ecole Polytechnique (Paris)

AUTRES MEMBRES DU JURY :

Mme. ROMBY Pascale	Directeur de recherche, Université de Strasbourg
M. KOLB Vyacheslav	Directeur de recherche, Académie des Sciences, Russie

ACKNOWLEDGEMENTS

First of all my gratitude goes to the members of the jury, Dr. Ciarán Condon, Dr. Yves Mechulam, Dr. Pascale Romby, Dr. Vyacheslav Kolb. Thank you for reading these pages and for accepting to evaluate my work.

I must say I was really lucky to have such an outstanding supervisor like Gulnara, who supported and guided me from the beginning of my PhD. I am thankful for motivating and pushing me in a positive way. I also appreciate involvement of Marat who was always ready to share his ideas; together with Gulnara they possess unmatched experience. I learned many different methods in biochemistry and structural biology and I can say that I was shaped as a scientist in Gulnara's and Marat's laboratories.

I would like to express my deep gratitude to Natasha Demeshkina and Lasse Bohl Jenner for their patience and sharing their knowledge with me through constructive and fruitful discussions. I learn so much from you!

I am thankful to the structural biology platform of IGBMC: Catherine, Pierre and Alastair, who taught me a lot of techniques of biophysics and crystallization; local contact personal at PX1 beamline at SLS synchrotron who are ready to help 24/7; and people from IGBMC administration and PhD program Francine, Paulo and Annick – they are always there to rescue from technical organizational matters.

I want to thank all the former members of the lab for creating pleasant working environment and wish good luck to present members of our ribosome team. I hope our paths will cross some day in the future. Many thanks to Irina for her precious ribosome and protein samples, and to Alexey for sharing countless sleepless nights on synchrotron.

And of course big credits to all my friends and family who support me no matter what and are always there when I need them. I appreciate how you help me to struggle through difficult situations in my life no matter how far we may be.

And last but not least special thanks to my girlfriend Rachel. Truth be told even full page will not be enough to express what she did for me. She made a huge impact if not on my whole life then definitely on my manuscript!

TABLE OF CONTENTS

TABLE OF FIGURES

ABBREVIATIONS

aa-tRNA	aminoacyl-tRNA
A-site	aminoacyl site, (A-tRNA – A-site tRNA)
E. coli	Escherichia coli
EF	elongation factor (eEF – eukaryotic EF)
E-site	exit site (E-tRNA – E-site tRNA)
IF	initiation factor (eIF – eukaryotic IF)
ML	mother liquor
mRNA	messenger ribonucleic acid
PreTC	premature termination codon
PTC	peptidyl transferase centre
P-site	peptidyl site, (P-tRNA – P-site tRNA)
rRNA	ribosomal ribonucleic acid
S. cerevisiae	*Saccharomyces cerevisiae*
tRNA	transfer ribonucleic acid

RESEARCH PROJECTS

During my PhD studies, I have been working on three different projects. All of them were designed to study structural aspect of protein synthesis machinery of eukaryotes by means of X-ray crystallography. All of the components used to form various 80S ribosome translation states in vitro were purified from *Saccharomyces cerevisiae.*

The projects will be presented in the following order:

1. Structural investigation of functional *S. cerevisiae* 80S ribosome complexes with mRNA and tRNAs.
2. Aminoglycoside interactions and impacts on the eukaryotic *S. cerevisiae* 80S ribosome
3. Structural studies of eukaryotic *S. cerevisiae* 80S elongation complex

INTRODUCTION

The ribosome

In all living organisms, protein synthesis is an essential process that allows each cell to live and reproduce. This activity consumes major part of the energy generated by the cell. Therefore, it is tightly regulated by numerous factors in order to ensure that only necessary proteins are produced in the required amount at the right time. Genetic information, encoded in genes, is transcribed from DNA into messenger RNA (mRNA) in the process called transcription. Afterwards information contained in the mRNA is translated into the protein on a special macromolecule called ribosome. This process is called translation since molecular substrate containing information is translated from nucleic acid “language” to amino acid one.

Common core and domain related diversity of the ribosome.

The ribosome is a giant ribonucleoprotein cellular assembly that catalyze and coordinate every step required to translate mRNAs into proteins in any living cell. While the core aspects of translation are highly conserved across eukaryotes, bacteria and archaea, there are substantive differences in the ribosome structures. Solving the first high resolution structure of eukaryotic ribosome from *Saccharomyces cerevisiae* (Ben- Shem et al., 2011) by means of X-ray crystallography in combination with early genetic data and structural information of prokaryotic ribosome enable detailed analysis of bacteria and eukaryotic ribosomes revealing that both ribosomes share a common structural core (Figure 1), comprising 34 conserved proteins (15 in the small subunit and 19 in the large subunit) and ~4,400 RNA bases, which harbors the major functional centers of the ribosomes, such as the decoding site, peptidyl transferase center and tRNA-binding sites (Klinge et al., 2012; Melnikov et al., 2012).

Despite the universal conservation of the core, ribosome composition varies between domains of life, taxonomic subgroups, organelles and even within a single individual, although to a smaller extent. The bacterial ribosome (*Escherichia coli* or *Thermus thermophilus*) contains 21 bacteria- specific proteins, a few extensions of the conserved proteins and of ribosomal RNA. The eukaryotic ribosome of *S. cerevisiae* contains 46 eukaryote- specific proteins (800 kDa) and extensions and insertions in most of the proteins of the core (200 kDa), and the rRNA harbors several extensions in the conserved rRNA chains (about 800 nucleotides that account for 350 kDa) (Ben- Shem et al., 2011; Melnikov et al., 2012). The molecular weight of the ribosomes may vary from 2.3 MDa in bacteria to 4.3 MDa in higher eukaryotes (Figure 1).

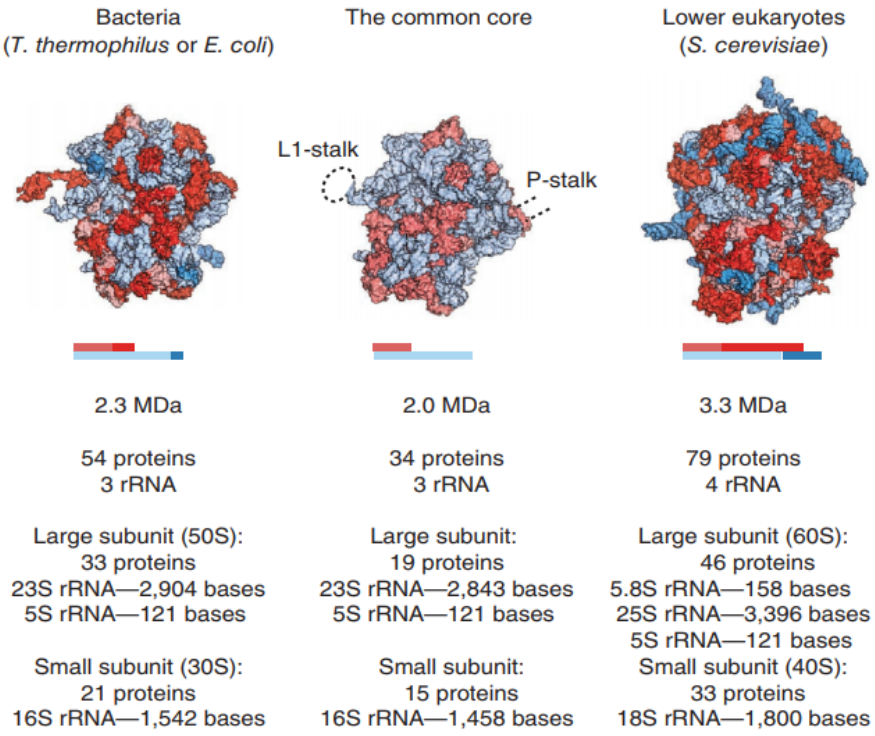

Figure 1. Comparison of the bacteria and eukaryote ribosomes. Adapted from Melnikov et al., 2012.

Main functional sites

The ribosome is an asymmetric macromolecule that consist of a large (LSU) and a small (SSU) subunit that are composed of a ribosomal RNA (rRNA) and proteins with average ratio of 2:1 RNA to protein (the exceptions are mitochondrial and chloroplast ribosomes which have ratios 1:2 and 3:2 respectively (Sharma and Agrawal, 2012). Molecular weight and composition of subunits are different and each has a specific sedimentation coefficient that is used to characterize and to name isolated or associated subunits. In eukaryotes, large subunit is 60S (50S in bacteria) and small subunit is 40S (30S in bacteria). And when associated in a complete ribosome it is 80S (70S in bacteria) (Figure 2).

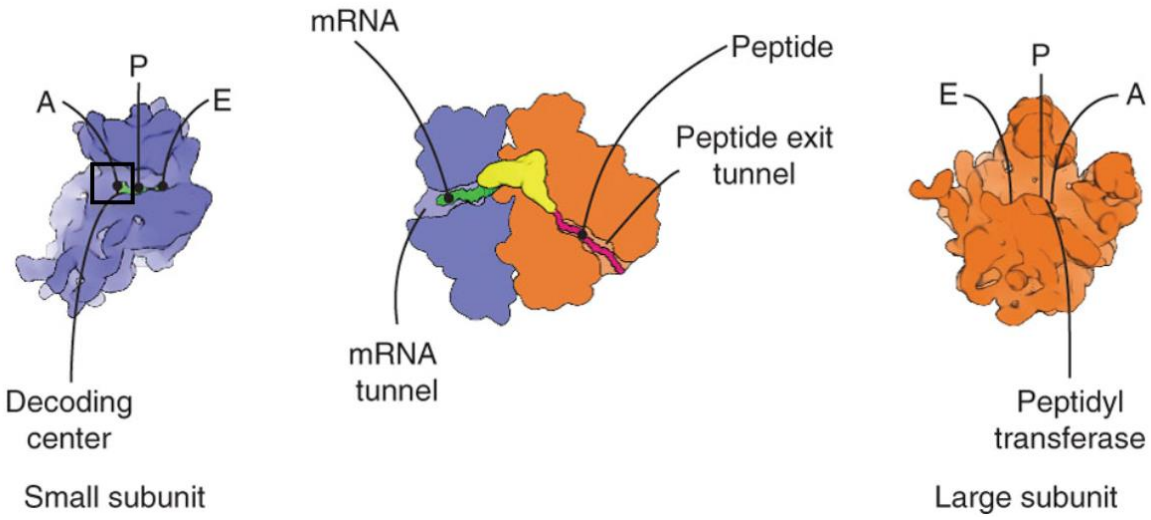

Figure 2. Structural organization with annotation of main functional sites of the ribosome and two separated subunits. Adapted from Melnikov et al., 2012.

Both subunits contain A-, P- and E-tRNA binding sites and each subunit makes different contribution into the process of protein synthesis. SSU accommodates and conduct mRNA through mRNA path during translation. It is also responsible for decoding process where aminoacyl- tRNA (aa-tRNA) is selected according to the mRNA sequence (Figure 2).

The small ribosomal subunit

The small subunit is more dynamic than the large subunit, it has an extended shape and can be divided in three distinct domains: head, body and platform (Figure 3). The functional sites are located in the neck formed between the head and the body/platform. The three tRNA binding sites make contacts with the anticodon stem- loop of the tRNA. The path of the messenger RNA runs all along the neck from the A to the E site (Yusupova et al., 2001). In fact, the ribosome covers about 30 nucleotides of the mRNA as first revealed by footprinting experiments (Steitz, 1969). During translocation, the head swivels relative to the body/platform to facilitate mRNA and tRNA translocation (Frank et al, 2007; Ratje et al., 2010).

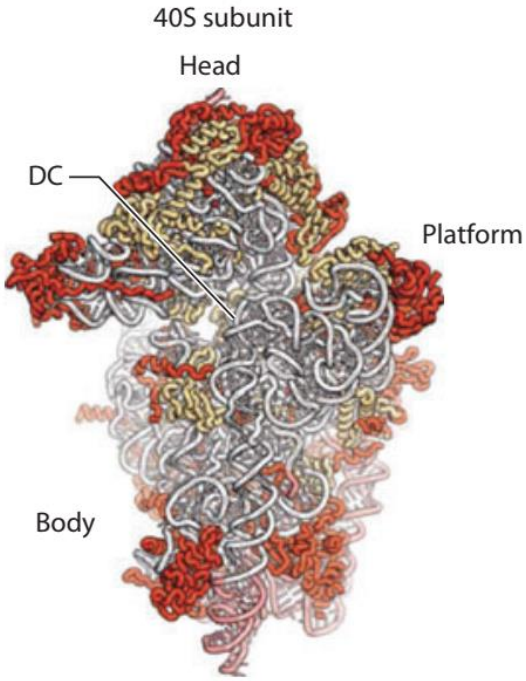

Figure 3. *S. cereviseae* 40S subunit from the interface side, DC stands for decoding center. Adapted from Yusupova et al., 2014.

The large ribosomal subunit

The large subunit catalyzes peptide bond formation, and structurally is more compact relative to the small subunit and apart from its body three distinct features can be observed: the L1 stalk, the P- stalk (L7/L12 stalk in bacteria) and the central protuberance (CP) (Figure 4). The L1 stalk is a dynamic element that participates in the release of deacetylated tRNA while the P-stalk is required for binding and activity of translation factors. The central protuberance contains 5S rRNA together with some proteins. Protein L41e on the LSU forms the only eukaryote-specific bridge eB14 that is positioned at the center of the ribosome. The tRNA binding sites interact with the acceptor stem of the three tRNA (Yusupov, 2001). The peptidyl transferase center (PTC) is located at the convergence of 3' end of the A- and P- tRNAs and opens onto the peptide exit tunnel that runs through the bulk of the subunit and exits at the back on the solvent side (rim of the peptide tunnel). The peptide tunnel has a length of 80–100 Å and a diameter of approximately 10- 20 Å. Together with factors binding sites, the rim of the exit tunnel is the most protein rich regions of the large subunit. The PTC is responsible for peptide bond formation, it is a conserved region on the interface of LSU that is mainly composed of rRNA.

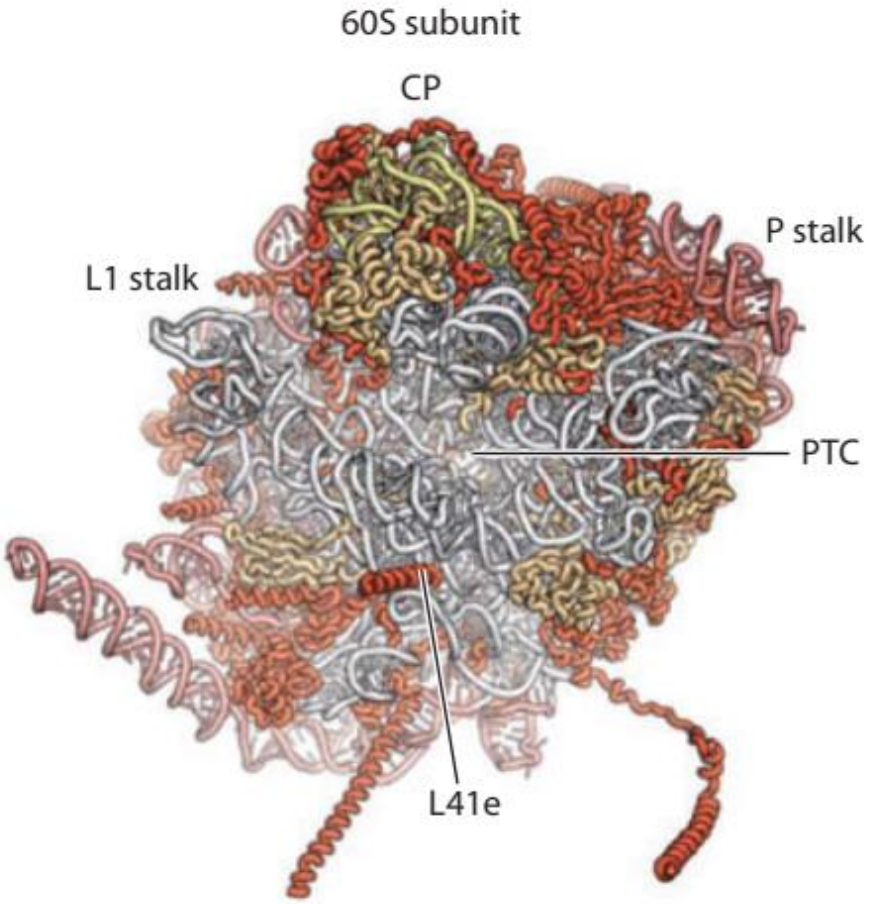

Figure 4. *S. cereviseae* 60S subunit from the interface side, CP stands for central protuberance. Adapted from Yusupova et al., 2014.

During protein synthesis aatRNA enters into the ribosome through the A site, the P site holds tRNA carrying the nascent polypeptide chain (peptidyl- tRNA), and the E site (exit) is where deacylated-tRNA dissociates from the ribosome. During translation, after the nascent polypeptide chain is transferred from the peptidyl- tRNA in the P site to the aa- tRNA in the A site, tRNAs are translocated from the A to the P site and from the P to the E site, thus extending the nascent chain by one amino acid.

Protein synthesis

Recent advances in the field of protein synthesis on the ribosome undergo constant analysis and summarize in up-to date reviews. (Dever et al 2018; Rodnina 2018; Jobe et al 2018; Frank 2017; Ling et al 2016; Yusupova and Yusupov, 2014; Voorhees and Ramakrishnan, 2013). It could be explained by a highly important role protein translation occupies in all living organisms and therefore it remains popular for many decades and bothers minds of many outstanding researchers. Progress in ribosome crystallography brought unprecedent amount of information, as well as advances in cryo-EM technique demonstrate that structures of different ribosome complexes became more detailed and higher in resolution. As a result, number of structural studies on ribosomes was significantly increased, providing more new insights on the ribosome translation in various organisms. However, despite the recent breakthrough the mechanism of translation is yet to be completely understood.

In this chapter I will make a brief overview of all main stages of translation, with more in-depth focus on the elongation cycle.

A rapidly dividing yeast cell growing on rich medium is estimated to synthesize nearly 13,000 proteins per second (von der Haar 2008), limited by the availability of ribosomes (Shah *et al.,* 2013). The average cell contains nearly 200,000 ribosomes (Warner 1999; Firczuk *et al.,* 2013) and 15,000–60,000 messenger RNA (mRNA) molecules (with ~1/3 encoding ribosomal proteins) (Warner 1999) (Zenklusen et al., 2008). With levels ranging from 10^5 to 10^6 molecules per cell, translation elongation factors are among the most abundant proteins in the cell (Firczuk *et al.,* 2013). Given the vast resources the yeast cell devotes to protein synthesis, a thorough understanding of protein synthesis is critical to understanding the biology of the living organisms.

Protein synthesis or translation is a complicated process, regulated by a number of protein factors that takes place on the ribosome. It can be divided into four main stages:

- Initiation – assembling of small and large ribosomal subunits and positioning P-site with initiator $tRNA^{met}$ on mRNA start codon (AUG).
- Elongation – a cycle that begins with an aminoacyl-tRNA selection followed by the catalysis of peptide transfer from the P- to the A-site and mRNA-tRNA translocation. The longest phase of translation.
- Termination – termination of protein synthesis and release of the synthesized protein triggered by the stop codon on mRNA

- Recycling – ribosomal subunits dissociation and preparation for the next translational iteration

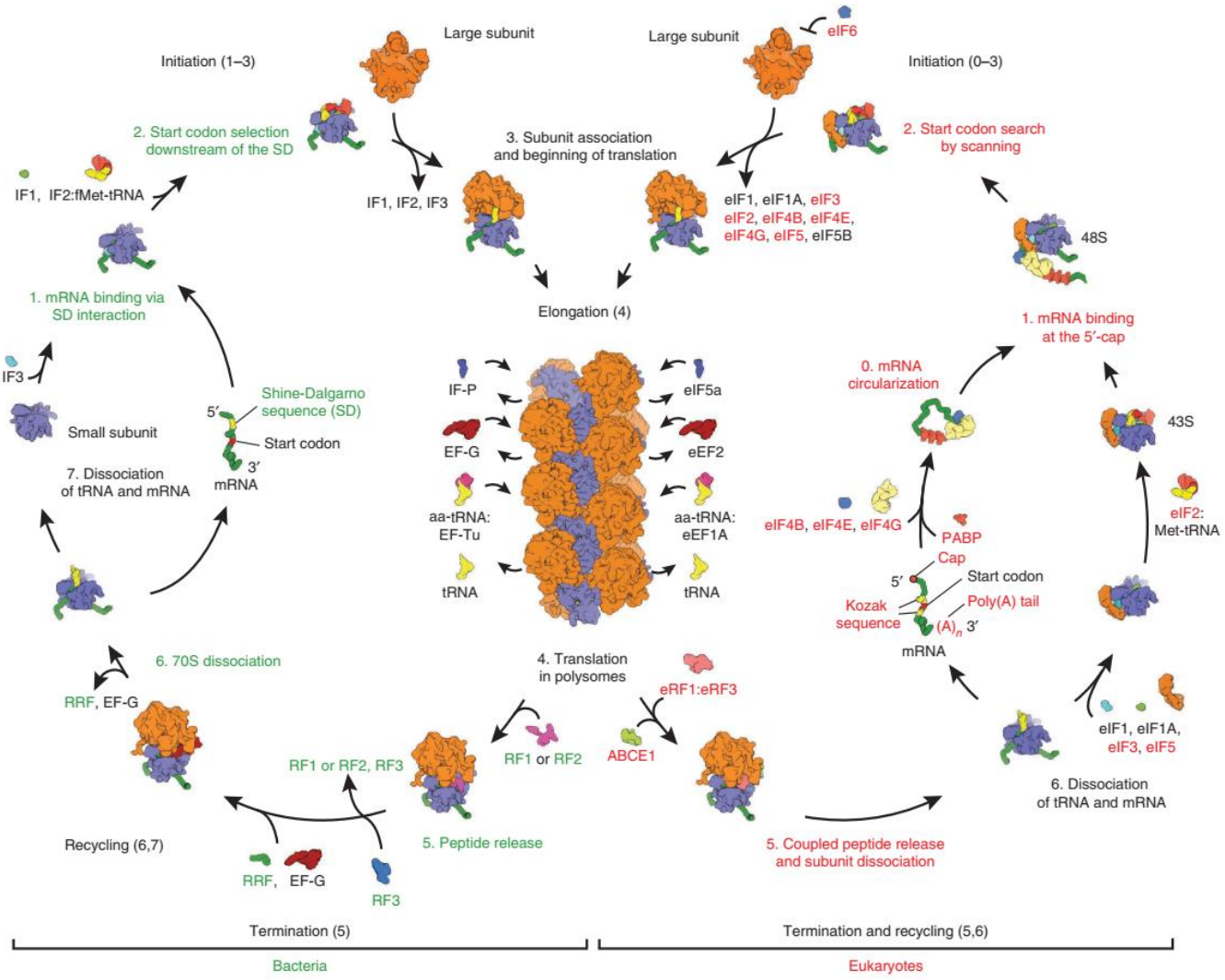

Figure 5. The translation cycle in bacteria and eukaryotes. Homologous factors and common steps of translation between bacteria and eukaryotes are labeled black, bacteria specific factors and steps are labeled green, while eukaryote specific ones are red. More details are provided in the main text. Adapted from Melnikov et al., 2012.

Each of these stages is assisted by protein factors termed initiation factors (IFs in bacteria or eIFs in eukaryotes), elongation factors (EFs or eEFs), release factors (RFs or eRFs) and recycling factors.

Initiation in bacteria is generally tied to mRNA Shine- Dalgarno sequence (SD). mRNA often exhibits a specific conserved SD sequence upstream to the AUG start codon that is

complementary to the 3' end of the 16S rRNA in the small subunit (anti- SD). Formation of an SD/anti- SD duplex allows the 30S subunit to bind the mRNA and orient the AUG in the P- site. Initiator $tRNA^{fMet}$ (N-formylmethionine) is subsequently recruited and the large subunit joins the complex.

For eukaryotes translation initiation is a more complicated. The three bacterial translation factors, IF1, IF2, and IF3 (Laursen *et al.,* 2005; Schmeing and Ramakrishnan 2009), are replaced by 11 factors in yeast (Dever et al 2016). It also includes, beside 40S and 60S ribosomal subunits, mRNA and Met-$tRNA_i^{Met}$. As detailed in the scheme (Figure 5), translation initiation factors function in an ordered fashion to assemble the 80S ribosomal complex that synthesizes proteins. Before being enrolled in translation initiation, the 40S subunit associates with factors to form the 43S preinitiation complex (PIC). The eIF4 family of factors are thought to prepare the capped mRNA (m^7G mRNA) for binding to the 43S PIC to form a 48S PIC. After binding near the 5′ end of the mRNA, the ribosomal complex scans down the mRNA in search of an AUG start codon. Reaching the start codon by 48S PIC promotes binding of the 60S subunit to form an 80S ribosome and subsequent dissociation of the initiation factors. At this step, initiation is over, leaving the ribosome associated with the mRNA and initiator Met- $tRNA_i^{Met}$ in P- site ready to engage the elongation stage.

As is seen from the Figure 5, elongation step is the most conserved between bacteria and eukaryotes with homologous elongation factors. It is the longest stage of protein synthesis during which ribosomes are assembled in large helical complexes, termed polysomes, when single mRNA is translated by multiple ribosomes at the same time. During each cycle of elongation one amino acid is added to the nascent peptide chain. More detailed review of elongation step will be presented in the next chapter.

Elongation cycle is continued until a stop codon (UAG, UGA or UAA) enters the A-site, which will trigger termination of translation. The stop codon recruit release factor that hydrolyzes polypeptide chain from P-site tRNA, which eventually leaves ribosome. After termination ribosome undergoes recycling step – two subunits disassociate and prepare for another translation cycle.

Elongation

Following initiation, the ribosome is ready to enter in the elongation stage during which the mRNA open reading frame is translated into protein. As it was already mentioned, the elongation cycle is highly conserved, unlike initiation and termination, which differ significantly between bacteria and eukaryotes. Elongation is an iterated process composed of three major steps: aminoacyl- tRNA selection, peptide bond formation and mRNA-tRNA translocation. Each cycle lasts from around 0.1 to 1 seconds (Munro et al., 2009) and corresponds to the incorporation of one amino acid in the nascent polypeptide chain. It is the most conserved stage and includes key features of translation: fidelity, catalysis and structural dynamics. All this is achieved under tight control of elongation factors. Before diving into the elongation process, elongation factors will be reviewed.

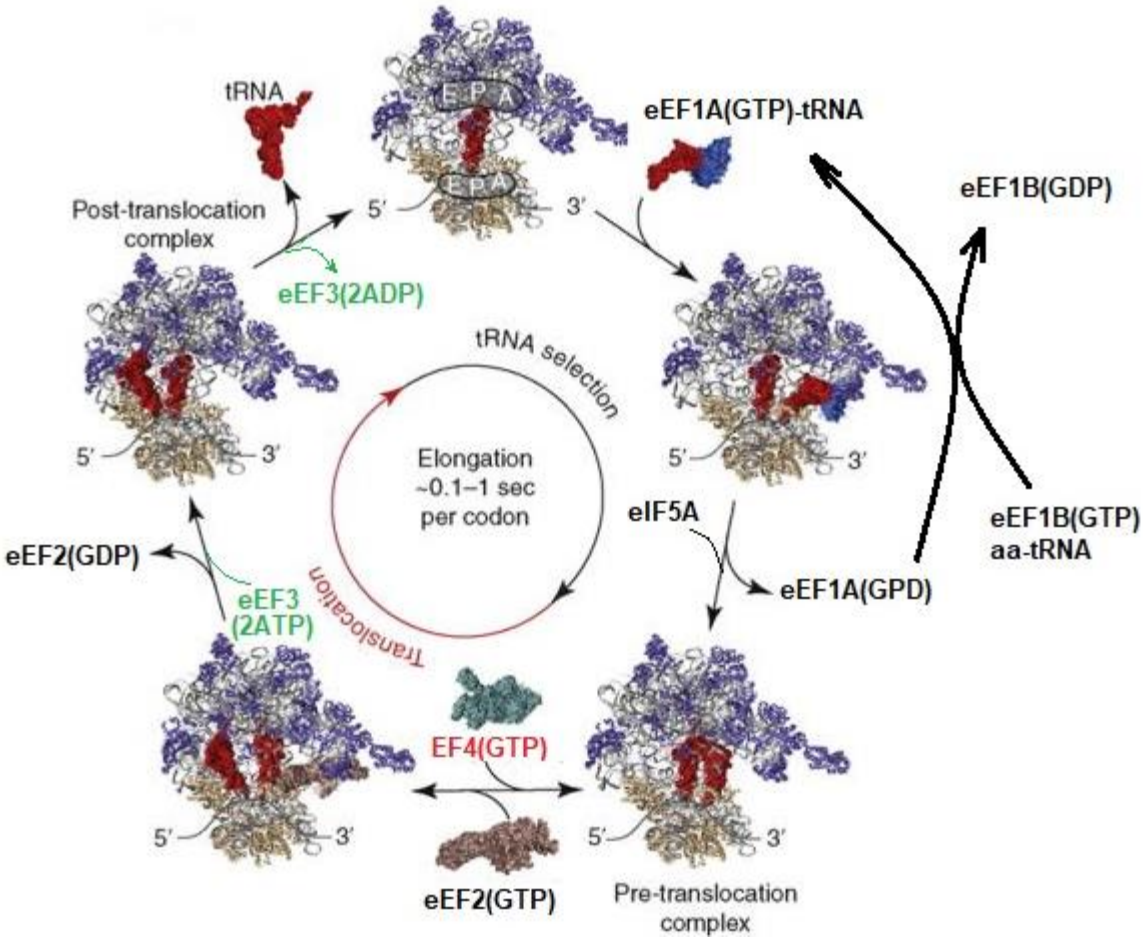

Figure 6. Scheme of the elongation cycle. EF4 is bacteria specific and labeled in red. eEF3 is presented in fungi only and labeled in green. The rest factors are named accordingly to eukaryotes, however they all have homologues in prokaryotes. eIF5A is assumed to assist during peptide bond synthesis and dissociates after. Details are presented in the main text. Adapted from Munro et al., 2009.

Elongation factors		
Eukaryote name	**Bacterial homolog**	**Function**
eEF1	EF-Tu	GTPase that delivers of aminoacyl-tRNA
eEF1B	EF-Ts	Nucleotide exchange factor required for re-activation of eIF1
eEF2	EF-G	GTPase that mediates translocation of tRNA and mRNA
eEF3	None	ATPase fungi-specific that stimulates release of E-site tRNA
None	EF4 (LepA)	GTPase mediates reverse translocation tRNA and mRNA
eIF5A	EF-P	Cooperate with eEF2 during elongation

Elongation factors

Elongation factor 1A and 1B (EF-Tu and EF-Ts in bacteria)

Elongation factor 1A (eEF1A), like its bacterial ortholog elongation factor Tu (EF-Tu), starts elongation cycle by carrying and delivering aminoacyl- tRNA to the A-site of the ribosome. eEF1A/EF-Tu, is activated upon binding guanosine triphosphate (GTP) and forms a ternary complex upon binding an aminoacyl-tRNA. The GTPase eEF1A binds aminoacyl-tRNA in a ternary complex with GTP. Following GTP hydrolysis on the ribosome, the eIF1A is released in a binary complex with GDP. As with EF-Tu, the spontaneous rate of GDP dissociation from eEF1A is slow and the guanine nucleotide exchange factor eEF1B is required to recycle inactive eEF1A•GDP to active eEF1A•GTP (Gromadski et al., 2007).Whereas the complementary factor EF-Ts in bacteria is a single polypeptide, eEF1B is composed of two or three subunits (depending on the organism) and destabilizes GDP binding to eEF1A by a mechanism that is distinct from that employed by EF-Ts (Andersen et al., 2001)(Rodnina et al., 2009).

Elongation factor 2 (EF-G in bacteria)

Elongation phase of protein biosynthesis catalyzed by elongation factor 2 (eEF2) in eukaryotes proceeds by repetitive translocations of mRNA and tRNA on the ribosome. eEF2 belongs to the family of G-proteins, which consume the energy of GTP to fulfill their function. The bacterial factor EF-G and the archaeal aEF2 are structurally and functionally homologous with eEF2. Both eEF2 and EF-G contain six structural domains (Figure 7). Domains I–V have folds as first described for the bacterial EF-G, although insertions are found in domains I, II and IV of eEF2 (Jorgensen et al., 2003) (Laurberg et al., 2000). Like other GTP-binding proteins, domain I contains five conserved sequence elements, forming the binding pocket for GTP/GDP. The G′ domain in eEF2 is somewhat bigger and shares no structural similarity with the corresponding domain in EF-G.

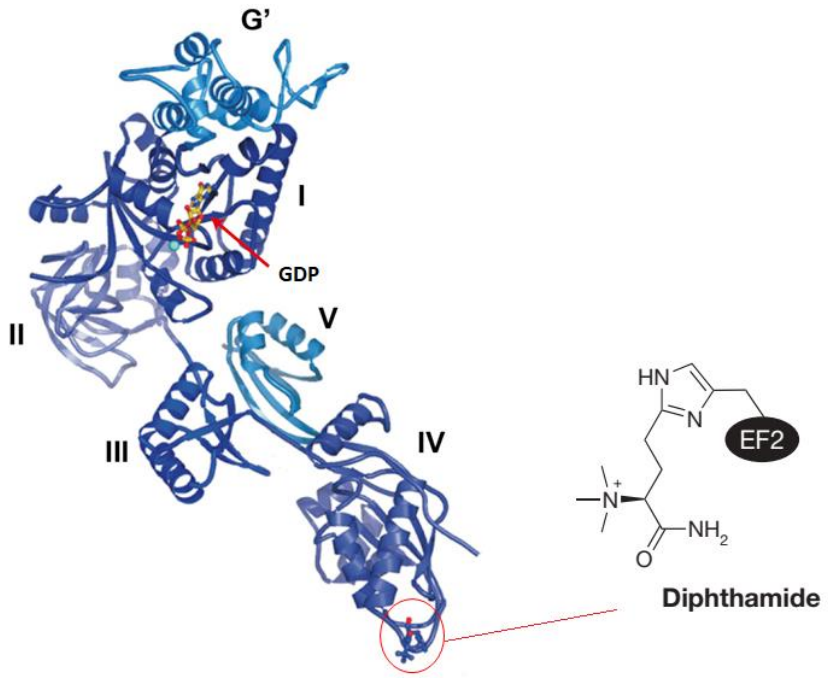

Figure 7. Elongation factor 2 from yeasts. Adapted from Jorgensen et al., 2006.

eEF2, like EF-G, is a structural mimic of the eEF1A•GTP•aminoacyl-tRNA ternary complex (Jorgensen et al., 2003). Domain IV of eEF2, like the anticodon loop of tRNA, binds deep in the A-site decoding center to promote translocation of the tRNAs and mRNA on the ribosome following peptide bond formation.

eEF2 is well conserved among eukaryotes, and it carries a unique post-translational modification, covalently bound to a conserved histidine residue (His699 in yeast and His715 in human) at the tip of domain IV and called diphthamide (2-[3-carboxyamido-3-(trimethylammonio)propyl]histidine). This diphthamide modification is conserved in eukaryotes and archaea (Su et al., 2013; Schaffrath et al., 2014) but is absent in bacteria. Replacement of this histidine with lysine or arginine decreases the rate of tRNA translocation at least 100-fold (Savelsbergh et al., 2000).

Diphthamide biosynthesis is accomplished by a set of highly conserved proteins: yeast strains lacking these enzymes display increased mRNA frame-shifting, pointing to a crucial role of the modification in protein synthesis fidelity (Ortiz et al., 2006).

Mice lacking the diphthamide biosynthetic enzymes DPH1, DPH3, or DPH4 exhibit severe developmental defects or embryonic lethality (Chen and Behringer 2004; Liu et al., 2006; Webb

et al., 2008), indicating that diphthamide synthesis or perhaps another function of these enzymes is required during development.

The diphthamide residue is targeted by well-known virulent factors as diphtheria toxin, Pseudomonas aeruginosa exotoxin A and cholix toxin from Vibrio cholera, which inactivate eEF2 by ADP-ribosylation (Schaffrath et al., 2014). Inactivation of eEF2 blocks protein synthesis, and impairs cell growth; however, the molecular basis for how ADP-ribosylation impairs eEF2 function has not been fully resolved (Davydova and Ovchinnikov 1990; Nygard and Nilsson 1990; Jorgensen et al., 2004; Taylor et al., 2007; Mateyak and Kinzy 2013).

In yeast, eEF2 can be also shut off by an antifungal drug sordarin that does not affect mammalian eEF2 in spite of a very high conservation of the factor among eukaryotic species. Sordarins are fungicides that inhibit translocation in yeast and certain filamentous fungi through inhibition of eEF2. The sordarin-stabilized eEF2–80S complex resembles the 70S–EF-G complex stabilized by fusidic acid. Like fusidic acid, sordarin prevents release of the eEF2 from ribosome (Justice et al., 1998).

It was shown that eEF2 also works as mediator of global physiologic processes and metabolic pathways of eukaryotic cells such as mTOR, cell cycle, stress response and cancer (Proud, 2002; White-Gilberson et al., 2009). eEF2 is regulated by an endogenous Ca2+-activated kinase (eEF2K) that inactivates the factor by reversible phosphorylation upon cellular stimuli. In such a way cells can quickly halt protein synthesis when required.

Elongation factor 3

The translation elongation factor eEF3 is restricted to fungi and appears to be specifically required for protein synthesis with yeast ribosomes. Whereas yeast eEF1 and eEF2 will functionally substitute for their mammalian counterparts to promote translation with mammalian ribosomes in vitro, the mammalian factors eEF1 and eEF2 will only work with yeast ribosomes when eEF3 is added as well (Skogerson and Engelhardt 1977). eEF3 contains two ATP binding cassettes and possesses ribosome-stimulated ATPase activity. A low-resolution cryo-EM structure of eEF3 bound to the ribosome revealed that eEF3 contacts both the central protuberance of the 60S subunit and the head of the 40S subunit (Andersen et al., 2006). eEF3 may promote release of deacylated tRNA from the E site following translocation (Triana-Alonso et al., 1995; Andersen et al., 2006). It is unclear why yeast ribosomes require eEF3 when similar ATPases are neither required for translation nor are obviously present in the genomes of higher eukaryotes.

Eukaryotic translation initiation factor 5A (EF-P in bacteria)

Another universally conserved factor, eIF5A/EF-P, also functions in translation elongation. eIF5A and EF-P were originally identified based on their abilities to stimulate the yield of methionyl-puromycin in a model assay of first peptide bond formation (Glick and Ganoza 1975; Kemper et al., 1976), and, so, eIF5A was considered an initiation factor with a critical role in first peptide bond formation. However, it is noteworthy that puromycin is a poor substrate because of unfavorable positioning in the PTC (Youngman et al., 2004; Wohlgemuth et al., 2008). Moreover, the results of dipeptide synthesis assays employing canonical aminoacyl-tRNA substrates argue strongly against a critical role for eIF5A in first peptide bond formation (Gutierrez et al., 2013; Schuller et al., 2017; Shin et al., 2017). In another study addition of eIF5A stimulated the rate of peptide synthesis in in vitro elongation assays and of release in termination assays in the presence of eRF1 and eRF3. It was also shown that rapid inactivation of temperature-sensitive eIF5A mutants in yeast resulted in the accumulation of polysomes. (Saini et al., 2009). Taken together, these findings argue that the factor plays a critical role in translation elongation, but not in translation initiation or first peptide bond formation.

Further studies into the function of EF-P revealed that the factor stimulated the synthesis of proteins containing runs of consecutive proline residues (Doerfel et al., 2013; Ude et al., 2013). Complementary studies in yeast cells revealed that inactivation of eIF5A impaired translation of reporter genes containing runs of polyproline residues and that eIF5A and its hypusine modification are required for the synthesis of polyproline peptides in vitro (Gutierrez et al., 2013).

Recent structural studies (Blaha et al., 2009; Schmidt et al., 2016; Melnikov et al., 2016) of EF-P/eIF5A bound to the bacterial/yeast ribosome revealed the factor binding in the E site. In these structures, the factor abuts the peptidyl-tRNA in the P site and the hypusine residue interacts with the acceptor arm of the peptidyl-tRNA.

Based on findings obtained from both structural and biochemical studies, a model was proposed, in which the hypusine side chain acts sterically to position the acceptor arm of the P-site tRNA for favorable interaction with the A-site substrate in the ribosome PTC. Although this repositioning is likely to assist synthesis of all peptide bonds, some substrates like polyproline may show a greater requirement because of their inherently poor positioning in the PTC (Dever et al., 2018).

Elongation factor 4

EF4, also known as Leader peptidase A (LepA), is ubiquitously conserved in bacterial (only known exceptions are Streptococcus pyogenes and Carsonella ruddii) as well as mitochondrial and chloroplast genomes (Margus et al., 2007) (Leipe et al., 2002) (Caldon et al., 2003). It was reported that, in vitro, EF4 can catalyze reverse translocation (also called back-translocation), the movement of tRNAs from E and P to P and A sites, respectively (Qin et al., 2006). Based on the observation that EF4 binds to the POST state with higher affinity than to the PRE state, and that EF4-dependent GTP hydrolysis has a higher turnover rate with the former, it was proposed that the POST complex serves as the substrate of EF4 (Connell et al., 2008). EF4 likely interacts with the bacterial translational machinery in response to certain conditions explaining why its deletion affects bacterial growth or fitness under conditions such as low pH (Yang et al., 2014) or high magnesium (Mg2+) concentrations (Pech et al., 2011) but is a non-essential protein during growth in both rich and poor medium (Qin et al., 2006) (Shoji et al., 2010) (Dibb et al., 1986) (Colca et al., 2003) (Badu-Nkansah et al., 2010). While the fidelity of translation in *vivo* does not seem to be affected by the absence of EF4, addition of the purified EF4 has been shown to increase the fraction of active protein synthesized *in vitro* (Qin et al., 2006).

Structural basis of elongation process

tRNA selection: decoding, proofreading

After highlighting key players of elongation cycle we can proceed to the process. Elongation phase starts directly after initiation step with AUG start codon of mRNA and methionyl-$tRNA^{iMet}$ (FMet-$tRNA^{fMet}$ in bacteria) positioned in the P site of the ribosome and extends until the ribosome reaches the termination codon at the end of the ORF. Ribosomes decode one codon of the mRNA sequence per elongation cycle by using tRNA substrates and append the encoded amino acid to the nascent peptide. Translation elongation is composed of three basic steps that take place at the incorporation of each amino acid in the elongating peptide chain: tRNA selection (or decoding), peptide-bond formation and translocation of the mRNA–tRNA complex.

During protein synthesis, the ribosome accurately selects transfer RNAs (tRNAs) in accordance with the messenger RNA triplet in the decoding centre. The decoding pathway comprises two subsequent selection steps, initial selection and proofreading. tRNA selection is initiated by elongation factor eEF1A (EF-Tu in bacteria), which delivers tRNA to the aminoacyl tRNA-binding site (A site) and hydrolyses GTP upon establishing codon–anticodon interactions

in the decoding centre. At the following proofreading step the ribosome re-examines the tRNA and rejects it if it does not match the A codon (Rodnina, 2012). Based on extensive early footprinting, cross-linking, and mutagenesis data, it was demonstrated that several regions in 16S ribosomal RNA (16S rRNA) are implicated in decoding of aa-tRNA recognition (for recent review see Noler, 2007). Recent breakthroughs in X-ray crystallography of ribosomes and their subunits, together with cryo-EM and kinetic data, a model to provide the structural basis for tRNA recognition acceptance of aa-tRNA was proposed (see for review Voorhees and Ramakrishnan, 2013). The mechanistic model of "induced fit" of the decoding centre, where isolated 30S subunit and mimics of tRNAs and mRNA were used, focuses on A1492,A1493, G 530 of 16S ribosomal RNA (*E.coli* nomenclature). Upon binding of tRNA mimic the decoding nucleotides A1492/93 flip out of the 16S helix 44 to form A-minor interactions with the cognate codon–anticodon helix, thus monitoring the Watson–Crick geometry of the first and second base pairs, also accompanying by the domain closure of 30S subunit. It was also claimed that in ribosomal interactions with near-cognate tRNA, deviation from Watson-Crick geometry (G-U pair was found in wobble geometry) results in uncompensated desolvation of hydrogen-bonding partners at the codon-anticodon minor groove (Figure 8).

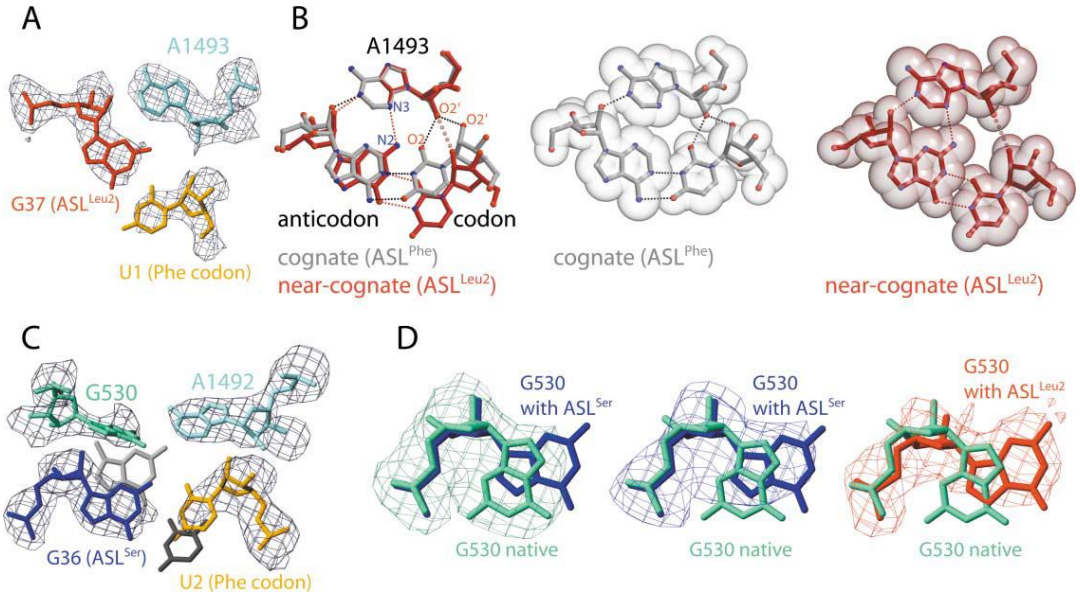

Figure 8. Discrimination at the First Two Codon Positions adapted from Ogle et al., 2002.

This idea, however, has been questioned by observations that the decoding centre in entire 70S ribosome with long messenger RNA and full size tRNAs interacts similarly with mismatched codon–anticodon helices formed by fully accommodated near-cognate tRNAs (Demeshkina et al., 2012; Rozov et al., 2016).

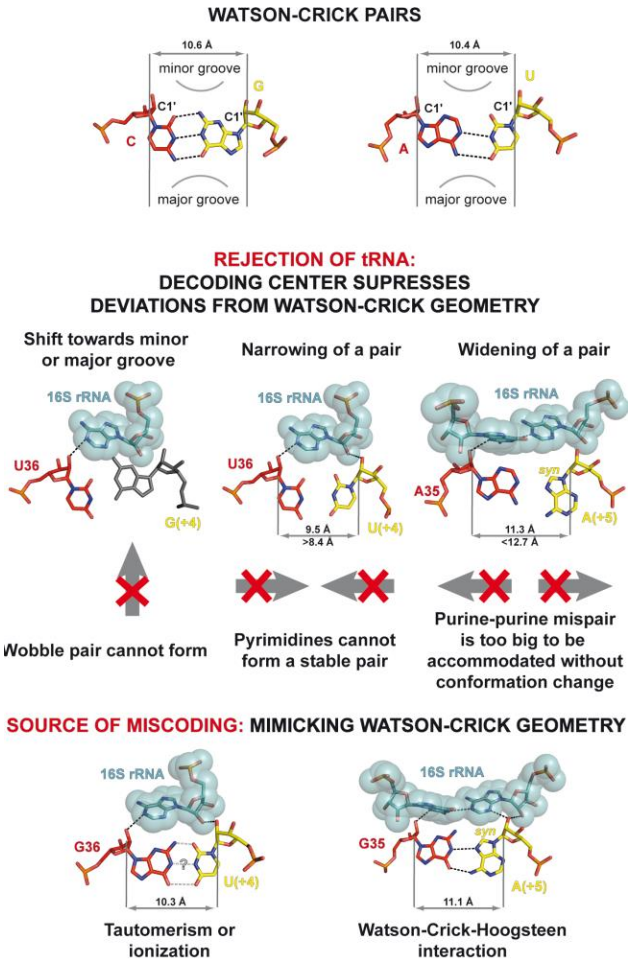

Figure 9. The Ribosome Closely Monitors the Geometry of Base Pairs in the First and Second Positions of the Codon–Anticodon Duplex. Adapted from Rozov et al., 2016.

Integrative scheme of decoding suggested that upon any (cognate, near or non-cognate) aa-tRNA binding to the A site of the ribosome the small subunit undergoes "shoulder locking" , which results in formation of a tight and rigid decoding center by local rearrangements of A1492, A1493 and A1913 (Demeshkina et al., 2012; Rozov et al., 2015). This leads to the formation of minor groove interactions mRNA that restricts the first two nucleotides of the A codon to form exclusively Watson–Crick base pairs with the tRNA anticodon. (Figure 9). These rearrangements essentially define the decoding pocket from the side of mRNA. The slight movement of the shoulder domain of the small subunit towards the anticodon loop brings together G530 (which switches its conformation from *syn* to *anti*) with the second anticodon position and finalizes the formation of the decoding center (Figure 8b-ii). This model bring structural basis to understanding of translational infidelity. The average efficiency of miscoding is estimated to be as high as 10^{-3} – 10^{-4} per amino-acid site (Kurland et al., 1996). Under normal physiological conditions, 18% of the

proteins expressed from an average 400-codon-long gene contain at least one misincorporated amino acid (Drummond et al., 2008).

During the step of initial aa-tRNA selection the codon recognition leads to a complex rearrangement of the tRNA that initially binds to the ribosome in the A/T-state with ASL in the A-site of 30S subunit and acceptor arm remaining simultaneously bound to eEF1A/EF-Tu, which in turn interacts with the ribosome's factor binding site (Schmeing et al., 2009; Voorhees et al., 2013; Loveland et al., 2017).

The conformational rearrangements of the ternary complex, combined with changes in the ribosome, transmit decoding signals from cognate codon-anticodon interactions to EF-Tu stimulating GTP hydrolysis and subsequent dissociation of EF-Tu•GDP. Similarly, in the cryo-EM structure, near-cognate and cognate EFTu•GTP/tRNA ternary complex induced the same local and global conformational changes (Loveland et al., 2017).

The X-ray structures demonstrate that cognate or in some cases near-cognate tRNAs tend to sustain this selection (Demeshkina et al 2012) (Rozov et al 2015, 2018) and subsequently it is assumed to trigger GTP hydrolysis and dissociation of EF-Tu•GDP. However, only a minor portion of the near-cognate ternary complexes reaches the GTPase-activation (Rodnina et al., 2017) suggesting either the existence of additional verification instrument or high sensitivity of the current proposed mechanism at the intermediate stage.

After eEF1A/EF-Tu•GDP release another event of selection referred as proofreading that takes place. When the elongation factor dissociates, the aa- tRNA, which is in the A/T state is not yet fully accommodated in the ribosome. Since its acceptor stem was in the complex with eEF1A/EF- Tu, it has to reach the PTC in the large subunit after release of factor. The aa- tRNA, bound in this conformation is not favorable energetically. Hence, it exerts transition to the PTC, a most favorable state, by rotation the acceptor arm towards the A- site in the large subunit while maintaining strong interactions in the decoding center (Valle et al., 2002; Valle et al., 2003). A near- cognate tRNA by the presence of mismatch with the codon will not be able to stay strongly bound to the small subunit and as consequence will dissociate. However, some near-cognate pairs (especially with mismatch as G·U pair) will maintain Watson–Crick geometry via rare tautomeric or anionic forms and will be accommodated in the decoding centre and further translocated to the P-site, resulting in misincorporation of an amino acid into a polypeptide chain (Figure 9) (Rozov et al., 2016b). The frequencies of occurrence of minor enolic or anionic base states were estimated to fall in the range of 10^{-5} to 10^{-3} (Kimsey et al., 2015). This scenario agrees

with the studies of the tRNA selection process using the single-molecule fluorescence resonance energy transfer approach (Geggier et al., 2010) (Blanchard et al., 2004).

It could be objected that mistakes at tRNA aminoacylation stage by aminoacyl-tRNA synthetases also contribute to the attachment of wrong amino acid into the peptide chain. However, studies reviewed in (Francklyn, 2008) showed the aminoacylation reaction proceed with high accuracy and the chance of attaching incorrect amino acid to the tRNA once in 10^4–10^5 events. Thus, it is assumed that fidelity is mostly dictated by mistakes caused by the ribosome (Zaher and Green, 2009)

Peptidyl transferase reaction

The fully accommodated aa-tRNA is immediately engaged in the peptidyl transferase reaction. This reaction is characterized by the formation of a peptide bond following the attack of the peptidyl-tRNA carbonyl group in P-site by the aa-tRNA amino group in A-site (Figure 10). This attack induces formation of a tetrahedral intermediate on the carbonyl group, which breaks to release the products. This reaction is catalyzed in vivo by the ribosome in the peptidyl transferase center (PTC) that allows increasing the rate of peptide bond formation up to 10^6 times (Beringer et al., 2007) (Rodnina et al., 2007).

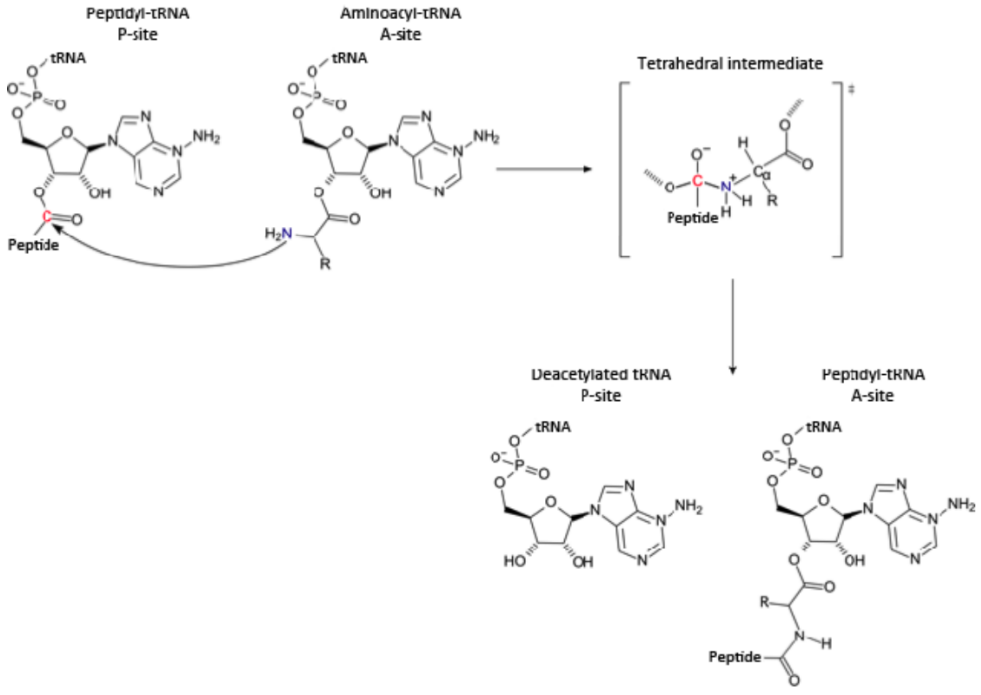

Figure 10. Peptide bond formation reaction.

Biochemical data and X-ray structures showed that both aa-tRNA in A-site and peptidyl-tRNA in P-site orient their acceptor ends in the PTC via two loops of the large subunit rRNA (Moore and Steitz, 2011). One of the catalytic mechanisms the ribosome uses is correct positioning of substrate that decrease the entropy of activation.

Correct positioning of substrate decrease the entropy of activation and represents the first catalytic mechanisms applied by the ribosome (Rodnina et al., 2007; Schmeing et al., 2005; Steitz, 2008). The 2' hydroxyl group of A76 in P-site tRNA makes a direct hydrogen contact with the amino group of the amino acid bound to A-site tRNA, playing an important role in the reaction (Weinger et al., 2004). Current model suggests that the A76 2'OH serve as a proton shuttle. The nucleophilic amino group in A-site donates a proton to A76 2'OH that subsequently transfer it to the 3' in P-site (Figure 11)(Zaher and Green, 2009).

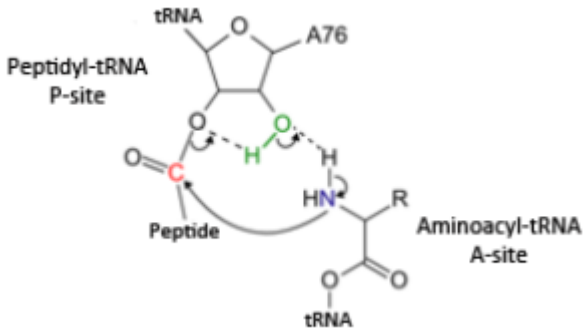

Figure 11. Proton shuttle mechanism by the 2'OH of A76 in the P-site tRNA.

Translocation

After peptidyl transferase reaction, nascent peptide is transferred from the P site tRNA to the amino group of the A site tRNA, this state is called pre-translocation state (PRE). Early mapping of tRNA binding sites on the ribosomes using chemical probing revealed that PRE-state triggers the spontaneous movement of the acceptor stems of the resulting peptidyl- tRNA and deacylated tRNA from A and P to P and E sites of the large subunit, respectively, while tRNA ASLs remain in the A and P sites of the small subunit. This position of the tRNAs inside ribosome is referred as the hybrid A/P and P/E (Figure 12a-b) (Moazed et al 1989). Recent X-ray and Cryo-EM studies, together with single molecule experiments revealed, that in addition to classical (A/A, P/P) and hybrid (A/P, P/E) states, the ribosome can adopt several intermediate conformations that differ in the positions of the tRNAs with respect to the SSU head and body domains and the

A and P site loops on the LSU. These intermediate translocational states are referred to as chimeric states (e.g., ap/P and pe/E (Ramrath et al., 2013); ap/ap (Zhou et al., 2014); or noncanonical states identified by smFRET (Chen et al., 2011) (Adio et al., 2015) (Wasserman et al., 2016). FRET, chemical probing and cryo- EM experiments suggested that, in pretranslocation ribosomes, the spontaneous movement of tRNAs into the hybrid state is coupled to rotation of the platform and body domains of the small ribosomal subunit by 8–10° (Figure 13) (Ermolenko et al., 2007) (Agirrezabala et al., 2008) (Julian et al., 2008). The intersubunit rotation is often described as a ratchet- like movement or simply 'ratcheting' (Frank et al., 2000). smFRET experiments show that, in the absence of EF- G (eEF2 in eukaryotes), pretranslocation ribosomes spontaneously fluctuate between nonrotated (classical) and rotated (hybrid) state conformations (Blanchard et al., 2004) (Munro et al., 2007) (Cornish et al., 2008) (Fei et al., 2008).

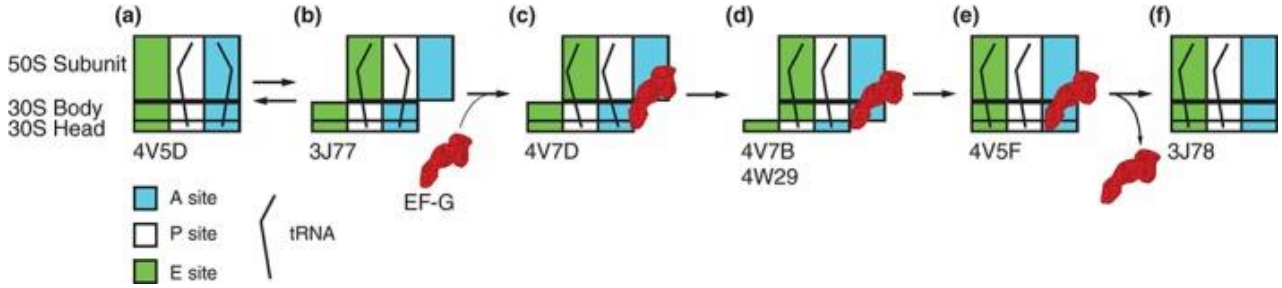

Figure 12. Scheme demonstrating movement of tRNAs and ribosome during EF-G catalyzed translocation. Details are provided in the main text. Adapted from Ling et al., 2016.

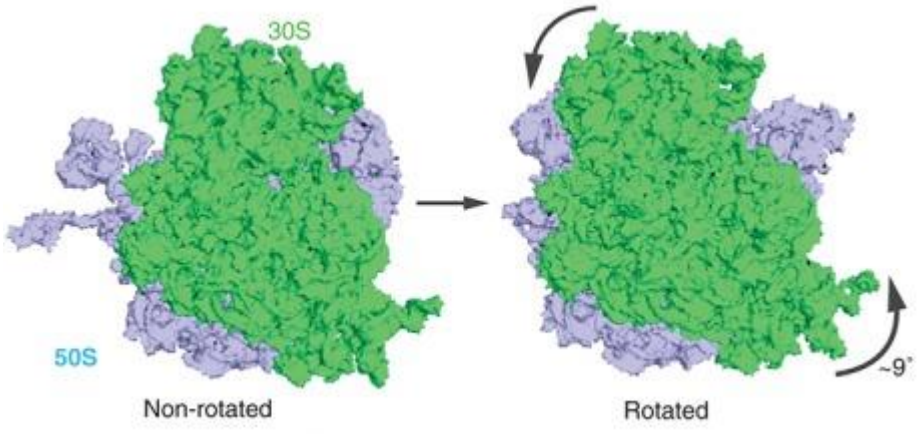

Figure 13. Ratcheting intersubunit movement. The small subunit is shown in light green and the large subunit is shown light blue. Curved arrows indicate the counter-clockwise rotation of the small subunit relative to the large subunit. Adapted from Ling et al., 2016.

To initiate a new elongation cycle, both tRNAs and the mRNA have to be moved for one codon distance. Transition from the pre- translocation state to the post- translocation state (POST) is catalyzed by the conserved GTPase elongation factor EF- G and relies on dynamic of both the ribosomal subunits.

Majority of early published reports suggested that EF- G binds to the ribosome with high affinity and induces translocation only in GTP- bound form (Inoue- Yokosawa et al., 1974) (Belitsina et al., 1975). EF- G · GDP and nucleotide- free EF- G do not show significant translocation activity (Inoue Yokosawa et al., 1974) (Zavialov et al 2005) (Pan et al., 2007) (Spiegel et al., 2007). Intrinsic GTPase activity of EF- G is low, but it is dramatically enhanced via interaction of the G domain of EF- G with the universally conserved sarcin- ricin loop (SRL) of the 23S rRNA of the large ribosomal subunit (Parmeggiani et al., 1981) (Moazed et al., 1988) (Gao et al., 2009). GTP hydrolysis and the subsequent release of inorganic phosphate trigger EF- G dissociation from the ribosome (Belitsina et al., 1975), (Savelsbergh et al., 2003).

Spontaneous fluctuations in the absence of EF-G, of the pre-translocation ribosome between non-rotated (classical) and rotated (hybrid) states do not lead to efficient translocation of tRNA/mRNA on the small subunit, which evidently requires EF-G that accelerates translocation by ~50,000- fold (Rodnina et al., 1997) (Katunin et al., 2002). EF-G is considered to bind to the rotated state of pre-translocation complex and translocate the mRNA–tRNA complex inside the ribosome bringing the tRNAs to the ‘classical’ P/P and E/E states (Ferguson et al., 2015) (Spahn et al., 2004), (Taylor et al., 2007), (Ling et al., 2016), (Shoji et al., 2009). In X-ray study of translocation complexes with use of fused EF-G protein, which N-terminus was bound to the N-terminal domain (NTD) of ribosomal protein L9, it was shown that EF-G can adopt compact conformation with significantly inverted domains III, IV, V (Figure 14) and bind to unrotated state PRE-ribosome with tRNAs in A/A and P/P positions (Lin et al., 2015), which may represent the very early steps of translocation. However, current structure was obtained in presence of GDP nucleotide. Therefore, despite interesting insight on compact conformation of EF-G interacting with non-rotated PRE-state ribosome this model brings, it should be considered cautiously. As all structural studies on pre-translocation complexes (Zhou et al., 2013) (Tourigny et al., 2013) show EF-G in elongated form with rotated ribosome, that is also aligned with biochemical studies. (Spiegel et al., 2007) (Ermolenko et al., 2011) (Frank et al., 2000) (Valle M, Zavialov et al., 2003).

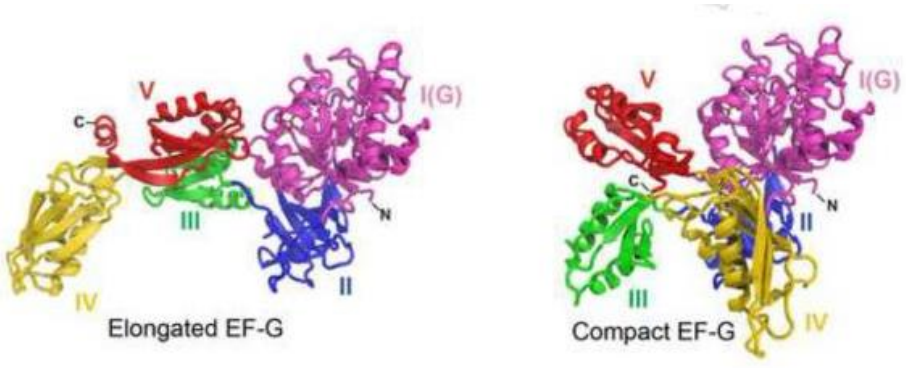

Figure 14. Elongated and compact EF-G conformations with five domains colored differently. Adapted from Lin et al., 2015.

Upon binding to the pretranslocation ribosome, EF- G was shown to transiently stabilize the rotated, hybrid state (Spiegel et al., 2007) (Ermolenko et al., 2011) (Frank et al., 2000) (Valle et al., 2003) and subsequently induce the transition into the nonrotated, classical state conformation of the ribosome (Figure 15c-e) (Chen et al., 2013) (Ermolenko et al., 2007). It could be mediated by the domain IV of EF-G that is disposed in a proximity to intersubunit B2a bridge where it can form contacts. In one of the X-ray crystallography studies (Chen et al 2013) the authors describe interaction of domain IV with a decoding center, however deep analysis of published data (PDB entry 4V90) showed very weak experimental electron density for the tip of domain IV, in particular highly conserved loop I (496-509) and loop II (567-579), and decoding center. While at density map contour level at root-mean-square deviation (rmsd) = 1 there are some traces of density for backbone, it changes drastically at contour level rmsd = 1.5 (Figure 15, Figure16-A). Another region of EF-G from the same PDB entry was examined (Figure 16, A) with two different rmsd levels the same way as it was done for the tip of domain IV, in order to verify that density deterioration is not caused by low EF-G occupancy or overall weak signal from protein. Comparison of the density with 1 and 1.5 rmsd contour levels for this region around domain III, that does not form secondary structure such as α-helix or β-sheet, did not show significant map deterioration (Figure 16-B and C) indicating that weak signal from loop I and II is likely due to flexible conformation of the tip of domain IV. Suggesting that in current crystal packing loop I and II do not have strong interaction with DC. However, the presence of density traces indicates on slightly more favorable conformation.

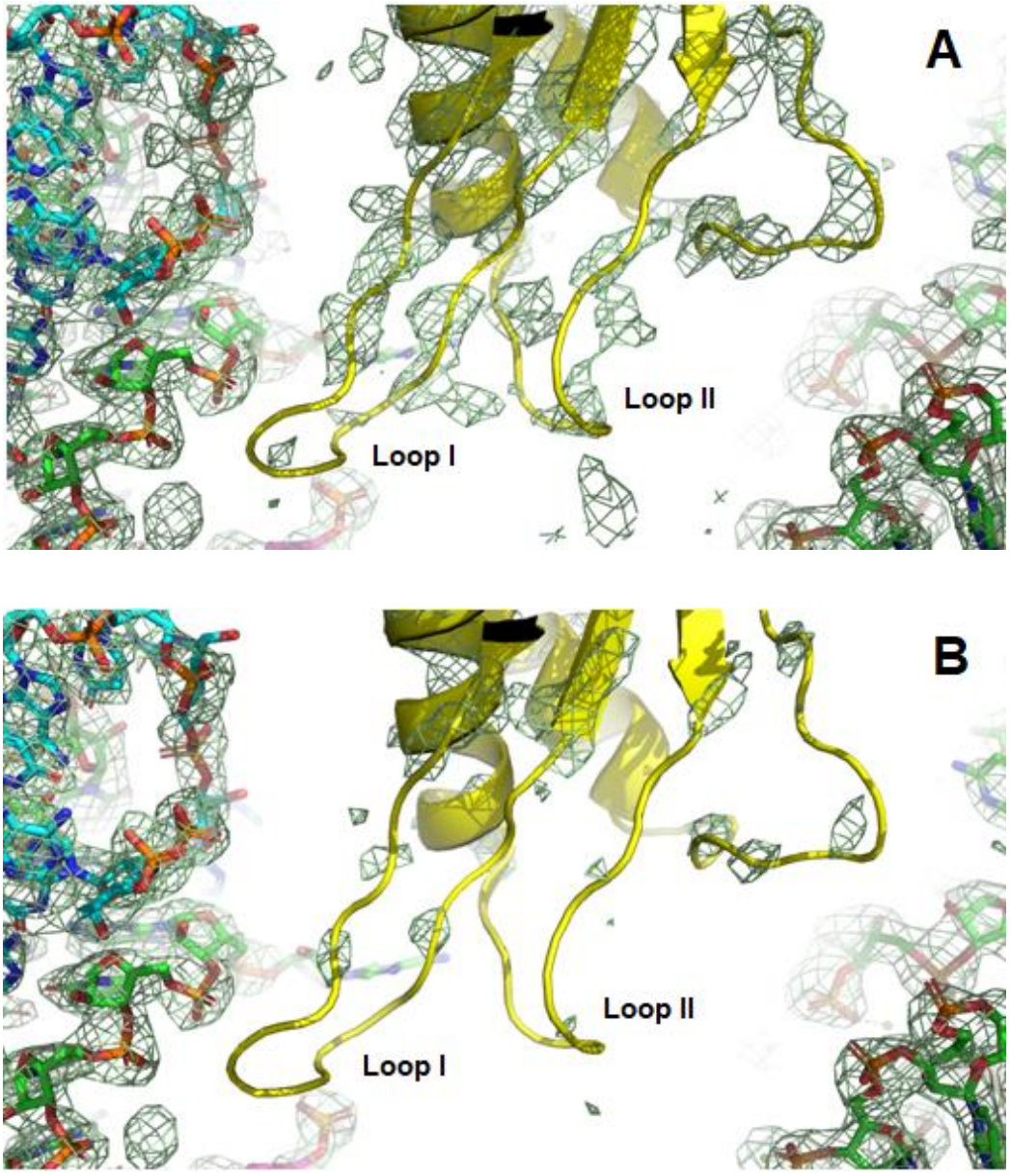

Figure 15. Close insight into the domain IV of EF-G near to decoding center (PDB entry 4V90). (A) – Rmsd at level 1, (B) – Rmsd at level 1.5 EFG-yellow, cyan-23S, green 16S. Model and 2fo-fc density map was obtained from PDB entry 4V90 (Chen et al 2013).

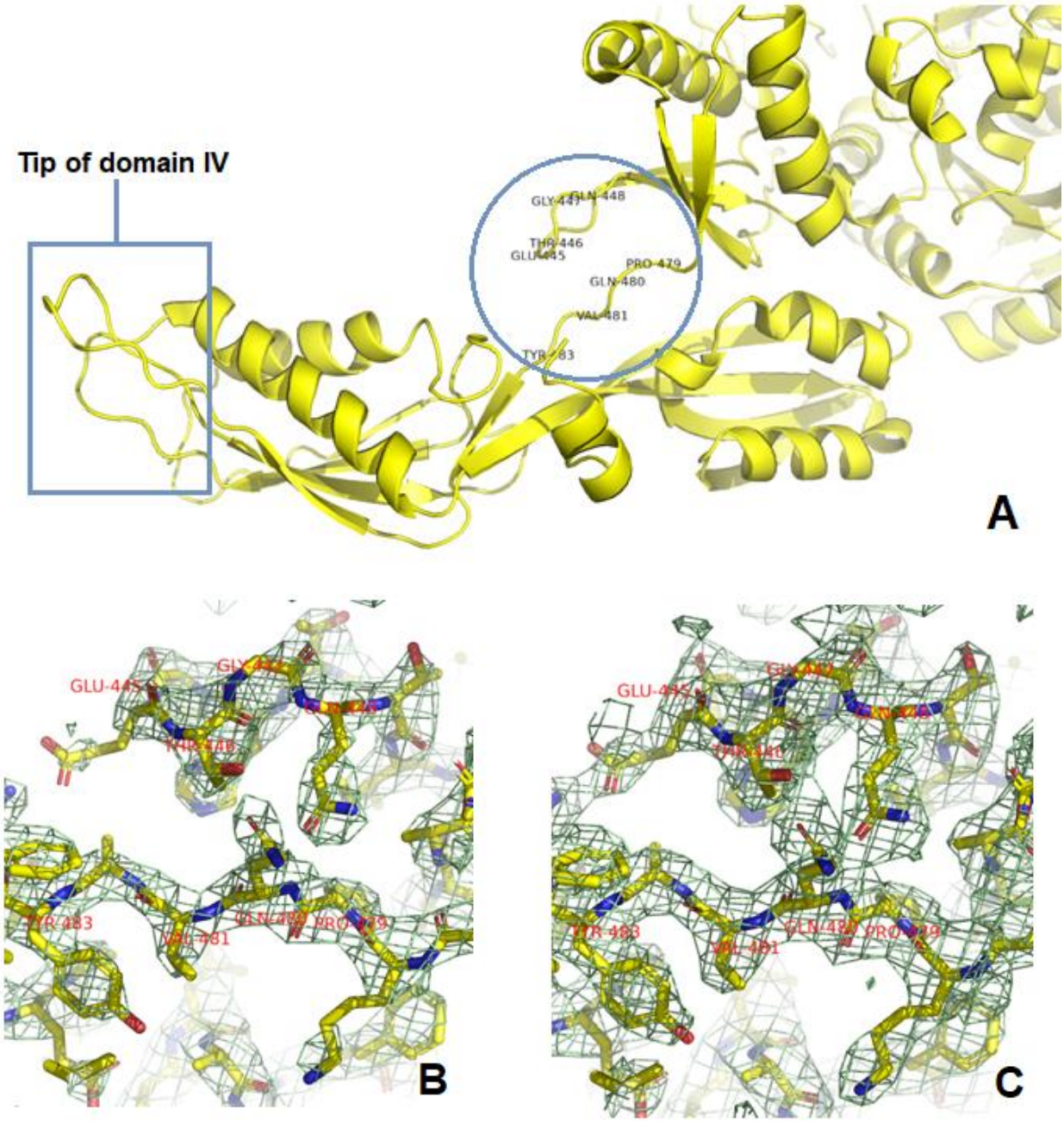

Figure 16. Analysis of the region (in a circle) around domain III of EF-G used for density examination (A). Comparison of the density map at rmsd 1.5 (B) and 1 (C). Model and 2fo-fc density map were obtained from PDB entry 4V90 (Chen et al 2013).

Analysis of experimental densities of presently available high-resolution structures of pretranslocation-intermediate complexes weather bound with one (Tourigny et al., 2013) (Chen

et al 2013) or two tRNAs (Zhou et al., 2014), revealed weak to no density for loop I and II that are in proximity to DC (Figure 17). Therefore, there are no structural evidence that could unbiasedly demonstrate how exactly EF-G interacts with this region during translocation.

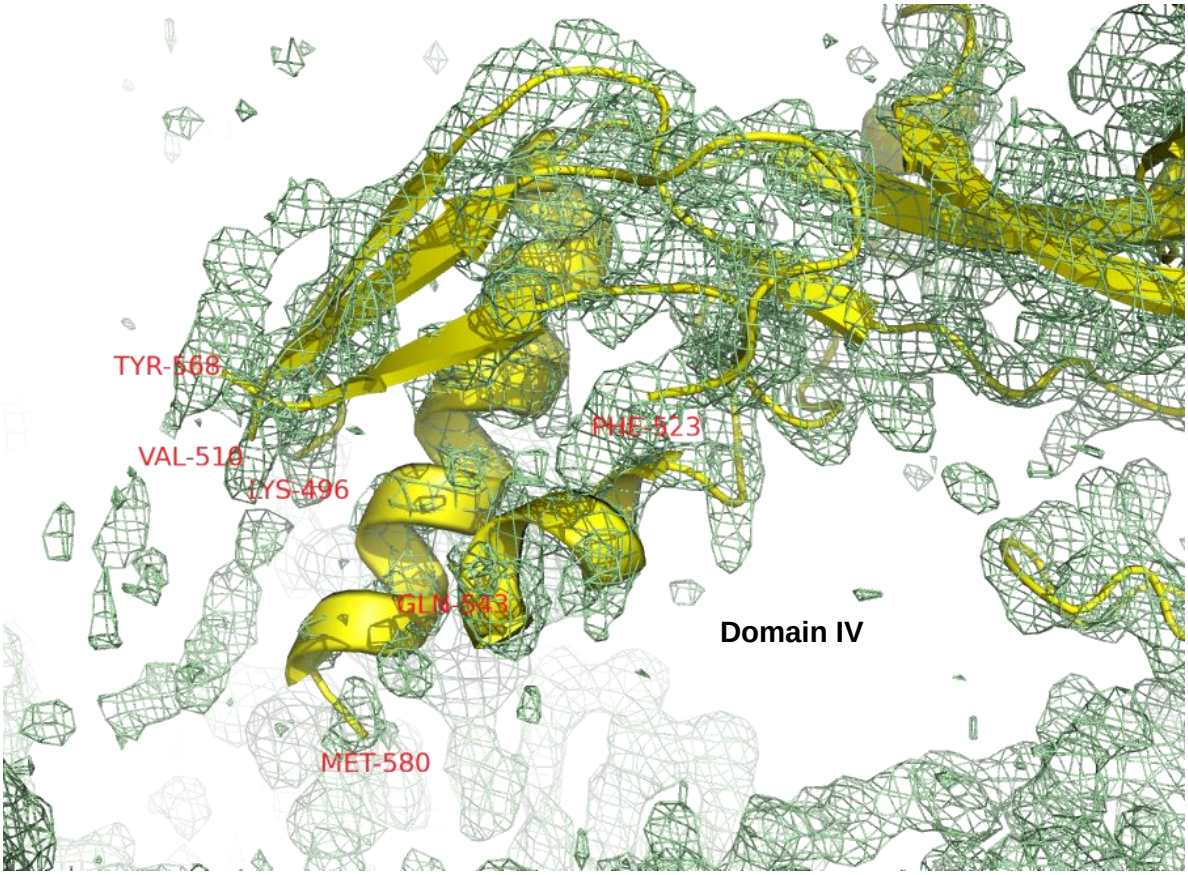

Figure 17. Model and 2fo-fc density map at rmsd 1 of EF-G from PDB entry 4JUW (Tourigny et al., 2013). Due to the absence of the density authors had to cut the tip of domain IV model.

When the SSU body begins moving backward to nonrotated state the SSU head remains in swiveled state (Guo and Noller 2012; Belardinelli et al., 2016b; Wasserman et al., 2016). This may open the decoding region sufficiently to uncouple the tRNAs from the interactions with the ribosome elements that hold the mRNA and the tRNA anticodons in the A and P site, respectively. It also explains how chimeric states are formed: while the tRNA positions on the SSU head domain are retained, the SSU body moves, leading to the displacement of the tRNAs. After the unlocking of the codon–anticodon complexes from the SSU, the SSU head domain starts to move backward (Guo et al., 2012) (Wasserman et al., 2016). The tRNAs adopt their canonical POST positions in P and E sites and EF-G releases Pi (Savelsbergh et al., 2003). While the SSU head moves further

backward, the E-site tRNA moves further away from the P-site tRNA, which is accompanied by the loss of the E-site codon–anticodon interaction (Adio et al., 2015).

In contrast to structures of pretranslocation states, GDP posttranslocation state with two tRNAs in the P, E sites and mRNA provides more details (Figure 18) (Gao et al., 2009). In this model loop I of EF-G is inserted into the minor groove between P site tRNA and codon. There is also a network of interactions between conserved residues Q500 in loop I, H573 in loop 2 and P site tRNA phosphate oxygen in position U37; but no direct contacts of domain IV with the A-site codon. It could be speculated that above mentioned contacts might help to avoid frameshifting in case if they occur at the beginning and maintained throughout the translocation.

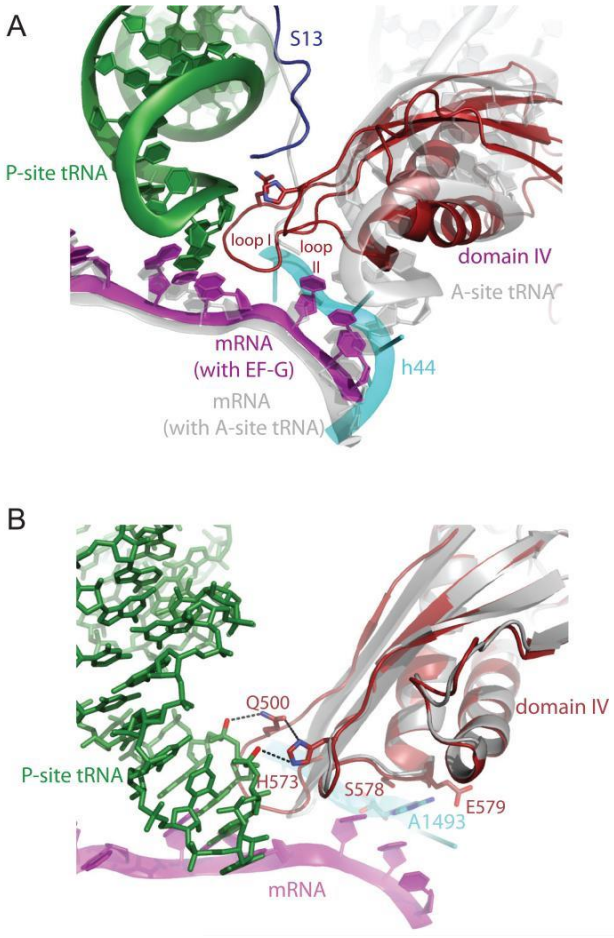

Figure 18. Interactions of domain IV of EF-G with tRNA and mRNA. A. Interactions of domain IV of EF-G with P-site tRNA and mRNA. Loop 1 is inserted into the minor groove between P-site tRNA and its codon. In gray are shown elements from a superposition of the 70S structure with A-site tRNA (20), showing conformational changes in the mRNA and protein S13 on EF-G binding. B. Details of interactions with domain IV in the decoding site. Domain IV of the isolated protein in gray (PDB entry 2BM0). Residues S578 and E579 make interactions with the universally conserved A1493 of 16S RNA. Adapted from Gao et al., 2009.

In the kinetic experiments translocation of mRNA and tRNA on the small subunit was shown to occur at the same rate as reverse rotation of the small subunit from rotated to nonrotated conformations (Ermolenko et al., 2011). Inhibition of translocation with the antibiotics spectinomycin or hygromycin B slows down mRNA translocation and the reverse movement of the small subunit to the same extent, further supporting the idea that the translocation of mRNA and ASLs of tRNA are coupled to the reverse rotation of the small subunit.19 Consistent with these results, the antibiotics viomycin and neomycin, inhibitors of translocation, were shown to perturb intersubunit rotation by trapping the ribosome in conformations in which subunits are rotated relative to each other by ~10° (Ermolenko et al., 2007) (Brilot et al 2013) and 6° (Wang et al., 2012), respectively. Furthermore, a cross- link introduced between proteins S6 of the 30S and L2 of the 50S subunits to block intersubunit rotation was shown to completely abolish ribosomal translocation (Horan et al., 2007) demonstrating that intersubunit rotation is essential for translocation.

mRNA is translocated in three nucleotides (one codon) at a time inside the ribosome (Joseph et al., 1998) (Qu et al., 2011), indicating that it is probably coupled to the movement of associated tRNA by anticodon stem-loop (ASL). It is confirmed by toeprinting experiments (Joseph et al., 1998) that show necessity of ASL bound in the A site of the small subunit and a full- length deacylated tRNA bound in the P site for mRNA translocation. While binding of EF- G · GTP to ribosomes containing a single tRNA bound in the P site does not induce translocation, translocation of two tRNAs through the ribosome can be induced by EF- G in the absence of an mRNA template (Belitsina et al., 1981). Complexes with mutated tRNAs that led to basepairing of four instead of three nucleotides with mRNA performed translocation of mRNA by four nucleotides (Phelps et al., 2006). It suggests that mRNA translocation is driven by tRNA movement, however ribosome rearrangement should also contribute to the process since mRNA have multiple contacts with ribosome along all mRNA track 42 (Interactions of the ribosome with mRNA and tRNA (Jenner et al., 2010).

After translocation event is finished the ribosome is left with the peptidyl-tRNA in the P-site and deacetylated tRNA in the E-site waiting for departure. The empty A-site with a subsequent mRNA codon is awaiting to accommodate next tRNA, so the new elongation cycle can begin.

Eukaryote-specific features of translocation

The majority of structural studies studies of translational apparatus were performed on prokaryotic systems. Despite the fact that the structure and function of the ribosome is substantially conserved across the domains of life, there comparatively much less is known about detailed mechanism of eukaryotic translation. As it was mentioned above the eukaryotic (80S) ribosome is significantly larger and more complex than its bacterial counterpart (Melnikov et al., 2012; Yusupova and Yusupov, 2014), and thus structural investigations of the translation mechanisms in higher organisms are more difficult. Main differences in the translation mechanism between eukaryotic and prokaryotic systems are observed at initiation, termination and recycling stages, requiring numerous additional factors in eukaryotes (Melnikov et al., 2012). In comparison to that elongation phase is defined as conserved because core elements of the ribosome, including the substrate binding sites and the general elongation factors present highly similar. However, the existence of conserved posttranslational modification diphthamide on eukaryote and archaea elongation factor 2 (Su et al., 2013; Schaffrath et al., 2014), eEF3 that was found in fungi only (Andersen et al., 2006) or specific for bacteria EF4 and antibiotic that target domain specific ribosomes (Wilson, 2009) (Garreau de Loubresse et al., 2014), indicate differences in translation mechanisms.

Currently only one X-ray structure of vacant entire 80S eukaryotic ribosome from S. cerevisiae is available (Ben-Shem, 2010, 2011). Thus all current structural information on molecular mechanisms of eukaryotic ribosome translation provided by cryo-EM technique. There are three major conformational states that were revealed for eukaryotic ribosome elongation complexes by cryo-EM. In the first state unrotated ribosome is observed after peptidyl transferase reaction with peptidyl-tRNA in the A site and deacylated tRNA in the P-site. The other two states represent ribosome in rotated conformation with deacylated tRNA adopting hybrid P/E state while peptidyl-tRNA either fully remains in the A site (rotated-1) or moves in the hybrid A/P state (rotated-2) (Budkevich et al., 2011) (Behrmann et al., 2015). Pioneer low-resoultion cryo-EM studies have revealed that similar to EF-G eEF2 binds in the A site of the ribosome (Spahn et al., 2004). Main structural knowledge about dynamics of the eukaryotic translocation, in the presence of mRNA and tRNA, has been provided by low to intermediate-resolution cryo-electron microscopy reconstructions that enabled the understanding of the major conformational rearrangements responsible for guiding the translocation process (Spahn et al., 2004) (Sengupta et al., 2008) (Taylor et al., 2007). There are no structures of translocation intermediates (eEF2 bound with mRNA and two translocating tRNAs) in eukaryotes at the present, however based on similarity with structural data from bacteria head swiveling of the small subunit and reverse

rotation of the small subunit body relative to the large subunit are thought to accompany movement of the tRNAs into the canonical P and E sites (P/P and E/E states) (Ratje et al., 2010) (Ermolenko et al., 2011) (Ramrath et al., 2013) and to allow release of eEF2•GDP from the posttranslocation ribosome.

Due to the limited resolution and "detalization" of the existing cryo-EM reconstructions, a structural understanding of the mechanism by which eEF2 catalyzes translocation in eukaryotes remained unclear. Until the recent cryo-EM study of elongation complex with resolution limit at approximately 4Å shed light on some details on eukaryotic elongation mechanism (Pellegrino et al., 2018). In particular obtained structure of GMPPCP state revealed diphthamide, eukaryote specific posttranslational modification of eEF2, interacting mRNA at position + 4. While in GDP•AlF_4^- complex, mimicking transition-like state after phosphate hydrolysis but still remaining in the pocket, diphthamide points toward the DC and interacts with the sugar-phosphate backbone of decoding nucleotides A1755/56 (A1492/93 in *Escherichia coli*) (Figure 19).

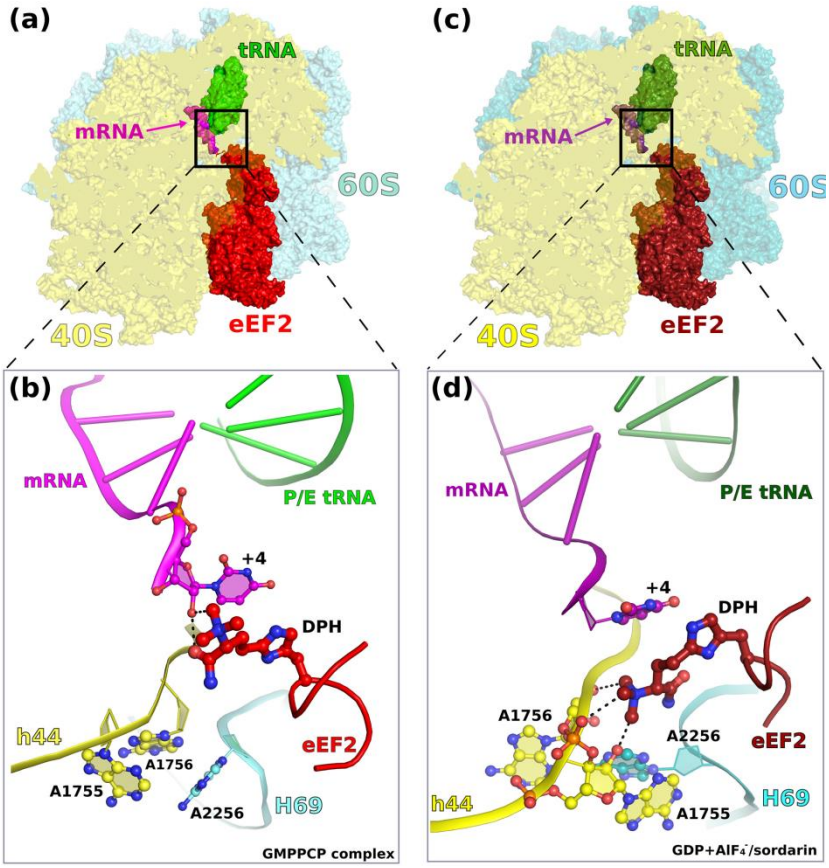

Figure 19. Diphthamide interactions within the reported translocating 80S complexes at different GTP-hydrolytic states. (a), "AlF4−/sordarin" (c) and "GMPPCP/sordarin". (b, d) Atomic model of the DC from the different reported translocating complexes, highlighting the interacting network of diphthamide. Adapted from Pellegrino et al., 2018.

Suggesting that diphthamide might function as a “pawl” (Figure 20) preventing slippage or frame-shifting of mRNA, hence ensuring the fidelity of translocation, that is in line with the results of functional studies. Increased levels of programmed -1 ribosomal frameshifting was observed in both yeast (Ortiz et al., 2006) and mammalian (Liu et al., 2012) cells.

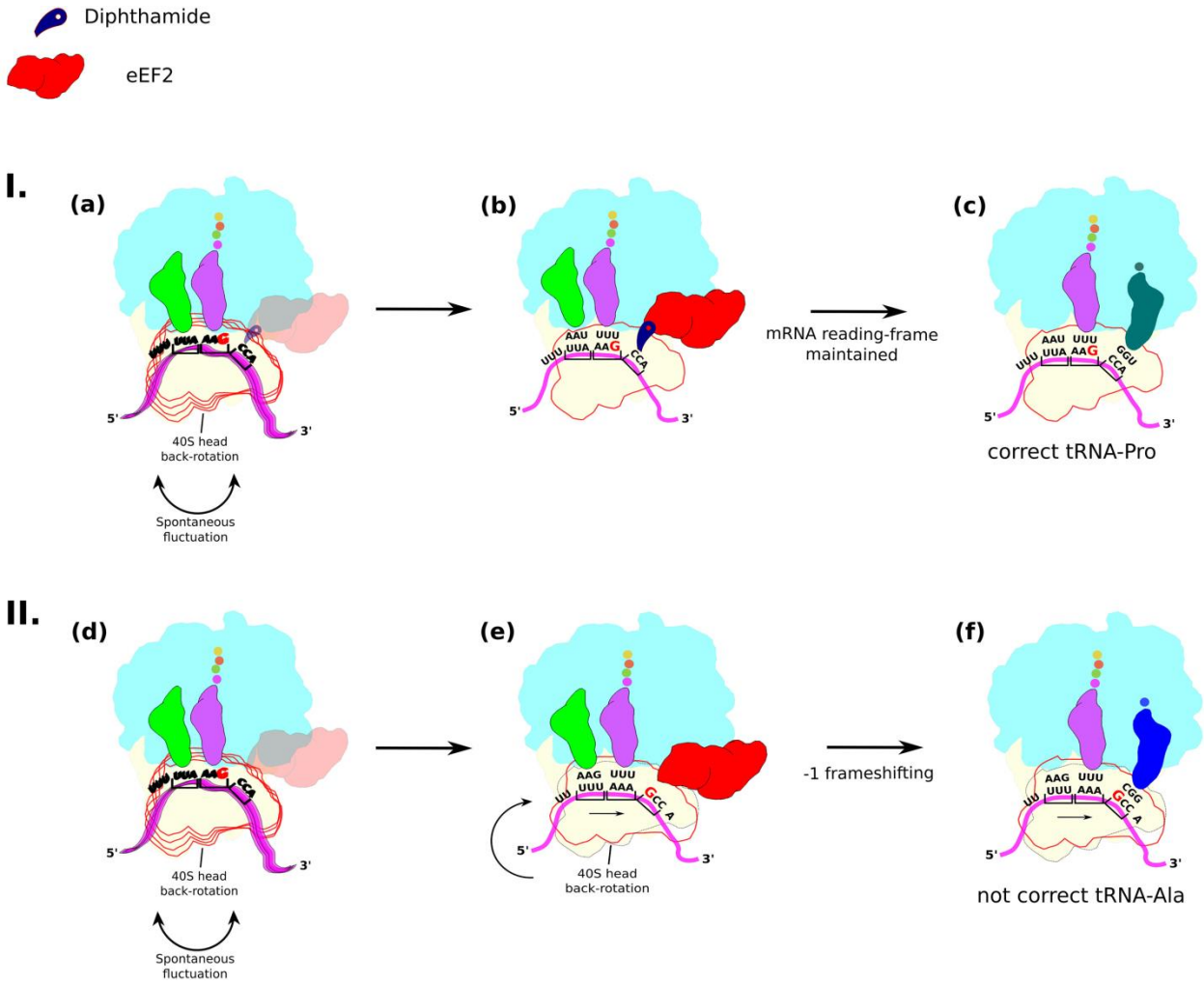

Figure 20. Proposed mechanism of action of diphthamide during ribosomal translocation in eukaryotes. (a). The obtained structure revealed that eEF2 might prevent the head domain to back-rotate by binding directly to the mRNA via diphthamide, and more specifically at the residue in + 4 position (b). In turn, this interaction might keep the correct reading frame of the mRNA and allow for the loading of the correct aminoacylated-tRNA once translocation has finished (c). However, when diphthamide is not expressed or the tip of domain IV is not properly folded (II). The deficient eEF2 is not able to prevent back-rotation of the head of the SSU (d), which in turn might cause mRNA frameshift and load the non-correct aminoacylated-tRNA or introduce premature stop codons (e, f). Adapted from Pellegrino et al., 2018.

Apart from classical translocation substrate, eEF2 is also involved in translocation of the internal ribosome entry sites (IRESs). In order to start translation on IRESs from the cricket paralysis virus (CrPV) or the Taura syndrome virus (TSV) initial translocation reaction is required to move Pseudoknot I (PKI) that binds in the A site and mimics tRNA bound to its mRNA codon, to the P-site (Butcher et al., 2016). It was shown that peptide synthesis initiated on the CrPV IRES is impaired when eEF2 lacks the diphthamide modification (Murray et al., 2016). This could be due to a heightened requirement for diphthamide to promote high fidelity translocation by the IRES. It is supported by cryo-EM structures of translocation complexes that reveal interactions between diphthamide and PKI (Abeyrathne et al., 2016; Murray et al., 2016).

Antibiotics and inhibitors of translation

Antibiotics are small and active against bacteria compounds that revolutionized medicine in the 20th century. They are widely used as a powerful tool in the treatment and prevention of bacterial infections. However, abuse of antibiotics since they have been commercially produced worldwide led to development of antibiotic resistance in bacteria. Therefore, there is a constant need in searching for new compounds that would be active against infection diseases.

On molecular level antibiotics can target different processes like impairing cell wall or nucleic acid synthesis. However, given the central role of protein synthesis in the cell, ribosome constitutes the main target for more than fifty percent of antibiotics. In fact, they inhibit almost every step of translation, although with differing degrees of specificity (Figure 21). Antibiotics or compounds (e.g. in eukaryotes) that impair translation process are called translation inhibitors.

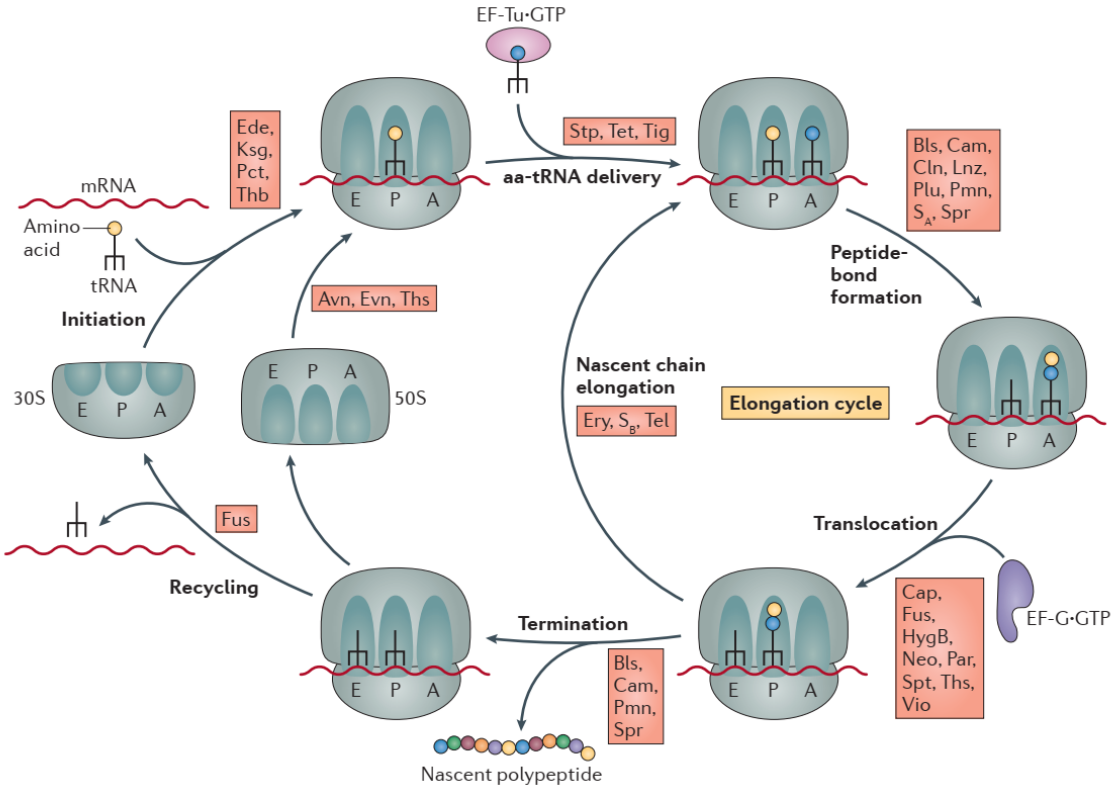

Figure 21. Different targeting sites of antibiotics during bacterial translation. Ede - edeine, Ksg - kasugamycin, Pct – pactamycin, Thb – thermorubin, Avn – avilamycin, Evn - evernimicin, Ths – thiostrepton, Stp - streptomycin, Tet – tetracyclines, Tig – tigecycline, Bls - blasticidin S, Cam - chloramphenicol, Cln - clindamycin, Lnz - linezolid, Plu - pleuromutilins, Pmn - puromycin, S_A - streptogramin A, Spr – sparsomycin, Cap – capreomycin, Vio - viomycin, Hyg B - hygromycin B, Neo – neomycin, Par – paromomycin, Fus - fusidic acid, Spt – spectinomycin, Ery - erythromycin, S_B streptogramin B, Tel - telithromycin. Adapted from Wilson 2014.

X-ray crystallography of ribosomes has opened a new field of investigation of translation inhibitors and ribosome modulators. Decades of studies have revealed the great diversity of molecular mechanisms used by a multitude of antibiotics (review Wilson 2009, 2014). Atomic structures of prokaryotic ribosomes provided the basis for the development of novel antibiotics and in turn ribosome inhibitors served as tools to study protein synthesis in bacteria (Zhou et al., 2008).

Similar to bacteria, the eukaryotic ribosome is also a major target for broad-spectrum as well as eukaryote-specific small-molecule inhibitors. However structural studies of translational inhibitors on 80S ribosome were performed years after they were made for bacteria. High-resolution X-ray crystallography of the 80S ribosome from Ben Shem et al., 2011 opened a new area of investigation. And a number of eukaryote-specific and broad -spectrum ribosome inhibitors were studied for the first time on structural aspect (Garreau de Loubresse et al., 2014). These studies shed light on inhibitor's binding sites, modes of action, determinants of species selectivity and resistance. In particular it was demonstrated for eukaryote specific inhibitors such as cycloheximide, lactimidomycin that bind in the E-site of the ribosome. This binding in the most diverse across species E-site, which is different in nucleotide and protein content in bacteria, archaea and eukaryotes, revealed specific interaction with 80S ribosome that are not possible in bacteria (Figure 22).

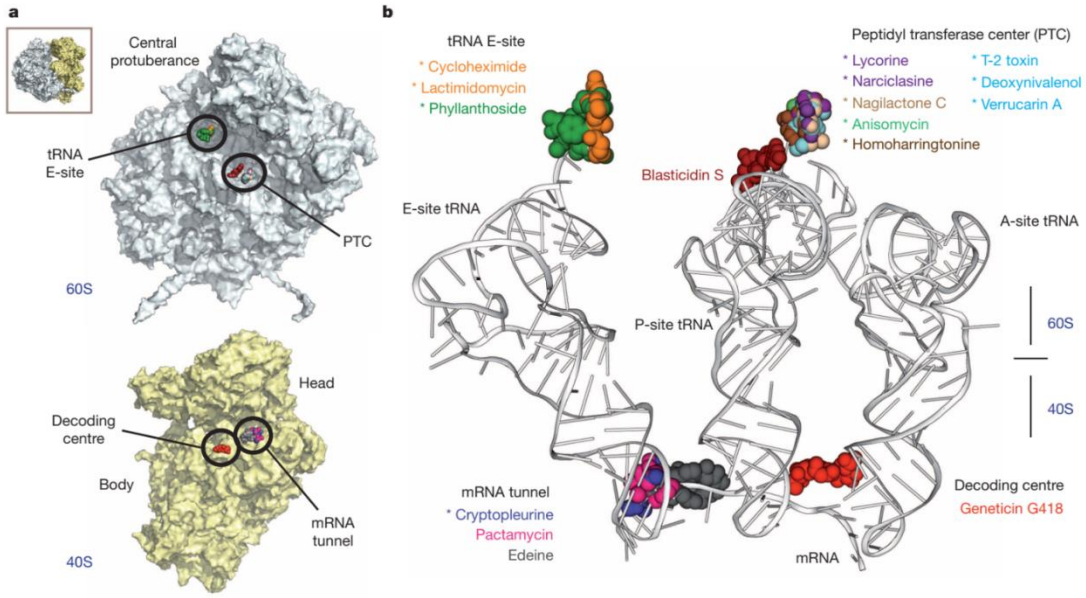

Figure 22. Binding sites of translation inhibitors on yeast ribosome. a) View from subunits interface, binding sites in four functional regions. b) Inhibitors targeting mRNA and tRNA binding sites. Eukaryotic-specific inhibitors are marked with an asterisk.

In more recent years, a number of inhibitors of eukaryotic translation have been identified and shown to affect distinct components of the complicated eukaryotic translation machinery from initiation to elongation. Due to their higher proliferation rate and consequently higher demand for newly synthesized proteins, cancer cells in general appear more vulnerable to inhibitors of translation, creating a therapeutic window, albeit a narrow one, for those inhibitors as potential anticancer drugs. In Yusupov's goup several high-resolution crystal structures of the 80S eukaryotic ribosome from S. cerevisiae in complex with several anticancer drugs were obtained, revealing multiple conformational changes in the ribosome accompanying the binding of inhibitors (Pellegrino et al., 2018b).

Derived structures highlight general principles for drug targeting and provide foundations for structure-based drug design. These structures facilitate the development of next-generation antibiotics with reduced adverse effects and new therapeutics against infectious diseases, cancers and genetic disorders caused by premature termination codons (Bidou et al., 2012; Darnell and Klann, 2013; Lu et al., 2011; Santagata et al., 2013).

RESEARCH PROJECTS

STRUCTURAL INVESTIGATION OF FUNCTIONAL EUKARYOTIC *S. CEREVISIAE* 80S RIBOSOME COMPLEX WITH mRNA AND tRNAs.

Project outline

Structural investigation of "Functional eukaryotic *S. cerevisiae* 80S ribosome complex with mRNA and tRNAs" was the first project I started to work on when I joined the laboratory. The aim was first to obtained *S. cerevisiae* 80S ribosome complexes programmed with long messenger RNA and naturaly modified eukarytoic tRNAs in A- and P-sites in crystal form and then to determine a high-resolution X-ray crystal structure of these complexes. The development of this system would allowed to conduct accurate studies on molecular mechanism of decoding in eukaryote system as it was made for bacteria (Demeshkina et al., 2012; Rozov et al., 2016). At the moment, most of structural studies that allowed scientists to deepen the understanding of mechanisms of translation had been made on prokaryote ribosome.

Although prokaryotic 70S and eukaryotic 80S ribosomes share conservative core, there are big number of eukaryote specific features (reviews: Melnikov et al., 2012; Yusupova and Yusupov, 2014), developed through the process of evolution, role of which are yet to be determined. It is also the case for eukaryote specific tRNA modifications, such as wybutosine on phenylalanine tRNA and others. The discovered alterations in translational mechanism could be exploited for antibiotic drug design, making them less harmful for humans.

Advancement in determination of the first atomic structure of the yeast *S. cerevisiae* 80S ribosome by the groups of Dr. Gulnara Yusupova and Dr. Marat Yusupov opened new prospects for investigation of complex protein biosynthesis in eukaryotes with atomic resolution. However, the obtained crystal form of a vacant *S. cerevisiae* 80S ribosome was not suitable to model functionally relevant states of the 80S ribosome because it was bound with a stress protein Stm1, which was caused by the shock treatment (glucose starvation) that *S. cerevisiae* cell culture was exposed to in order to transfer polysomes to 80S monosomes (Ashe et al., 2000). Binding to the ribosome Stm1 protein blocked major mRNA and tRNA binding sites, hence yeast strain with disrupted Stm1 gene was used.

The classical pipeline for any crystallography project starts from the development of the protocol of obtaining the molecules of interest in a homogeneous state, which will lead to obtaining of crystals. It is known that the main bottleneck in crystallograpic studies is that the well-diffracting

crystal must be found. Thus, the crystallography project includes search for crystallization conditions, collection of the data from crystals treated with post-crystallization solution on X-ray source and finally build the model. As I begin the project "*ab initio*" I started with screening for crystallization conditions, which is a time consuming and challenging task considering the large size and high flexibility of 80S ribosome.

Material and methods

JD1370-ΔStm1 Yeast strain

The described crystal form of the vacant yeast 80S ribosome that gave the first 3 Å resolution structure of the full eukaryotic ribosome is based on the shock treatment of the *S. cerevisiae* cell culture (Ben-Shem et al., 2011). Namely, the ribosome purification protocol includes a key step of glucose starvation that quantitatively converts actively translating ribosomes (or polysomes) into a highly homogeneous fraction of dormant 80S monosomes allowing cells to survive through nutritional deprivation (Ashe et al., 2000). The crystallographic analysis revealed that monosomes purified from starved cells were stoichiometrically bound to protein Stm1, which was described as a translation stress factor (Cherry et al., 2012). Further examination of the crystal structure demonstrated that the Stm1-binding site overlapped with the mRNA and tRNA binding sites on the ribosome (Figure 23), hence, for the first time demonstrating a mechanistic rationale of the 80S ribosome inactivation upon glucose starvation. It is worth to mention that Stm1 was bound to the 80S ribosome in one of its rotated or ratcheted states, which can be adopted naturally by the yeast ribosome without additional stabilization (Spahn et al., 2004).

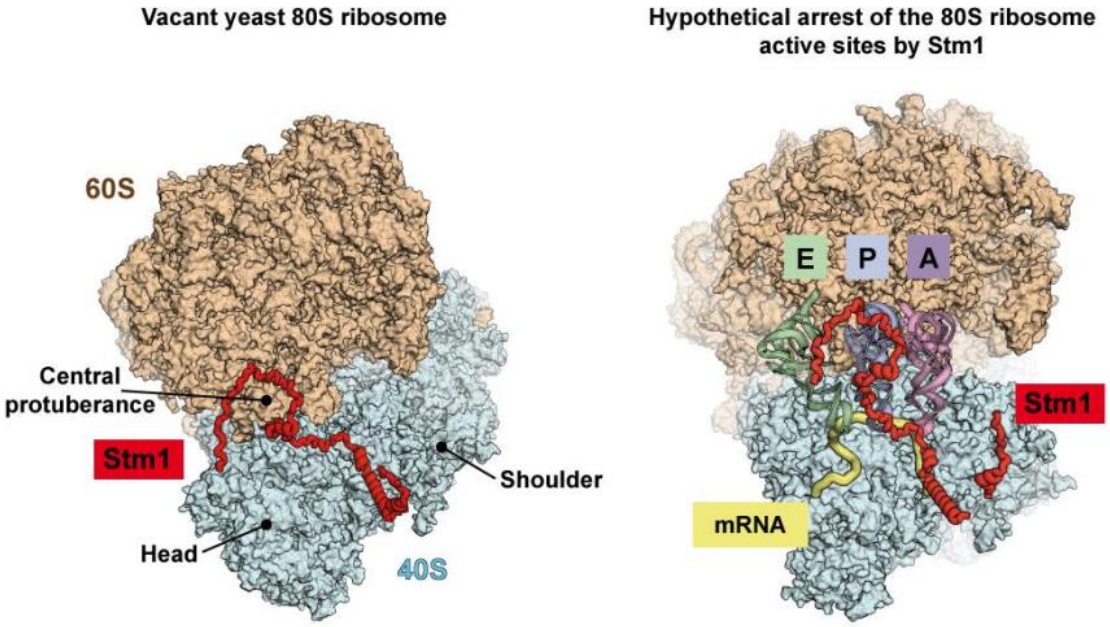

Figure 23. Stm1 functionally arrests the yeast 80S ribosome. (**a**) The model of the complete 80S ribosome based on the original crystal form (Ben-Shem et al., 2011) in two slightly different orientations. The stress protein Stm1 inactivates 80S ribosome by steric hindrance on the major binding sites of mRNA and tRNA. The PDB ID used: 4V88 (ribosome A).

Because of the mentioned above limitation of the original crystal form, attempts to model functionally relevant states of the 80S ribosome would be precluded by the presence of protein Stm1. Therefore, to use the robust protocol developed for the yeast 80S ribosomes purification, it was decided to disrupt the Stm1 encoding gene from S. cerevisiae genome. The same yeast strain JD1370 was used (Ben-Shem et al., 2010) and a homology recombination approach with the TRP1 marker to follow disruption (Figure 26). The resultant strain JD1370-ΔStm1 showed no phenotypic difference with the JD1370 strain demonstrating identical growth curve. However, analysis of the 80S ribosomes isolated from the strain lacking Stm1 revealed a co-purified high-molecular weight contaminant, which was further identified by mass spectrometry as eukaryotic elongation factor 3. The eEF3 protein is a ribosome-dependent ATPase, which is specific to yeast and facilitates release of deacylated tRNA from the ribosomal exist site. It was shown earlier that ribosomes isolated from yeast lacking Stm1 had elevated amount of bound eEF3; at the same time, increased levels of Stm1 reduced association of ribosomes with eEF3. These results indicated that Stm1 and eEF3 might regulate protein biosynthesis through a coupled negative feedback mechanism. Consequently, to avoid possible hindrance of co-purified eEF3 on the capacity of the 80S ribosomes to form crystals, the published protocol of ribosome isolation had to be modified. One of the most important alterations was addition increasing the concentration of monovalent cations to sucrose density gradients that helped to eliminate the eEF3 contamination from the final sample of the 80S ribosomes.

Vacant ΔStm1 S. cerevisiae 80S ribosome purification

Cell culture of the strain *S. cerevisiae* JD1370-ΔStm1 is grown in 5L flasks in standard YPAD media overnight from a fresh single colony pre-culture. Cells are harvested by centrifugation when OD_{600} reaches 1.2-1.3 and are subjected to the glucose starvation treatment. Glucose starvation is used to homogenize ribosome population in vivo by rapidly and reversibly inducing translation inhibition. After few minutes only, all translating ribosomes in polysomes are transferred to inactive 80S monosomes (Ashe et al., 2000). Practically, the treatment requires to re-suspend the pellet in YPA media (i.e. without glucose) and to incubate the flasks at 30°C for 10 minutes. The pellet is then recovered by centrifugation and left in ice at 4°C for 60 minutes. All further steps are performed at 0-4°C. Cells are washed 3 times with pre-cooled buffer M: 30mM Hepes-KOP pH 7.5, 50 mM KCl, 10 mM $MgCl_2$, 8.5% mannitol, 2mM DTT, 0.5 mM EDTA pH 7. Typically, 5-6 grams of cells are obtained from 4L culture.

After the washing steps, cells are prepared for lysis. The pellet is resuspended in 1.35 ml of buffer M per 1 gram of cells and supplemented with additional 740 µL of protease inhibitor

cocktail (PIC, Roche), 100 µL RNasin (Promega), 150 µL Pefablock 100 mM and 70 µL of Na-heparin 100 mg/ml, 30 µL DTT 1M per 6g of cells. Heparin concentrations were found to participate in ribosome solubility thus affecting the amount of PEG required at later steps to precipitate the ribosomes. Cells are disrupted with glass beads by hard vortexing the tube 6 times for 1 minute with 1 min breaks on ice between each shake (Lang et al., 1977) in order to prevent heating. This approach was originally used to isolate yeast mitochondria and introduced here to avoid contamination by mitochondrial ribosome.

All further steps require working fast and on ice. Beads are removed by short centrifugation (20,000g - 2 min) and the lysate is further clarified by centrifugation (31,000g - 9 min) before being subjected to a differential precipitation by polyethylene glycol (PEG). This step is used to fractionate quickly the lysate in order to recover the ribosome-containing fraction. Thus, PEG 20,000 is added from a 30% w/v stock (Hampton Research) to a final concentration of 4.5% w/v for the first fractionation. The solution is clarified by centrifugation (20,000g - 5 min), the supernatant is recovered and the KCl concentration is adjusted to 130 mM final concentration. PEG 20,000 concentration is increased to 8.5% for the second fractionation. Ribosomes are pelleted (17,500g - 10 min) and the supernatant is discarded. Ribosome pellet is re-suspended (6.5-7 mg/ml) in buffer M+, which is composed of buffer M with KCl concentration adjusted to 150 mM and supplemented with protease inhibitors and heparin. At this stage, typically 30-35 mg of ribosomes is obtained from 5-6 grams of yeast cells.

Ribosomes are further purified by a 10-30% sucrose gradient in buffer A (20 mM Hepes-K pH 7.5, 120 mM KCl, 8.3 mM $MgCl_2$, 1 mM DTT, 0.3 mM EDTA pH 7, 2.5mM spermidine) using the SW28 rotor (18,000 rpm - 15h). The appropriate fractions are pooled and both KCl and $MgCl_2$ concentrations are adjusted to 150 mM and 10 mM respectively. In order to precipitate ribosomes, PEG 20,000 is added to a final concentration of 6.9% w/v. Ribosomes are pelleted by centrifugation (17,500g - 10 min). The white pellet is gently suspended in buffer G (10 mM Hepes-K pH 7.5, 50 mM KAc, 10 mM NH_4Cl, 2 mM DTT, 5 mM $Mg(Ac)_2$) to a final concentration of 20 mg/mL. Typically, 15 -20 mg of pure ribosomes were obtained from 5-6 grams of cells (Ben-Shem et al., 2010).

One of the first characteristic of sample quality is the A260 curve after centrifugations in sucrose density gradients (Figure 24), the peak of which corresponds to the fractions with highest concentration of 80S ribosomes. Although no obvious contaminations could be seen from the chart, there are always impurities in a form of 110S or 60S around the peak. Therefore, only the fractions close to the tip are used for crystallization.

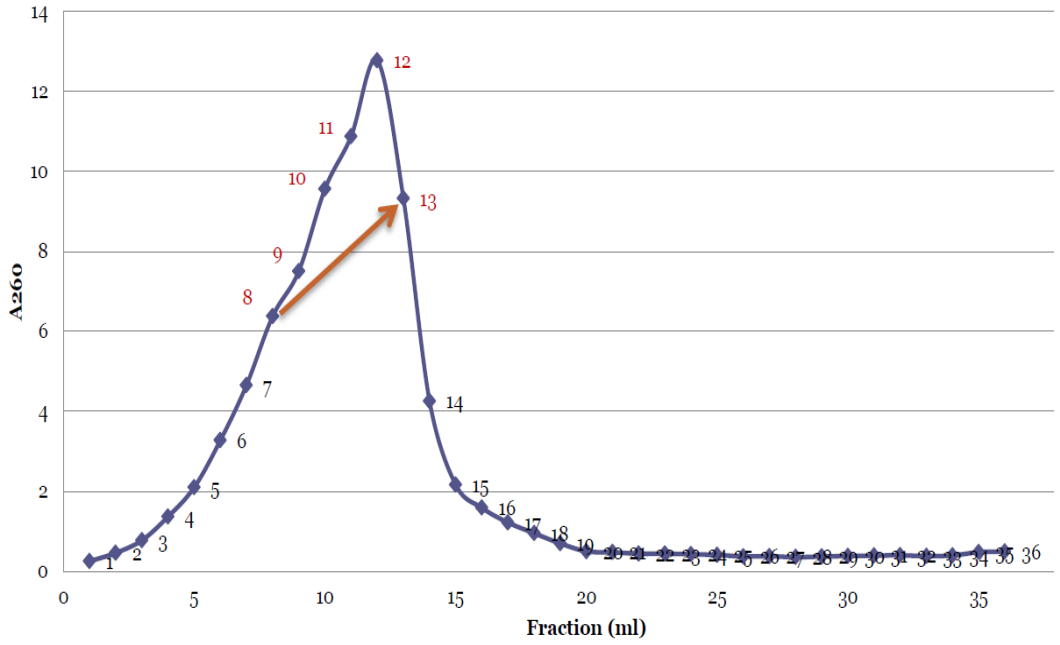

Figure 24. Obtained fractions of S. cerevisiae ΔStm1 80S ribosome after 10-30% sucrose gradient centrifugation. The peak fractions, corresponding to 80S ribosome, were pooled for crystallization experiments (labelled red).

Results

Ribosome characterization:

Since ribosomes with Stm1 protein were previously proven to be suitable for crystallography studies, they were used as a control for a quality check for ΔStm1 ribosome sample.

1% agarose gel for ribosome subunit test

This method is a simplest test for homogeneity of ribosome subunits. Subunits are moving in the agarose gel, as RNA-protein complexes containing all ribosome proteins on ribosomal RNA. This test is convenient to use before and after chemical treatment in order to follow intactness of ribosome subunits.

Agarose gel electrophoresis was performed according to the standard protocol (Sambrook et al., 1989) with the following buffers.

TAE buffer x50	
Tris	24.2g
Acetic acid	5.7ml
EDTA-Na_2	1.86g
mQ	to 100ml

1% agarose in TAE x1	
Agarose	0.5 g
TAE x50	1 ml
mQ	to 50ml
Ethidium bromide (10mg/ml)	2.5 µl

Sample buffer:	
TAE x50	20 µl
5%	50 µl
Bromophenol	
50% glycerol	0.5 ml
mQ	0.43 ml

Ribosome samples were loaded directly on the gel. The gel has demonstrated the intactness of both subunits (Figure 25), subunit size of delta Stm1 ribosomes are comparable to the subunit size of plus Stm1 ribosomes.

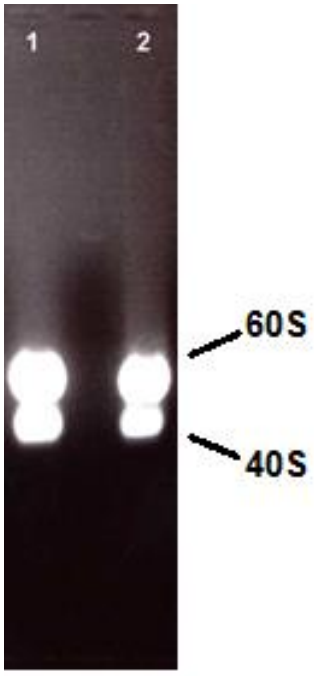

Figure 25. 1% agarose gel separating S. cerevisiae 80S ribosome on two subunits 60S and 40S. 1 – ΔStm1 ribosome sample, 2 – ribosome sample containing Stm1 protein.

SDS-PAGE (sodium dodecyl sulfate–polyacrylamide gel electrophoresis)

SDS PAGE separates proteins in denaturating conditions according their molecular weight. Ribosome samples from Delta Stm1 yeast strain JD1370 and JD1370 strain with Stm1.

The standard Laemmli method (Laemmli, 1970) with slight modifications was used. The working gel was prepared with 15% acrylamide, while concentrating gel had only 4.5%. Ribosome samples were incubated with sample buffer for 10 minutes at 60^{o}C before applying on the gel. The gel was stained in Coomassie Brilliant Blue R-250 according to standard protocols.

The gel demonstrated purity of both ribosomal samples with no contaminations by high molecular weight proteins. Except for Stm1 band, two samples had identical band pattern indicating comparable quality of the sample (Figure 26).

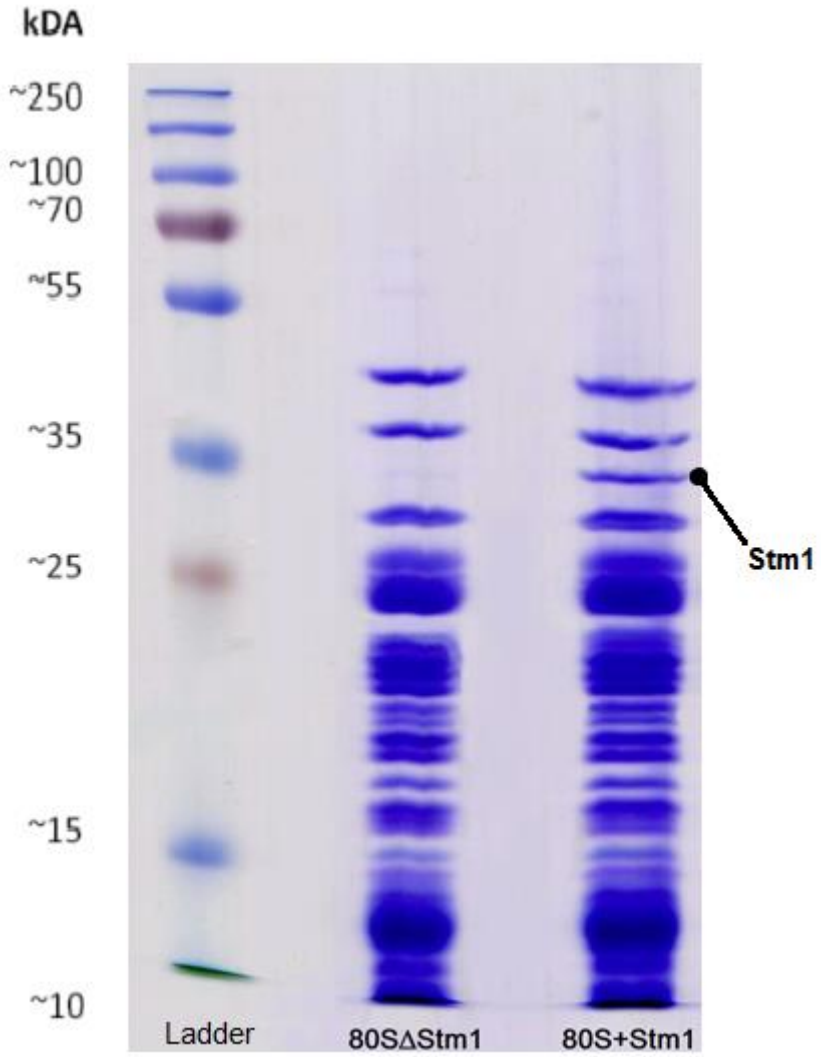

Figure 26. 15% SDS-gel electrophoretic analysis of the protein content of the S. cerevisiae 80S ribosome samples purified from strain JD1370-ΔStm1 and JD1370. The Stm1 band is indicated for the 80S+Stm1 ribosomes.

rRNA extraction from the ribosomes.

This is a fine test for the quality of ribosomal RNAs, showing the level of RNA degradation in ribosomes (Figure 27).

200 µg of *S. cerevisiae* 80S ribosomes were mixed with 4 µl 10% SDS, 1 µl 0.2M EDTA-Na2 and 32 µl of mQ, and incubated for 10 min at 37oC. After adding 40 µl of phenol the mixture was vortexed for 2 minutes and centrifuged at 12000 rpm on Heraeus pico 17 centrifuge for 3 minutes. 250 µl of 100% diethyl ether were added and vortex for 2 minutes. The ether phase was

discarded after a short spinning on a centrifuge. The tube was left open for 10 min to let diethyl ether leftovers to evaporate. For one volume of obtained RNA 3 volumes of cold 100% EtOH and 1/10 volume of 3M NaAc pH 5.2 were added to incubate for 3 hours at –20oC. After 12000 rpm centrifugation for 5-7 minutes RNA pellet was washed with 70% EtOH and dried on the air for 15-20 minutes at room temperature. Finally, RNA was dissolved in water to required concentration.

100 ml of 4% polyacrylamide gel electrophoresis containing 4 % AA/bisAA 19:1, 10 ml TBE x10, 48g urea and milli Q up to 100 ml. 1/100 of 10 % PSA and 1/1000 of 100% TEMED was added right before gel formation. TBE was used as an electrode buffer.

Loading buffer containing 20 µl 5 % bromophenol blue, 20 µl 5% xylene cyanol and 960 µl formamide was mixed in a ratio 3:1 with a sample and heated to 90^{o}C for 2 minutes with fast cooldown on ice for 2 minutes.

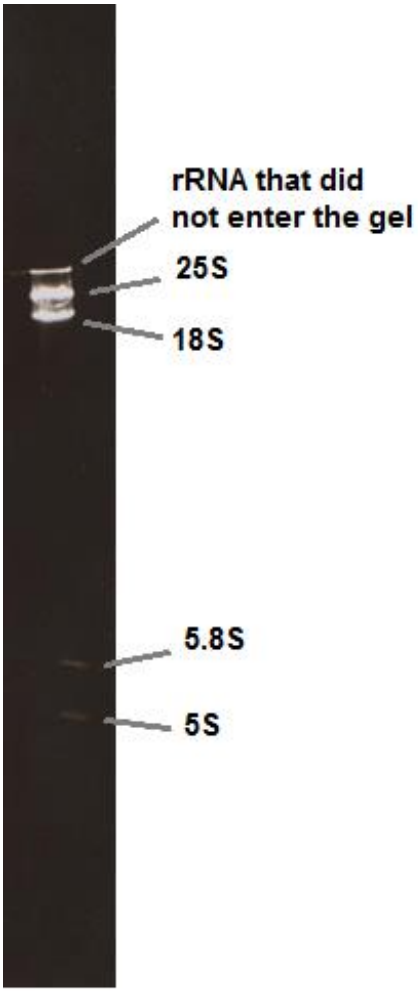

Figure 27. 4% PAGE of yeast 80SΔStm1 ribosomal RNA. 25S – 3392 nucleotides, 18S – 1798 nucleotides, 5.8S – 158 nucleotides, 5S – 121 nucleotides

The gel demonstrated that all rRNAs from the sample were separated and intact, with no signs of degradation or contamination.

Analytical ultra-centrifugation.

Analytical ultracentrifugation allows quantitative analysis of macromolecules in solution. As the sample is being centrifuged, the components separate out into layers forming boundaries due to movement of particles. Sedimentation is observed (measuring absorbance/fluorescence) in real time and used to calculate the Svedberg's coefficient (S) for the molecule. Sedimentation coefficient values, in turn, depend on the size, shape and interactions of macromolecules in solution. Experiments were conducted using Beckman Coulter Proteome Lab XL-I analytical ultracentrifuge with the 8-hole Beckman An-50Ti rotor at 4°C.

For this experiment three samples of ribosomes were used. One of 80S ribosomes with Stm1 protein as a control (Figure 28 (A)) and two samples of 80S ribosomes without Stm1 protein (Figure 28 (B-C)). Before analytical ultra-centrifugation one of the delta Stm1 ribosome samples was incubated for 1 hour at 30^{o}C and left at 4^{o}C for 20 hours (Figure 28 (C)), in order to verify that ribosomes do not dissociate rapidly in the absence of Stm1 protein in these conditions. The rest two samples were thawed not long before analysis and all samples were diluted to 1.0 OD_{260}/ml in buffer G.

Prepared samples (400 µl) were loaded into quartz cuvettes of the centrifuge tube. Additional cuvette was filled with 410 µl of buffer G. Sedimentation at 16000 rpm was monitored by absorbance at 280 nm and 260 nm with scans made at 4 min intervals. The solution density and viscosity for re-suspension buffer were calculated using SEDNTERP software. Data were analysed using a c(s) model in SEDFIT.

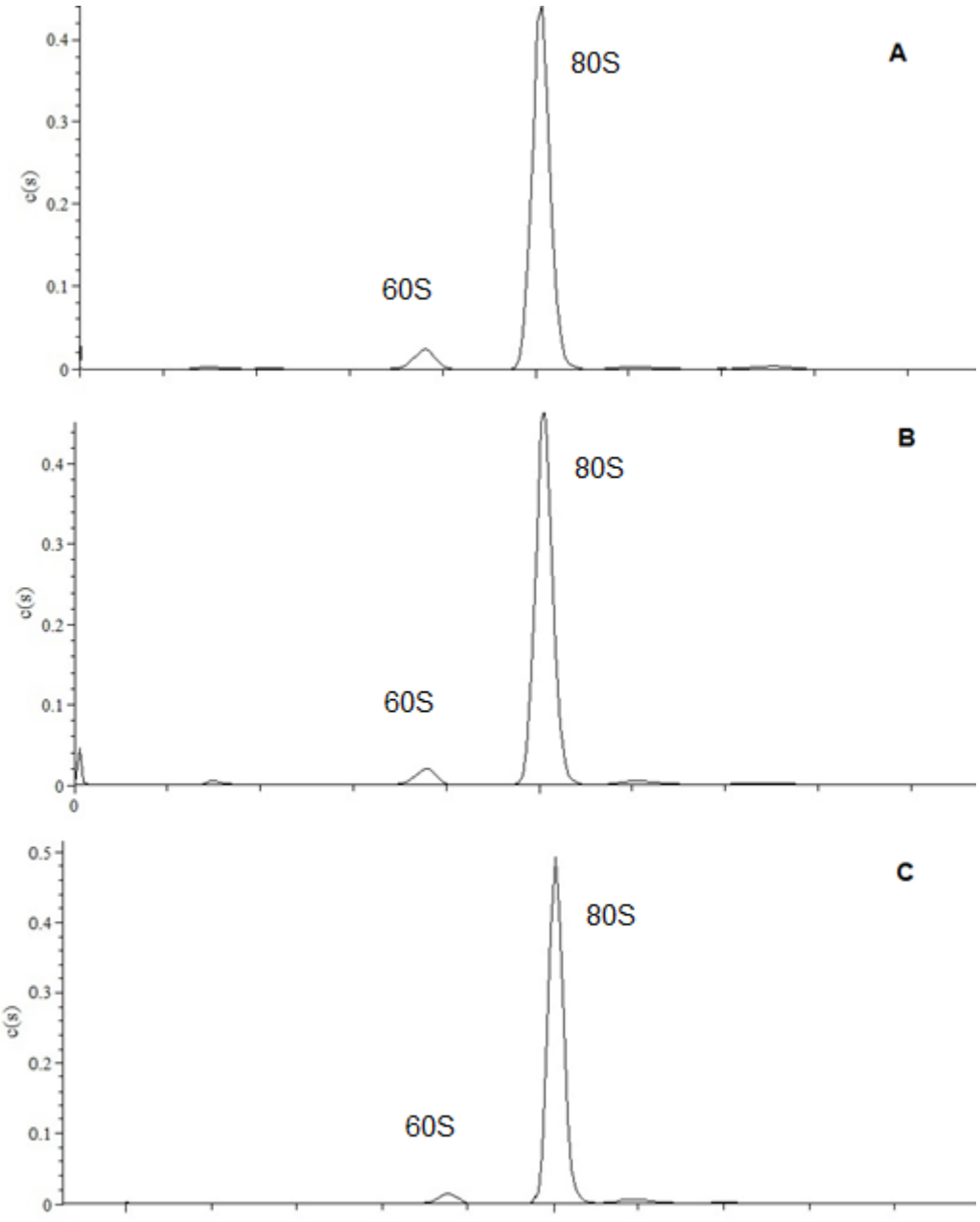

Figure 28. Sedimentation profile of S. cerevisiae 80S ribosomes with Stm1 (A), without Stm1 (B) and preliminary incubated without Stm1 (C). Details are in the main text.

The analysis demonstrated all samples remained in major part in 80S form with only a minor contamination of 60S. The incubated sample did not show any signs of dissociation.

Overview of X-ray crystallography technique.

X ray crystallography is one of the main techniques in structural biology. Currently, total number of molecules in Protein Data Base solved by X-ray crystallography is around 130000. The first protein structure solved using this technique was in the late 1950s. Since then it has been maturing and advancing, with more and more people getting involved. Given the vast amount of information molecular structures can bring and how it can extend our understanding of living organisms, a field of structural biology emerged. The discovery of DNA structure by Francis Crick and James Watson is one of the brightest examples that eventually led to the birth of molecular biology.

X-ray crystallography relies on crystals and is used for determining their atomic and molecular structure. Incoming X-ray beam on the crystal is diffracted into many specific directions. The diffraction is registered on the detector allowing us to measure angles and intensities. Using special software three-dimensional picture of the electrons density of substance building the crystal can be produced. High resolution density maps allow scientists to unambiguously build the structure of the compounds or molecules of study.

Crystal is a highly ordered microscopic structure, forming a lattice that extends in all directions. Crystallization of biological material can be a challenging task depending on the nature of the molecule. In our field proteins are the common subject for crystallization. The more ordered and still the protein is the more likely it is to crystallize. Symmetrical molecules tend to crystallize easier. In order to make solved matter to crystallize it is necessary to bring it to the supersaturated state, where the protein tend to shift into other aggregation state and if proper conditions are granted it will crystallize. There are many parameters (temperature, pH, concentration of the sample and salt, polyamines) that effect protein solubility and there could be exploited for crystallization screening. And it is practically impossible to predict crystallization conditions required for a certain protein. Therefore, in general protein crystallization is a systematic screening by changing concentrations or different compounds (precipitant, salt, buffer etc) for conditions that yield optimal crystals for diffraction experiment. There are number of commercially available crystallization screens developed to facilitate a comprehensive search, which are based on successful proteins crystallization conditions found in the past.

The crystallization experiment is designed to drive initial soluble protein conditions into the supersaturated one, which could be achieved by increasing the concentrations of the sample and/or precipitant using one of the crystallization methods: vapor-diffusion, batch or liquid-diffusion. Simplistically crystallization experiment can be described as following. The protein sample is mixed with a crystallization solution containing precipitant, reducing protein solubility and shifting it to the supersaturation zone (Figure 29). In supersaturation zone maintaining solubilized state is energetically unfavorable therefore proteins interact with each other and form nucleus that serve as a growth point for crystals. Due to incorporation of proteins from the solution into the crystals the concentration reduces and moves to metastable zone, where the crystal growth continues. In vapor diffusion experiments concentrations are maintained in metastable zone through water diffusion from the drop to reservoir that continues until equilibrium state is reached.

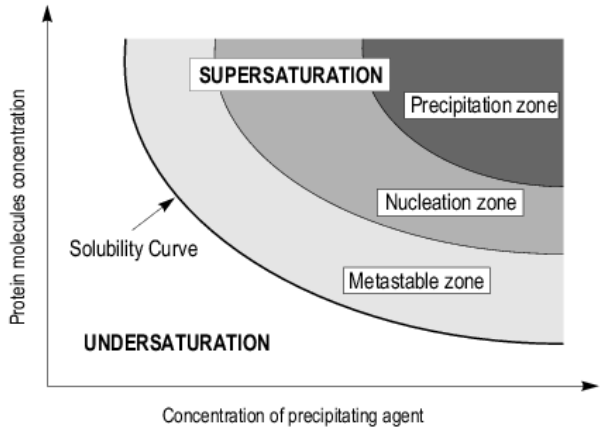

Figure 29. Schematic phase diagram of protein crystallization

Since the majorly used technique in the current study was vapor diffusion, it will be reviewed. Vapor diffusion, the most commonly used method, is performed in a special crystallization plates that are design either for sitting or hanging drops (Figure 30). Regardless of the plate geometry the idea is to slowly dehydrate a drop of protein solution preliminary mixed with a precipitant solution (usually in 1:1 ratio) by exposing it to a reservoir in a hermetic sealed well. The same precipitant solution is used as a reservoir but since the concentration of precipitant is higher it dehydrates the experiment drop. Water diffuses to the reservoir until it equilibrates, increasing the precipitant and protein concentrations in drop and driving it into supersaturated state. And in case if proper precipitant solution is used crystal growth will occur.

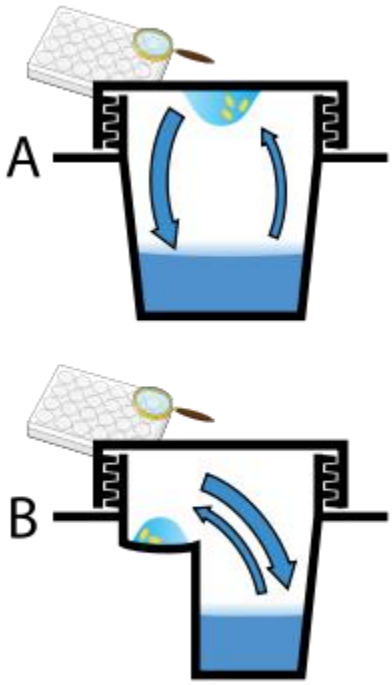

Figure 30. Vapor diffusion experiment in A) hanging drop and B) sitting drop well.

Crystallization of eukaryotic ribosome is a challenging task considering that it is an asymmetric macromolecule of a large size (3.5 MDa for yeast) and high flexibility. It is known that 80S ribosomes reside in a dynamic state with a rotation of two ribosome subunits with respect to each other (ratcheting), thus making the process of ordering and packing into the crystal very sophisticated. Therefore for quite a long time crystallization of 80S ribosome was considered almost impossible, until the determination of the first atomic structure of the yeast 80S ribosome (Ben-Shem et al., 2010) was solved. However, as it was mentioned above in material and methods the obtained ribosome was arrested by the Stm1 protein bound to both subunits and restricting intersubunit movement.

Formation of functional S.cerevisiae ΔStm1 80S ribosome complex with messenger RNA and tRNAs

Functional S.cerevisiae ΔStm1 80S ribosome complex with messenger RNA and tRNAs was formed in buffer G with 4 mM $Mg(Ac)_2$. For formation of the complex, 30 nucleotide long mRNA (5' – AGAAAAGAAAAGUUUUUUUUUUUUUUUUU – 3') was used, where the molar ratio for 80S ribosome, mRNA and yeast $tRNA^{Phe}$ was 1:3:5 respectively. First, 95 µl S.cerevisiae

ΔStm1 80S ribosomes (1.86 mkM) were pre-incubated for 10 minutes at 30°C, then mRNA (5.7 mkM) was added and incubation continued for 10 more minutes. Then preliminary annealed tRNAphe (9 mkM) for 2 minutes at 55°C with slow cooldown at room temperature (RT) was added to ribosomal mixture and left to incubate for 30 minutes at 30°C to finish complex formation. Two batches of complex were used in presence of 2.1 mM Deoxy big CHAP detergent and without it. The mixture was cooled down in at 4°C for 15 minutes before crystallizing. (We obtained the mRNA sample from Dharmacon, Inc , and tRNAPhe from brewer's yeast from Sigma.)

Screening for crystallization conditions

The significant difficulties in crystallization of the ribosomes involve an absolute lack of commercial screens, which is in general developed for crystallization of small proteins. Therefore, search for a new crystal form of such big macromolecule as eukaryotic 80S ribosome with MW 3.3 MDa presents a challenging and time-consuming process that requires innovative ideas and big amount of the sample material.

Reservoirs for screening were prepared on a Freedom EVO® robotic system. 200 nl of reservoir was mixed using mosquito® crystallization system with 200 nl of prepared ribosome complex on the MRC 96 well sitting drop plate, 2 drops per well. The plates were stored at 4°C in automated imaging system ROCK IMAGER®.

In parallel to crystallization trials using mosquito® robotic system manual screening was performed in a big geometry 24 well VDX plates for a hanging drop vapor diffusion experiments. 2.5 µl of a sample was mixed with 2.5 µl of reservoir solution on a siliconized glass cover slides and was hermetically sealed with 400 µl reservoir. Crystallization procedure was performed in the cold room at 4°C.

Similarly, to commercial screens for proteins, published crystallization conditions prepared manually that yielded ribosomal crystals were used for initial screening trials with PEG 20k as a main precipitant. Unfortunately, they did not result in any positive hits. Then it was decided to make a screen based on the crystallization conditions of 80S ribosome with Stm1 with the following composition: PEG 20k in a range 3.5% - 9%, glycerol in a range 2.5% – 20%, KSCN in a range 100 – 300 mM, 4 mM MgAc2, 100 mM Tris-Ac pH 7.0 and 5 mM spermidine. Despite the fact that this screening did not lead to any crystal formation, there were some interesting drops with shaped formations (Figure 31).

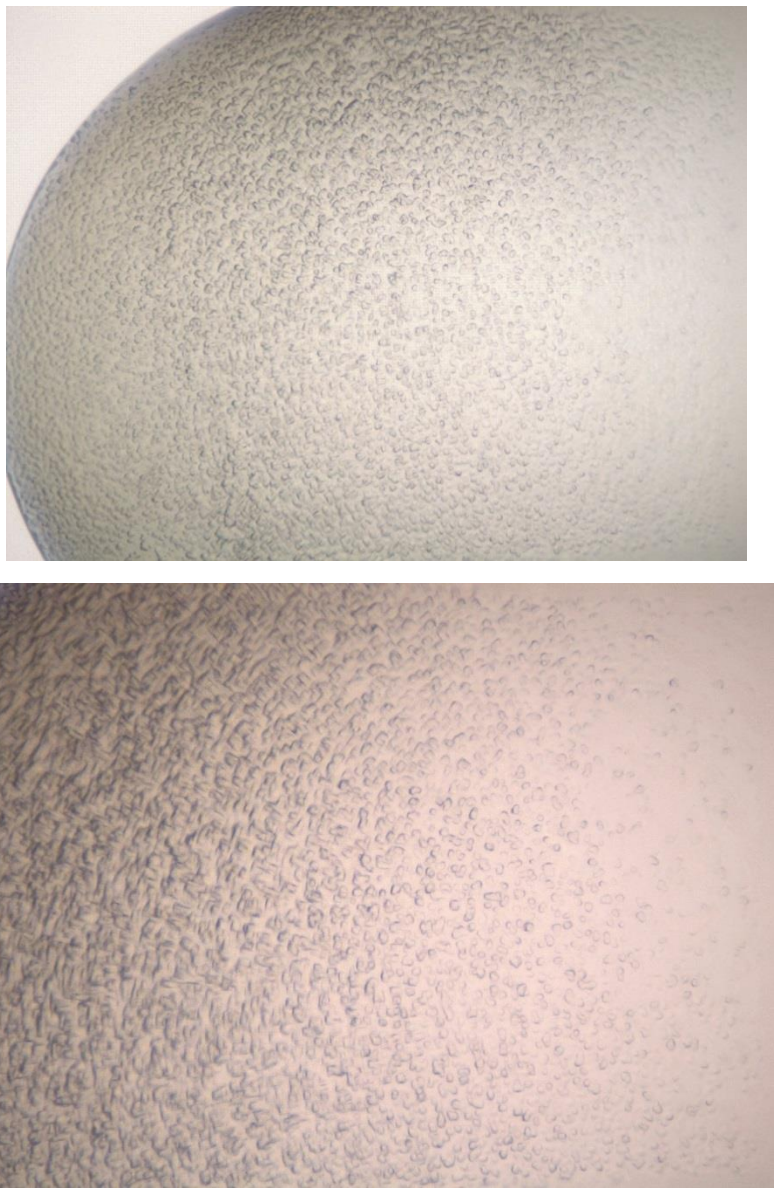

Figure 31. Crystallization drops of the samples of functional yeast 80S ribosome complexes with mRNA and tRNAs based on conditions, developed for the yeast vacant 80S ribosome with Stm1 (Ben Shem et al., 2011).

Those conditions were investigated further but with an attempt to reduce conformational flexibility which presents an entropic barrier to crystallization. One of the compounds that can have this effect on ribosome is polyamines. Polyamines are small positively charged compounds that bind to ribosome and stabilize negatively charged rRNA. spermine, spermidine and putrescine were used in the concentration range from 2 to 15 mM.

During search of the crystallization conditions emphasis was made on glycerol alongside with polyamines. There has been intensive studies of glycerol as a stabilizing agent (Sousa, 1995;

Vera et al., 2011) showing that proteins in solutions containing glycerol tend to reduce conformational flexibility and its application in crystallizing flexible proteins. The fact that glycerol concentration in crystallization conditions for vacant 80S ribosome was equivalent to 20% (Ben-Shem et al., 2011) indicated that it has a positive effect on eukaryotic ribosome. Therefore, significant amount of screens were made in the presence of glycerol in a range from 5% to 35% concentration.

The other approach was to restrict inter-subunit movement using specific ribosome targeting inhibitors. Mainly the ones that are known to inhibit ribosome translocation: viomycin, geneticin (G418) and hygromycin B.

Anti-tuberculosis antibiotic viomycin possesses high affinity to 70S ribosome. It was shown that viomycin binds to the well conserved intersubunit bridge B2a formed by the interactions of Helix 69 of the 23S rRNA and helix 44 of the 16S rRNA (Figure 32) (Stanley et al., 2010). It also effects on conformation of conserved nucleotides in the decoding center increasing affinity of tRNA to the A-site (Peske et al., 2004) and promotes the back translocation of the complex of tRNA with mRNA on the ribosome (Szaflarski et al., 2008). Due to low affinity to the 80S ribosome relatively high concentrations 0.7 – 3 mM of viomyicin were used for crystallization screening.

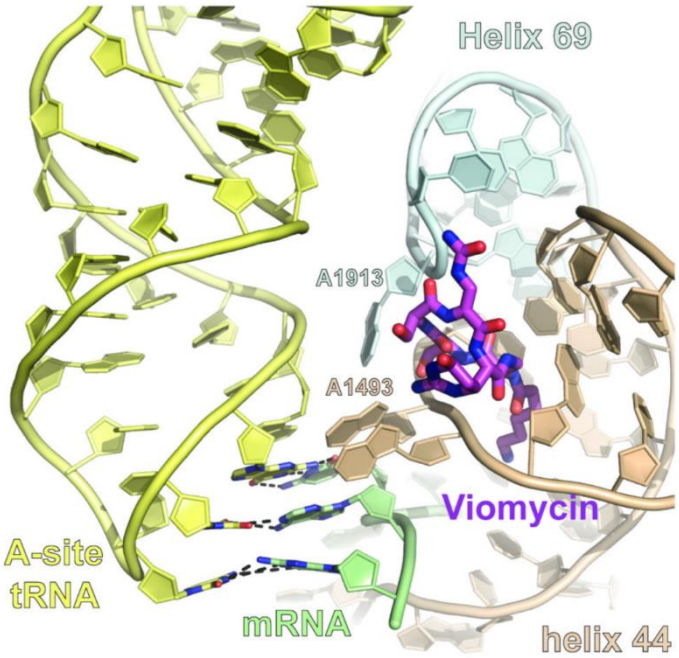

Figure 32. Viomycin bound to T. Thermophilus 70S ribosome. Adapted from (Stanley et al., 2010).

Geneticin (G418) is a representative of kanamycin subgroup of aminoglycosides with high affinity for the eukaryotic ribosome. It was shown to bind in the decoding center where it interacts with eukaryotic specific residues (Garreau de Loubresse et al., 2014) and it has a property to inhibit translocation.

Hygromycin B belongs to the aminoglycoside family of inhibitors and is known to bind both 70S and 80S ribosomes with high affinity. It was demonstrated bound in the decoding center of *E. coli* ribosome, where it could cause steric block to the movement of tRNAs between the A and P sites (Borovinskaya et al., 2008). Moreover, Hygromycin B binds to the ribosome in a place to contact the backbone of the P-site mRNA codon. Therefore, it was suggested that hygromycin B inhibits translocation by confining the movement of mRNA and by blocking the tRNA path between the A and P sites.

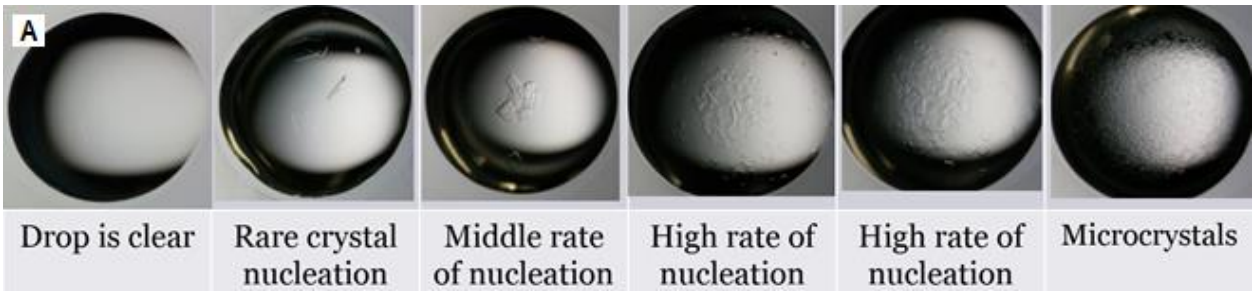

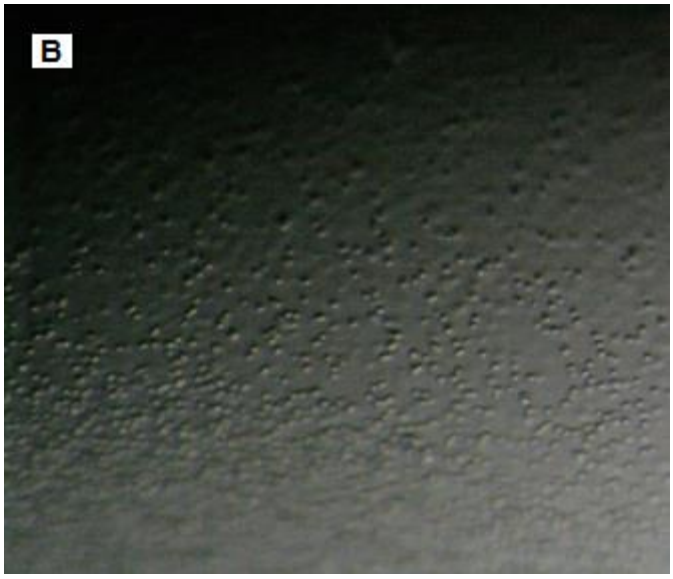

Figure 33. The effect of precipitant concentration on crystallization of 80S Stm1 ribosomes (Ben Shem et al., 2011). A) From left to right – 3.6% to 4.7% PEG 20k respectively; B) appearance of precipitant in a drop with 6% PEG 20k.

During crystal screening quite often, unless crystallization conditions are found, the sample precipitate directly. Therefore, with increasing concentration of the precipitant agent the appearance of the drop will change from empty to precipitant. In order to have some additional clues for the annotation of the droplets obtained during screening it was decided to investigate the appearance of Stm1 80S ribosome crystallization conditions in the low concentration of precipitant before the crystals appear to the high concentration when there is precipitate only. Gradually increasing the precipitant concentration the appearance of drops was changing from rare crystals to microcrystals and precipitate (Figure 33). The obtained result was helping in the estimation of new derived conditions.

Applying the all above mentioned approaches the new screening trials were made. Initial screening with inhibitors demonstrate that plates containing hygromycin B looked relatively better than the ones with geneticin or viomycin. After screening of dozens of different conditions two of them had the droplets with crystalline sample.

The reservoir composition of the first crystallization hit consisted of 4% - 6.2% PEG 20k, 100 mM BisTris Acetate pH 7.0, 20% glycerol, 3 mM $Mg(Ac)_2$, 4 mM spermidine, 100 mM KSCN, 100 mM KAc pH 7.2. Crystallization was performed on 24 well VDX hanging drop plates. After pretranslocation complex formation 0.5 mM hygromycin B was added. The little formations in the droplet around 10 µm long resembled microcrystals (Figure 34)

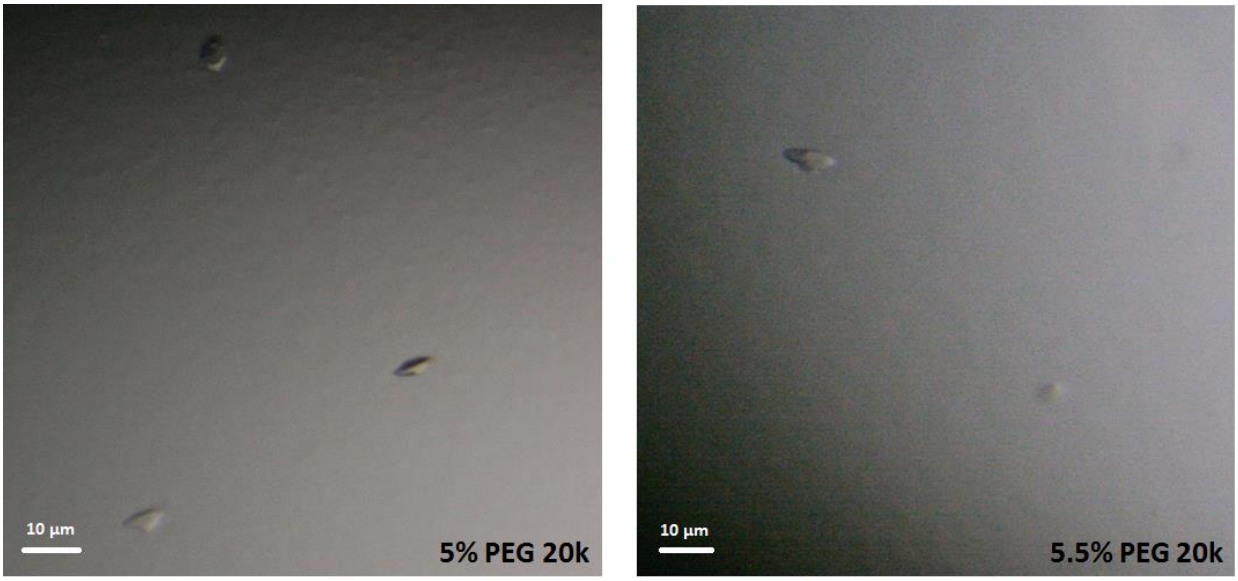

Figure 34. Microcrystals in the first hit crystallization conditions: 5-5.5% PEG 20k, 100 mM Bis-Tris Acetate pH 7.0, 20% glycerol, 3 mM $Mg(Ac)_2$, 4 mM spermidine, 100 mM KSCN, 100 mM KOAc pH 7.2

There was also strong similarity of the precipitate with the one from vacant 80S Stm1 ribosome (Figure 35).

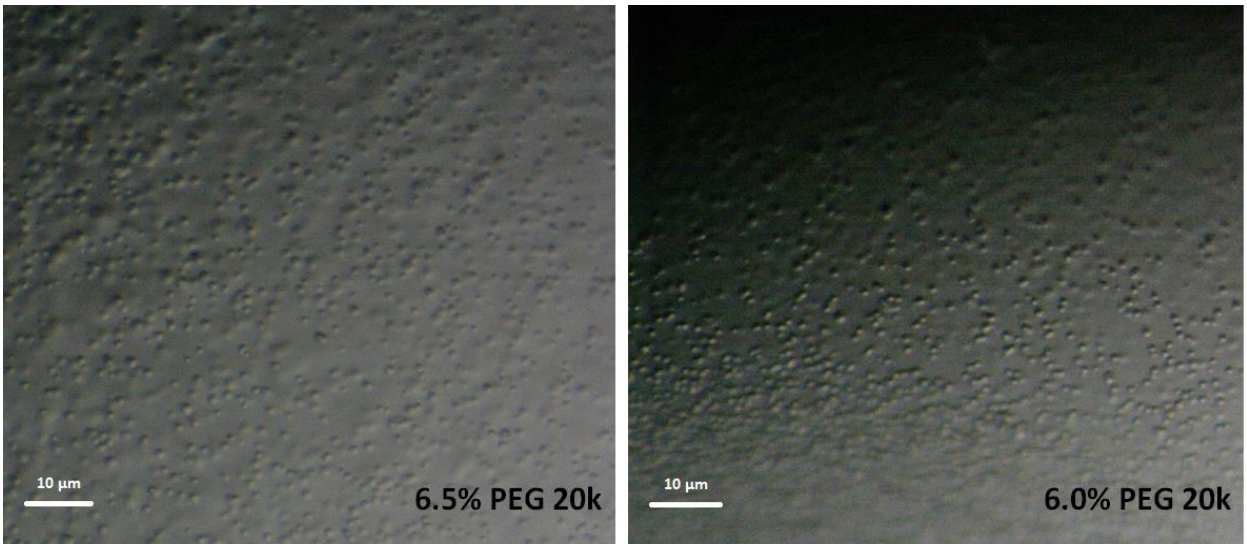

Figure 35. Precipitate comparison of new obtained conditions of pretranslocation complex on the left and vacant 80S ribosome on the right.

In parallel to this plate another one was made with the following conditions 3.5% - 9% PEG 20k, 100 mM Tris-Ac pH 7.0, 30% Glycerol, 4 mM $Mg(Ac)_2$, 5 mM spermidine and 100 mM KSCN in 24 well VDX hanging drop plate and 0.5 mM of hygromycin B to stabilize functional yeast 80S ribosome complexes with mRNA and tRNAs. This condition, which are mostly based on the one from (Ben-Shem et al., 2011), resulted in the second crystallization hit (Figure 36). The length of the obtained crystals was in the range from 15 to 20 µm. Crystals in comparison with the ones from the first hit had larger body and more nucleation points. Therefore, the focus was made to the second crystallization hit.

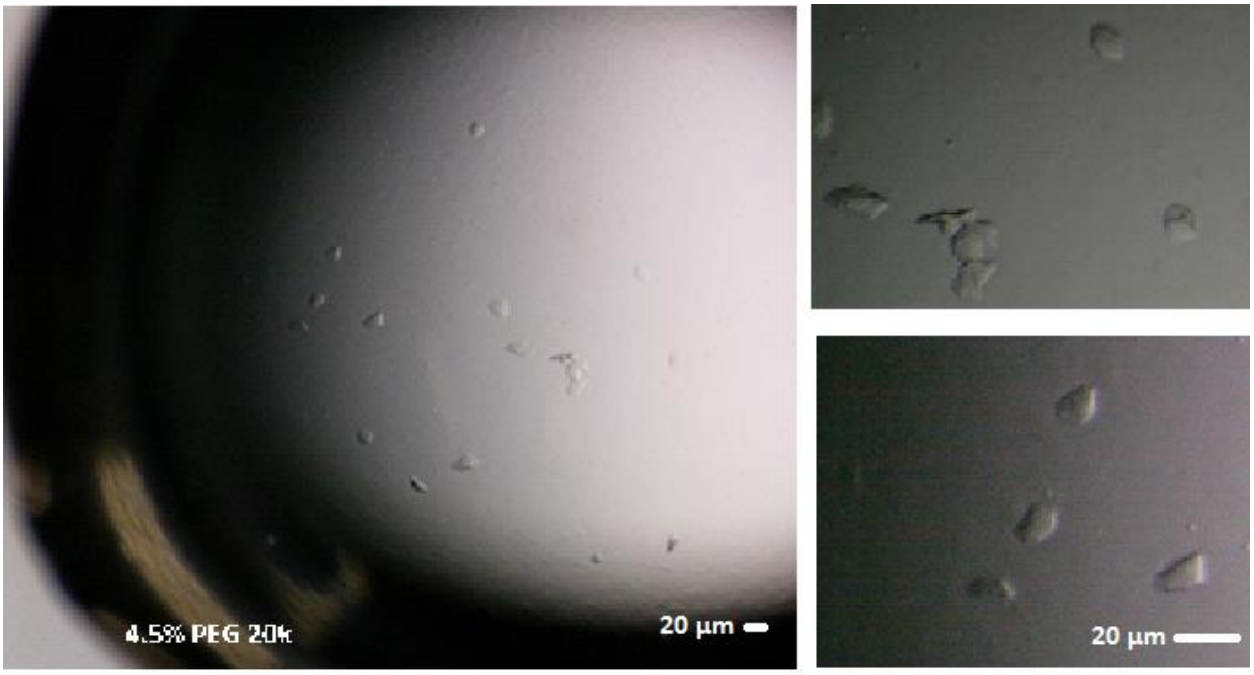

Figure 36. The look of the droplet of the second found crystallization conditions:4.5% PEG 20k, 100 mM Tris Acetate pH 7.0, 30% Glycerol, 4 mM $Mg(Ac)_2$, 5 mM spermidine and 100 mM KSCN.

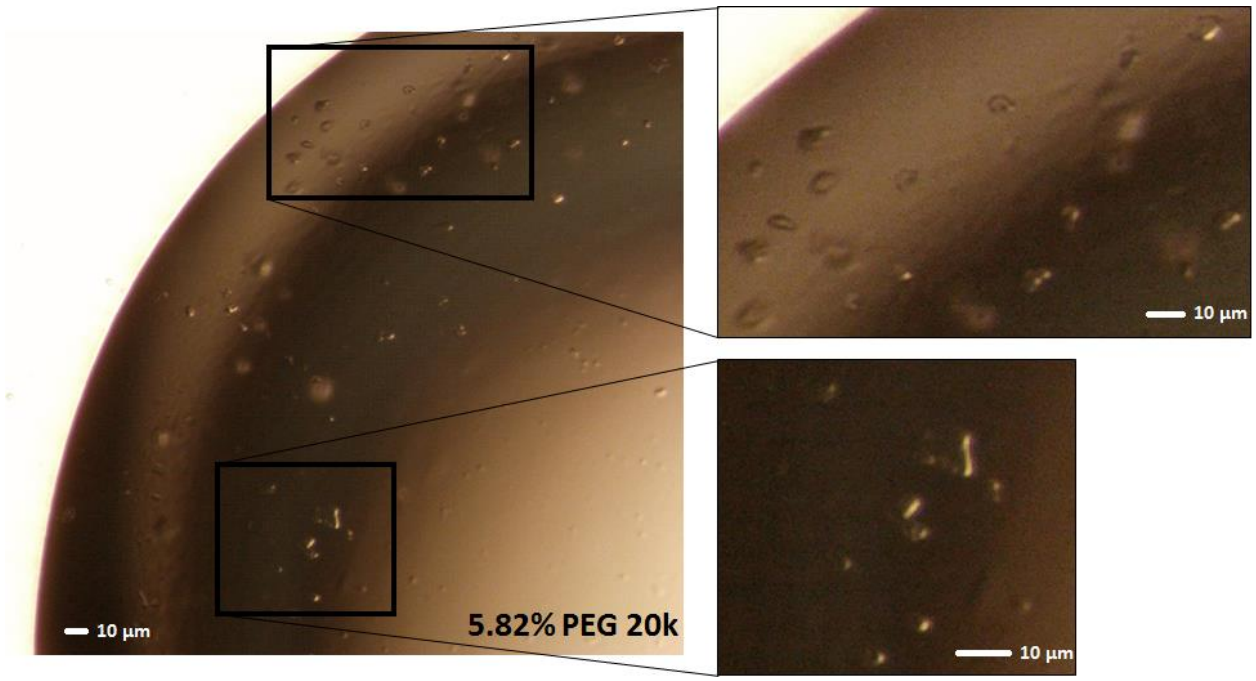

Figure 37. The look of the droplet obtained by reproduction of the second crystallization conditions: 5.8% PEG 20K, 100 mM Tris-Ac pH 7.0, 30% Glycerol, 4 mM $Mg(Ac)_2$, 5 mM spermidine and 100 mM KSCN.

The attempt to reproduce crystal growth was successful; however, the obtained crystals had smaller body around 5-10 µm (Figure 37).

Inspection of the droplet revealed that the surface was covered with a crust. It was possibly caused by an elevated viscosity of the droplet due to high concentrations of glycerol and relatively fast diffusion process. Droplets with the same composition but with 20% glycerol did not form crust surface. The rate of water evaporation from the surface is faster than it manages to diffuse evenly inside the droplet, which leads to decreased concentration of water on the surface and crust formation (Figure 38). This could be one of the reason why crystals did not grow larger, as the crust impairs vapour diffusion experiment.

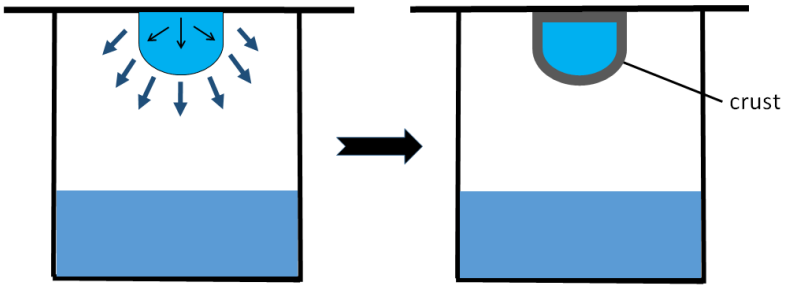

Figure 38. Scheme of the hanging drop diffusion experiment. Arrows show water diffusion, details are provided in the main text.

There are several ways that can be applied to overcome this problem. One of which is to decrease diffusion rate either by diluting reservoir or changing the plate to smaller geometry with less reservoir surface exposure could equilibrate water diffusion inside and from the droplet. The other option is to use microbatch method. In microbatch crystallization the droplet is sealed under a layer of oil. Varying the oil allows to adjust water diffusion rate through it. Generally, a mineral oil of branched paraffins in the C_{20}+ range or 1:1 mixture of silicon and paraffin oil are used.

At this stage of the project, after one year of work, following the decision of my supervisor Dr. Yusupova, I have changed the direction of my PhD study, and started to work on the project entitled "Accuracy of gene expression through understanding structural basis of a translation cycle on the eukaryotic ribosomes". Initially, this project of was initiated by Natalia Demeshkina, a Postdoctoral Fellow of Dr. Yusupova, who worked X-ray structural investigations of eukaryotic elongation ribosome complexes trapped at translocation state. During her staying, Natalia Demeshkina was able to obtain crystals of the complex, which contained *S. cerevisiae* ΔStm1

80S ribosome and *S. sereviceae elongation factor 2 (in the absence of messenger RNA and tRNA)*. Preliminary X-ray analysis of obtained crystals demonstrated low resolution diffraction limit (about 9 A resolution), and showed very low occupancy of elongation factor 2 in the 80s ribosome.

Nevertheless, it was the first step towards to development of new crystal forms of eukaryotic 80S ribosomal functional complexes.

Discussion

The main objective of the project 'Functional *S. cerevisiae* 80S ribosome complexes with mRNA and tRNAs studied by X-ray analysis'' is to provide structural aspect of translation mechanism in eukaryotes in a similar way as it has been done for bacteria (Ramakrishnan, 2002; Demeshkina et al., 2012; Rozov et al., 2016b). The ultimate goal was to solve high-resoultion structure of *S. cerevisiae* 80S ribosome complex with mRNA and with tRNAs bound to three A-, P- and E-site. The obtained structure would present the first structural insight of naturaly modified tRNA and mRNA interactions with 80S ribosome, enable studying eukaryotic decoding mechanism and provide a functional model for targeted drug design.

The advancement in determination of the first atomic structure of the eukarytoic entire *S. cerevisiae* 80S ribosome in 2011 (Ben-Shem et al., 2011) opened new prospects for investigation of complex protein biosynthesis in eukaryotes with high resolution. However, X-ray structure determination of 80S ribosome is an extremely challenging task that requires the unprecedented knowledge of the ribosome as a biochemical object and a unique crystallographic expertise. This explains the lack of other crystal structures of eukaryotic entire 80S ribosome either in vacant state or in complex with functional ligands. Nowadays cryogenic electron microscopy cryo-EM is the main technique used to study ribosome structures. The recently developed detectors and software allow obtaining high resolution of the ribosome especially in the less flexible regions. And many new structures of eukaryotic ribosomes were solved using cryo-EM technique. However there is still no atomic resolution structure of functional 80S ribosome complexes with mRNA and tRNAs available. The available cryo-EM reconstructions provide interesting insight of 80S ribosomes in this state, but cannot reveal precise atomic interactions of ribosome functional ligands such as mRNA and tRNAS inside the ribosome (Behrmann et al., 2015). One of the main reasons why cryo-EM structures of functional eukaryotic 80S ribosome complexes have not reached high resolution is the ribosome flexibility. The dynamic ratcheting of the small subunit relative to the large one also leads to the tRNAs shifting between A/A, P/P classical state and A/P, P/E hybrid state. The cryogenic freezing of the sample results in obtaining multiple intermediate states on the grid.

For the exactly same reason crystallization of not stalled ribosomes presents a challenging task. The dynamic intersubunit movement interferes with binding in the ordered fashion into crystal structure. Moreover higher eukaryotic organisms developed additional protein-rRNA or RNA layers on the surface of ribosomes (Melnikov et al., 2012;M Anger et al., 2013) that possess supplementary level of flexibility (Figure 1). It explains the larger number of solved crystallography

structures for bacterial ribosomes relatively to the only one high-resolution crystals structure of entire *S. cerevisiae* 80S ribosome, few crystal structures of 60S and 40S subunit from (Klinge et al., 2012) and complete absence crystal structure of the ribosomes from high eukaryotes.

Despite all the challenges the proper crystallization conditions can stabilize the flexible parts of the macromolecules, which is why it is important to consider compounds with stabilizing effect it during the crystallization trials. As it was demonstrated in the current project screening with stabilizing agents yielded two crystallization conditions. Several approaches were implemented in order to reduce macromolecular flexibility. From special inhibitors of translocation that tend to bind in a proximity to B2a intersubunit bridge reducing ratcheting motions, to the viscous compound like glycerol that is known to conserve molecular conformations.

The result of the project presents the accomplished the first step of crystallography studies – finding the first hits of crystallization conditions. Giving limited amount of time and the complexity of the object of study the result, despite it is still a long way until obtaining the complete structure, nevertheless presents considerable progress demonstrating that based on proper strategy even the large and highly flexible macromolecular complexes like yeast ribosomes are still possible to crystallize. However significant amount of work is still needed to be done. The obtained crystals are relatively small in size and optimization of crystallization conditions is required to make them grow larger. Even after obtaining a large size they might not diffract at atomic resolution. Crystals should be already cryoprotected considering high concentration of glycerol in the reservoir, however additional crystal treatment might be needed to reduce the water content to make them firmer and improve diffraction limit. The search for the post-crystallization treatment might be even more complicated than the search for crystallization conditions. Successful completing all the remaining steps most likely will require additional time of research.

AMINOGLYCOSIDE INTERACTIONS AND IMPACTS ON THE EUKARYOTIC RIBOSOME

Project outline

The project that I was working on together with one of the Postdocs of our laboratory Prokhorova Irina who had initialized and led the project. I was participating at the most stages of the study including 80S+stm1 ribosome purification, crystallization, crystal treatment and crystal screening and data collection at the synchrotron.

The project was devoted for an investigation of a structural rearrangements that aminoglycosides induce in the *S. cerevisiae* 80S ribosome and how they impact on translation. Aminoglycosides are known to bind with the ribosome and inhibit translation. The focus was made on four aminoglycosides: Paromomycin, Geneticin (G418), Gentamicin, TC007. It was demonstrated before that they can promote read-through of premature termination codons (PreTC) during translation and for this reason are considered as potential therapies for PreTC-associated human diseases. Thus it was the scope of the study.

Previously established crystal form of 80S yeast ribosomes was exploited for the current project (Ben-Shem et al., 2010). However, necessary modifications were made for crystal treatment procedure in order to provide more natural conditions for aminoglycosides to bind to ribosome avoiding artefacts. Osmium hexamine, which is normally present in initial procedure, binds rRNA, including the aminoglycoside-binding site (Ben-Shem et al., 2011). Obtained structural data were complemented with single molecule FRET analysis from our collaborators. The performed research culminated into publication article (Prokhorova et al., 2017) demonstrating molecular basis of the impact aminoglycosides make by binding to the eukaryotic ribosome, supplemented by dynamics rearrangements of the pretranslocation complex.

Materials and methods

Ribosome purification from JD1370 yeast strain

The first *Saccharomyces cerevisiae* engineered strain JD1370 was provided by Jonathan Dinman (University of Maryland, USA) (Ben-Shem et al., 2010). The L-A virus is a double-stranded RNA virus that infects and replicates in the yeast S. cerevisiae. In order to avoid

observed contaminations by viral particles of the ribosome preparation, the L-A virus was depleted from this strain. In addition, the JD1370 strain harbors deletions of key proteases and RNAses that are liberated upon cell lysis: PEP4 vacuolar protease and NUC1 mitochondrial nuclease.

Purification and crystallization procedures follow the protocols developed previously (Ben-Shem et al., 2010). The ribosome purification protocol was described in details in the material and methods part of the first research project.

Crystallization of ribosomes bound with Stm1 protein

For crystallization, ribosome sample is prepared as following: 5 mg/mL ribosomes in buffer G, 2.5 mM Hepes-K pH 7.5, 2.5 mM NH4Cl, 3.33 mM $Mg(Ac)_2$, 1.6 mM DTT, 0.055 mM EDTA, 2.8 mM Deoxy Big Chap, 40 mM KOAc, 5.5 mM NH4OAc, 5.5 mM Tris-Acetate pH 7.0. The ribosome solution is incubated at 30°C for 10 min and left to cool down in the cold room before crystallization for 30 minutes. Ribosomes are crystallized in 24-well VDX hanging drop plates (Hampton Research®) with a 400 µL reservoir solution (100 mM Tris-Acetate pH 7.0, 100 mM KSCN, 3 mM $Mg(Ac)_2$, 20% glycerol, 4-4.5% w/v PEG 20,000, 5 mM spermidine), using the hanging drop method at 4°C by mixing 2-2.4 µL of ribosome solution with 1.6 µL of reservoir solution. Typically, crystals appear within 7-10 days in hermetically closed wells and reached their full size after two additional (Figure 39).

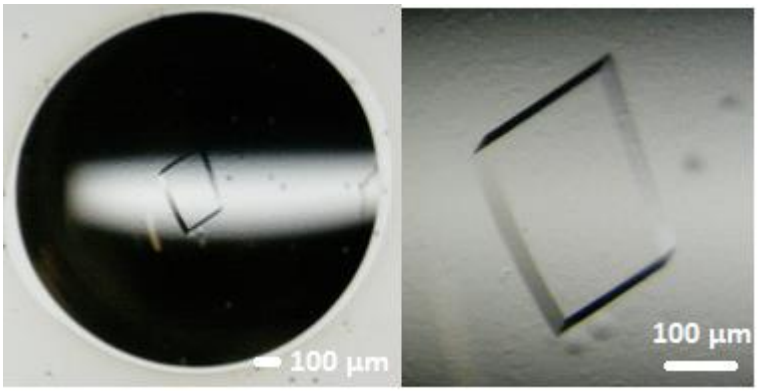

Figure 39. Crystal of S. cerevisiae 80S ribosome with Stm1 protein. Dimensions: Length = 250µm; 160 µm width; thickness ≈ 30µm

Post-crystallization treatment

Post-crystallization treatment is used to cryoprotect crystals from ice formation, make them more stable and improve diffraction. However, obtained crystals of 80S ribosome diffracted very poorly (20-30 Å) with cryoprotectant post-crystallization treatment. Therefore, treatment induced dehydration was implemented, as it is known that the reduction of the solvent content inside the crystal produces internal strengthening often leading to an improvement of diffraction. Initially crystals were treated by previously established protocol (Ben-Shem et al., A 2011), which implies addition of osmium hexamine in order to reach high resolution diffraction. It is known that osmium hexamine binds to RNA with high affinity by mimicking fully hydrated magnesium (Cate and Doudna, 1996) thus it is able to stabilize rRNA inside the ribosome. However, as was observed in the previous study (Ben-Shem et al., 2011) it competes with aminoglycosides for binding and creates artificial conformation in the decoding site (Figure 40). In order to study aminoglycoside interactions with a decoding center in a natural conformation, osmium hexamine was removed from treatment conditions, which impaired crystal diffraction to around 5 Å. To improve resolution limit empiric investigations of different modifications of previously established post-crystallization treatment were conducted. PEG 6K was replaced with one of the following PEGs 400, 1K, 2K MME, 3350, 4K or 8K.

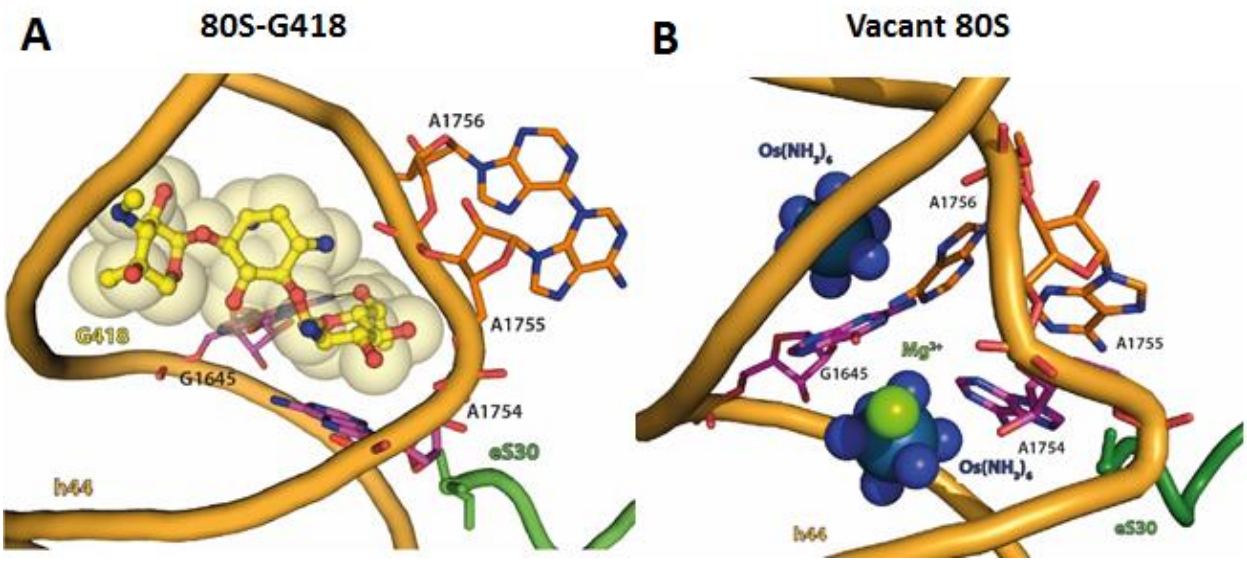

Figure 40. The decoding site of (A) 80S ribosome bound with aminoglycoside G418 (Garreau de Loubresse et al., 2014) and (B) vacant ribosome with osmium hexamine crystal treatment (Ben-Shem et al., 2011) demonstrating the common binding site.

Also, incubation time was tested in a range from 1h to 8h or incubation of the drop sealed back in the well with the reservoir for 18h. As well as different concentration of aminoglycosides. Crystals were treated and frozen in the stream of gaseous nitrogen in the laboratory and brought to the Swiss Light Synchrotron in a nitrogen dewars. Each condition was tested at the PX1 X06SA beamline headed by Takashi Tomizaki. Crystals treated with PEG 2K MME, 3350 or 4K with incubation time of 1h or 4h had the highest diffraction limit. Data was collected with a beam size around 70x70 µm focused on the detector with flux around $2x10^{11}$ ph/sek. Oscillation range was set to 0.1° and exposure time to 0.1 second.

Aminoglycoside interactions and impacts on the eukaryotic ribosome

Irina Prokhorova[a,1], Roger B. Altman[b,1], Muminjon Djumagulov[a], Jaya P. Shrestha[c], Alexandre Urzhumtsev[a,d], Angelica Ferguson[b,e], Cheng-Wei Tom Chang[c], Marat Yusupov[a,2], Scott C. Blanchard[b,e,2], and Gulnara Yusupova[a,2]

[a]Department of Integrated Structural Biology, Institut de Génétique et de Biologie Moléculaire et Cellulaire, INSERM U964, CNRS UMR7104, Université de Strasbourg, 67404 Illkirch, France; [b]Department of Physiology and Biophysics, Weill Cornell Medicine, New York, NY 10065; [c]Department of Chemistry and Biochemistry, Utah State University, Logan, UT 84322; [d]Département de Physique, Faculté des Sciences et des Technologies, Université de Lorraine, 54506 Vandoeuvre-lès-Nancy, France; and [e]Tri-Institutional PhD Training Program in Chemical Biology, Weill Cornell Medicine, Rockefeller University, Memorial Sloan-Kettering Cancer Center, New York, NY 10065

Edited by Joseph D. Puglisi, Stanford University School of Medicine, Stanford, CA, and approved November 8, 2017 (received for review September 1, 2017)

Aminoglycosides are chemically diverse, broad-spectrum antibiotics that target functional centers within the bacterial ribosome to impact all four principle stages (initiation, elongation, termination, and recycling) of the translation mechanism. The propensity of aminoglycosides to induce miscoding errors that suppress the termination of protein synthesis supports their potential as therapeutic interventions in human diseases associated with premature termination codons (PTCs). However, the sites of interaction of aminoglycosides with the eukaryotic ribosome and their modes of action in eukaryotic translation remain largely unexplored. Here, we use the combination of X-ray crystallography and single-molecule FRET analysis to reveal the interactions of distinct classes of aminoglycosides with the 80S eukaryotic ribosome. Crystal structures of the 80S ribosome in complex with paromomycin, geneticin (G418), gentamicin, and TC007, solved at 3.3- to 3.7-Å resolution, reveal multiple aminoglycoside-binding sites within the large and small subunits, wherein the 6′-hydroxyl substituent in ring I serves as a key determinant of binding to the canonical eukaryotic ribosomal decoding center. Multivalent binding interactions with the human ribosome are also evidenced through their capacity to affect large-scale conformational dynamics within the pretranslocation complex that contribute to multiple aspects of the translation mechanism. The distinct impacts of the aminoglycosides examined suggest that their chemical composition and distinct modes of interaction with the ribosome influence PTC read-through efficiency. These findings provide structural and functional insights into aminoglycoside-induced impacts on the eukaryotic ribosome and implicate pleiotropic mechanisms of action beyond decoding.

ribosome | aminoglycosides | PTC read-through | translation | protein synthesis

Aminoglycosides are broad-spectrum, bactericidal antibiotics of critical importance to the treatment of life-threatening infections. Despite their proven clinical utility, these therapeutics can lead to potential toxic side effects, including ototoxicity and nephrotoxicity, and an increased prevalence of resistance (1, 2). The most heavily employed and extensively investigated aminoglycosides contain a central 2-deoxystreptamine (2-DOS) ring. This class is comprised of both natural products (such as neomycin and paromomycin) and semisynthetic derivatives (such as dibekacin and amikacin).

The 2-DOS aminoglycosides effectively inhibit protein synthesis in bacteria by targeting the mechanisms of translation elongation, termination, and recycling (3–6). These activities have, in part, been distilled to the capacity of the 2-DOS rings to engage chemical features within the deep and narrow major groove of the 16S rRNA secondary structure (7). Structural insights into the mechanisms of 2-DOS aminoglycoside action were first obtained through chemical footprinting methods (8) and later using RNA fragments of the bacterial ribosome (7, 9) and isolated *Thermus thermophilus* 30S ribosomal subunits (10–12). These investigations revealed that aminoglycosides interact within the major groove of a conserved, asymmetric internal loop within the helix 44 (h44) decoding center of 16S rRNA within the small ribosomal subunit to affect the decoding mechanism.

Structural investigations using isolated 30S ribosome subunits led to the hypothesis that the universally conserved A1492, A1493, and G530 residues within the h44 decoding center actively "monitor" the interaction between the tRNA anticodon and the mRNA codon (12). To do so, A1492/A1493 must extrude from the helical axis of h44 to "recognize" the codon–anticodon helix through A-minor groove interactions. This local conformational change then couples to global conformational changes in the ribosome (domain closure) that enable tRNA accommodation. It was also suggested that the inability of mismatched near-cognate tRNA to form proper A-minor groove interactions prevents domain closure, thereby favoring tRNA rejection (11). The binding of paromomycin and neomycin to helix 44 in the crystals of isolated 30S subunits also extrudes both decoding nucleotides A1492 and A1493, leading to the hypothesis that stabilization of extrahelical A1492/A1493

Significance

Aminoglycosides are well known as antibiotics that target the bacterial ribosome. However, they also impact the eukaryotic translation mechanism to promote read-through of premature termination codons (PTCs) in mRNA. Aminoglycosides are therefore considered as potential therapies for PTC-associated human diseases. Here, we performed a comprehensive study of the mechanism of action of aminoglycosides in eukaryotes by applying a combination of structural and functional approaches. Our findings reveal complex interactions of aminoglycosides with eukaryotic 80S ribosome caused by their multiple binding sites, which lead to inhibition of intersubunit movement within the human ribosome that impact nearly every aspect of protein synthesis.

Author contributions: M.Y., S.C.B., and G.Y. designed research; I.P., R.B.A., M.D., and A.F. performed research; J.P.S. and C.-W.T.C. contributed new reagents/analytic tools; I.P., R.B.A., A.U., and S.C.B. analyzed data; and I.P., R.B.A., M.D., J.P.S., A.U., A.F., C.-W.T.C., M.Y., S.C.B., and G.Y. wrote the paper.

The authors declare no conflict of interest.

This article is a PNAS Direct Submission.

Data deposition: Atomic coordinated and structure factors for crystal structures have been deposited in the Protein Data Bank, https://www.rcsb.org/pdb/home/home.do {PDB ID codes 5NDV (80S–paromomycin), 5OBM (80S–gentamicin), 5NDW (80S–TC007), 5NDG [80S–geneticin (G418)], 5NDK (70S–tRNA–mRNA–TC007 cocrystallized), and 5NDJ (70–tRNA–mRNA–TC007 soaked)}.

[1]I.P. and R.B.A. contributed equally to this work.

[2]To whom correspondence may be addressed. Email: marat@igbmc.fr, scb2005@med.cornell.edu, or gula@igbmc.fr.

This article contains supporting information online at www.pnas.org/lookup/suppl/doi:10.1073/pnas.1715501114/-/DCSupplemental.

positions is directly related to the misincorporation of near- and noncognate tRNAs into the ribosome during translation (10, 12). However, later studies of the fused-ring 2-DOS aminoglycoside apramycin demonstrated that extrahelical A1492/A1493 positions alone are insufficient to induce miscoding (13). The non-DOS aminoglycoside streptomycin, which also promotes translation errors, exerts distinct conformational changes in the decoding site such that residues A1492 and A1493 remain intercalated within the h44 helical axis (14).

Recent structural studies of the functional 70S ribosome in complex with mRNA and tRNAs in the P- and E-sites (peptidyl- and exit-tRNA–binding sites, respectively) show that the A1493 nucleotide adopts an extrahelical positon in the absence of tRNA within the decoding site (15). By contrast, the decoding-specific changes in positions of nucleotides A1492 and G530 and domain closure require the binding of either cognate or mis-incorporated near-cognate tRNAs (16, 17). In the context of the 70S ribosome, paromomycin binding to the decoding center was also shown to elicit moderate structural rearrangements in the A-site tRNA-binding pocket, which may influence translation accuracy (16, 18, 19).

Binding of 2-DOS aminoglycosides to the ribosome has also been documented within the major groove of Helix 69 (H69) of the large ribosomal subunit, which forms a critical intersubunit bridge (B2a) that directly contacts the h44 decoding site of the small subunit (3). Paromomycin or neomycin binding to H69 alters the conformation of bridge B2 and the process of small subunit rotation with respect to the large subunit that accompanies nearly every aspect of the translation mechanism (4, 20). These impacts also hinge on interactions of the 6′-OH group of h44-bound aminoglycosides with the universally conserved A1913 residue located within the apical tip of the H69 stem loop (21).

The basis of 2-DOS aminoglycoside-class antibiotic selectivity is understood to arise from structural differences in the h44 decoding sites of bacterial and eukaryotic ribosomes. In eukaryotes, the presence of A1408G and G1491A base substitutions (bacterial numeration) within h44 (Fig. 1*A*) alter key binding interactions mediated by aminoglycoside rings I and II (22, 23). Nonetheless, specific 2-DOS aminoglycosides such as geneticin (G418) retain the capacity to bind eukaryotic ribosomes. G418 belongs to the 4,6-linked aminoglycoside class that contains a ring I 6′-OH group (Fig. S1). Its interactions with the eukaryotic h44 decoding region are accommodated by conformational plasticity within both the target and drug that enables a network of specific, stabilizing interactions (24).

Investigations of aminoglycoside activity in both human cells and the wheat embryo system revealed that aminoglycosides such as paromomycin and G418, which both possess a 6′-OH group in ring I, are efficient in promoting missense errors during protein synthesis (25, 26). Paromomycin and, with much less efficiency, neomycin were also recognized as being effective suppressors of nonsense mutations (27). Since that time, gentamicin, G418, tobramycin, and amikacin, which possess either a 6′-OH or 6′-NH_2 moiety in ring I, have all been shown to induce suppression of premature termination codons (PTCs) (28). Mutations that introduce PTCs are understood to be causative in ∼11% of the >5,000 human genetic diseases identified to date, including sporadic cancers arising from mutations in tumor-suppressor genes such as *TP53* (29, 30). Consequently, aminoglycosides are regarded as potential therapies for the treatment of human disease.

The application of aminoglycosides for suppression therapies has been limited in practice by their toxicities and their low efficiencies of stop-codon read-through (31, 32). Despite these shortcomings, aminoglycosides have been enrolled in clinical trials for the treatment of cystic fibrosis (33) and Duchenne muscular dystrophy (34) and have shown therapeutic potential for the treatment of dystrophic epidermolysis bullosa (35) and Werner syndrome (36) as well as specific cancers (37). The neomycin derivative TC007 has also been tested in the context of spinal muscular atrophy (SMA) in both human fibroblasts (32) and mouse models of disease (38).

As the molecular basis of aminoglycoside action against eukaryotic ribosomes is currently lacking, we have examined the

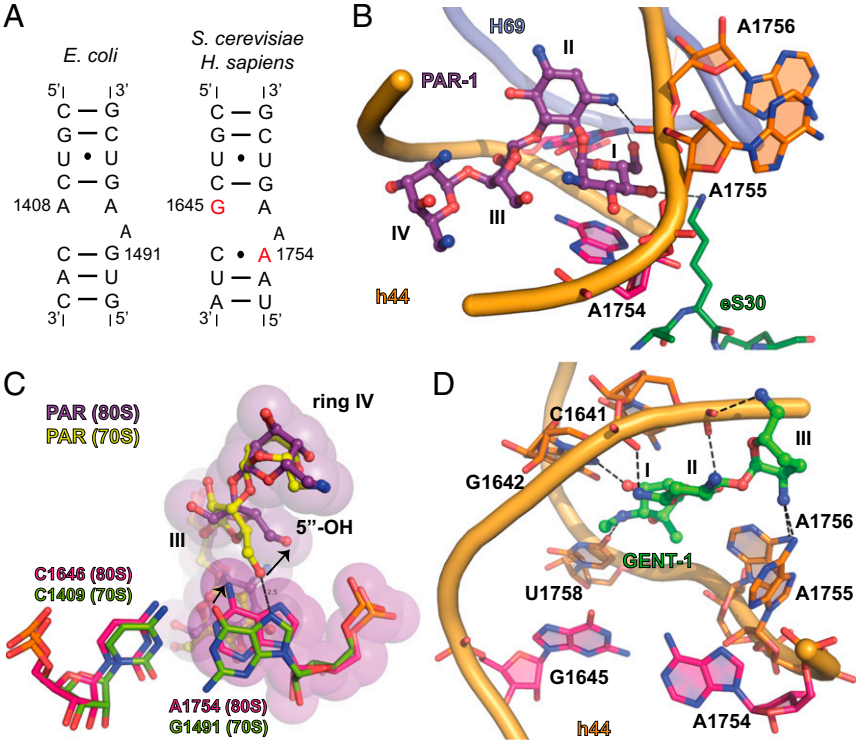

Fig. 1. Aminoglycosides target the decoding center of the 80S ribosome in a different ways. (*A*) Secondary structure of h44 of the small ribosomal subunit from bacteria (*E. coli*) and eukaryotes (identical in *S. cerevisiae* and *Homo sapiens*). Substituted nucleotides implicated in the selectivity of aminoglycosides are marked in red. (*B*) Binding of paromomycin (PAR-1) to h44 in the 80S ribosome from *S. cerevisiae*. Paromomycin is colored violet, and rings I, II, III, and IV of paromomycin are marked. Ring I is in stacking with A1754. Residues A1754, and G1645 are colored pink. h44 is shown in orange; H69 of the large ribosomal subunit is shown in light blue; and the eukaryote-specific protein eS30 is shown in green. Oxygen atoms are colored red, and nitrogen atoms are colored blue. (*C*) Comparison of PAR-1 binding to h44 in the 70S ribosome from *T. thermophilus* (PDB ID code 5EL6) and the 80S ribosome from *S. cerevisiae*. Paromomycin in complex with 70S is shown in yellow; residues of 16S rRNA of 70S are in green; other color-coding is as in *B*. The shift in the position of A1754 and the movement of 5′-OH group in ring III of paromomycin are marked with arrows. (*D*) Binding of gentamicin (GENT-1) to h44 in the 80S ribosome from *S. cerevisiae*. Gentamicin is shown in green; other color-coding is as in *B*. Rings I, II, and III of gentamicin are marked, and atoms located at a hydrogen bonding distance are connected by dashed lines.

interactions of aminoglycosides with 80S eukaryotic ribosomes using X-ray crystallography and single-molecule FRET (smFRET) imaging. X-ray structural analyses of *Saccharomyces cerevisiae* 80S ribosomes in complex with paromomycin, G418, gentamicin, and TC007 reveal that aminoglycosides interact at multiple sites within both 18S and 28S rRNA. Multivalent aminoglycoside–ribosome interactions were further corroborated by the impact of aminoglycosides on the spontaneous dynamics within the human ribosome and their propensities to promote errors in tRNA selection. These investigations further revealed that TC007 exhibited distinct modes of interaction with and miscoding and structural impacts on the eukaryotic ribosome at ∼20-fold lower concentrations than observed for G418, paromomycin, or gentamicin. These findings are consistent with the efficacy profiles of TC007 in human cells and with this compound's unique capacity to promote PTC readthrough.

Results

Aminoglycoside Binding to the Eukaryotic h44 Decoding Site. To investigate the binding mode of aminoglycosides with low affinity to the 80S ribosome, we first sought alternative experimental conditions for *S. cerevisiae* 80S ribosome crystal treatment. Osmium hexamine, which is normally present in this procedure, binds rRNA, including the aminoglycoside-binding site within the h44 decoding region (39). Hence, to examine the binding of aminoglycosides that exhibit low affinities for the 80S ribosome, we removed osmium hexamine and instead treated crystals of the ribosome in the presence of high concentrations (up to 4 mM) of aminoglycosides (*Materials and Methods*).

Under these conditions, we obtained a structure of the 4,6-linked aminoglycoside G418 bound to the *S. cerevisiae* 80S ribosome at 3.7-Å resolution (Table S1). A similar structure had been previously solved in the presence of osmium hexamine [Protein Data Bank (PDB) ID code 4U4O] (24), where it was shown that G418 can compete with osmium hexamine for h44 binding. In both structures, G418 was found to exhibit canonical binding to the h44 decoding site with ring I of the antibiotic stacking on nucleotide A1754 (G1491 in bacterial numbering), displacing the conserved nucleotides A1755 (A1492) and A1756 (A1493) away from the helical axis (Fig. S2). There, the 6′-OH group of ring I is positioned within hydrogen bonding distance (2.7 Å) of the N2 atom of G1645 (A1408) (Fig. S2). Replacement of the 6′-OH group in ring I with a hydrogen bond acceptor, such as a 6′-NH2 group, could create repulsion from the N2 atom of G1645 (A1408) precluding aminoglycoside binding. Likewise, the presence of adenosine instead of guanosine at position 1754 (1491) would disrupt Watson–Crick base pairing with C1646 (C1409), a structural component of the bacterial h44 decoding site that is essential to aminoglycoside binding (7, 24, 40).

Using similar osmium hexamine-free conditions, we solved an 80S–paromomycin structure at 3.3-Å resolution (I/σ = 0.96, $CC_{1/2}$ = 34.9) (Table S1). Like G418, the 4,5-linked aminoglycoside paromomycin contains a 6′-OH group in ring I (Fig. S1). As for G418, at high drug concentration (4 mM for soaking of paromomycin), we observed weak, positive electron density for paromomycin (PAR-1) in the h44 decoding site (Fig. 1*B*). Within this site, rings I and II of paromomycin adopted a position globally similar to that of G418, wherein ring I of the antibiotic stacked on nucleotide A1754 (G1491 in bacterial numbering), and the contact between the 6′-OH group in ring I and the N2 atom of G1645 (A1408) was maintained (3.3 Å distance) (Fig. S3*A*). To avoid steric clash with the 6-NH_2 group of A1754 (G1491), ring III of paromomycin was found to be rotated compared with the structure of paromomycin bound to the bacterial 70S ribosome (Fig. 1*C*) (18). This repositioning reoriented ring IV within the major groove, breaking the hydrogen bond between the 5′-OH in ring III and the N7 atom of G1491 present in the 70S–paromomycin complex. Interestingly, the 4′-OH group in ring I of paromomycin is positioned within hydrogen bonding distance (3.5 Å) of the ζ-NH2 group of lysine 3 of the eukaryote-specific protein eS30, which approaches h44 from the minor groove face (Fig. 1*B*). This interaction, which is absent in both the paromomycin–70S ribosome complex and the 80S–G418 structures (18, 24), may partially compensate for the reductions in binding affinity arising from sequence changes within the h44 decoding site (Fig. 1*A*) so that low levels of miscoding are maintained (25, 26).

Gentamicin, a 4,6-linked aminoglycoside produced as a mixture of C1, C1a, C2, and C2a isoforms (29) and which contains amine along with a few methyl groups in the 6′ position of ring I (Fig. S1) (41), does not induce errors in translation but competes with paromomycin-induced miscoding (26). These data suggest a common binding site within h44 but a unique mode of interaction with the 80S ribosome. As for paromomycin, the crystal structure of the 80S ribosome in complex with gentamicin, solved at 3.4 Å resolution (I/σ = 0.94, $CC_{1/2}$ = 33.5) (Table S1), exhibits positive electron density in h44 (GENT-1) at a high drug concentration (4 mM) (Fig. S3*B*). Under these conditions, gentamicin's ring I does not stack upon A1754 (G1491), and nucleotides A1755 (A1492) and A1756 (A1493) adopt only semiextruded positions relative to the axis of h44 so that their N2 atoms are within hydrogen bonding distance of the 2′-NH_2 group of ring III. Thus, positioned, rings I–III also make sequence-specific contacts with O4 of U1758 (U1495) and N7 of G1642 (G1405) (Fig. 1*D* and Fig. S3*C*). This noncanonical pose, which appears to be enforced by repulsion between the N1 and N2 atoms of G1645 (A1408) and the NH_2-group in the 6′ position of ring I, rationalizes gentamicin's capacity to compete with paromomycin binding while being unable to support miscoding.

Interactions of TC007 with the 80S Ribosome and Implications for PTC Read-Through. SMA, a leading genetic cause of infantile death, is an autosomal recessive disease for which there is currently no cure (42). SMA is associated with the loss of full-length SMN protein (43). Initial screens for small molecule-mediated suppression therapies for potential treatment of SMA led to the discovery of TC007, a three-ring 4,5-linked aminoglycoside bearing a 6′-NH_2 group on ring I (Fig. S1) (32). TC007 testing in fibroblasts from SMA patients and in SMA mouse models showed good toxicity profiles and prolonged the lifespan of SMA mice while partially lessening the severity of disease (44).

To gain insight into TC007 interactions with the 80S ribosome, we solved the X-ray structure of the 80S–TC007 complex at 3.7-Å resolution (I/σ = 0.98, $CC_{1/2}$ = 36.1) (Table S1). Consistent with a steric clash between the 6′-NH_2 and the G1645 (A1408) residue (24), TC007 was not observed to bind the small subunit decoding center, despite being present at 4 mM concentration. Accordingly, no electron density was evidenced for the disordered nucleobases of residues A1755 (A1492) or A1756 (A1493). However, positive electron density was observed for TC007 (TC007-1) immediately below the canonical decoding site and above intersubunit bridge B3, spanning between h44 of the small subunit and Helix 71 (H71) of the large subunit at the intersubunit space (Fig. 2*A* and Fig. S4*A*). A second TC007 molecule (TC007-2) was also evidenced between Helix 68 (H68) and Helix 70 (H70) in the large ribosomal subunit, proximal to the highly conserved H69 element of intersubunit bridge B2. This binding site is close to (within ∼10 Å) but is distinct from the noncanonical aminoglycoside-binding site observed within the H69 major groove in the bacterial ribosome (3, 20, 21) and distorts the H69 conformation (Fig. 2 *A* and *B* and Fig. S4*B*).

Interactions of TC007 with Bacterial 70S Ribosome. To shed light on the selectivity of TC007, we solved the structure of the bacterial 70S ribosome from *T. thermophilus* cocrystallized in complex with three tRNAs, mRNA, and TC007 at 2.95 Å (I/σI = 1.38,

$CC_{1/2}$ = 47.1) (Table S1), where the drug was at 50-fold excess over the ribosome (*Materials and Methods*). As expected, we observed strong positive electron density in the h44 decoding site, where rings I and II were observed to overlap with those of paromomycin (Fig. S4*C*). In contrast to ring III of paromomycin, which interacts with the Hoogsteen face of G1491 (*Escherichia coli* numbering), the O7 atom of ring III of TC007 is positioned within hydrogen bonding distance of N4 of C1407. When TC007 was soaked into preformed crystals of the same 70S–tRNA–mRNA complex (500 μM for 24 h), we were able to obtain a structure at 3.05 Å resolution (I/σI = 1.25, $CC_{1/2}$ = 39.9) (Table S1) in which TC007 was bound in an identical position within h44 (TC007–h44) (Fig. S4*D*). As for neomycin, gentamicin, and paromomycin binding to H69 within the *Escherichia coli* 70S ribosome (3, 20, 21), TC007 was observed to make an array of hydrogen bonding contacts with bases lining the H69 major groove, including sequence-specific contacts with residues G1921 and G1922 (Fig. S4 *B* and *E*). Remarkably, the orientation of TC007 is different from that in a previously reported 70S–neomycin structure (21): The position of ring II is similar in the two antibiotics, but the positions of rings I and III are swapped. As for gentamicin, intersubunit bridging contacts present in both paromomycin and neomycin structures were not observed due to the absence of ring IV. As H69 is sterically accessible within the eukaryotic 80S ribosome, we attribute the observed differences in TC007 binding to Ψ2264 (G1921) and C2265 (G1922) substitutions present in the 80S ribosome (Fig. S4 *B* and *F*), which likely disrupt the drug's capacity to pack tightly against the floor of the major groove. These findings confirm that the TC007-binding sites in the *T. thermophilus* 70S ribosome are distinct from those found in the 80S ribosome of *S. cerevisiae* (Fig. S4*B*).

Aminoglycosides Inhibit Intersubunit Rotation of the Eukaryotic Ribosome. To assess the impact of aminoglycosides on the dynamics of subunit rotation within functional 80S ribosome complexes, we performed smFRET imaging on surface-immobilized human 80S pretranslocation (PRE) complexes in the absence and presence of paromomycin, G418, gentamicin, and TC007 (45). As previously reported (45), in the absence of drug, human PRE complexes predominantly exhibited a mixture of lower-FRET (H2: ∼0.2 and H1: ∼0.4) hybrid state configurations in which the 3′-CCA end of deacylated tRNA occupies the large subunit E-site and the 3′-CCA end of peptidyl-tRNA occupies either the aminoacyl (A)- or P-site, respectively (A/A and P/E; A/P and P/E) (Fig. 3 *A* and *B*, *Left*). The addition of paromomycin to the 80S PRE complex first lowered the average FRET value of the hybrid-state tRNA configurations, suggesting a relative stabilization of the H2 hybrid state in which peptidyl-tRNA returns to its classic (A/A) position while deacylated tRNA remains in its hybrid (P/E) state (46). This impact was maximized at a drug concentration of ∼10 μM. Above this concentration, we observed the appearance of an intermediate-FRET (∼0.55) state, followed by stabilization of a high-FRET, classic (C) PRE complex conformation (Fig. 3*B*). The estimated EC_{50} of this effect was ∼35 μM. These data are consistent with a multivalent impact of paromomycin binding to the 80S PRE complex, which first stabilizes peptidyl-tRNA in its classic position within the A-site, followed by a shift of deacylated P-site tRNA from its hybrid to its classic position. By contrast, G418, which also bears a ring I 6′-OH substituent, only stabilized at an intermediate-FRET state (∼0.55) (Fig. 3*C*). Notably, consistent with the concentration range used to inhibit mammalian cell culture growth (47), the EC_{50} of this impact was ∼2 mM. By analogy to bacterial systems, the intermediate-FRET state may reflect a reversal of subunit rotation from the P/E hybrid state, which promotes a chimeric, intersubunit hybrid configuration of deacylated P-site tRNA associated with the global inhibition of translation factor binding (20, 21).

Analogous investigations of gentamicin, which contains a 6′-NH2 group on ring I, also led to intermediate-FRET (∼0.55) state stabilization, but the EC_{50} of its impact was approximately an order of magnitude lower (∼100 μM) than that of G418 (Fig. 3*D*). TC007, which also has a 6′-NH_2 group on ring I, exhibited impacts on the 80S PRE complex that shared characteristics of G418 and gentamicin as well as paromomycin, in which drug binding was bimodal in nature. At concentrations below 2 μM, TC007 predominantly promoted a lower-FRET PRE complex conformation, in line with H2 hybrid state stabilization (A/A; P/E). Higher TC007 concentrations increasingly stabilized an intermediate-FRET (∼0.55) state, similar to that evidenced in the presence of subsaturating paromomycin and saturating G418 and gentamicin concentrations (Fig. 3*E*). At 10 μM, both H2 and intermediate-FRET PRE complex conformations persisted. Above

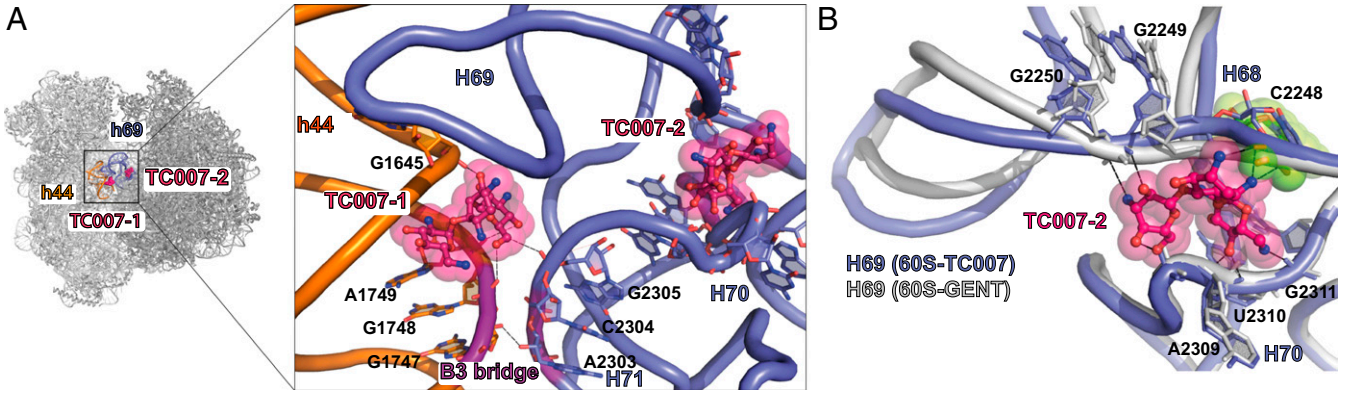

Fig. 2. Interactions of the aminoglycoside derivative TC007 with the 80S ribosome. (*A*, *Left*) The view from the A-site of the ribosome is indicated. (*Right*) Enlarged view showing binding sites of TC007-1 and TC007-2 in close proximity to h44 of the small ribosomal subunit and H69 of the large ribosomal subunit, respectively. The regions of h44 of the small ribosomal subunit and H71 of the large ribosomal subunit, which form intersubunit bridge B3, are colored violet. The 40S subunit is shown in orange. Contacts of TC007 and rRNA residues are depicted by dashed lines. The 60S subunit is shown in blue, and TC007 is in magenta. Oxygen atoms are colored red, and nitrogen atoms are colored blue. (*B*) Close-up view of the second binding site of TC007-2 located between helices H68, H69, and H70 of the large ribosomal subunit. Local alignment demonstrates that TC007-2 would clash with the phosphate group of C2248 if H69 adopted the conformation characterized by the different rotational state of the ribosomal subunits as observed in the 80S–gentamicin structure. The 60S subunit from the 80S–gentamicin structure is colored gray; residue C2248 is colored lime and is marked with spheres; other color-coding is as in *A*.

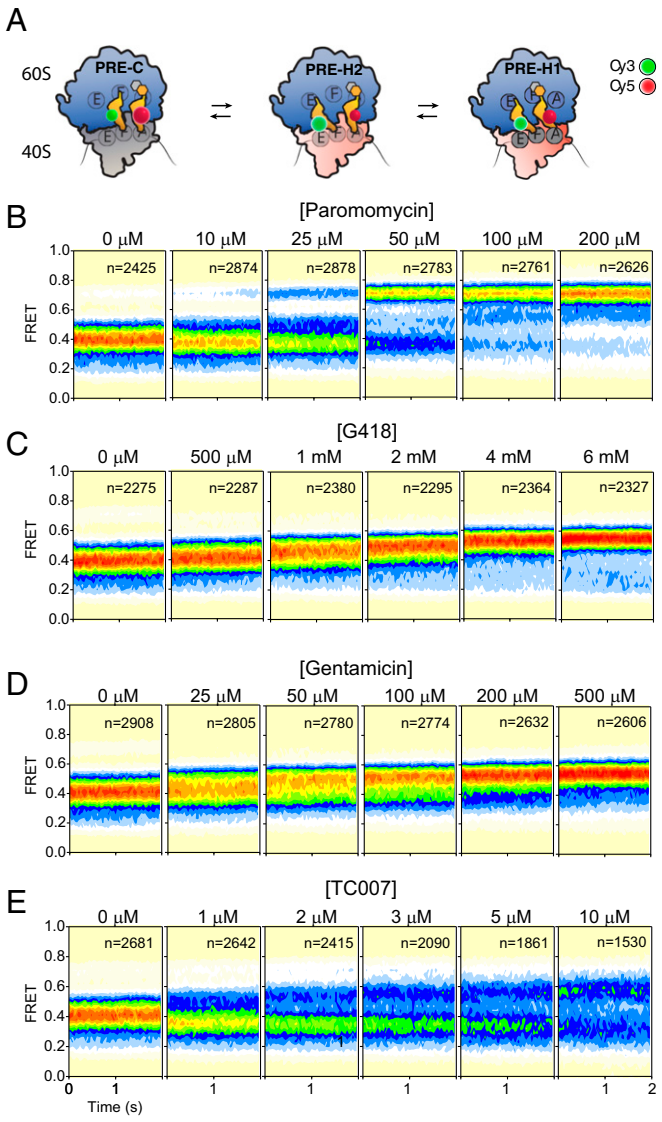

Fig. 3. Aminoglycoside-induced changes in human 80S PRE complex conformation. (*A*) Schematic showing classic (C) and hybrid (H2 and H1) states of the human PRE ribosome complex. Large (60S) and small (40S) subunits (unrotated, gray; rotated, pink), tRNAs (orange), and sites of donor (Cy3, green) and acceptor (Cy5, red) fluorophore labeling on tRNA in the P- and A-sites, respectively, are indicated. (*B–E*) Population FRET histograms showing the impact of paromomycin (*B*), G418 (*C*), gentamicin (*D*), and TC007 (*E*) on the equilibrium distribution of FRET states exhibited by the 80S PRE complex. The concentration of antibiotic is indicated; *n*, number of single-molecule observations made in each experiment.

this concentration the FRET distribution broadened substantially, consistent with an increase in dynamic PRE complex behaviors.

Aminoglycoside-Induced Errors in tRNA Selection on the Eukaryotic Ribosome. To evaluate the impact of aminoglycosides on aminoacylated tRNA (aa-tRNA) miscoding at the A-site, we examined the extent of aa-tRNA misincorporation of Phe-tRNA^{Phe} into surface-immobilized 80S initiation complexes (ICs) containing (Cy3)Met-tRNA$_i^{Met}$ in the P-site, in which the A-site codon was changed from the cognate UUU codon to the near-cognate UCU codon. To provide adequate time for miscoding, the eEF1A(GTP)-(Cy5)Phe-tRNA^{Phe} ternary complex (20 nM) was incubated with surface-immobilized ribosome complexes for 2 min (*Materials and Methods*) followed by buffer exchange to remove unbound ternary complexes. Using this approach, we could specifically examine the extent of PRE complex formation in the absence of convoluting signals arising from transient ternary complex binding events. Consistent with a high-fidelity decoding mechanism, near-cognate ternary complexes were efficiently rejected from the A-site in the absence of drug so that little or no PRE complex formed (Fig. 4 *A* and *B*, *Left*). By contrast, increasing levels of A-site miscoding were observed as a function of paromomycin, G418, gentamicin, and TC007 concentration. In each case, the extent of miscoding correlated with the concentrations of drug, where the EC_{50} of miscoding closely mirrored that observed for drug binding to the cognate PRE complex (Figs. 3 and 4). Strikingly, the distribution of FRET values exhibited by precomplexes bearing near-cognate tRNA at the A-site were distinct from those bearing cognate tRNAs; the near-cognate complexes were found to exhibit multiple distinct FRET states (compare far right panels in Figs. 3 and 4). Inspection of individual FRET trajectories of PRE complexes bearing near-cognate tRNA in the A-site showed that the FRET states observed were in dynamic exchange. These findings suggest that the nature of the codon–anticodon pair in the A-site influences the ribosome's interaction with antibiotics and tRNA in a manner that affects both the conformation and dynamics of the PRE complex.

Secondary Binding Sites: Hot Spots Targeted in the Eukaryotic 80S Ribosome by Aminoglycosides. Aminoglycosides are positively charged and are well known to bind a diverse range of RNA molecules, including catalytic RNAs such as ribonuclease P, self-splicing introns, and ribozymes (48–50). Crystal structures of the isolated small ribosomal subunit as well as intact 70S ribosomes from bacteria have all shown evidence of multiple aminoglycoside-binding sites (3, 13, 14, 20, 21). The positively charged anticancer drug cisplatin also has several binding sites in the 70S ribosome (51).

As high aminoglycoside concentrations were used in each of our crystallographic investigations under conditions of relatively low ionic strength (~130 mM salt concentration) and neutral pH (7.0–7.5), secondary binding sites were observed for each of the aminoglycosides examined. While it is difficult to link the binding sites observed with the impairment of specific ribosome functions due to the presence of numerous copies of rRNA genes in the genome, we note that several of the secondary aminoglycoside-binding sites map to key functional centers of the ribosome (Fig. 5*A*). These findings are consistent with the known propensities of aminoglycosides to show diverse impacts on the bacterial translation mechanism (20, 52).

The peptide exit tunnel, which spans the peptidyl-transferase center to the solvent side of the ribosome, is subjected to translation regulation by small molecules and peptides that induce translational stalling (53). We find that gentamicin, G418, and TC007 each bind to the peptide exit tunnel (Fig. 5*B*). Paromomycin was not found in the exit tunnel, suggesting that only aminoglycosides with a maximum of three rings can be accommodated within this pocket. Superposition with the structure of the 50S ribosome subunit from *Haloarcula marismortui* complexed with erythromycin shows that aminoglycosides and erythromycin bind opposite sides of the exit tunnel wall (Fig. S5*A*) (54). Interestingly, although each drug interacts with the same 25S rRNA residues, the orientations of G418 and gentamicin within the exit tunnel, which are very similar, are distinct from TC007 (Fig. 5*B*). These distinctions likely reflect the unique ring topologies of the 4,6-linked (G418 and gentamicin) and 4,5-linked (TC007) aminoglycosides. Alignment of each of these structures with that of the *Escherichia coli* ribosome containing the SecM stalling peptide (55) suggests that aminoglycoside occupancy within the exit tunnel wall is unlikely to be sufficient to

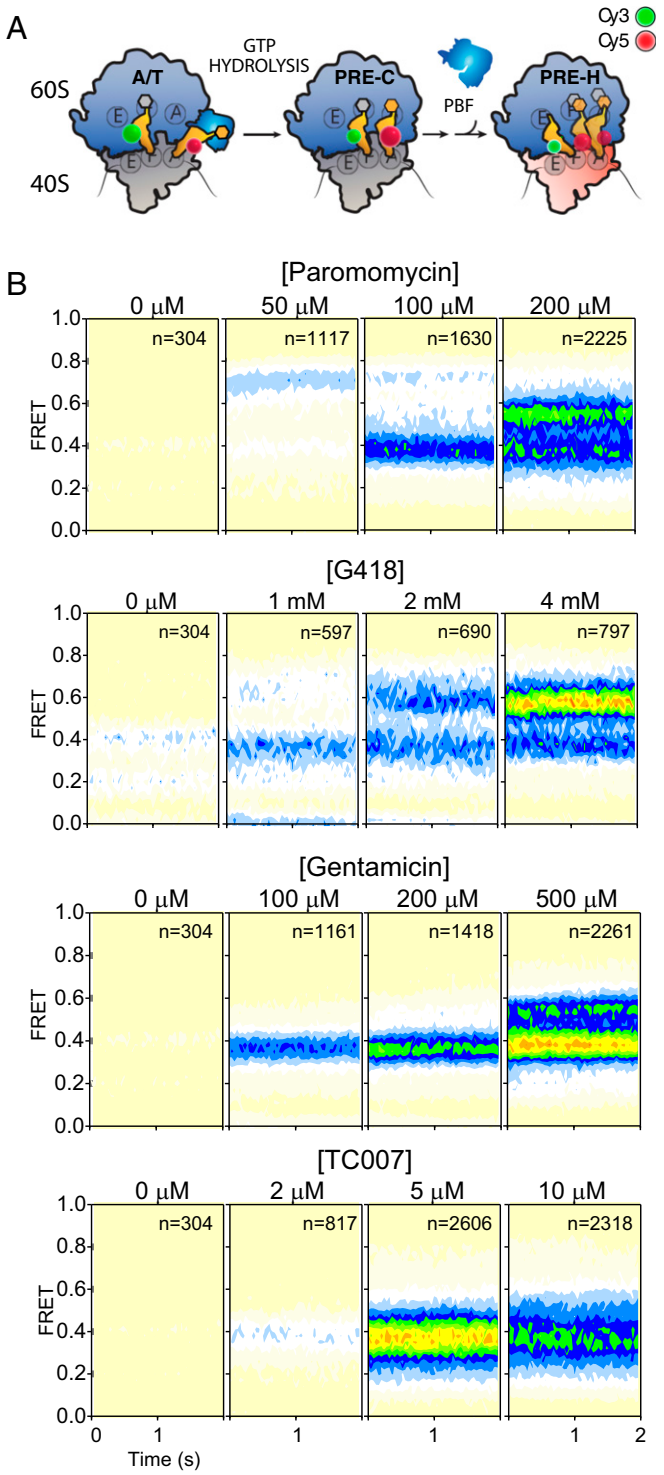

Fig. 4. Aminoglycoside-induced miscoding during tRNA selection on the human ribosome. (*A*) Schematic showing the process of tRNA selection, in which the ternary complex of eEF1A (blue), GTP, and aa-tRNA (orange) enters the A-site of the 80S ribosome. The process of tRNA selection proceeds through the A/T state in which codon–anticodon pairing on the small subunit occurs while the 3′-aminoacylated CCA-end of tRNA remains bound to eEF1A. GTP hydrolysis by eEF1A facilitates the aa-tRNA release from eEF1A and the accommodation of its 3′CCA end into the large subunit A-site on the classically (C) configured (unrotated) PRE complex. Peptidyl- and aminoacyl-tRNAs in the P- and A-sites, respectively, then undergo peptide bond formation (PBF), enabling deacylated P-site tRNA and peptidyl-tRNA to achieve hybrid (H2 and H1) states. Large (60S) and small (40S) subunits (unrotated, gray; rotated, pink), tRNAs (orange), and sites of donor (Cy3, green) and acceptor (Cy5, red) fluorophore labeling on tRNA in the P- and A-sites, respectively, are indicated. (*B*) Population FRET histograms showing that aminoglycoside-induced errors in tRNA selection lead to the accumulation of PRE ribosome complexes bearing near-cognate tRNA in the A-site. The concentration of antibiotic is indicated; *n*, number of single-molecule observations made in each experiment.

block the path of nascent peptides lacking bulky amino acid side chains (Fig. S5*B*) (56, 57).

The E-site of the small ribosomal subunit is a potential point of regulation of eukaryotic protein synthesis (45, 58, 59). We observe that paromomycin (PAR-3), geneticin (G418-3), and gentamicin (GENT-2) bind in the space normally occupied by the E-site mRNA codon and exhibit similar ring I and II positions (Fig. 5*C*). Aminoglycoside binding in this region may have important impacts on tRNA occupation within the translating ribosome (45) and/or alter the mRNA-binding and -scanning mechanism required for translation initiation (60). Similar to the binding mode of streptomycin to the bacterial 30S subunit (14), gentamicin (GENT-3) was also found within <4 Å of the mRNA backbone wedged between helices 1, 44, 18, and 27 within the A-site, where it interacts with the phosphate groups of residues U9 and A11 (Fig. S6 *A–C*). In contrast to streptomycin, however, gentamicin does not appear to induce substantial conformational changes in h44 and h45. This same pocket was also occupied by geneticin (G418-4) (Fig. S6*C*). In addition to potential impacts on the initiation mechanism, binding in such proximity to the decoding region may influence tRNA selection and translocation of the mRNA–tRNA module during the elongation phase of protein synthesis.

Aminoglycosides interact extensively with the intersubunit region of the ribosome. Paromomycin (PAR-3) provides additional contacts between the subunits in the vicinity of bridge B2c formed by h24 of the small subunit and H66 of the large subunit (Fig. 5*D*). Gentamicin (GENT-4, 5) is also observed to bind bridge B2c (Fig. 5*E*), and GENT-6 binds bridge B4, a protein–RNA bridge comprised of H34 of the large subunit and protein uS15 of the small subunit (Fig. 5*F*). The interactions of the GENT-5 molecule with bridge B2c are expected to preclude bridge B2c rearrangements relative to h24 in the small subunit (Fig. 5*E*). These findings, together with the observation that TC007 binds close to bridge B2c (Fig. S6*D*) and B3 (Fig. 2*A*), are consistent with aminoglycosides interfering with intersubunit rotation in distinct ways to affect the translation mechanism. Such distinctions may impact the mechanism of translocation in particular, which requires dramatic remodeling events within the central bridge B2 domain (20, 21), as well as rearrangements in B4 (61, 62).

Additional impacts on the elongation mechanism may also arise from aminoglycoside binding in proximity to the peptidyl-transferase center. Paromomycin (PAR-4) is located just 3 Å away from the phosphate groups of the catalytic residues A2820 (A2450) and C2821 (C2451) and 3.4 Å away from C75 of the A-site tRNA (Fig. S7*A*). Aminoglycosides are also observed to bind the base of the P-stalk and sarcin–ricin loop (H95), elements of the large ribosomal subunit that interact with translation elongation factors (Fig. 5*G* and Fig. S7*B*).

Discussion

The structural and functional insights into aminoglycoside interactions with the 80S eukaryotic ribosome obtained through the present investigations serve as a foundation for exploring the molecular mechanisms of aminoglycoside action in eukaryotes. Although the impairment of mitochondrial translation is considered one of the main causes of side effects produced by aminoglycosides in eukaryotic cells (63, 64), emerging evidence

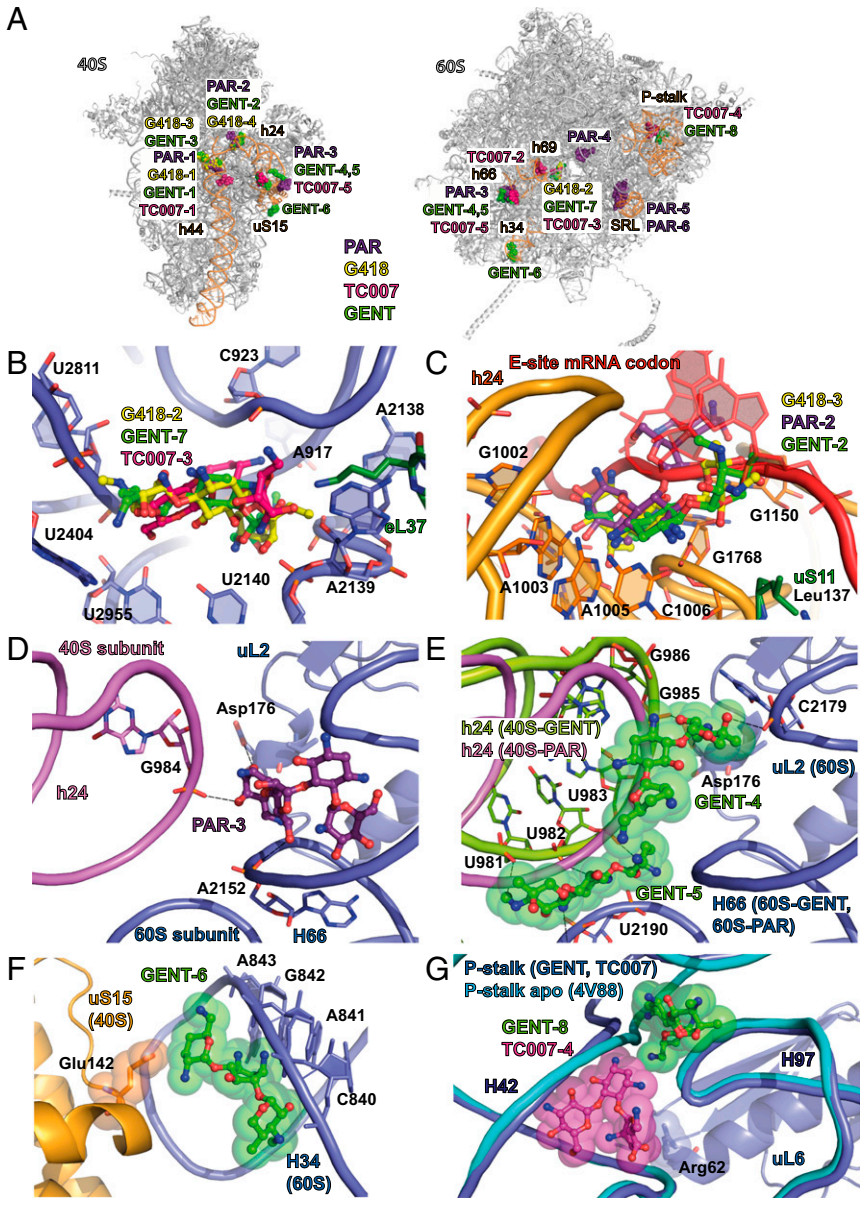

Fig. 5. Overview of the secondary binding sites of aminoglycosides in 80S ribosome. (*A*) Binding sites of gentamicin (GENT), G418, TC007, and paromomycin (PAR) in the 80S ribosome from *S. cerevisiae*. All structures were aligned either on 18S rRNA or on 28S rRNA, for small and large subunits, respectively, in the 80S–gentamicin structure. The ribosome is colored light gray; elements of the binding pockets of aminoglycosides are colored light orange; gentamicin is colored green; G418 is colored yellow; TC007 is colored magenta; and paromomycin is colored violet. (*B*) Binding of GENT-7, G418-2, and TC007-3 to the peptide exit tunnel of the 80S ribosome. G418 is colored yellow; gentamicin is colored light green; TC007 is colored magenta; the large ribosomal subunit is colored blue; and the eukaryote-specific protein eL37 is colored green. Similar poses are observed for G418-2 and GENT-7, but the orientation of TC007-3 is different. Oxygen atoms are colored red, and nitrogen atoms are colored blue. (*C*) Binding sites of PAR-2, GENT-2, and G418-3 in the E-site of the small ribosomal subunit overlapping the position of the mRNA. Structures of the 80S ribosome in complex with paromomycin, gentamicin, and G418 were locally aligned on the structure of the 70S ribosome from *T. thermophilus* in complex with tRNAs and mRNA (PDB ID code 5EL6). mRNA is colored red; elements of the 70S ribosome are omitted for clarity. The 40S subunit is colored orange; paromomycin is colored violet; the universal protein uS11 is colored green; and other color-coding is as in *A*. (*D*) Interactions of PAR-3 with the elements of the intersubunit bridge B2c. Contacts made between paromomycin and G984 of the 40S subunit, A2152 of the 60S subunit, and Asp176 of uL2 are marked with dashed lines. The 40S subunit is colored light pink; paromomycin is colored violet; the 60S subunit is colored blue; and the universal protein L2 (uL2) is colored blue. Oxygen atoms are colored red, and nitrogen atoms are colored blue. (*E*) GENT-4 and GENT-5 stabilize particular conformations of bridge B2c. The 80S–paromomycin structure was aligned on the 80S–gentamicin structure based on the 28S rRNA. The alignment demonstrates that rearrangement of the bridge B2c would be blocked by gentamicin due to a clash with h24 of the 40S subunit in the 80S–paromomycin structure (colored in pink). 80S–gentamicin contacts are marked with dashed lines. The 40S subunit from 80S–gentamicin structure is colored lime; other color-coding is as in *A*–*C*. (*F*) GENT-6 targets bridge B4 formed by the universal protein uS15 protein and H34 of the large subunit. uS15 is shown in yellow; other color-coding is as in *D*. Glutamine 142, which interacts with GENT-6, is depicted as spheres. (*G*) Interactions of GENT-8 and TC007-4 with the elements of the ribosomal P-stalk. Different conformation of the helices 42 and 97 of the P-stalk are shown in blue for 80S-GENT and 80S-TC007 structures and in cyan for the 80S-apo structure (PDB ID code 4V88). H42 in the apo conformation would clash with GENT-8. Arg62 in the uL6 protein approaching TC007 is shown as spheres. Color-coding is as in *A*–*E*.

suggests that aminoglycosides also exert effects on cytosolic ribosomes to alter translation elongation and termination in a manner that induces read-through of PTCs (27, 65). These findings have led to their consideration as potent drugs to treat human diseases caused by PTCs (28). Aminoglycosides also operate against eukaryotic human pathogens, including *Leishmania* and *Trypanosoma* families (66, 67), due to sequence variations in their canonical h44 decoding sites (Fig. S8).

The concentrations of aminoglycosides required for eukaryotic cell growth inhibition and the EC_{50} values measured for the inhibition of eukaryotic translation by distinct aminoglycosides in vitro generally correlate with their affinities for the canonical h44 decoding region within the small subunit A-site (23, 68). As illustrated by crystal structures of the 80S ribosome with gentamicin and TC007, which adopt noncanonical poses in the vicinity of the h44 decoding site, the eukaryotic-specific G1645 residue (equivalent to A1408 in bacteria) within h44 tends to preclude the binding of aminoglycosides containing a 6′-NH_2 substituent in the ring I (Figs. 1*D* and 2*A*). Paromomycin and G418, which contain a 6′-OH substituent, can achieve canonical interactions with the h44 decoding site, but the absence of Watson–Crick base pairing between C1646 and A1754 impedes drug-binding interactions that hinge on ring I interactions with the floor of the aminoglycoside-binding site (Fig. 1*B* and Fig. S1). Human mitochondrial ribosomes contain an adenosine at the 1408 position (bacterial numbering), making it a good target for aminoglycosides with both 6′-OH and 6′-NH_2 substituents in ring I (63). However, aminoglycoside affinity to mitochondrial ribosomes is likely to be attenuated by two consecutive noncanonical base pairs [C1494–A1555 (A1410–U1490) and C1493–C1556 (C1409–G1491)] that are likely to strongly disrupt ring I interactions (Fig. S8). Consistent with this notion, the reestablishment of

Watson–Crick interactions in the floor of the aminoglycoside-binding site by the naturally occurring mutations A1555G or C1494T leads to aminoglycoside hypersusceptibility in humans (69, 70).

Our smFRET experiments indicate that each of the aminoglycosides tested increases the error rate of A-site decoding (Fig. 4). However, the behaviors of the miscoded 80S precomplexes bearing near-cognate tRNA in the A-site are unique for each drug. These findings suggest that aminoglycosides may promote PTC read-through by distinct mechanisms. Aminoglycosides containing 6′-OH substituent in ring I likely induce miscoding and PTC read-through due to residual binding to the canonical binding site in h44 of the eukaryotic ribosome. In this case, near-cognate or noncognate tRNA may efficiently accommodate at the stop codon-programmed A-site to compete with the termination factors. Aminoglycosides containing a 6′-NH_2 constituent in ring I, including gentamicin and TC007, do not bind h44 in a canonical fashion. Their impacts on PTC read-through may entail alternative mechanisms, including intersubunit rotation effects that are anticipated to hamper RF1 interactions with the classically configured ribosome (Fig. S9) (71).

The propensity of eukaryotic ribosomes to adopt rotated states and the impact of aminoglycosides in enforcing closer interactions (higher FRET) between deacylated and peptidyl-tRNA within the 80S human PRE complex suggest that aminoglycoside binding to intersubunit regions of the ribosome (bridges B2c and B4 for gentamicin and bridge B3 for TC007) facilitate conformational changes in the PRE 80S–ribosome complexes that shift peptidyl tRNA toward the P-site. Such impacts may relate to the stabilization of partially rotated ribosome configurations that move deacylated tRNA toward the A-site (20, 21).

The nature of the observed aminoglycoside interactions with the eukaryotic ribosome hint at potentially multiple modes of action on the translation mechanism. These insights also provide an important framework for understanding the diversity of aminoglycoside interaction sites and drug-binding modes with the 80S ribosome. The combined perspectives afforded by X-ray crystallography and direct imaging of aminoglycoside impacts on functional ribosome complexes using smFRET has the potential to facilitate the design of new antibiotic derivatives and may be particularly suited for the identification of compounds capable of mediating efficient PTC read-through. Such efforts will be greatly aided by in-depth functional investigations of a diversity of functional ribosome complexes relevant to termination. In this regard, the present findings suggest that nonspecific impacts on decoding may be reduced by avoiding aminoglycoside scaffolds bearing a ring I 6′-OH moiety, which exhibit generally higher affinity for the h44 decoding site, and instead focusing on aminoglycosides, other compounds, or mixtures of compounds that give rise to stop codon-specific miscoding in the absence of dominant-negative downstream impacts.

Materials and Methods

Yeast and Bacterial Ribosome Purification, Crystallization, and Crystal Treatment. Ribosomes from *S. cerevisiae* were purified and crystallized as described (39). The crystal treatment procedure was modified based on the procedure described previously (39). Briefly, crystals were transferred to the solution containing 80 mM Tris·acetate (pH 7.0), 70 mM KSCN, 10 mM $Mg(OAc)_2$, 20% (vol/vol) glycerol, 5% (wt/vol) PEG 20,000, 6.5 mM spermidine, 7.5 mM NH_4OAc, 1.4 mM *N,N′*-bis-(3-D-gluconamidopropyl) deoxycholamide (Deoxy Big Chap), 2 mM DTT, and stepwise increasing concentrations of PEG 4000, PEG 3350, or PEG 2000 MME up to 20%. The crystals were incubated for 1 h or 4 h and were flash-frozen in a stream of liquid nitrogen. All manipulations were performed at 4 °C. Aminoglycosides G418, paromomycin, and gentamicin were ordered from Sigma. TC007 was obtained as described in ref. 32. High-concentration stocks of aminoglycosides were prepared and introduced during the last steps of treatment. We observed that soaking in high concentrations of paromomycin or gentamicin improves the diffraction of the crystal. For example, crystals prepared in the same conditions and soaked in 2 mM of paromomycin diffracted up to 3.7-Å resolution. Ribosomes from *T. thermophilus* were purified and crystallized as described in ref. 72. TC007 was added for cocrystallization in 50-fold excess over the ribosome concentration (70S = 1.25 μM; TC007 = 62.5 μM). The crystal treatment was performed as described. If necessary, TC007 was added for soaking during all steps of the crystal treatment procedure at a concentration of 500 μM.

Purification of 40S and 60S Ribosomal Subunits from Human Cells. Preparation of small (40S) and large (60S) human ribosomal subunits was adapted from refs. 45 and 73. Specific deviations implemented for the purification of polysome fractions from human tissue culture are described here. Cell pellets were resuspended in lysis buffer [20 mM Tris HCl (pH 7.5), 2.5 mM $MgCl_2$, 10 mM KCl, and 1 mM freshly prepared DTT] with the RNase inhibitor RNase Out (Invitrogen), EDTA-free Halt Protease Inhibitor (Thermo Scientific), and cycloheximide (Sigma) at 100 μg/mL (~350 μM). The solution was incubated on ice for 10 min before centrifugation in a Microfuge 22R Refrigerated Centrifuge (Beckman Coulter) at 14,000 rpm for 10 min at 4 °C to pellet cell debris. The supernatant was loaded onto precooled 10–50% sucrose density gradients and spun at 35,000 rpm for 3 h at 4 °C in an Optima L-100 XP ultracentrifuge (Beckman Coulter). The gradients were then fractionated using a BR-186-1 Fractionator and a UA-6 UV/Vis detector (Teledyne Isco). Fractions corresponding to polysomes were collected and subsequently pelleted and dissociated into subunits according to ref. 73. Pelleted subunits were resuspended with storage buffer [30 mM Hepes (pH 7.5), 15 mM $MgCl_2$, 50 mM NH_4Cl, 2 mM spermidine, 5 mM putrescine, 1 mM DTT, and 6% sucrose] for stable, long-term storage in liquid nitrogen.

Data Collection, Crystal Structure Determination, and Analysis. Diffraction data were collected at 90 K using 0.05° oscillation on beamline PROXIMA I at the Soleil synchrotron (Saint-Aubin, France) equipped with a Pilatus 6M detector (Dectris) or on the PXI beamline at the Swiss Lightsource synchrotron (Villigren, Switzerland) equipped with an Eiger 16M detector (Dectris). Two to eight crystals were used for each dataset. Data were reduced and scaled using the XDS suite (74). Coordinates of vacant 80S ribosome from *S. cerevisiae* from PDB 4V88 were used to determine structures of 80S–paromomycin, 80S–gentamicin, and 80S–TC007. Phenix software was used for structure refinement, starting with several rounds of a rigid body refinement, and validation (75, 76). P-stalk elements were disordered and were removed from the structures except for P-stalk rRNA in the 80S–paromomycin structure and P-stalk rRNA and protein L12 in the 80S–gentamicin structure. Due to weak electron density, protein S31 was removed from the 80S–paromomycin structure, and a few structural elements were remodeled, in particular, amino acids 103–113 of protein uL16 and residues 80–87 of 5.8S rRNA. An unbiased difference electron density map ($F_{obs} - F_{calc}$) was used to locate the binding sites of aminoglycosides. Ligand fitting was performed in Coot (77). Geometry restraints for antibiotics were generated with the help of Grade web server (Global Phasing, grade.globalphasing.org/cgi-bin/grade/server.cgi). Peaks of positive electron density maps were inspected manually to add magnesium ions, with coordinated water molecules often replacing osmium hexamine molecules. Manual corrections were followed by several iterations of reciprocal space refinement of atomic coordinates, B-factors (one isotropic B-factor per residue), and occupancies (one occupancy value per ligand and individual occupancies for magnesium ions). Real-space refinement in Phenix was applied to fit rotamer outliers. Finally, translation–libration–screw-rotation (TLS) refinement was performed with two TLS groups. For structure determination of 70S–tRNA–mRNA–TC007 complexes, coordinates of the 70S ribosome from PDB 4WSM and tRNAs and mRNAs coordinates from PDB 4V6F were used for two rounds of rigid-body refinements. The electron density maps were inspected manually, and the molecules of TC007 were localized in the peaks of positive electron density. Secondary binding sites of TC007 (four in total) were located on the periphery of the ribosome far from the functional centers. Additionally, one binding site of TC007 to the intersubunit region was detected. Here TC007 interacts with the low part of h44 of the 30S subunit and the junction of helices 62 and 64 in the 25S rRNA of the 50S subunit between intersubunit bridges B5 and B6. Geometry restraints for TC007 were generated with the help of Grade web server (Global Phasing, grade.globalphasing.org). Manual modeling was done in Coot and was followed by several rounds of reciprocal space refinement of atomic coordinates and B-factors. Crystallographic statistics are reported in Table S1. All figures were generated using PyMOL 1.5 (https://pymol.org/2/) (Schrödinger). Local structure alignments were performed in Coot (77). Ribosomal proteins are named throughout the paper according to the newly established nomenclature (78). Atomic coordinated and structure factors for structures

of 80S–paromomycin, 80S–gentamicin, 80S–TC007, 80S–geneticin (G418), 70S-tRNAs-mRNA–TC007 (cocrystallization), and 70S–tRNAs–mRNA–TC007 (soaking) have been deposited in the Protein Data Bank (https://www.rcsb.org/pdb/home/home.do) under ID codes 5NDV (80S–paromomycin), 5OBM (80S–gentamicin), 5NDW (80S–TC007), 5NDG [80S–geneticin (G418)], 5NDK (70S–tRNA–mRNA–TC007 cocrystallized), and 5NDJ (70–tRNA–mRNA–TC007 soaked).

Preparation of Native and Fluorescently Labeled tRNAs. *E. coli* $tRNA^{fMet}$ and $tRNA^{Phe}$ were purified as previously described (79, 80). Aminoacylation and fluorescent labeling of tRNAs ($tRNA_i^{Met}$ at $4sU^8$ and $tRNA^{Phe}$ at acp^3 U47 positions) were performed following established protocols.

In Vitro Reconstitution of 80S ICs. As previously described (45), 80S ICs were assembled following a procedure that bypasses the need for exogenous initiation factors (81). Purified 40S subunits were mixed with an equal volume of 80S association buffer [30 mM Hepes (pH 7.5), 5 mM $MgCl_2$, 50 mM NH_4Cl, 2 mM spermidine, 5 mM putrescine, 1 mM DTT] and then were heat activated at 42 °C for 5 min. Fourfold excess of mRNA with the sequence 5′-CAA CCU AAA ACU UAC ACA CCC UUA GAG GGA CAA UCG AUG UUU UUU UUU UUU UUU UUU UUU-3′ (Dharmacon) (henceforth referred to as "*MFF* mRNA") or 5′-CAA CCU AAA ACU UAC ACA CCC UUA GAG GGA CAA UCG AUG UCU UUC UUC UUC UUC UUC UUC-3′ (henceforth referred to as "MFF near-cognate mRNA") was added, heated to 37 °C for 10 min and subsequently cooled on ice. To this mixture, a twofold excess of fluorescently labeled Met-$tRNA_i^{Met}$ (prepared as described in ref. 82) was added, and the reaction was heated and cooled as above. At this time, equimolar amounts of 60S subunits were heat activated at 42 °C for 5 min. The 60S subunits were then added to the mixture of 40S/tRNA/mRNA. After an additional heating and cooling cycle, the $MgCl_2$ concentration of the reaction was raised to 15 mM, and the mixture remained on ice for 5 min. It was then loaded on a 10–30% sucrose gradient in 80S association buffer and was ultracentrifuged in a Beckman SW41 rotor at 35,000 rpm for 1.5 h at 4 °C before fractionation. The peak corresponding to 80S complexes was collected and aliquoted before storage in liquid nitrogen. To achieve surface immobilization, the mRNA was hybridized to a double-stranded, biotinylated DNA oligonucleotide (sequence 1: 5′-GTA AGT TTT AGG TTG CCC CCC TTT TTT TTT TTT TTT TTT TTT TTT TTT TTT-3′; sequence 2: 5′-AAA AAA AAA AAA AAA AAA AAA AAA AAA AAA AAA-3′) before its mixture with the 40S subunit.

Formation of the eEF1A(GTP)–aa-tRNA Ternary Complex. aa-tRNAs ($tRNA^{Phe}$, $tRNA^{Met}$) were first generated as previously described (82) and were mixed with 1 mM GTP, 6 mM phosphoenolpyruvate, 12 units/mL pyruvate kinase, and 12 units/mL myokinase. A twofold excess of eEF1A isolated from rabbit reticulocyte lysate (45), which bears 100% sequence identity with human eEF1A, was then added, and the mixture was incubated at 37 °C for 5 min to form the ternary complex.

Single-Molecule Fluorescence Imaging. Complexes were surface-immobilized via the biotin–streptavidin interaction in PEG-passivated quartz chambers. All imaging experiments were performed in Hepes (KOH)-Polymix buffer (pH 7.5) containing 5 mM $MgCl_2$, 50 mM NH_4Cl, 2 mM spermidine, and 5 mM putrescine, as well as an oxygen scavenging system (2 mM protocatechuic acid, 50 nM protocatechuate 3,4-dioxygenase) together with a mixture of solution additives (1 mM Trolox, 1 mM cyclooctatetraene, 1 mM nitrobenzyl-alcohol) (83) to reduce photobleaching. As previously described (82), single-molecule fluorescence imaging was performed using a custom prism-based total internal reflection fluorescence microscope. Cy3 fluorophores were illuminated with an Opus 532-nm solid-state laser (Laser Quantum), and fluorescence emissions from Cy3 and Cy5 fluorophores were collected using a 60×, 1.27 NA Plan-Apo water immersion objective (Nikon) and were spectrally separated using a MultiCam-LS device (Cairn) equipped with a T635lpxr-UF2 dichroic mirror (Chroma) and imaged onto ORCA-Flash 4.0 v2 sCMOS cameras (Hamamatsu). Data were acquired at 40-ms time resolution using custom software implemented in LabVIEW (National Instruments).

Single-Molecule tRNA Selection Assay. As previously described (45), the process of tRNA selection on the ribosome was performed by stopped-flow injection of a 20-nM solution of ternary complex [eEF1A(GTP)–aa-tRNA] containing (Cy5)Phe-$tRNA^{Phe}$ into surface-immobilized ribosome complexes containing (Cy3)$tRNA_i^{Met}$ in the P-site. Here, 80S ICs were formed with the near-cognate UCU mRNA codon in the A-site, and the period of incubation with the ternary complex was extended from 30 s to 2 min. To prevent spurious, nonenzymatic binding of deacylated $tRNA^{Phe}$ to the E-site, tRNA selection experiments were performed in the presence of 500 μM cyclohexamide. Subsequent steady-state imaging of PRE complexes was performed following buffer exchange into a solution lacking the ternary complex.

Analysis of smFRET Data. Analysis of single-molecule fluorescence data was performed using the SPARTAN analysis software package MATLAB (84). Single-molecule fluorescence traces were extracted from wide-field movies and were corrected for background, spectral crosstalk, and unequal apparent brightness (85). FRET trajectories were calculated as $E_{FRET} = I_A/(I_A + I_D)$, where I_A and I_D are the acceptor and donor fluorescence intensities at each frame, respectively. Traces were selected for further analysis according to the following criteria: (*i*) single-step photobleaching; (*ii*) signal-to-background noise ratio >8; (*iii*) fewer than four donor blinking events; and (*iv*) >0.12 FRET efficiency for at least 50 frames (2 s). FRET histograms were calculated from the first 50 frames of all individual molecules passing the aforementioned criteria from each dataset with bin sizes of 0.03.

ACKNOWLEDGMENTS. We thank Daniel S. Terry for helpful discussions and support with smFRET data analysis; the French Infrastructure for Integrated Structural Biology ANR-10-INSB-05-01 and Instruct, which is part of the European Strategy Forum on Research Infrastructures; all staff members of SOLEIL synchrotron PROXIMA-1 beamline; and all staff members of Swiss Lightsource synchrotron PX-1 beamline. This work was supported by French National Research Agency (ANR) Grant ANR-15-CE11-0021-01 (to G.Y.); Fondation ARC pour la Recherché sur le Cancer (G.Y.); La Fondation pour la Recherche Médicale Grant DBF20160635745, France (to G.Y.); European Research Council Advanced Grant 294312 (to M.Y.); the Russian Government Program of Competitive Growth of Kazan Federal University (M.Y.); an Association Française Contre les Myopathies Telethon Postdoctoral Fellowship (I.P.); and Grant ANR-10-LABX-0030-INRT from a French State Fund managed by the ANR under the frame program Investissements d'Avenir ANR-10-IDEX-0002-02 (to M.D.). M.D. is an International PhD Program fellow of the Institute of Genetics and Molecular and Cellular Biology supported by LabEx Integrative Biology: Nuclear Dynamics, Regenerative and Translational Medicine funds. Funding support for S.C.B., R.B.A., and A.F. was provided by NIH Grant GM079238 and the Tri-Institutional Stem Cell Initiative supported by the Starr Foundation.

1. Fosso MY, Li Y, Garneau-Tsodikova S (2014) New trends in aminoglycosides use. *MedChemComm* 5:1075–1091.
2. Davies J (1994) Inactivation of antibiotics and the dissemination of resistance genes. *Science* 264:375–382.
3. Borovinskaya MA, et al. (2007) Structural basis for aminoglycoside inhibition of bacterial ribosome recycling. *Nat Struct Mol Biol* 14:727–732.
4. Feldman MB, Terry DS, Altman RB, Blanchard SC (2010) Aminoglycoside activity observed on single pre-translocation ribosome complexes. *Nat Chem Biol* 6:244.
5. Youngman EM, He SL, Nikstad LJ, Green R (2007) Stop codon recognition by release factors induces structural rearrangement of the ribosomal decoding center that is productive for peptide release. *Mol Cell* 28:533–543.
6. Davies J, Gorini L, Davis BD (1965) Misreading of RNA codewords induced by aminoglycoside antibiotics. *Mol Pharmacol* 1:93–106.
7. Fourmy D, Recht MI, Blanchard SC, Puglisi JD (1996) Structure of the A site of Escherichia coli 16S ribosomal RNA complexed with an aminoglycoside antibiotic. *Science* 274:1367–1371.
8. Moazed D, Noller HF (1987) Interaction of antibiotics with functional sites in 16S ribosomal RNA. *Nature* 327:389–394.
9. Recht MI, Fourmy D, Blanchard SC, Dahlquist KD, Puglisi JD (1996) RNA sequence determinants for aminoglycoside binding to an A-site rRNA model oligonucleotide. *J Mol Biol* 262:421–436.
10. Carter AP, et al. (2000) Functional insights from the structure of the 30S ribosomal subunit and its interactions with antibiotics. *Nature* 407:340–348.
11. Ogle JM, Murphy FV, Tarry MJ, Ramakrishnan V (2002) Selection of tRNA by the ribosome requires a transition from an open to a closed form. *Cell* 111:721–732.
12. Ogle JM, et al. (2001) Recognition of cognate transfer RNA by the 30S ribosomal subunit. *Science* 292:897–902.
13. Matt T, et al. (2012) Dissociation of antibacterial activity and aminoglycoside ototoxicity in the 4-monosubstituted 2-deoxystreptamine apramycin. *Proc Natl Acad Sci USA* 109:10984–10989.
14. Demirci H, et al. (2013) A structural basis for streptomycin-induced misreading of the genetic code. *Nat Commun* 4:1355.
15. Jenner L, Demeshkina N, Yusupova G, Yusupov M (2010) Structural rearrangements of the ribosome at the tRNA proofreading step. *Nat Struct Mol Biol* 17:1072–1078.
16. Demeshkina N, Jenner L, Westhof E, Yusupov M, Yusupova G (2012) A new understanding of the decoding principle on the ribosome. *Nature* 484:256–259.
17. Rozov A, Demeshkina N, Westhof E, Yusupov M, Yusupova G (2016) New structural insights into translational miscoding. *Trends Biochem Sci* 41:798–814.
18. Rozov A, et al. (2016) Novel base-pairing interactions at the tRNA wobble position crucial for accurate reading of the genetic code. *Nat Commun* 7:10457.
19. Rozov A, Westhof E, Yusupov M, Yusupova G (2016) The ribosome prohibits the G•U wobble geometry at the first position of the codon-anticodon helix. *Nucleic Acids Res* 44:6434–6441.

20. Wang L, et al. (2012) Allosteric control of the ribosome by small-molecule antibiotics. *Nat Struct Mol Biol* 19:957–963.
21. Wasserman MR, et al. (2015) Chemically related 4,5-linked aminoglycoside antibiotics drive subunit rotation in opposite directions. *Nat Commun* 6:7896.
22. Recht MI, Douthwaite S, Puglisi JD (1999) Basis for prokaryotic specificity of action of aminoglycoside antibiotics. *EMBO J* 18:3133–3138.
23. Fan-Minogue H, Bedwell DM (2008) Eukaryotic ribosomal RNA determinants of aminoglycoside resistance and their role in translational fidelity. *RNA* 14:148–157.
24. Garreau de Loubresse N, et al. (2014) Structural basis for the inhibition of the eukaryotic ribosome. *Nature* 513:517–522.
25. Wilhelm JM, Jessop JJ, Pettitt SE (1978) Aminoglycoside antibiotics and eukaryotic protein synthesis: Stimulation of errors in the translation of natural messengers in extracts of cultured human cells. *Biochemistry* 17:1149–1153.
26. Wilhelm JM, Pettitt SE, Jessop JJ (1978) Aminoglycoside antibiotics and eukaryotic protein synthesis: Structure—function relationships in the stimulation of misreading with a wheat embryo system. *Biochemistry* 17:1143–1149.
27. Palmer E, Wilhelm JM, Sherman F (1979) Phenotypic suppression of nonsense mutants in yeast by aminoglycoside antibiotics. *Nature* 277:148–150.
28. Lee HL, Dougherty JP (2012) Pharmaceutical therapies to recode nonsense mutations in inherited diseases. *Pharmacol Ther* 136:227–266.
29. Baradaran-Heravi A, et al. (2017) Gentamicin B1 is a minor gentamicin component with major nonsense mutation suppression activity. *Proc Natl Acad Sci USA* 114: 3479–3484.
30. Mort M, Ivanov D, Cooper DN, Chuzhanova NA (2008) A meta-analysis of nonsense mutations causing human genetic disease. *Hum Mutat* 29:1037–1047.
31. Xue X, et al. (2014) Synthetic aminoglycosides efficiently suppress cystic fibrosis transmembrane conductance regulator nonsense mutations and are enhanced by ivacaftor. *Am J Respir Cell Mol Biol* 50:805–816.
32. Mattis VB, et al. (2006) Novel aminoglycosides increase SMN levels in spinal muscular atrophy fibroblasts. *Hum Genet* 120:589–601.
33. Keeling KM, Wang D, Conard SE, Bedwell DM (2012) Suppression of premature termination codons as a therapeutic approach. *Crit Rev Biochem Mol Biol* 47:444–463.
34. Wagner KR, et al. (2001) Gentamicin treatment of Duchenne and Becker muscular dystrophy due to nonsense mutations. *Ann Neurol* 49:706–711.
35. Cogan J, et al. (2014) Aminoglycosides restore full-length type VII collagen by overcoming premature termination codons: Therapeutic implications for dystrophic epidermolysis bullosa. *Mol Ther* 22:1741–1752.
36. Agrelo R, et al. (2015) A novel Werner syndrome mutation: Pharmacological treatment by read-through of nonsense mutations and epigenetic therapies. *Epigenetics* 10:329–341.
37. Bordeira-Carriço R, Pêgo AP, Santos M, Oliveira C (2012) Cancer syndromes and therapy by stop-codon readthrough. *Trends Mol Med* 18:667–678.
38. Mattis VB, Tom Chang CW, Lorson CL (2012) Analysis of a read-through promoting compound in a severe mouse model of spinal muscular atrophy. *Neurosci Lett* 525: 72–75.
39. Ben-Shem A, et al. (2011) The structure of the eukaryotic ribosome at 3.0 Å resolution. *Science* 334:1524–1529.
40. Pfister P, et al. (2005) Mutagenesis of 16S rRNA C1409-G1491 base-pair differentiates between 6′OH and 6′NH3+ aminoglycosides. *J Mol Biol* 346:467–475.
41. Byrne KM, Kershner AS, Maehr H, Marquez JA, Schaffner CP (1977) Separation of gentamicin C-complex into five components by Craig distribution. *J Chromatogr A* 131:191–203.
42. Iannaccone ST, Smith SA, Simard LR (2004) Spinal muscular atrophy. *Curr Neurol Neurosci Rep* 4:74–80.
43. Lefebvre S, et al. (1995) Identification and characterization of a spinal muscular atrophy-determining gene. *Cell* 80:155–165.
44. Mattis VB, Ebert AD, Fosso MY, Chang CW, Lorson CL (2009) Delivery of a read-through inducing compound, TC007, lessens the severity of a spinal muscular atrophy animal model. *Hum Mol Genet* 18:3906–3913.
45. Ferguson A, et al. (2015) Functional dynamics within the human ribosome regulate the rate of active protein synthesis. *Mol Cell* 60:475–486.
46. Munro JB, Altman RB, O'Connor N, Blanchard SC (2007) Identification of two distinct hybrid state intermediates on the ribosome. *Mol Cell* 25:505–517.
47. Bar-Nun S, Shneyour Y, Beckmann JS (1983) G-418, an elongation inhibitor of 80 S ribosomes. *Biochim Biophys Acta* 741:123–127.
48. Stage TK, Hertel KJ, Uhlenbeck OC (1995) Inhibition of the hammerhead ribozyme by neomycin. *RNA* 1:95–101.
49. von Ahsen U, Davies J, Schroeder R (1991) Antibiotic inhibition of group I ribozyme function. *Nature* 353:368–370.
50. Mikkelsen NE, Brännvall M, Virtanen A, Kirsebom LA (1999) Inhibition of RNase P RNA cleavage by aminoglycosides. *Proc Natl Acad Sci USA* 96:6155–6160.
51. Melnikov SV, Söll D, Steitz TA, Polikanov YS (2016) Insights into RNA binding by the anticancer drug cisplatin from the crystal structure of cisplatin-modified ribosome. *Nucleic Acids Res* 44:4978–4987.
52. Weisblum B, Davies J (1968) Antibiotic inhibitors of the bacterial ribosome. *Bacteriol Rev* 32:493–528.
53. Gupta P, et al. (2016) Nascent peptide assists the ribosome in recognizing chemically distinct small molecules. *Nat Chem Biol* 12:153–158.
54. Tu D, Blaha G, Moore PB, Steitz TA (2005) Structures of MLSBK antibiotics bound to mutated large ribosomal subunits provide a structural explanation for resistance. *Cell* 121:257–270.
55. Zhang J, et al. (2015) Mechanisms of ribosome stalling by SecM at multiple elongation steps. *Elife* 4:09684.
56. Arenz S, et al. (2016) A combined cryo-EM and molecular dynamics approach reveals the mechanism of ErmBL-mediated translation arrest. *Nat Commun* 7:12026.
57. Tsui WH, et al. (2004) Dual effects of MLS antibiotics: Transcriptional modulation and interactions on the ribosome. *Chem Biol* 11:1307–1316.
58. Budkevich T, et al. (2011) Structure and dynamics of the mammalian ribosomal pretranslocation complex. *Mol Cell* 44:214–224.
59. Wilson DN, Nierhaus KH (2006) The E-site story: The importance of maintaining two tRNAs on the ribosome during protein synthesis. *Cell Mol Life Sci* 63:2725–2737.
60. Kozak M (1978) How do eucaryotic ribosomes select initiation regions in messenger RNA? *Cell* 15:1109–1123.
61. Bock LV, Blau C, Vaiana AC, Grubmüller H (2015) Dynamic contact network between ribosomal subunits enables rapid large-scale rotation during spontaneous translocation. *Nucleic Acids Res* 43:6747–6760.
62. Liu Q, Fredrick K (2013) Contribution of intersubunit bridges to the energy barrier of ribosomal translocation. *Nucleic Acids Res* 41:565–574.
63. Hobbie SN, et al. (2008) Genetic analysis of interactions with eukaryotic rRNA identify the mitoribosome as target in aminoglycoside ototoxicity. *Proc Natl Acad Sci USA* 105: 20888–20893.
64. Böttger EC, Springer B, Prammananan T, Kidan Y, Sander P (2001) Structural basis for selectivity and toxicity of ribosomal antibiotics. *EMBO Rep* 2:318–323.
65. Manuvakhova M, Keeling K, Bedwell DM (2000) Aminoglycoside antibiotics mediate context-dependent suppression of termination codons in a mammalian translation system. *RNA* 6:1044–1055.
66. El-On J, Bazarsky E, Sneir R (2007) Leishmania major: In vitro and in vivo antileishmanial activity of paromomycin ointment (Leshcutan) combined with the immunomodulator Imiquimod. *Exp Parasitol* 116:156–162.
67. Hobbie SN, et al. (2011) Genetic reconstruction of protozoan rRNA decoding sites provides a rationale for paromomycin activity against Leishmania and Trypanosoma. *PLoS Negl Trop Dis* 5:e1161.
68. Hobbie SN, et al. (2007) Engineering the rRNA decoding site of eukaryotic cytosolic ribosomes in bacteria. *Nucleic Acids Res* 35:6086–6093.
69. Zhao H, et al. (2004) Maternally inherited aminoglycoside-induced and nonsyndromic deafness is associated with the novel C1494T mutation in the mitochondrial 12S rRNA gene in a large Chinese family. *Am J Hum Genet* 74:139–152.
70. Prezant TR, et al. (1993) Mitochondrial ribosomal RNA mutation associated with both antibiotic-induced and non-syndromic deafness. *Nat Genet* 4:289–294.
71. Brown A, Shao S, Murray J, Hegde RS, Ramakrishnan V (2015) Structural basis for stop codon recognition in eukaryotes. *Nature* 524:493–496.
72. Rozov A, Demeshkina N, Westhof E, Yusupov M, Yusupova G (2015) Structural insights into the translational infidelity mechanism. *Nat Commun* 6:7251.
73. Bommer UA, et al. (1996) *Ribosomes and Polysomes*, eds Graham JM, Rickwood D (IRL at Oxford Univ Press, Oxford), pp 271–300.
74. Kabsch W (2010) Xds. *Acta Crystallogr D Biol Crystallogr* 66:125–132.
75. Adams PD, et al. (2010) PHENIX: A comprehensive Python-based system for macromolecular structure solution. *Acta Crystallogr D Biol Crystallogr* 66:213–221.
76. Afonine PV, et al. (2012) Towards automated crystallographic structure refinement with phenix.refine. *Acta Crystallogr D Biol Crystallogr* 68:352–367.
77. Emsley P, Lohkamp B, Scott WG, Cowtan K (2010) Features and development of Coot. *Acta Crystallogr D Biol Crystallogr* 66:486–501.
78. Ban N, et al. (2014) A new system for naming ribosomal proteins. *Curr Opin Struct Biol* 24:165–169.
79. Dunkle JA, et al. (2011) Structures of the bacterial ribosome in classical and hybrid states of tRNA binding. *Science* 332:981–984.
80. Wang L, Altman RB, Blanchard SC (2011) Insights into the molecular determinants of EF-G catalyzed translocation. *RNA* 17:2189–2200.
81. Burgess AB, Mach B (1971) Formation of an initiation complex with purified mammalian ribosomal subunits. *Nature* 233:209–210.
82. Blanchard SC, Kim HD, Gonzalez RL, Jr, Puglisi JD, Chu S (2004) tRNA dynamics on the ribosome during translation. *Proc Natl Acad Sci USA* 101:12893–12898.
83. Dave R, Terry DS, Munro JB, Blanchard SC (2009) Mitigating unwanted photophysical processes for improved single-molecule fluorescence imaging. *Biophys J* 96: 2371–2381.
84. Juette MF, et al. (2016) Single-molecule imaging of non-equilibrium molecular ensembles on the millisecond timescale. *Nat Methods* 13:341–344.
85. Roy R, Hohng S, Ha T (2008) A practical guide to single-molecule FRET. *Nat Methods* 5: 507–516.

Discussion

The study provides structural details of aminoglycoside impact on eukaryotic ribosome from the interesting scope not just as a translation inhibitor but also as a modulator of protein synthesis, a potential treatment for diseases associated with premature termination codons mutations (PreTC). PreTCs appear as a result of point mutations in the genome and lead to the synthesis of non-functional truncated proteins by the ribosome and are responsible for a number of genetic disorders including cystic fibrosis, Duchenne muscular dystrophy, spinal muscular atrophy, Hurler syndrome and ataxia telangiectasia (A-T). Examined aminoglycosides posses a property of forcing the ribosome to bypass premature stop-codons in order to restore the synthesis of full-length functional proteins and can be exploited as a potential treatment strategy for all genetic disorders caused by nonsense mutations.

Current work revealed paromomycin and G418 bound in the decoding site where they directly affect the conformation of A1755 and A1756 that play important role in codon anticodon recognition. Interestingly TC007 due to its 6′-NH_2 group did not bind in the decoding center demonstrating that PreTC read-through could be triggered by rearranging several sites of the ribosome – one below the canonical decoding center and another one between Helix 68 and Helix 70 of the large subunit. Binding of gentamicin provides insight of conformational rearrangements in the decoding site that do not support miscoding.

Another interesting finding is a multiple binding sites that spread in peptide exit tunnel, E-site of the small ribosomal subunit, intersubunit bridge B2c and P-stalk. It should be considered that it might be a result of relatively high 4 mM concentration of aminoglycoside during crystal treatment. Additional studies are required to test the affinity of studied compounds to the secondary binding sites and if they might have any effect on promoting miscoding.

Single molecule FRET experiments that were performed in collaboration with Scott C. Blanchard contribute to our understanding of the aminoglycoside impact on the dynamics of the translational complex. It was demonstrated that depending on the concentration aminoglycosides promote different ribosomal states, which coincide with the effect of multiple binding. In the presence of high concentration they completely inhibit protein synthesis.

The results of the current study shed light on structural aspect of read-through mechanisms and provide structural basis to design compounds for efficient treatment of genetic disorders caused by nonsense mutations.

STRUCTURAL STUDIES OF EUKARYOTIC ELONGATION COMPLEX

Project outline

To date all structural knowledge about the elongation cycle in eukaryotes is provided by cryo-EM reconstructions that laid the groundwork for understanding major conformational rearrangements guiding translocation of tRNAs and mRNA. However, these reconstructions are either low in resolution or detalization in order to provide the structural details of the translocation mechanism. And the understanding of the process in eukaryotes is formed by available cryo-EM reconstructions and high-resolution X-ray structures of analogical complexes from bacteria.

The aim of the project is to narrow the gap in understanding of the eukaryote specific features of elongation cycle by obtaining high resolution X-ray structures of eukaryotic 80S ribosome trapped at different stages of translocation.

During protein synthesis, the macromolecular ligands of the ribosome, that are, messenger RNA, tRNAs, as well as the nascent peptide chain, move through the ribosome in a precise and controlled manner. This is a multistep process in which substrates move in 10-30 Å steps, through structurally and spatially distinct binding sites within a solvent -accessible channel formed by the interface of large and small subunits. Large-scale movements of the ribosome accompany the translocation reaction. During this step, the ribosome changes from the pre-translocational (PRE) to the post-translocational (POST) state as the A- (acceptor) and P- (peptidyl) site bound tRNAs move to the P and E (exit) sites, respectively. The translocation is catalyzed by elongation factor G (EFG) in prokaryotes and elongation factor 2 (eEF-2) in eukaryotes and coupled to the ratchet-like rotation of the small subunit relative to the large subunit. In the classical view of translocation, EF-G/eEF-2 acts by a GTPase switch mechanism similar to a regulatory G protein (Figure 66). One of the main factors contributing to the accuracy of protein synthesis on the ribosome is maintenance of the mRNA reading frame. This maintenance is pivotal and is mainly achieved by the action of the elongation factor 2 in eukaryotes. Interruption of this process can bring disastrous consequences and lead to dysfunction of the cell. Spontaneous shifts in the reading frame result in severe human diseases. However, induction of mRNA slippage like read-through of premature termination codons is shown to have therapeutic potential for the treatment of different diseases associated with premature termination codons.

Main goal of my new PhD project was to solve crystal structures of eukaryotic yeast (*Saccharomyces cerevisiae)* 80S ribosome with messenger RNA, naturally modified eukaryotic

transfer RNAs (tRNAs) and *S. cerevisiae* eEF-2 with non-hydrolysable analogue of GTP in the canonical elongation states (pre-translocation complex).

Current project was started in 2012 by a Postdoc Natalia Demeshkina, who adapted a) 80S ribosome purification from JD1370 (Ben-Shem et al., 2010) to JD1370-ΔStm1 yeast strain; and b) eEF2 protein purification from *S. cerevisiae* (Jørgensen et al., 2002) establishing it in our laboratory. She also found and optimized crystallization conditions of eukaryotic elongation complex of ΔStm1 S. cerevisiae 80S ribosome with eukaryotic S. cerevisiae elongation factor 2 (eEF-2), but in the absence of mRNA and tRNA. However, despite numerous post-crystallization treatment that she tried in order to improve diffraction limit, it stayed around 9 Å.

During my PhD study on this project, the main strategy was the developing the protocols to obtain well-diffracting crystals first for a "minimized" binary complex of ΔStm1 S. cerevisiae 80S ribosome with eukaryotic S. cerevisiae elongation factor 2 (eEF-2) and with non-hydrolysable analogue of GTP, GDPNP, (80S/eEF2/GDPNP) then for more complex, "complete", pre-translocation *S.cerevisiae* 80S ribosome/eEF2/GDPNP/mRNA/tRNAs complex. Thus the project was divided in two parts. During developing the first part of the project the main goal was obtaining of significant improvement in resolution of the binary complex 80S/eEF2/GDPNP. (Inhibitor sordarin was added to lock eEF2 on ribosome and reduce movement while it is bound. Hygromycin B as it was discussed earlier is expected to decrease ratcheting intersubunit movements of the ribosome).

Upon succeeding with the first part the second one was to study functional elongation complexes of *S.cerevisiae* 80S ribosome bound not only with eEF2 and with non-hydrolysable analogue of GTP (GDPNP), but also in the presence of mRNA and natural tRNAs.

Material and methods

Saccharomyces cerevisiae ΔStm 80S ribosomes were purified as was previously described in material and methods of the "'Functional S. cerevisiae 80S ribosome complexes with mRNA and tRNAs studied by X-ray analysis" project.

Purification of elongation factor 2

Native eEF2 was purified from the same strain of *S. cerevisiae* as the 80S ribosomes (i.e. JD1370-ΔStm1) to preserve all natural modifications of the factor. The procedure of the eEF2 isolation published earlier (Jørgensen et al., 2002) was modified and proceed as follows below.

Yeast cells were grown in a 6 L YPAD medium and harvested at 5-6 AU. After breaking cells with microfluidizer, the lysate treatment and isolation of the S30 and S100 fractions, eEF2 was eluted from the SP Sepharose cation exchange chromatography at around 8 mS/cm conductivity. (Figure 41 (A)) A clearly visible band corresponding to eEF2 (93 kDa) was identified within the recovered fractions of the selected peak. Next, a peak at around 18 mS/cm conductivity of the Q Sepharose anion exchange chromatography was found to contain eEF2 (Figure 41 (B)). Fractions containing mostly eEF2 were selected for Superdex 200 column (Figure 41 (C)). The peak fractions were analyzed on PAGE. The final sample presents no major protein contaminants. (Figure 41 (D)) was flash frozen in the buffer with 10% glycerol and stored at minus 80^{o}C.

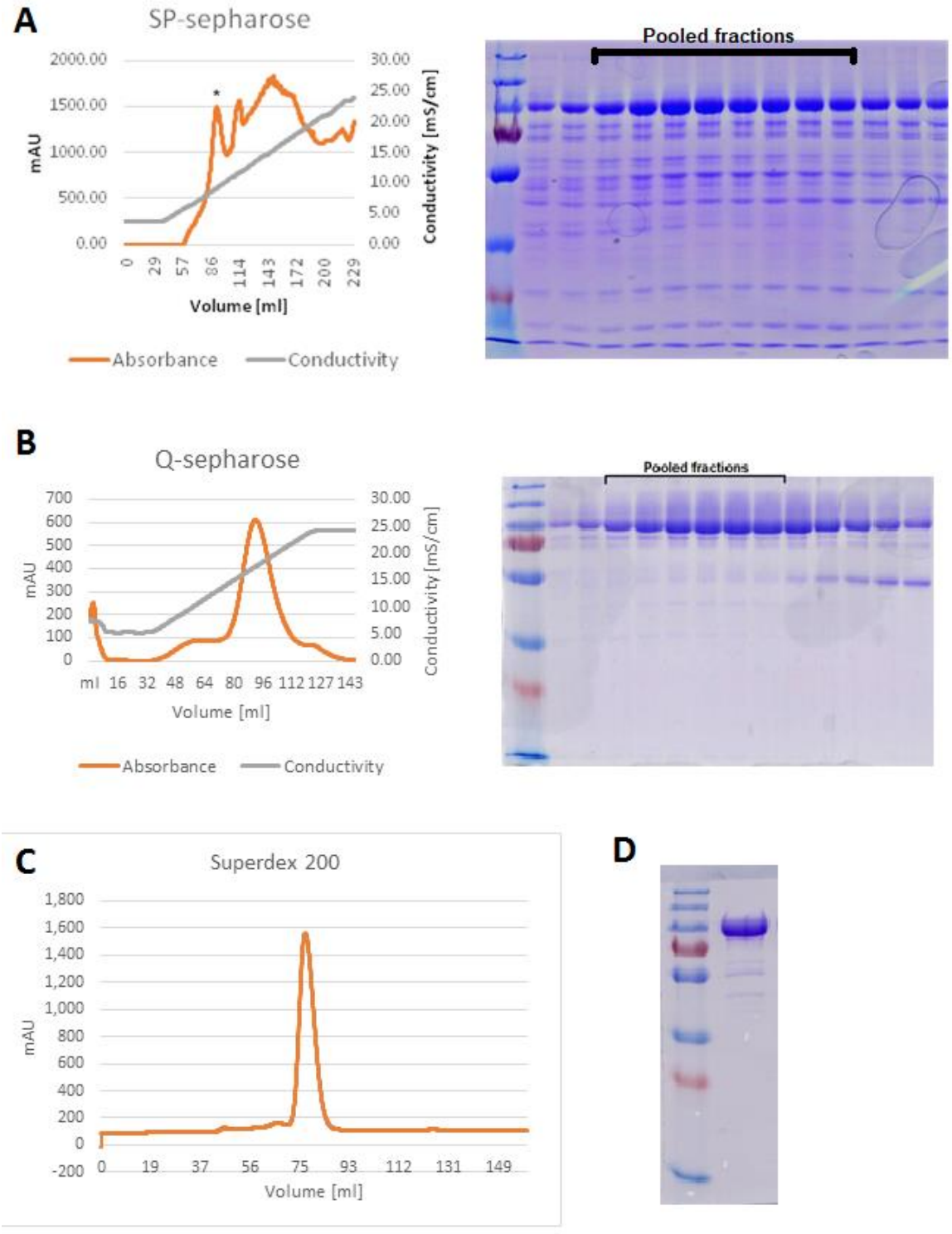

Figure 41. Purification steps of the native eEF2 from S. cerevisiae by three succeeding chromatography methods, and fractions analysis by SDS-PAGE. (A) Anion-exchange step (pooled fractions are marked with star), (B) cation exchange step, (C) gel-filtration chromatography and (D) SDS-PAGE of final sample. Pooled fractions are indicated.

Mass spectrometry

The identity of the protein product was confirmed by the mass spectrometry analysis at the Proteomics Platform of IGBMC. Additional mass of 146.1 Da was identified on VNILDVTLHADAIHR peptide (residues 686 – 700), that could refer to diphthamide. However, the PSM score for VNILDVTLHADAIHR peptide was 3, indicating that this peptide was detected with lower abundance.

Complex formation and crystallization

The initial trials were focused on a crystallization of a binary complex of the 80S ribosome with eEF2 bound in the presence of nonhydrolyzable analog of GTP, GMPPNP (5'-guanylyl imidodiphosphate) and an antifungal compound sordarin known to inhibit the release of the factor from the yeast ribosome (Jørgensen et al., 2003; Justice et al., 1998).

The 80S/eEF2/GDPNP/Sordarin complex was formed in buffer 10 mM Hepes-KOH, 4 mM $Mg(Ac)_2$, 40 mM KAc, 10 mM NH_4Cl, pH 7.5. The eEF2/GDPNP/Sordarin mixture was incubated for 30 min at room temperature before adding to the 80S ribosomes (7.5 mg/mL), which were also pre-incubated for 15 min at 30°C. The factor mix was incubated with the ribosomes for 25 min at 30°C. The eEF2 factor was used at four-fold excess over the ribosomes and concentrations of GDPNP and sordarin were 0.15 and 0.05 mM, respectively. Detergent deoxy big CHAPS (CalBioChem) was added to the complex to the concentration of 2 CMC and the complex was slowly cooled down to 4°C. The complex was crystallized at 4°C by vapor-diffusion in the MRC-48 siting drop plates (Hampton Research) by mixing 3 µL of the complex with 3 µL of the reservoir solution (100 mM bis-Tris-HCl, pH 7.0, 300 mM NH_4SCN, 100 mM KCl, 9.25% – 9.8% PEG 20,000, 3 mM $Mg(Ac)_2$, 2% glycerol, 1% sucrose, 5 - 7.5 mM putrescine or 0.5 – 1.0 mM spermidine). Crystals appeared after 3 days and grew to their full size during 14 days.

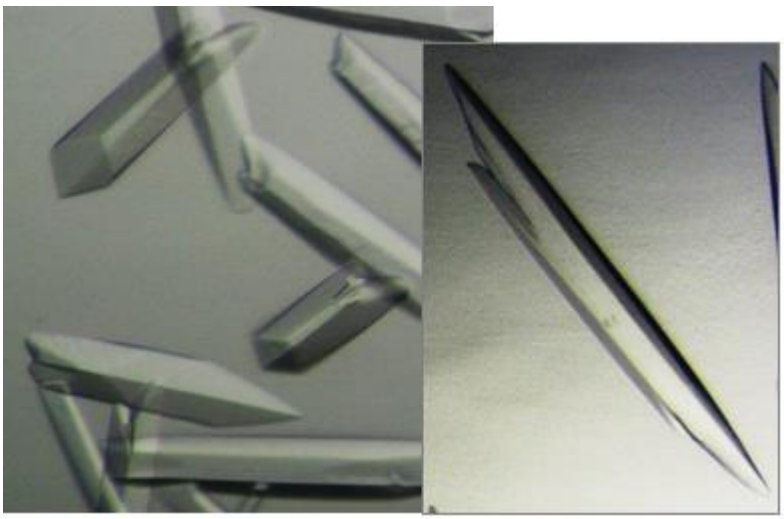

Figure 42.Obtained crystal form of binary complex of *S.cerevisiae* 80S ribosome with *S.cerevisiae* eEF2.

Results

Reproduction of the crystallization and treatment

Post-crystallization treatment is commonly used in X-ray crystallography to protect the crystals from the cryogenic temperature during X-ray data collection and to stabilize them by reducing the solvent content. Crystal treatment allows introducing cryo-protectant agents to prevent ice formation within the crystal to avoid that it is destroyed during freezing due to the fact that water when it crystallizes into ice expands and thereby explodes the crystal. Having cryo-protectant will make ice freeze as a glass where it is not ordered and does not expand. Furthermore collecting data at low temperatures also lowers radiation damage so that more data can be collected from each crystal.

Stabilized crystals are subsequently exposed to X-ray radiation at a synchrotron. Long-term experience in the ribosomal crystallography gathered in our laboratory suggests that each crystal form has a very narrow optimum of treatment that, in most of the cases, is found experimentally and is rarely deduced theoretically. Therefore, to overcome this obstacle an extensive search for post-crystallization treatment conditions has to be conducted in different projections. However before making any screening it was important to master all biochemistry methods relative to the project.

After successful reproduction of crystallization conditions and the best post-crystallization treatment established previously crystals were diffracting around 15 Å. The treatment included two step:

1 – incubating for 20h the droplet containing crystals with a ML solution in higher concentrations of 10.5% PEG 20k, 5 mM spermidine, 15 mM MgAc2 and finally 100 mM bis-Tris HCl pH 5.4. The idea was to stabilize ribosomes, which should make crystals firmer.

2 – inducing cryoprotectant solution by stepwise increase of either PEG 400 to 28% or MPD to 35%.

Despite stabilization step the crystals remained quite fragile. Few attempts were made to improve current crystal treatment by slight modifications in composition of cryoprotectant that did not result in any improvement. So it was clear that radical changes of crystal treatment are required.

Optimization of crystallization conditions and development of new crystal treatment

The first modification was introduced to crystallization conditions. Crystallization trials with different polyamines clearly indicated that putrescine had the best effect on crystal size and form.

Additionally 1.25 mM Dithiothreitol (DTT) a reducing agent was introduced to prevent forming of intramolecular and intermolecular disulfide bonds between cysteine residues of proteins. 0.6 mM Hygromycin B was another compound used in crystallization, as it comes from the positive experience obtained during the first project where it favored crystallization by supposedly reducing ratcheting movement between two ribosomal subunits. In the result crystals became larger (Figure 43).

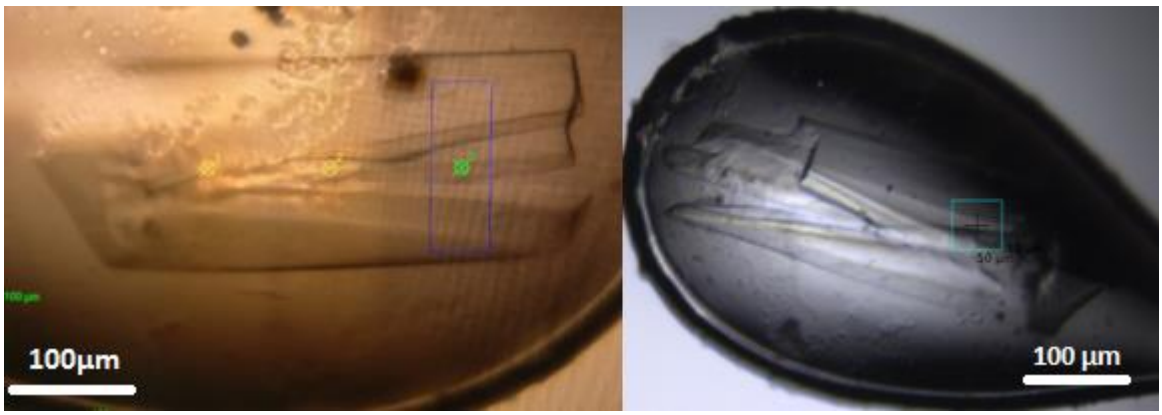

Figure 43. Appearance of crystals after introduced modifications in crystallization conditions

The next step was to identify the effect of different cryo-protectants on crystal diffraction. Among all cryoprotectants tested earlier glycerol was the best fit. Stepwise increase of glycerol up to 30% with prior 20h stabilization as described before improved diffraction limit to 7-8 Å. Which indicated that not only it worked as a cryo-protectant, but also has a positive effect on crystal order. And as expected cryo-protection alone was insufficient to obtain high resolution.

Crystals of macromolecules are often composed of approximately 50% solvent on the average, therefore they can be considered to be in an ordered gel state with a very few intermolecular contacts, which provide the lattice interactions essential for crystal maintenance. Decreasing water content by dehydration procedure usually makes molecules inside pack tighter and solidifies crystal. Usually alcohols like EG, PEG, MPD or salts like $(NH_4)_2SO_4$ are used as dehydration agents. There are several classic methods for protein crystal dehydration: simple air drying, vapour diffusion with salts or soaking with dehydrating compounds (Heras & Martin, 2005). Therefore it was decided to apply dehydration alongside with stabilization step.

Three saturated salts were empirically tested as an effective dehydration reservoir: LiBr, $MgCl_2$, and $Mg(NO_3)_2$. The crystallization reservoir was replaced by one of the salts and the droplet was sealed back to continue vapor diffusion. In agreement with the work of Greenspan,

1976 LiBr was the most efficient and dehydrated the droplet to approximately 2.5 µl in 8 hours, while $MgCl_2$, and $Mg(NO_3)_2$ required 18 and 25 hours respectively. It was decided to use $MgCl_2$ as it provides a relatively soft dehydration compared to LiBr, and the incubation time matches overnight range which allows for an efficient workflow.

Since the droplet is shrinking more than twice in the volume the concentration of all compounds is significantly increasing, therefore the stabilization solution had to be adapted for dehydration experiments accordingly. Testing of different procedures and buffers one approach gave significant improvement. The droplet with the crystals was mixed with the stabilization buffer based on mother liquor with following changes: 7% PEG 20k, 10% glycerol, 13 mM putrescine, 18 mM $Mg(OAc)_2$, 100 mM bis-Tris HCl pH 5.4 and 0.5 mM hygromycin B. Crystallization reservoir was replaced with saturated $MgCl_2$ solution and sealed back with the droplet. After 18 hours incubation 0.7 µl of 50% glycerol were added to assure cryoprotection. In 20-30 minutes crystals were fished and frozen. Diffraction experiments at the SLS synchrotron demonstrate crystals diffracting up to 4 Å limit (Figure 44). Complete dataset at 4.1 Å resolution with cell parameters 233.2 301.3 514.9 90 90 90 was collected using EIGER 16M detector on the PX1 X06SA beamline. The phase problem was solved by molecular replacement with 80S ribosome structure and the obtained electron map revealed clear density for the eEF2.

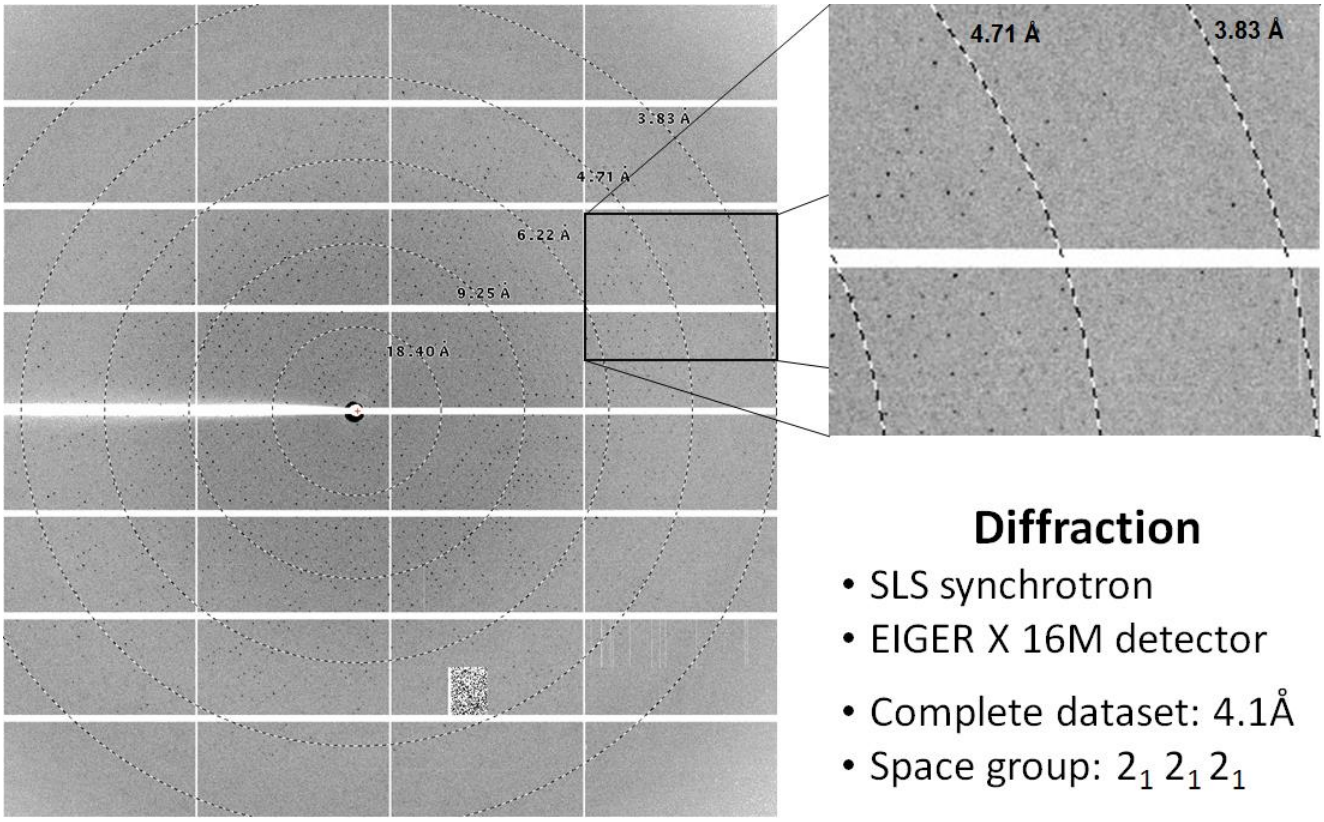

Figure 44.Diffraction image of the vacant 80S ribosome bound with eEF2 crystals.

At this point of the project it became clear that the crystals are capable diffracting at high resolution therefore the focus was switched from binary pre-translocation complex of *S.cerevisiae* 80S ribosome/eEF2/GDPNP to the functional pretranslocation complex of *S.cerevisiae* 80S ribosome/eEF2/GDPNP/mRNA/tRNAs.

Crystallization screening of different mRNAs constructs revealed that length of mRNA effects on the crystal growth, the longer the construct was the smaller the crystals grew. The mRNA construct of nine uracil long (U_9), containing three consecutive phenylalanine codons, and phenylalanine specific deacylated tRNA ($tRNA^{Phe}$) from *S.cerevisiae* were chosen as the substrates for the yeast 80S ribosome to form elongation (pre-translocation) *S.cerevisiae* 80S ribosome/eEF2/GDPNP/mRNA/tRNAs complex as this mRNA construct did not interfere crystal growth.

Thus, complex formation of functional pre-translocation complex of *S.cerevisiae* 80S ribosome with eEF2, GDPNP, U_9, $tRNA^{Phe}$ was performed in conditions as described for binary complex. The ratio of 80S ribosomes to eEF2, GDPNP, mRNA, tRNA was 1:1.3:2 respectively. Higher concentrations of functional ligands had a negative effect on crystal size.

To trap the translocation complex in second GTP-hydrolysis state "AlF_4^-/sordarin complex" was formed by addition of GDP and aluminium fluoride (AlF_4^-/) instead of GMPPCP. Previously, it was shown that AlF_4^-mimics the γ -phosphate of GTP (Salsi et al., 2016) during hydrolysis in GTPases. Thus, GDP- AlF_4^- presumably traps 80S ribosome-bound eEF-2 in a transition-like state of GTP hydrolysis with phosphate group still remaining in the pocket. (Ihibitors Hygromycin B and sordarin were added to the incubation mixtures when necessary as it was described for the formation of binary 80S ribosome/eEF2/GDPNP complex).

The crystals with the new mRNA construct and tRNA behave differently with the established post-crystallization treatment resulting in a decline of resolution limit to around 5 Å. So new screening trails were initiated. First major changes that helped to return to 4 Å resolution limit was increasing concentration of mother liquor components on 15% more and complete removal of the all salts in the stabilization solution. The second shift in diffraction limit to 3.5 Å was a result of diluting PEG 20k with PEG 10k. And the final touch that resulted in improving the resolution to 3.1 Å was adjusting concentration of putrescine. Although description of the research of post-crystallization conditions presented here is quite short, it represents constant iteration of sample purification, crystallization and crystal treatment followed by the diffraction examination. A wide range of combinations of components and concentrations could be tried for crystal

treatment that eventually has to be narrowed down to a very specific condition. Even slight deviation of obtained crystallization condition results in a loss of diffraction at high resolution. Majority of screened conditions turned out to be ineffective, some modifications in treatment represented minor changes and therefore were not worth mentioning, especially considering that main results of the project represent the description of obtained high resolution structures.

Part of the crystals was screened on local X-ray source of IGBMC (Rigaku FR-X generator coupled with Dectris Pilatus 300K pixel array detector), however the majority of them were screened directly at SLS synchrotron.

The most efficient conditions of crystallization and post-crystallization treatment were as follows:

a) crystallization - 100 mM bis-Tris-HCl, pH 7.0, 300 mM NH_4SCN, 100 mM KCl, 9.25% – 9.8% PEG 20,000, 1 mM $Mg(Ac)_2$, 2% glycerol, 1% sucrose, 5 mM putrescine

b) Solution for crystal treatment 4.0% PEG 20K, 4.5 mM PEG 10k, 115 mM bis-Tris-HCl, 15 mM putrescine, 15 mM $Mg(Ac)_2$, 10% glycerol, 0.75% sucrose, 1.80 mM DOBC, 2 mM DTT.

After applying above mentioned modifications for complex formation and crystallization the crystal looked as presented in Figure 45.

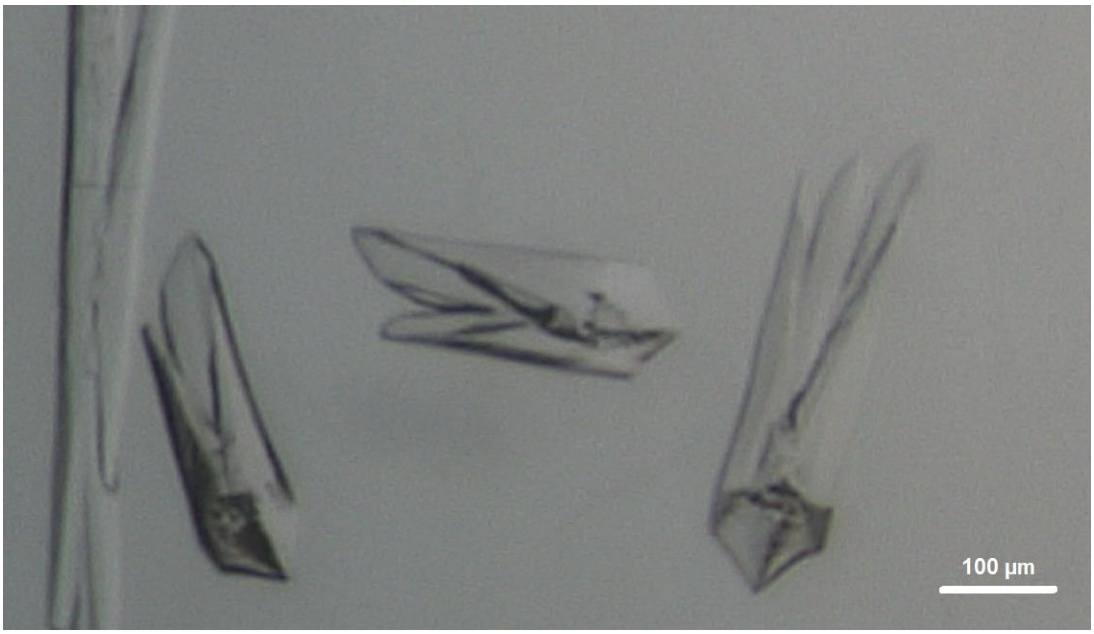

Figure 45.Diffraction image of the vacant 80S ribosome bound with eEF2 crystals.

As a result of the established procedure, we have already collected complete datasets for four *S.cerevisiae* 80S ribosome complexes trapped at the stage of translocation (Table 1). All of these elongation (pre-translocation) *S.cerevisiae* 80S ribosome/eEF2/GDPNP/mRNA/tRNAs complexes contained U_9 as an mRNA construct, $tRNA^{Phe}$ from *S.cerevisiae* and *S.cerevisiae* eEF2 with GDPCP or GDP/- AlF_4. In defined cases sordarin or hygromycin B were added. These were the measures to assure the stabilization of the "translocation intermediate complexes" in order to obtain high resolution diffraction.

Presently, we managed to obtain complete datasets for the following complexes

Number of complex*	**Resolution**	**Hygromycin B**	**Sordarin**	**Nucleotide**
1	3.1 Å	-	+	GDPCP
2	3.1 Å	+	+	GDPCP
3	3.2 Å	-	-	GDPCP
4	3.6 Å	-	+	GDP/AlF_4^-

Table 1. Summary of obtained structures. *Core of all analyzed complexes contained *S.cerevisiae* 80S ribosome with bound *S.cerevisiae* eEF2, U_9 mRNA and *S.cerevisiae* $tRNA^{Phe}$.

Table 2. Complexes of S.cerevisiae 80S ribosome bound with S.cerevisiae eEF2, U_9 as mRNA and S.cerevisiae $tRNA_{Phe}$: data collection and refinement statistics.

	1 - Sordarin/GDPCP	2 - Hygromycin B/Sordarin/GDPCP	3 - GDPCP	4 - Sordarin/AlF_4^-
Resolution range	152.9 - 3.12 (3.232 - 3.12)*	139.4 - 3.15 (3.263 - 3.15)*	139.4 - 3.23 (3.345 - 3.23)*	153.5 - 3.6 (3.729 - 3.6)*
Space group	P 21 21 21	P 21 21 21	P 21 21 21	P 21 21 21
Unit cell	226.56 308.79 528.1 90 90 90	227.34 309.87 529.37 90 90 90	227.34 309.87 529.37 90 90 90	228.1 310.96 529.65 90 90 90
Total reflections	138647657	78993072	35192844	47356657
Unique reflections	651009 (64638)	638636 (63442)	591488 (58811)	432263 (42864)
Multiplicity	217.0 (209.6)	123.7 (88.1)	59.5 (54.5)	109.5 (57.8)
Completeness (%)	99.98 (99.96)	99.97 (99.87)	99.77 (99.89)	99.96 (99.99)
Mean I/sigma(I)	18.17 (0.99)	14.81 (0.97)	14.97 (1.0)	8.24 (1.0)
Wilson B-factor	117.86	118.40	132.11	144.92
R-meas**	52.2% (1348.%)	56.6% (691.6%)	31.2% (819.8%)	92.1% (1072.9%)
CC1/2	100 (38.1)	99.7 (29.5)	99.8 (27.4)	99.9 (28.2)
Reflections used in refinement	651009 (64625)	638636 (63362)	591488 (58796)	432263 (42863)
Reflections used for R-free	1999 (199)	1913 (189)	1945 (193)	1409 (140)
R-work	0.2013 (0.3026)	0.2166 (0.3815)***	0.2213 (0.3768) ***	0.2284 (0.3435) ***
R-free	0.2918 (0.3663)	0.2166 (0.3808) ***	0.2213 (0.3878) ***	0.2284 (0.3419) ***
Number of non-hydrogen atoms	210022	210022	210022	210022
Protein residues	12217	12217	12217	12217
RMS(bonds)	0.013	0.016	0.016	0.004
RMS(angles)	1.73	1.97	1.91	0.69
Average B-factor	123.69	121.16	137.46	139.96
macromolecules	123.74	121.24	137.55	140.05
ligands	110.00	99.99	115.38	117.59

* Statistics for the highest-resolution shell are shown in parentheses

** As defined in Diederichs and Karplus, 1997. The elevated Rmeas is attributed to the high number of crystals and data-sets that were merged and to the method of data collection which results in a large number of relatively weak measurements of each reflection

*** Current structures were only refined and will be built accordingly later

X-ray data collection and integration

All X-ray data collection was performed on the beamline PX1 - X06SA of Swiss Light Source synchrotron. The data was collected with EIGER 6M detector allowing to utilize fine-slicing data collection strategy. As it was shown previously (Mueller et al., 2011) data measurement at a rotation width per image of half the mosaicity improves general statistics. This strategy was modified with highly redundant data collection at low exposure in order to measure accurately a maximum number of times each reflections. In order to reduce radiation damage the beam size was adjusted to around 65x60 µm with $1.87x10^{11}$ ph/s flux and focus on the detector. The oscillation angle was set to 0.01^{O} and exposure time 0.03 second. With the following parameters we were able to collect data in the 370^{O} range without any strong signs of radiation damage. The applied data collection strategy result in 37000 frames per 1 dataset. Considering on the size of the crystals we were able to collect data from multiple spots. The datasets from various crystals with high resolution were scaled together using XSCALE (XDS suite). The phase problem was solved by molecular replacement method utilizing vacant 80S ribosome bound by eEF2 that was previously obtained in the laboratory with cryo-EM technique.

Structure determination and composition

After molecular replacement we observed clear positive density for tRNA and mRNA in the difference map (fo - fc). The model for yeast $tRNA^{Phe}$ as well as mRNA with U_3 sequence were fitted into the density. The second round of rigid body refinement was made in phenix software with individual 6 bodies: large subunit, head, body, platform, eEF2 and tRNA. The model was further improved by 5 cycles of XYZ, real space and individual B-factors refinement with secondary structure restrains. Additional inter chain base pairing restrains, that were confirmed by previously obtained electron density map, were applied between 25S and 5.8S as well as two base pairs between tRNA and mRNA involved in codon anticodon interaction. The reflection data and the refined model were used to calculate feature enhanced map (FEM) (Afonine et al., 2015) in phenix. FEM maps can strengthen a weak signal, if present, and can reduce model bias and noise. Generally FEM maps also appear sharper than 2fo – fc ones (Figure 46).

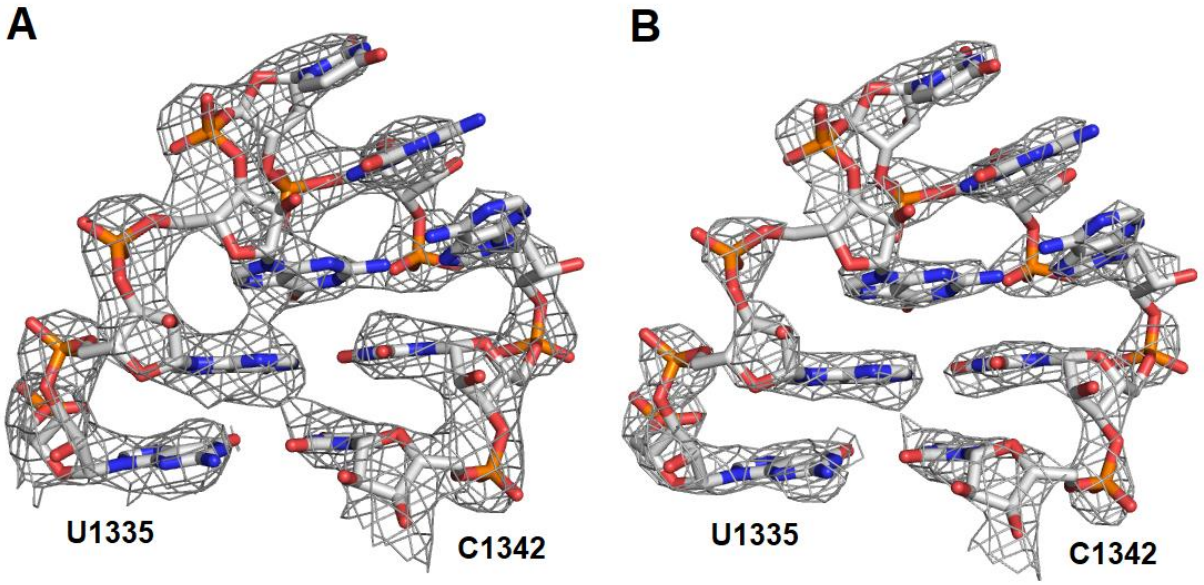

Figure 46. Comparison of obtained A) standart 2fo – fc and B) FEM maps. The region of 18S rRNA is presented.

The quality of the obtained maps at high resolution provided us with a detail information about the position and conformation of backbones and sidechains of the molecules (Figure 47).

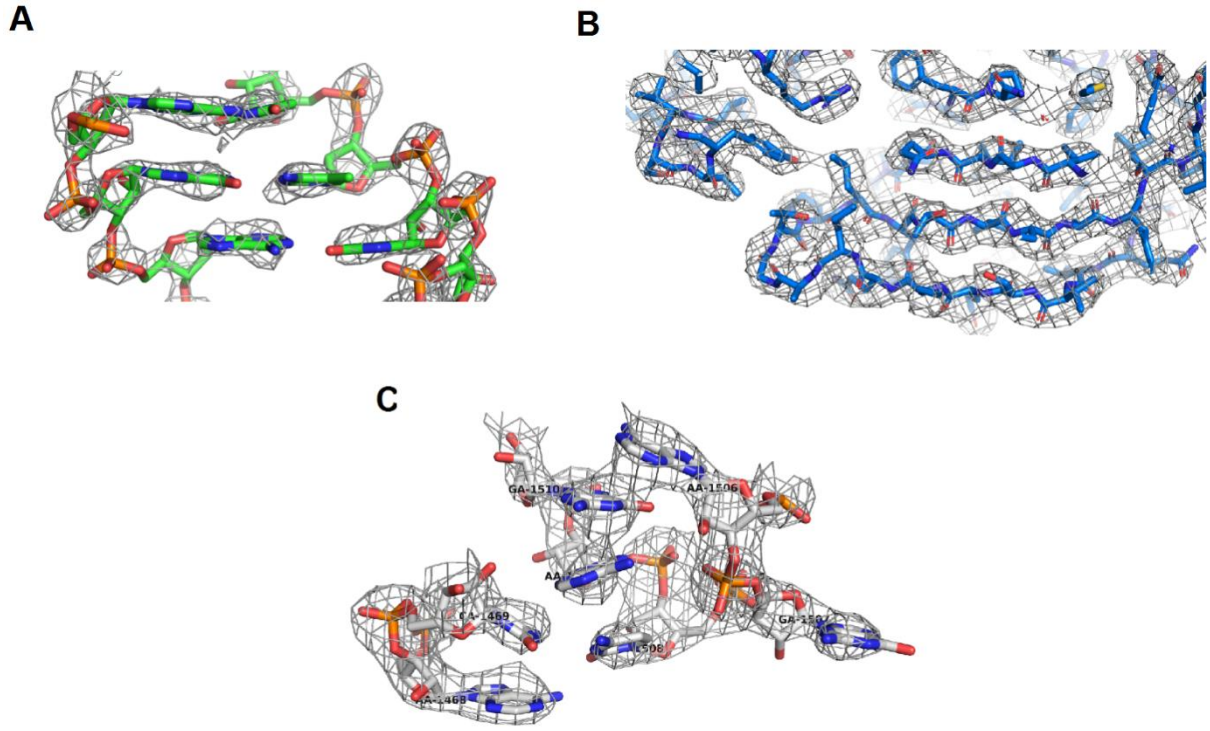

Figure 47. Demonstration of the quality of obtained maps. A) tRNA region (green) with a FEM map at rmsd 2.5. B) Region of eEF2 (blue) fitted in a FEM map at rmsd 2. C) Region of 25S rRNA (grey) with 2fo – fc map at counter level 2 rmsd.

Ribosomal components were manually inspected to fit the map. The majority of rRNA and ribosomal proteins were positioned in the newly obtained map. The regions of the model that deviated from the density were rebuilt. We observed electron density that allowed us to build L1 stalk, which was absent in the model of a vacant ribosome (Ben-Shem et al., 2011). The tRNA presented in our structure interacts with a L1 stalk stabilizing it. However the density of L1 stalk and L1 protein from the solvent side appeared rather weak indicating that it is remaining partially flexible (Figure 48).

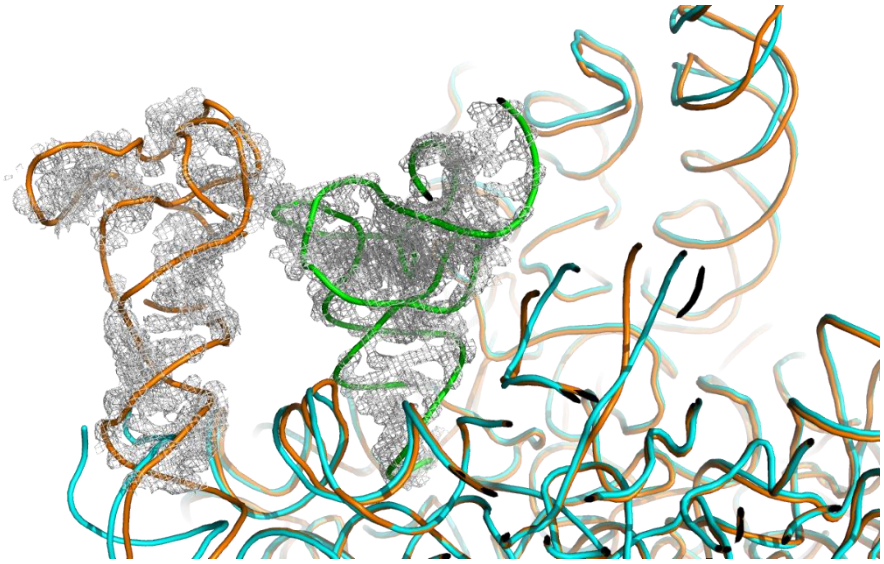

Figure 48. The L1 stalk region of 25S rRNA (orange) with tRNA (green) of obtained structure and superimposed 25S of a vacant ribosome (cyan). The electron density is presented (rmsd 1.5) around L1 stalk and tRNA.

Particular attention was made on functional regions of the ribosome as well as tRNA, mRNA and eEF2. The initially used model of eEF2 was replaced by the crystal structure of elongation factor 2 from *S. cerevisiae* in complex with sordarin (pdb entry 1N0U) that was previously solved at 2.12 Å by Jørgensen et al., 2003. The conformation of eEF2 is slightly different so that the domains had to be reoriented and partially rebuilt. In particular in the 1NOU crystal structure of eEF2 residues 48-67 were missing due to the lack of electron density; hence region from residue 38 to 74, which is situated in proximity to GDPCP, was rebuilt in our structure (Figure 49). It appears that binding to the ribosome fixate this part of eEF2. The density in the GTP binding pocket was clear and allowed us to unambiguously fit GTP (Figure 50). Moreover even this region was identified in the cryo-EM reconstruction the map quality did not allow to build it accurately (Pellegrino et al., 2018).

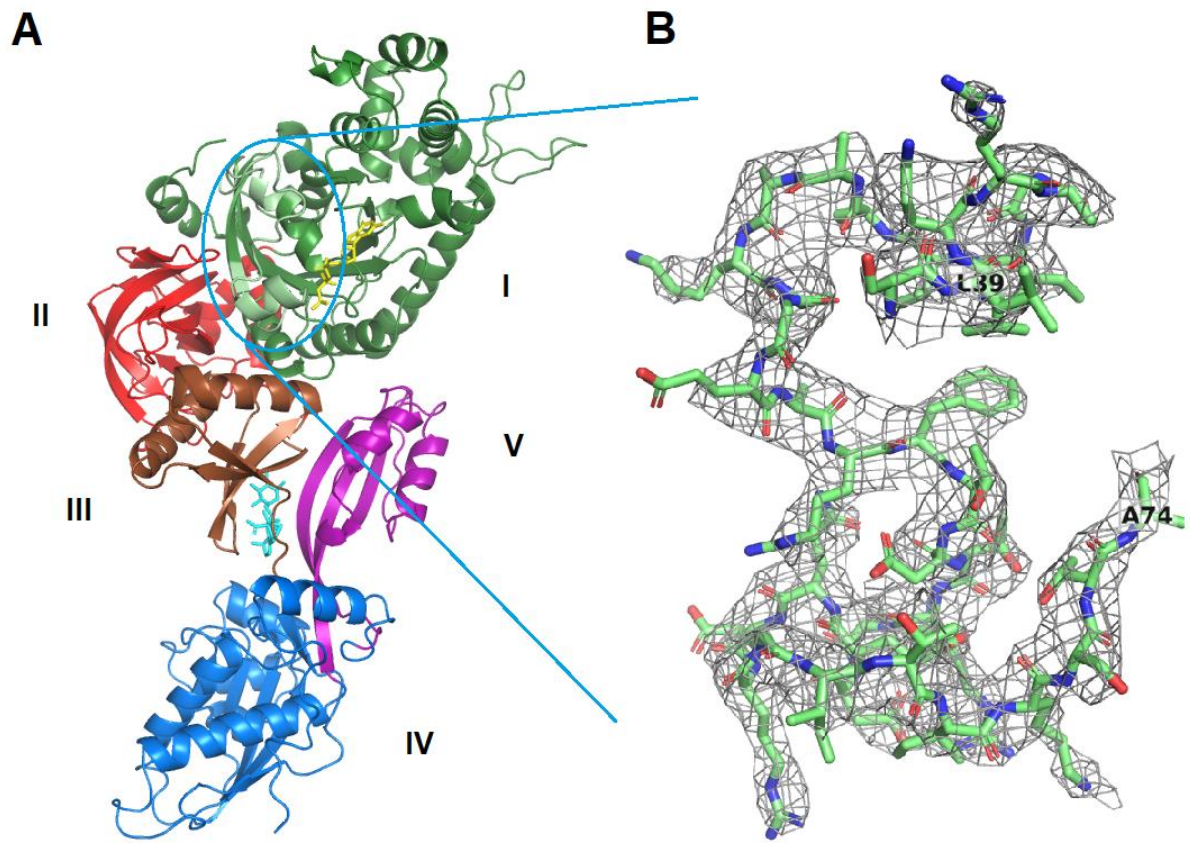

Figure 49. A) Conformation of eEF2 adopted in obtained structures. Domains are distinguished by color. Sordarin and GTP are presented in cyan and yellow colors respectively. Pale green color presents the region of domain I that was absent in 1N0U.B) Residues 38-74 of eEF2 built in the obtained density (contour level 1.8 rmsd)

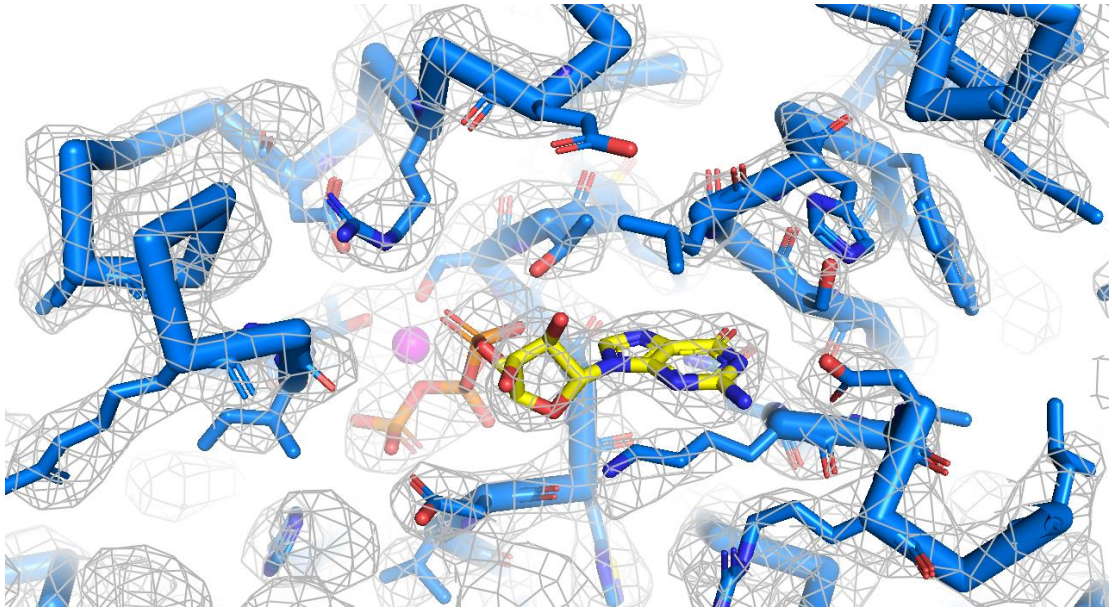

Figure 50. Conformation of the GTP (yellow) binding pocket of eEF2 (blue) with a FEM map at contour level 2 rmsd.

Analysis of the obtained structure

All of the obtained structures represent 80S ribosome in pretranslocation state with mRNA, one tRNA in a hybrid P/E conformation and bound by eEF2 (Figure 51).

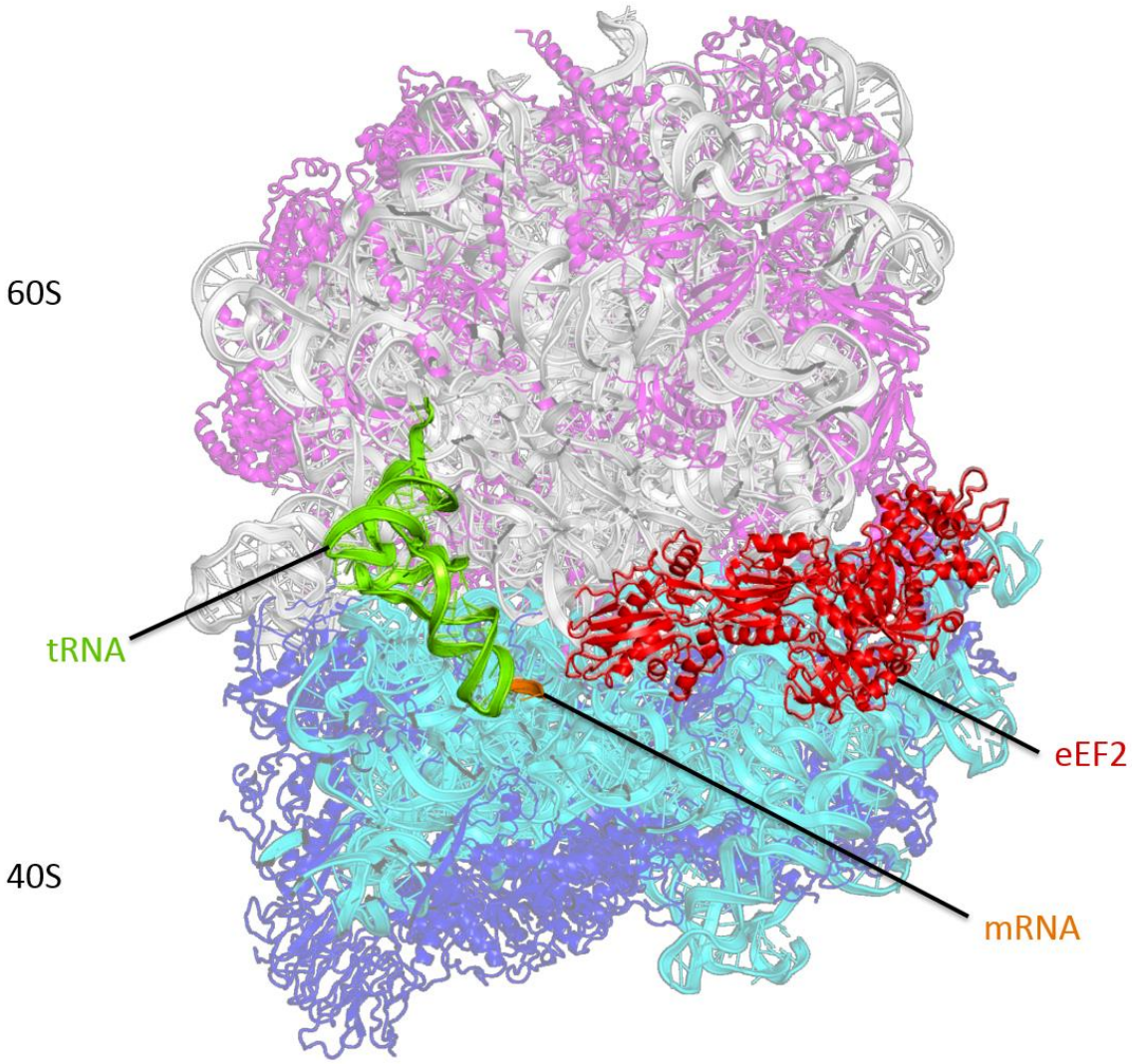

Figure 51. Overall view of obtained structure of 80S pretranslocation complex. 80S ribosome is presented slightly transparent in order to highlight functional ligands.

The structure of GDPCP complex with sordarin had the highest resolution 3.1 Å and therefore will be used for description.

Subunit rotation

The 40S ribosome subunit is counterclockwise rotated ~12° with respect to the 60S as viewed from the solvent side in comparison to the non rotated structure of cryo-EM reconstructed *S. cerevisiae* ribosome (Svidritskiy et al., 2014) (Figure 52). To measure this angle two ribosomes were superimposed on 60S subunits in PyMol. The command “angle_between_domains” was used to calculate the angle between two 40S subunits.

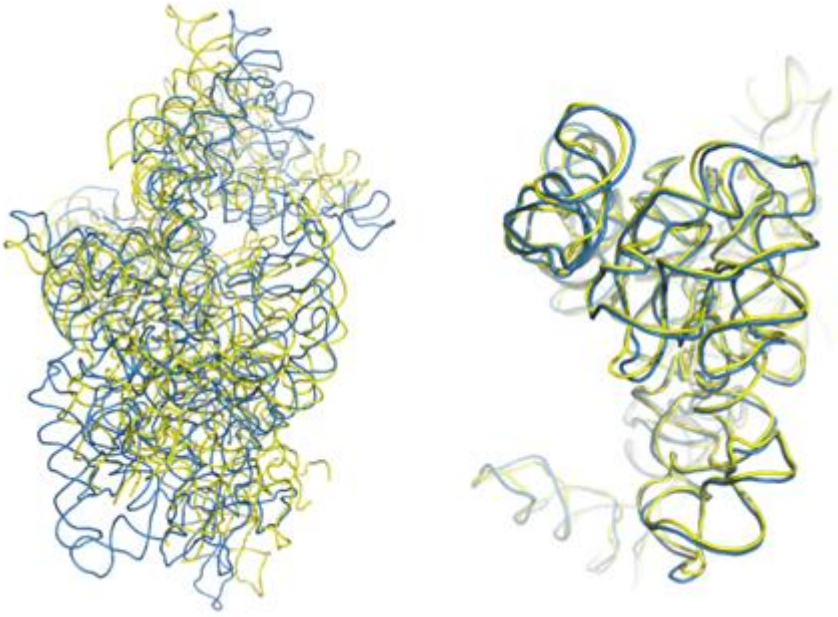

Figure 52. On the left view of the 40S subunits from the solvent side of the ribosome of obtained structure (yellow) aligned on 60S subunit with non rotated ribosome from 3J78 (blue). On the right view of the head of 40S subunit from the solvent side of the obtained structure and of non rotated ribosome 3J78. Ribosomal RNA presented only.

The head of the 40S subunit is swiveled by ~1.8° as compared to non rotated state (pdb entry 3J78) (Figure 52). In this case two ribosomes were superimposed on 40S subunits and the head region was input for the command angle_between_domains.

In comparison to cryo-EM reconstructions with eEF2 (6GQV) (Pellegrino et al., 2018a) rotation of the 40S is similar in both structure (~1.7°), while swiveling (rotation of the head of 40S) differ significantly ~9° (Figure 53).

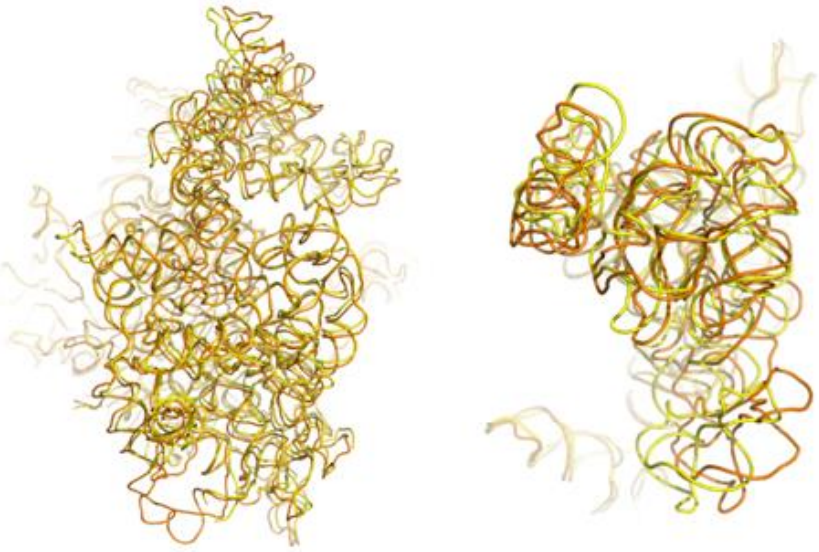

Figure 53. On the left view of the 40S subunits from the solvent side of the ribosome of obtained structure (yellow) aligned on 60S subunit with similar complex solved by cryo-EM 6GQV (orange). On the right view of the head of 40S subunit from the solvent side of the obtained structure and 6GQV. Ribosomal RNA presented only.

Superimposition with the analogous prokaryotic structure also with P/E state tRNA and EFG (4V90) (Chen et al., 2013) revealed the difference of ~5.6° of small subunit rotation and ~3° of the head (Figure 54).

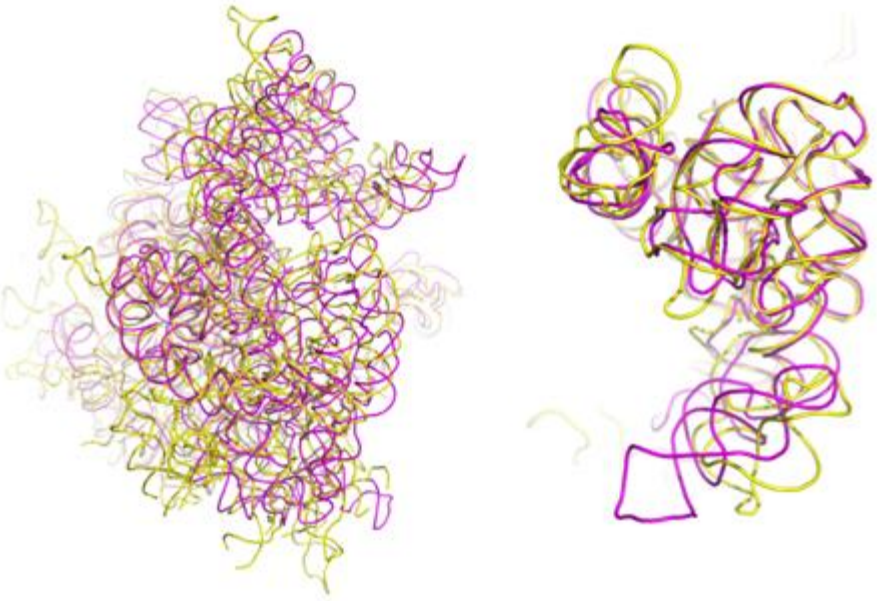

Figure 54. On the left view of the 40S subunits from the solvent side of the ribosome of obtained structure (yellow) aligned on 60S subunit with analogous complex in bacteria 4V90 (pink). On the right view of the head of 40S subunit from the solvent side of the obtained structure and 30S subunit from 4V90. Ribosomal RNA presented only.

Conformation of eEF2

The conformation that eEF2 adopts inside the ribosome is partially distinct from conformation in a crystal structure of eEF2 with sordarin (pdb entry 1N0U) (Jørgensen et al., 2003). Structural alignment demonstrates rather similar conformation between each domain but different orientation relative to each other (Figure 55).

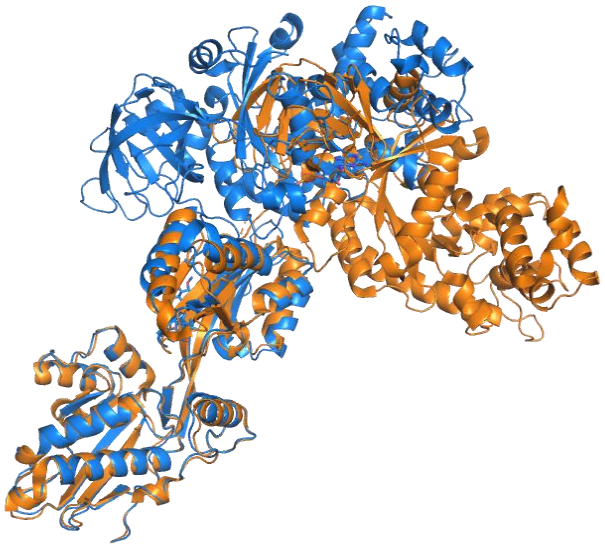

Figure 55. Overview of superimposition of domain IV eEF2 (blue) with a vacant eEF2-sordarin (orange) crystal structure (pdb entry 1N0U).

The superimposition between eEF2 of the obtained structure and derived from cryo-EM (6GQV) (Pellegrino et al., 2018a) revealed similar conformation with an average shift of 0.2 Å (Figure 56).

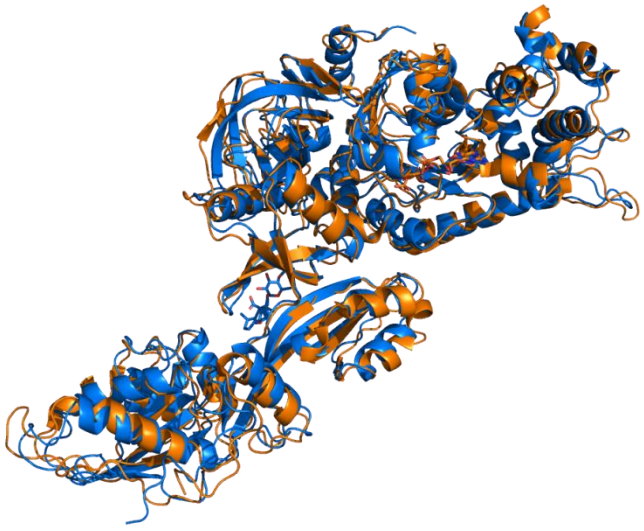

Figure 56. Overview of superimposition of eEF2 (blue) with cryo-EM structure of eEF2 from pretranslocation complex (orange) (pdb entry 6GQV). The structures are presented in cartoon.

The structures of two similar complexes were obtained in the presence and absence of sordarin. As it was amready mentioned, sordarin is an antifungal agent that inhibit protein synthesis by locking eEF2 on ribosome. High resolution structures of eEF2/sordarin bound to the ribosome has not been presented before. The quality of our maps demonstrate clear density for sordarin (Figure 57) and the absence of any direct contact between sordarin and ribosome.

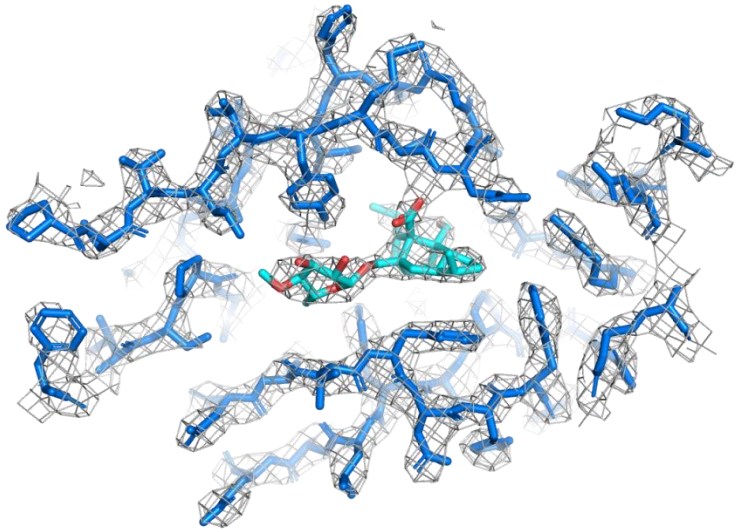

Figure 57. Sordarin (cyan) binding pocket of eEF2 (blue). FEM map contour level 2.5 rmsd.

The structure of the complex without sordarin did not reaveal any significant conformational changes of eEF2 or ribosome. Even the binding pocket of eEF2 has strikingly similar conformation to the one with sordarin (Figure 58).

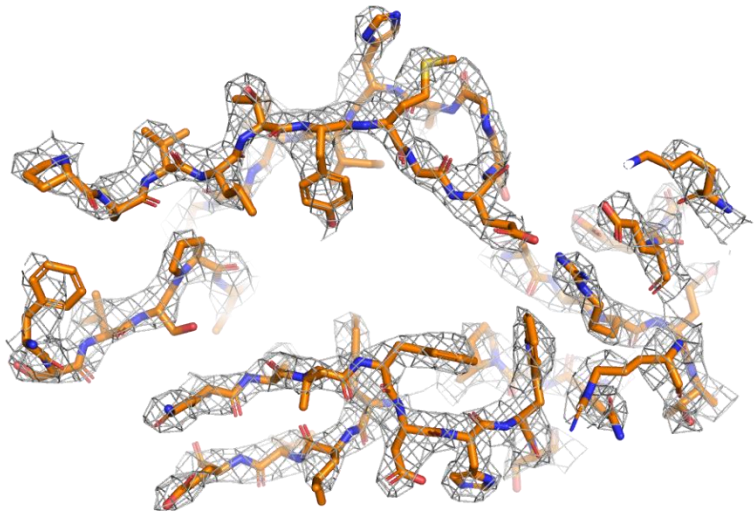

Figure 58. The conformation of sordarin binding pocket in eEF2 (orange) in the structure obtained without sordarin.

The only significant difference in eEF2 in the structure with sordarin that was observed is the presence of a density for an additional ion making contacts with domain IV, which is absent in the structure without sordarin (Figure 59). Mg^{2+} was fitted into the density into the density. However further investigation is required to determine the exact ion.

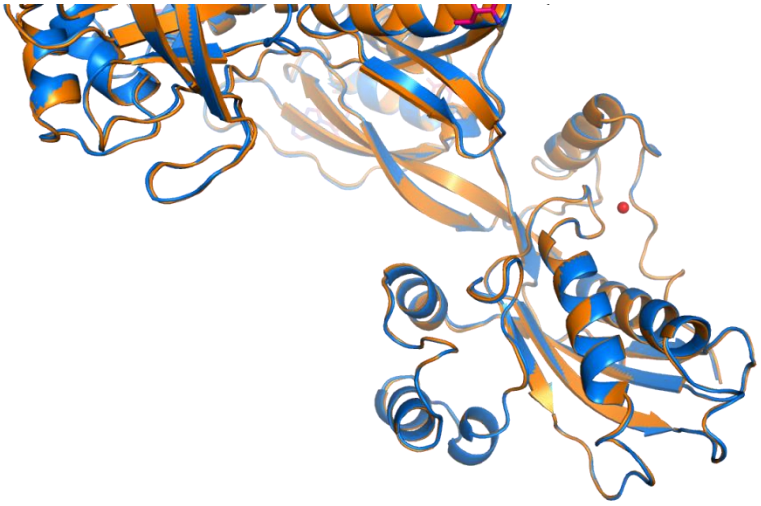

Figure 59. Superimposition of eEF2 from the structures with (blue) and without sordarin (orange). Mg^{2+} that is presented only in the structure with sordarin is shown as a red sphere.

Position of tRNA

At the beginning of translocation the ribosome resides in a dynamic state with peptidyl tRNA shifting between A/A - A/P states and deacylated tRNA in P/P and P/E-sites. At this point eEF2 binds and translocates mRNA and tRNA through the ribosome on +3 nucleotides. The state that we try to mimics resembles the beginning of translocation before GTP hydrolysis when eEF2 binds and locks rotated ribosome with tRNAs in the hybrid A/P P/E state. However in our studies only deacylated tRNAs were used to form this complex, which has lower affinity to the A-site of the ribosome in comparison to peptidyl tRNA. Therefore despite the addition of 2 fold ratio of tRNA to 80S ribosome at the complex formation stage, the obtained structure contained only one tRNA.

As it was expected for ribosomes in ratcheted conformation tRNA was positioned in a hybrid P/E state. Here we compare position of P/E $tRNA^{Phe}$ obtained in our high-resoultion crystal structure of translocation ribosomes complex with positions of tRNAs obtained in low resolution cryo-EM structures (6A) of *S. cerevisiae* ribosomes 80S ribosome complexes with mRNA and tRNA (Svidritskiy et al., 2014). Structural alignment was performed with 1^{st} – non rotated *S.*

cerevisiae ribosomes with two tRNAs bound in P- and E-sites, 2nd – rotated *S. cerevisiae* ribosomes with one tRNA in P/E conformation (Figure 60) (Svidritskiy et al., 2014).

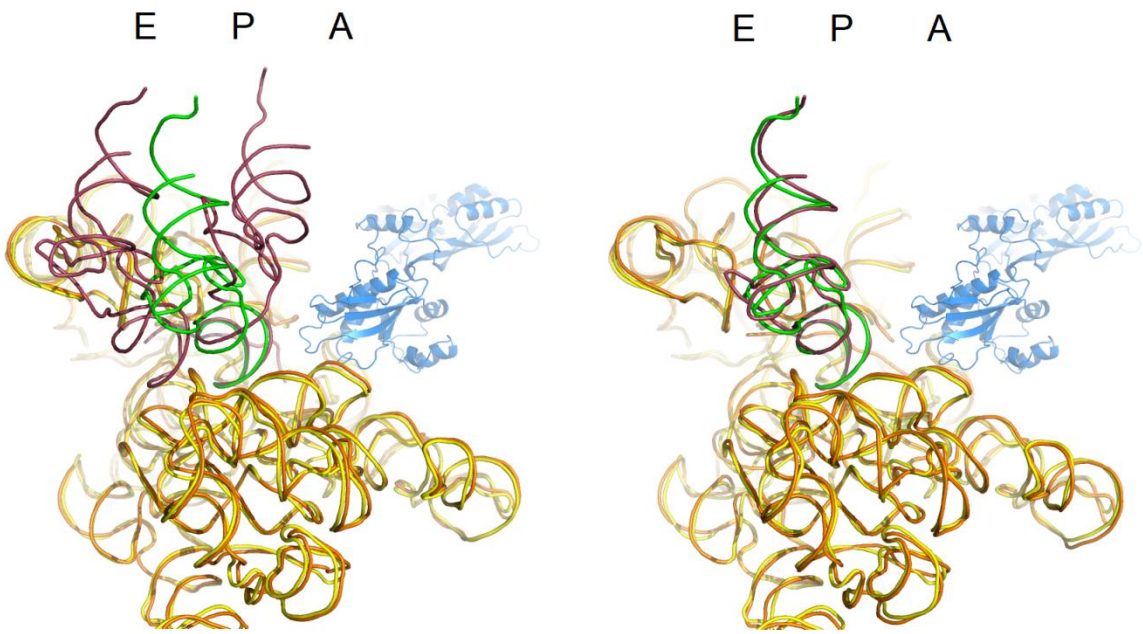

Figure 60.Structural alignment of 18S rRNA with cryo-EM reconstructed ribosomal complex in non rotated state (3J78) on the left and rotated state on the right. Color code of our complex: 18S rRNA – yellow, tRNA – green, eEF2 – blue. Color code of cryo-EM structures: 18S rRNA – orange, tRNAs – red. The location of A-, P- and E-sites are labeled.

As it is seen from the figure the position of our $tRNA^{Phe}$ corresponds with the tRNA in the rotated ribosome. While the anticodon stem loop is located in the P-site of the ribosome the CCA tail is shifted towards the E-site.

mRNA and codon-anticodon interactions in the P-site.

Clear density for three mRNA nucleotides was observed that allowed us to build U_3 sequence inside. These nucleotides are forming base pair interaction with anticodon stem loop of $tRNA^{Phe}$ (Figure 61), and correspond to the position of P codon of mRNA. Weak positive density was observed near the 3' end of mRNA model which might be from two additional mRNA nucleotides (corresponding to +4 and +5 position of A codon), however nothing was built in it (not illustrated).

We used native $tRNA^{phe}$ purified from yeast strain in order to be able to capture all the modifications and try to identify their function from a structural point. One of the most interesting $tRNA^{phe}$ modification is wybutosine, which is located on G37 in a close proximity to the mRNA (Figure 60). (MassSpec analysis of tRNAphe yeast showed the presence, probably not in equimolar concentration, of this modification in the sample of tRNA). But neither of our maps provide positive density in this region.

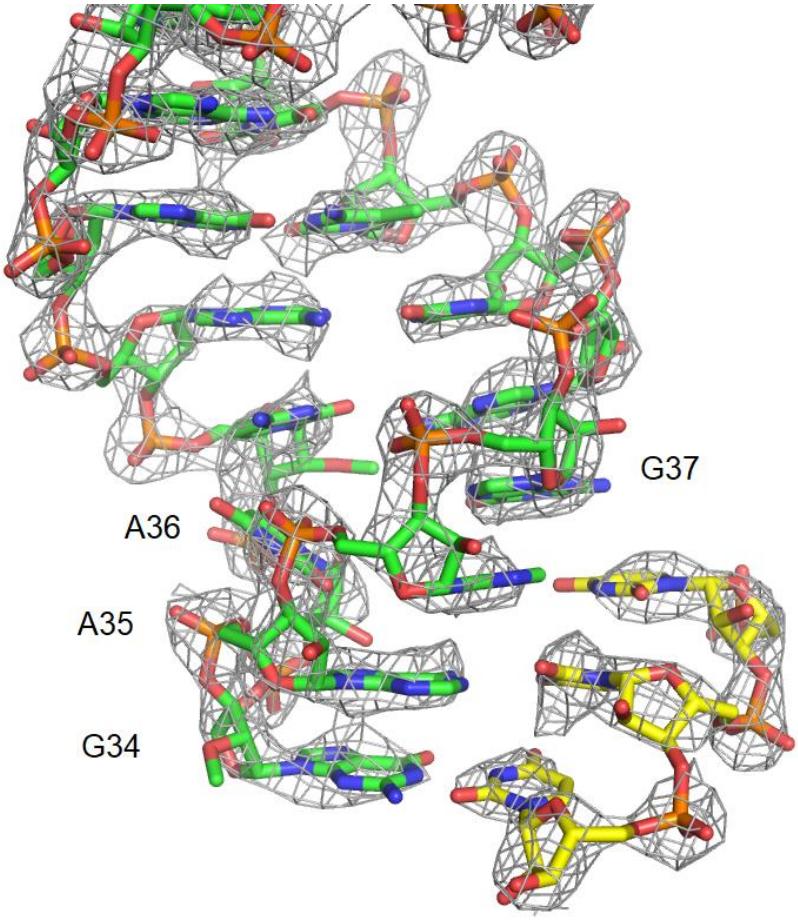

Figure 61. Codon anticodon interaction between mRNA (yellow) and tRNA (green). Four tRNA nucleotides are labeled. The FEM map contour level 2.5 rmsd.

Among all rRNA residues forming interactions with P codon of mRNA were observed for bases 1637-1640, 1150, 1761 and 1768 of 18S rRNA (Figure 62). Cytosine 1637 not only making contacts with mRNA with its phosphate-sugar backbone, but also have stacking interactions with G34 of $tRNA^{Phe}$.

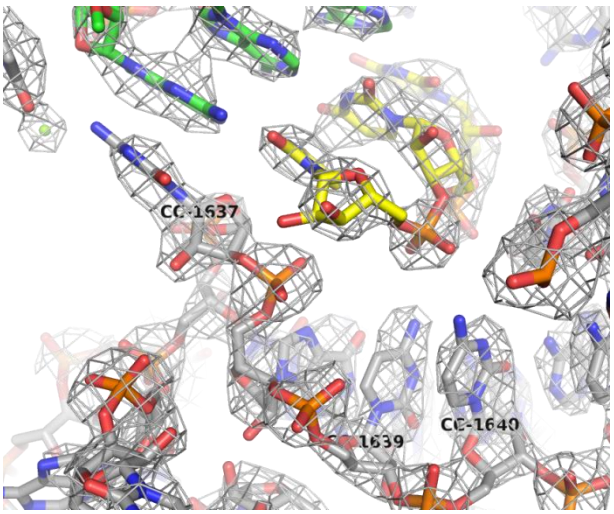

Figure 62. Interactions of 18S rRNA (gray) with P codon of mRNA (yellow) and P/E $tRNA^{Phe}$ (green). FEM map are presented with a contour level 2 rmsd.

Decoding center and hygromycin B.

In the obtained structures the density for conserved nucleotides A1755, A1756 (1492, 1493 in *E. coli*) that play important role in decoding process very weak. It is likely that in current conditions and in the absence of tRNA in A-site they reside in a flexible state (Figure 63), as it was observed in A-vacant site of bacterial 70S ribosome (Jenner, 2010).

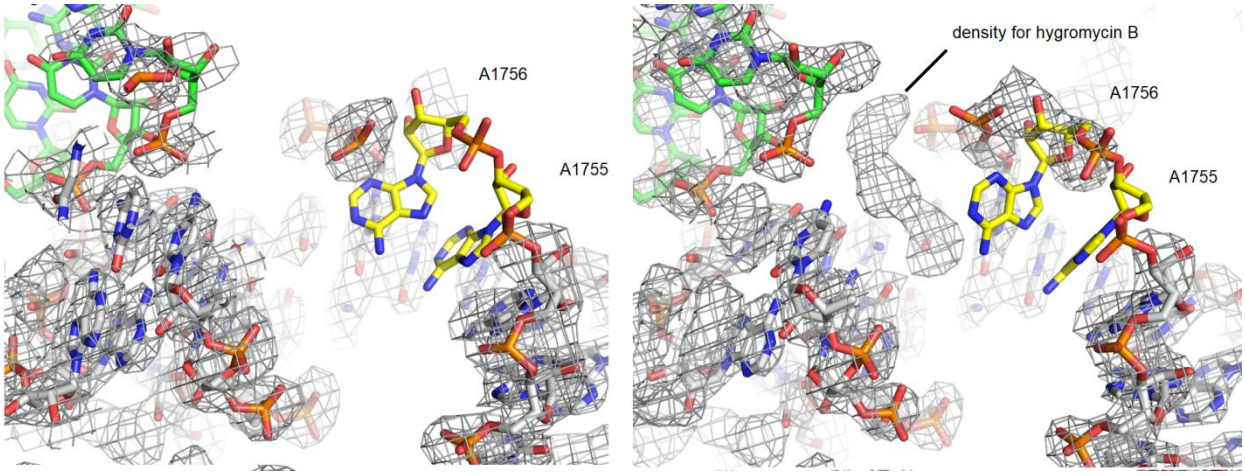

Figure 63. Overview of the decoding site and binding region of hygromycin B. On the left structure without hygromycin B and on the right with hygromycin B. A1755, A1756 are colored in yellow scheme, 18S rRNA in grey. FEM map contour level 1.7 rmsd.

In the 80S translocation structure (GDPCP/sordarin/hygromycin B) at 3.15 Å resolution new positive density was found in the region between mRNA and helix 44 (Figure 63). It is located close enough to make direct contacts with both mRNA and surrounding 18S rRNA nucleotides including A1756, G1757. (The model of hygromycin B will be fitted accurately in the structure later.)

In our structure the presence of hygromycin B has a stabilizing effect providing density for a backbone of A1756, which in in turn improves the density of neighboring A2256 of H69 25S from large 60S subunit (Figure 64).

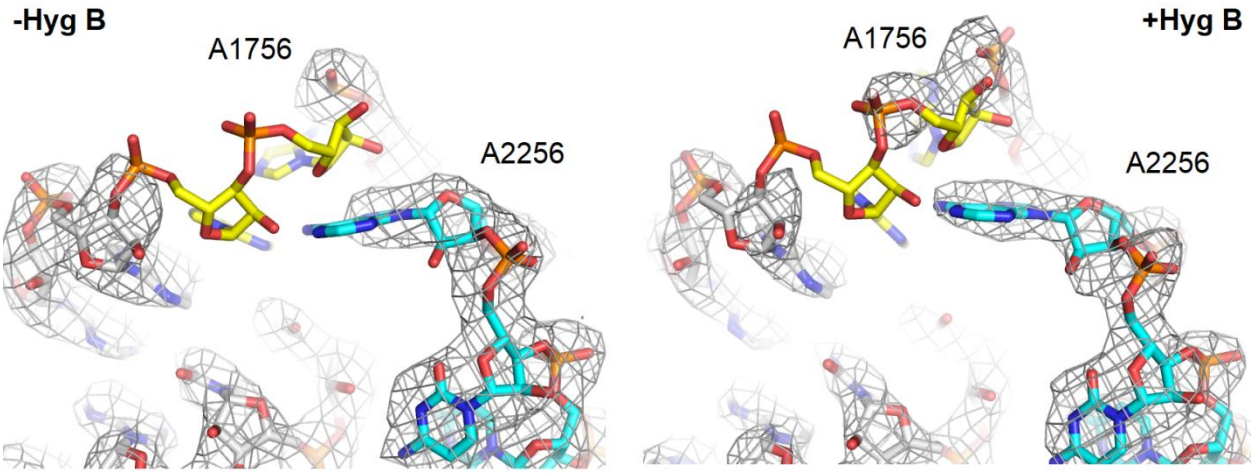

Figure 64. View from a backbone site of decoding region of helix 44. On the left structure without hygromycin B and on the right with hygromycin B. A1755, A1756 are colored in yellow scheme, 18S rRNA in grey and 25S rRNA in cyan. FEM map contour level 1.7 rmsd.

The tip of domain IV of eEF2 is not reaching 18S rRNA to have direct contacts, it is however interacts with the backbone of H69 of 25S from the large 60S subunit (Figure 65).

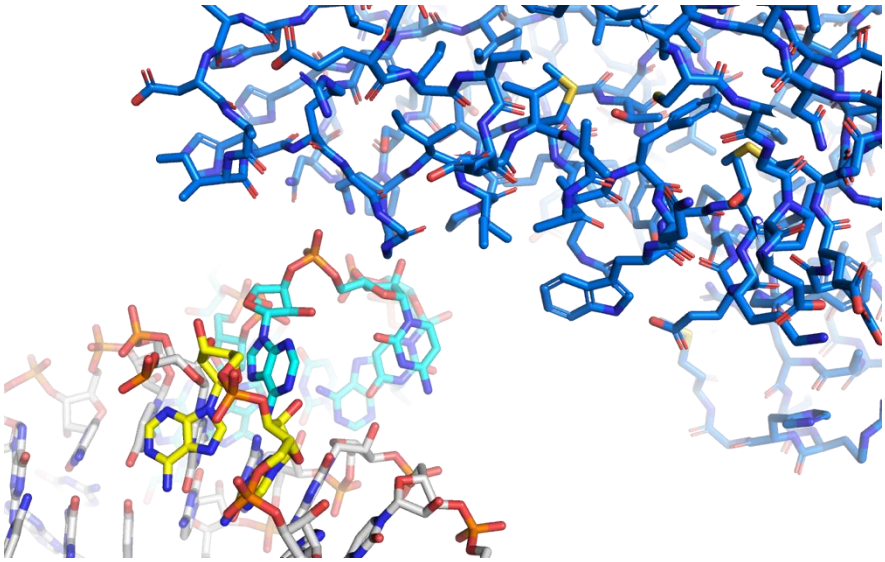

Figure 65. Part of domain IV of eEF2 (blue) reaching the A-site. Helix 69 of 25S from 60S ribosome subunit is colored in cyan, 18S rRNA in grey with decoding nucleotides colored yellow.

Comparison of the 80S ribosome translocation complexes structures with GDPCP and GDP-AlF$_4^-$

As it was mentioned previously GDP-AlF$_4^-$ mimics the transition state after GTP hydrolysis with γ –phosphate remaining in the GTP binding pocket of eEF2. The structure of this complex was obtained at 3.6 Å resolution. Just like in case of GDPCP we observed similar density for GDP-AlF$_4^-$. The rotation angle of 40S relative to 60S subunit and of the head of 40S relative to the body remained the same (Figure 66).

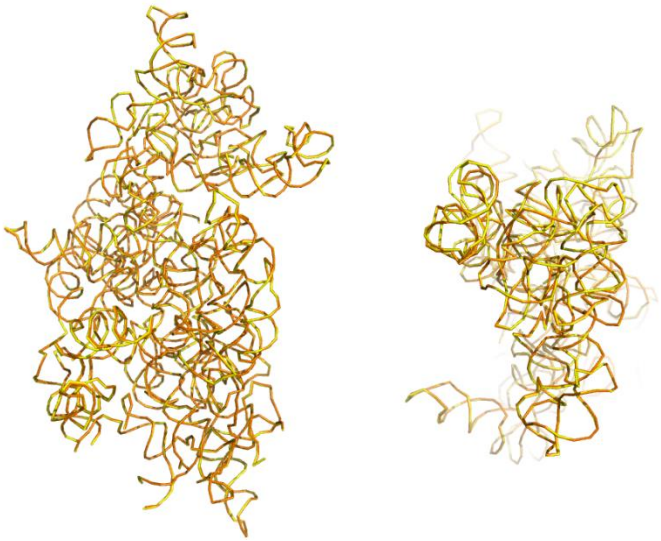

Figure 66. On the left superimposition of the 25S rRNAs from GDPCP (yellow) and GDP-AlF_4^- (orange) structures, 18S rRNAs are shown from the solvent side. On the right superimposition of the 18S rRNA, 18S rRNA of the head is shown from the solvent side.

The alignment of eEF2 in GDPCP and GDP-AlF_4^- states also did not reveal any significant changes (Figure 67). The additional in depth analysis is required to observe possible conformational changes of sarcin-ricin loop of 25S.

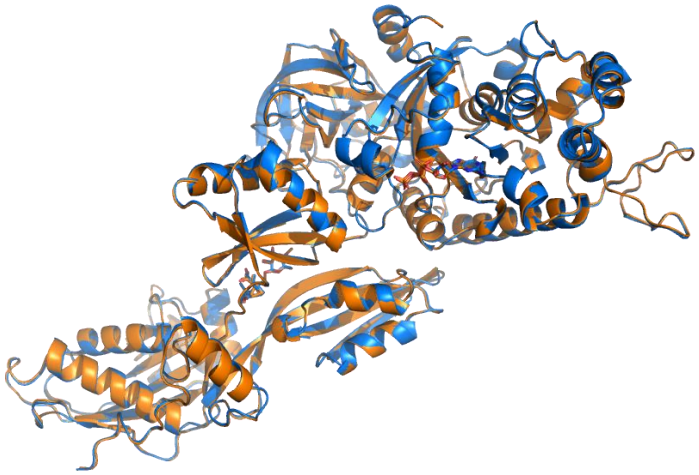

Figure 67. Superimposition of eEF2 from GDPCP (yellow) and GDP-AlF_4^- (orange) structures.

Discussion

The aim of the project was to study the different intermediate steps that take place during elongation in order to bring structural insight and broaden our understanding of this process in eukaryotes. More specifically we were addressing the lack of high-resoultion structural information of canonical translocation complexes of eukaryotic 80S ribosome bound with functional ligands mRNA, tRNA and eEF2, and the conformational changes that undergo inside this complex prior, during and after GTP hydrolysis.

Translocation is a very dynamic process that proceeds rapidly to allow cells efficiently synthesize proteins. In order to have a full overview of the mechanism structural information of various intermediate steps is required. Only combined together with functional studies it will allow complete understanding of the process. Functional studies on eukaryotic system were exceeding structural ones; therefore integrative structural biology approach was chosen as a research method. X-ray crystallography and cryo-EM are two major techniques in structural biology that allow study macromolecules. Given the profound knowledge in ribosome crystallization field and unique experience of group in solving high-resolution structure of first eukaryotic 80S ribosome from *S. cerevisiae* by X-ray crystallography it was decided to apply X-ray crystallography technique. Nevertheless solving a crystal structure of such large and complicated macromolecular complex (MW is more 3.3 MDa) remains very ambitious task, which explains why until presently only one eukaryotic vacant 80S ribosome structure has been solved at high resolution by X-ray crystallography technique (Ben-Shem et al., 2011).

Crystallization requires pure homogeneous and stable sample in high concentrations. The intense screening for crystallization conditions was made to find the one that yielded crystals. Further optimization screening was performed to obtain large and well shaped crystals suitable for X-ray diffraction experiment. However even obtained large crystals with cryoprotecting agent were not diffracting well and required further investigation of a specific post-crystallization treatment. Soft dehydration approach with an accurate screening for additional components and concentrations that had positive effect on crystal diffraction was developed. The established post-crystallization treatment significantly improved diffraction limit in a reproducible way and allowed us to collect complete datasets at high resolution.

Four structures of *S. cerevisiae* 80S ribosome bound with native *S. cerevisiae* eEF2 were obtained with resolution from 3.1 to 3.6 Å. All of the complexes were formed with U_9 mRNA and *S. cerevisiae* $tRNA^{phe}$. The complex of the first structure was formed in the presence of translocation inhibitors hygromycin B and sordarin, which prevents release of eEF2 from the ribosome (Hygromycin B/Sordarin/GDPCP). Then the focus was shifted to solve the structure of

translocation compex in the absence of inhibitor hygromycin B (Sordarin/GPDCP) and subsequently also in the absence of sordarin (GDPCP). To observe later state of translocation in the fourth complex GDPCP was replaced with GDP and AlF_4^- which mimics transition-like state of GTP hydrolysis with γ –phosphate still remaining in the pocket (Sordarin/GDP- AlF_4^-).

This work provides atomic models of eEF2 bound to the 80S ribosome (with and without translational inhibitors) in the presence of mRNA and tRNA in P/E state. The obtained structures present pretrasnlocation intrermediate state with eEF2 bound to the eukaryotic ribosome prior GTP hydrolysis.

To identify the ratcheting of the 40S subunit the model was compared to non rotated vacant S. cerevisiae 80S ribosomes (3J78). As expected the small subunit of our model is ~12° counterclockwise rotated. However, the head of the 40S subunit resides in approximately the same conformation. Interestingly when compared with the model of the same translocation complex derived from medium resolution cryo-EM reconstructions (6GQV) (Pellegrino et al., 2018a) originated from our group, rotation degree of the 40S is rather similar, but there is significant difference in the head rotation ~9°. The reason of such variation could be explain by differences in techniques. Indeed, in crystallography tight crystal packing might affect the conformation of the complex. While in cryo-EM, preferential orientation or beam induced movement may distort the resulting model. Besides, in cryo-EM without any restrains particles are presented in various conformational states which might also include different range of the head rotation. Indeed, it is known that this area is very flexible and lead to lower resolution in cryo-EM reconstruction (The resolution of cryo-EM translocation intermediates varied between 3.9 to 4.2 A (Pellegrino et al., 2018a)). Since translocation is a dynamic process both of the structures can present snapshots of different states that naturally occur on the ribosome. Nevertheless, it is important to underline that translocation ribosome complexes, which formed in vitro identically, but then analyzed by X-ray analysis (in this PhD study) or by cryo-EM as previously (Pellegrino et al., 2018a), were found in almost identical conformation translocation state and contained one tRNA in P/E state.

As presented in the results we built eEF2 in accordance to our high-resolution density map. By fitting model of eEF2 with modified conformation in cryo-EM maps (Abeyrathne et al., 2016; Murray et al., 2016; Pellegrino et al., 2018a) we saw that the applied changes allowed it to have more appropriate fit than original eEF2 from these structures. These cryo-EM ribosome complexes with eEF2 used original crystal model of eEF2 (Jørgensen et al., 2003) to fit in their density and the resolution of their structures do not allow to rebuild it accurately to see the specific conformational changes that EF2 undergoes upon binding to the ribosome.

During all this process of verification of our eEF2 conformation inside other cryo-EM maps we found very particular example of the impact of this small conformational changes and more precisely on diphthamide location. In the cryo-EM structure of (Murray et al., 2016; Pellegrino et al., 2018a) when they fit eEF2 they had an unfavorable conformation in the tip of domain IV as it is highlighted by not optimal geometry of aminoacids in Coot program (Figure 68).

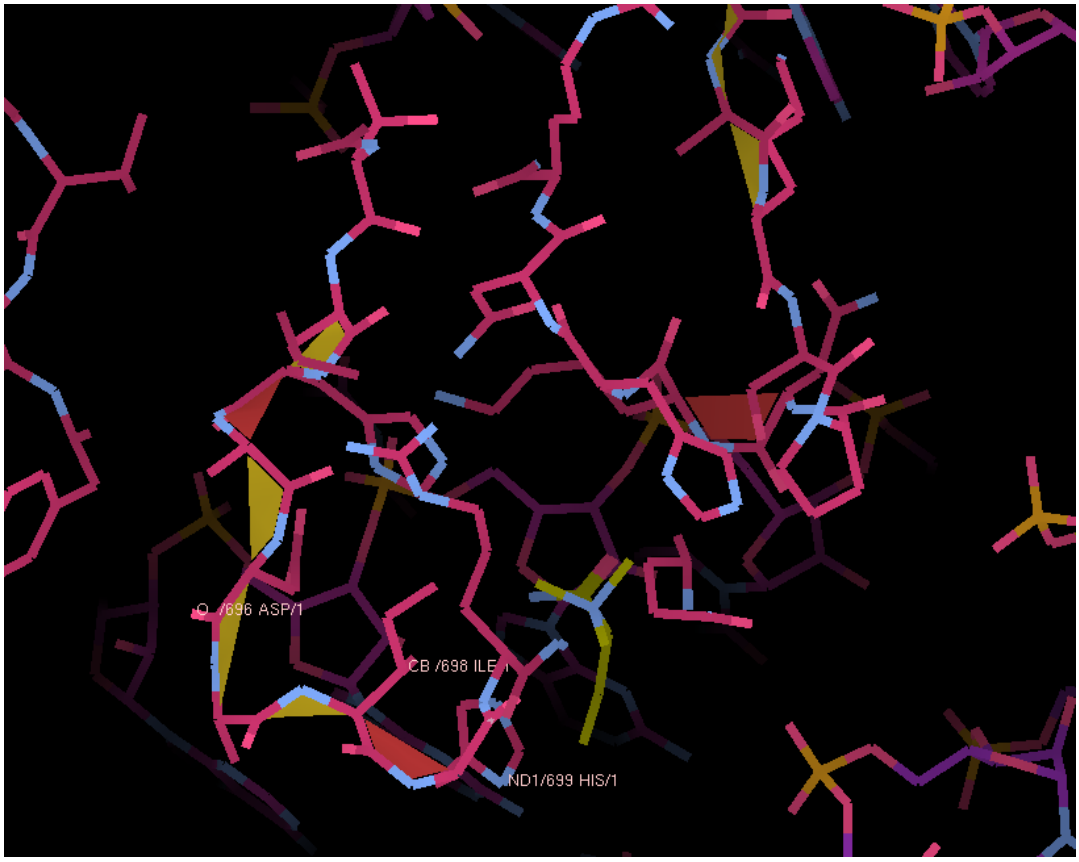

Figure 68. Original eEF2 structure (carbons colored in pink) from the cryo-EM reconstruction of ribosomal complex with IRES and eEF2 (Murray et al., 2016) (pdb entry 5IT7). Flat planes in the aminoacid residues indicate not optimal geometry.

This indicates that in this cryo-EM study the diphthamide might be located in a wrong place. When we replaced (without any refinement) eEF2 of PDB 5IT7 with our eEF2, we observed that the overall eEF2 model was not only fitted properly, but we also noticed additional density next to His699 for diphthamide. Despite the fact, that the density for diphthamide was not found in our crystal structures, but after replacing eEF2 in PDB 5IT7 we can clearly see the position of diphthamide between decoding center and pseudoknot I of IRES, which mimics codon- anticodon interactions. Based on proximity of diphthamide and His699 to decoding center we can now

suggest that it possess important role in translocation. Previously it was shown that this unique post-translational modification dipftamide, covalently bound to a conserved histidine residue (His699 in yeast) play cruicial role in mRNA frame-shifting (Figure 69-70).

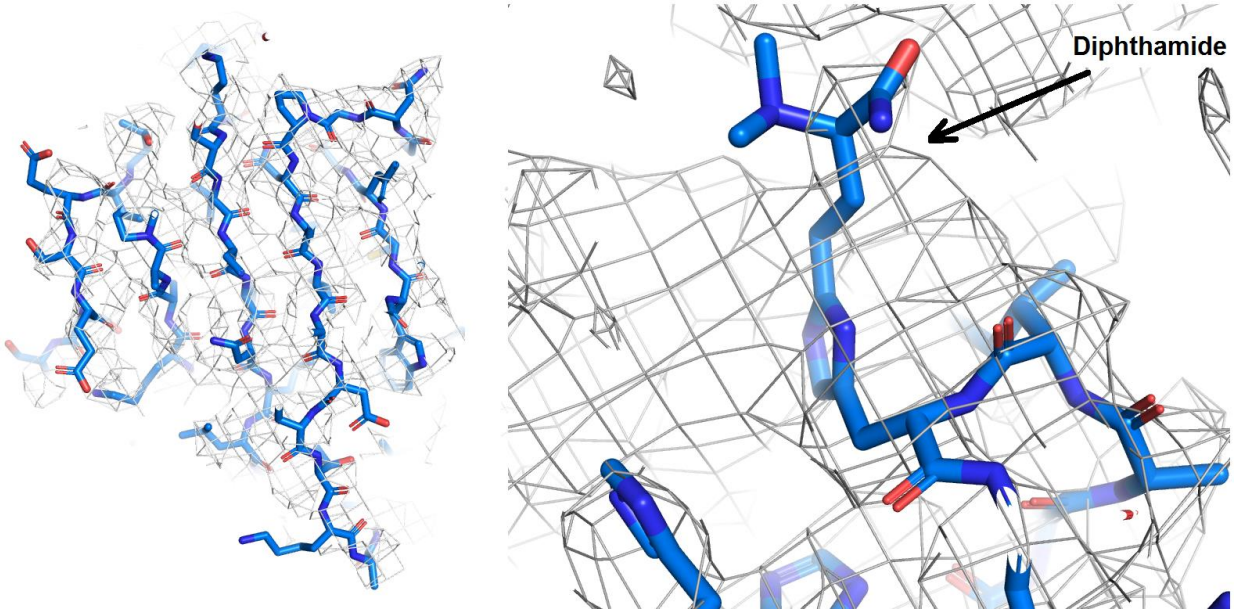

Figure 69. Domain IV of our eEF2 fitted into the cryo-EM density (rmsd 1.8) of ribosomal complex with IRES from pdb entry 5IT7. On the left region of domain IV presented to show matching electron map with our eEF2; on the right diphthamide loop is shown inside the density.

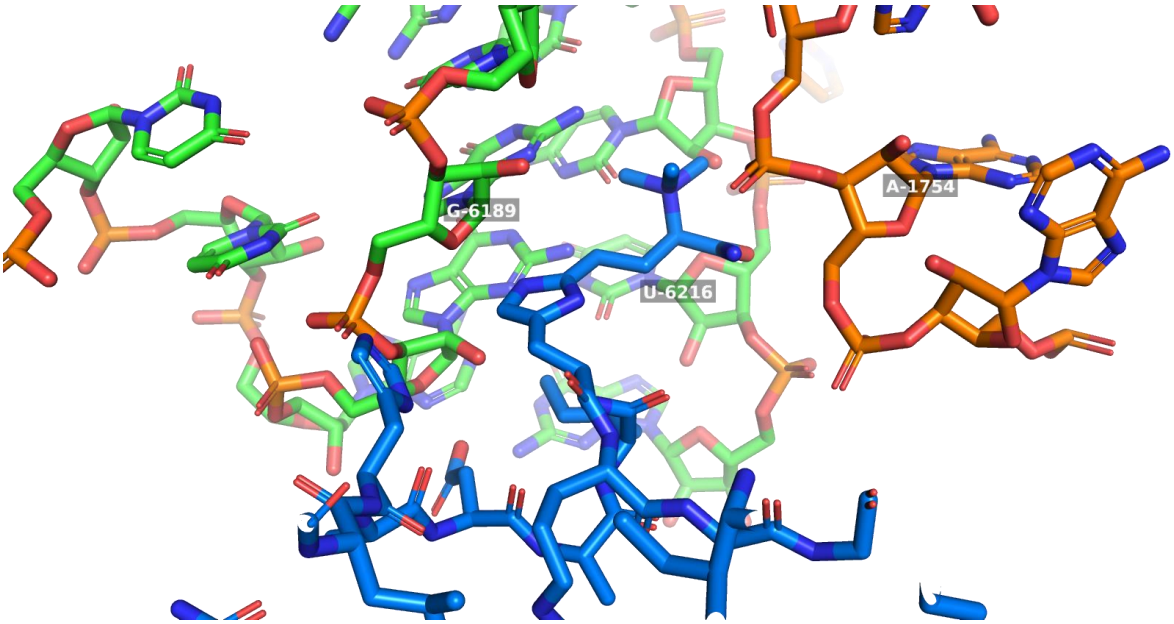

Figure 70. Interaction of diphthamide with part of IRES mimicking codon anticodon interaction are presented in green and decoding nucleotides are orange. eEF2 is colored blue.

Overlaying our eEF2 with the one in PDB 6GQV (Pellegrino et al., 2018a) demonstrated that the position of diphthamides is also different. Despite the fact that both of them were located in inside the cryo-EM electron density from 6GQV, it was difficult to propose any suggestions considering the intermediate resolution of the map (Figure 71).

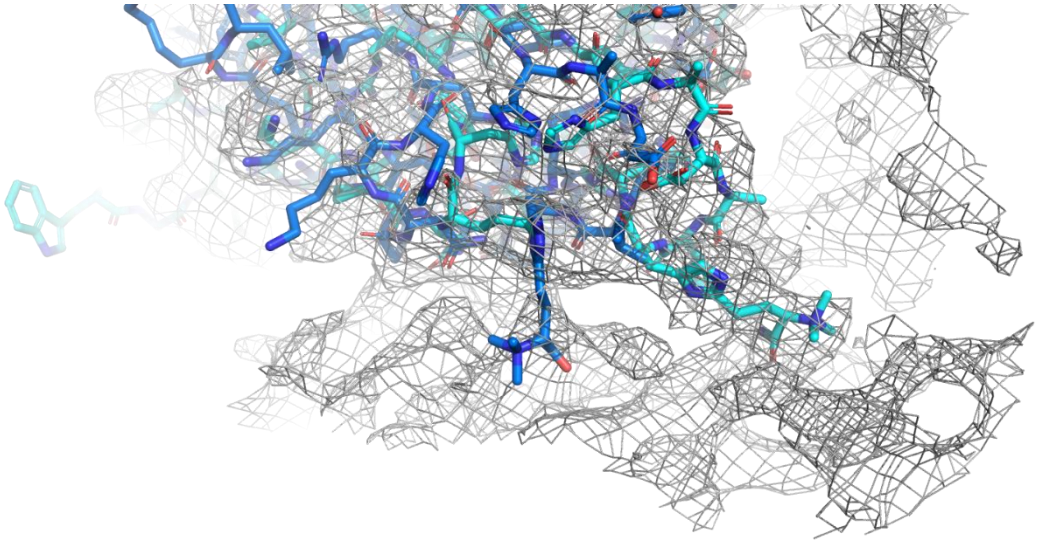

Figure 71. Overlay of our eEF2 (blue) and the one from cryo-EM structure (cyan) with original electron density map (rmsd 1.6) (6GQV) from Simone et. al.

It is likely that diphthamide interacts with the backbone of A1755-A1756 nucleotides of the decoding center in the 40S ribosome subunit (*S. cerevisiae* numeration) stabilizing them in flip in conformation and disrupting canonical contacts with codon anticodon bases. At the same time it is situated in proximity to have direct contact with the second and third mRNA bases of A-site codon. Moreover His699 is placed near to the first and second bases of A-site tRNA anticodon stem loop and together with the part of diphthamide that interacts with mRNA substitutes the canonical contacts of mRNA and tRNA with the decoding center. In this manner His699 together with its highly conserved modification diphthamide may unhitch mRNA and tRNA from the decoding center allowing the translocation.

The main reason why no density for diphthamide was observed in our structures is perhaps due to the absence of A site bound tRNA and as a consequence to the absence of codon anticodon base pairing in the A-site, which should interact with it and fix its conformation. In a natural conditions peptidyl-tRNA bound to the A-site (pre-translocation state), as a result of spontaneous peptidyl-transferase reaction, is translocated further on the ribosome. However in our structure despite the fact that our complex is formed with non hydrolysable analog of GTP (GDPCP) and high excess of tRNA, the ribosome contains only one tRNA in P/E state. Interestingly the same situation was observed for prokaryotic ribosome (Chen et al., 2013; Tourigny et al., 2013). In both of these studies, the obtained pretranslocation complex contained only one tRNA in P/E state. In the work of (Lin et al., 2015) the same situation appeared when regular aminoacyl-tRNAs were used to form elongation complex for their crystallography studies.

As my short-term future project, to solve this issue we will use non-hydrolysable aminoacyl-tRNA analogs that will probably prevents A-site tRNA from leaving from ribosome. The use of the same kind of compound is expected to allow us to obtain canonical complex with two tRNAs inside the ribosome.

Another impact of the absence of A-site tRNA is the conformational flexibility of decoding nucleotides A1755, A1756 of 18S and A2256 of H69 of 25S (large 60S subunit). However, in the structure with hygromycin B solved at 3.15 Å we observed stabilizing effect on flip out conformation of A2256 and on a backbone of A1756 that demonstrates in which manner this aminoglycoside increases A-site affinity to tRNAs and induces miscoding. On the other end hygromycin B is positioned close enough to mRNA to make direct contacts with it and in the same time based on the binding site inside the ribosome it is expected to make multiple contacts with the nucleotides of helix 44 and 45 of 18S rRNA (Figure 72). Considering distant location to any intersubunit bridges suggests that translocation inhibition affect that hygromycin B possesses is

be due to inducing additional restrains by binding to mRNA and preventing it to move further on the ribosome. In perspective the model of hygromycin B will be fitted into the density that will allow analyzing interaction more precisely.

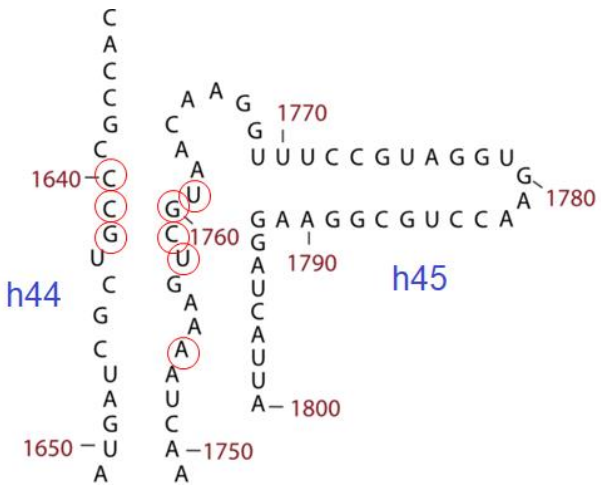

Figure 72. Secondary structure of the binding site of 18S rRNA. Nucleotides in circles are located in a close proximity to be able to form network of interaction with hygromycin B.

For the first time the P-site codon anticodon interaction was observed in eukaryotic ribosome at 3.1 Å high resolution.

Conclusions and Perspectives

To conclude, during these 4 years, all the work had been done in order to bring new structural insight in translation mechanism in eukaryotes.

In the project of structural investigation of functional complexes of *S. cerevisiae* 80S ribosome with mRNA and tRNAs the first step of crystallography studies – finding the first hits of crystallization conditions was accomplished. Giving limited amount of time and the complexity of the object of study the result, despite it is still a long way until obtaining the complete structure, nevertheless presents considerable progress demonstrating that based on proper strategy even the large and highly flexible macromolecular complexes like yeast ribosomes are still possible to crystallize.

Due to size limitation and crust formation on the surface (in one of the found conditions) it was not possible to investigate the content of obtained crystals by X-ray experiment. In order to overcome crust formation several approaches can be applied. One of which is to decrease diffusion rate either by diluting reservoir or changing the plate to smaller geometry with less reservoir surface exposure could equilibrate water diffusion inside and from the droplet. The other option is to use microbatch method. In microbatch crystallization the droplet is sealed under a layer of oil. Varying the oil allows to adjust water diffusion rate through it. Generally, a mineral oil of branched paraffins in the C_{20}+ range or 1:1 mixture of silicon and paraffin oil are used. Overcoming the crust formation issue should restore the process of vapour diffusion and have a positive effect on the crystal growth.

Significant amount of work is still needed to be done. The obtained crystals are relatively small in size and optimization of crystallization conditions is required to make them grow larger. Even after obtaining a large size they might not diffract at atomic resolution. Crystals should be already cryoprotected considering high concentration of glycerol in the reservoir, however additional crystal treatment might be needed to reduce the water content to make them firmer, less fragile and improve diffraction limit. The search for the post-crystallization treatment might be even more complicated than the search for crystallization conditions. Unfortunately, it is impossible to predict and suggest any specific changes neither in the crystallization nor crystal treatment as reaction of the current crystal form to these changes is unpredictable and must be defined empirically.

The structural and functional insights into aminoglycoside (paromomycin, geneticin (G418), gentamicin, and TC007) interactions with the vacant 80S eukaryotic ribosome were presented. Our findings revealed complex interactions of aminoglycosides with eukaryotic 80S ribosome caused by their multiple binding sites, which lead to inhibition of intersubunit movement within the human ribosome.

Both paromomycin and gentamicin bind into the decoding center, however due to the structural difference of these compounds (paromomycin has four rings and gentamicin - three) they have different impact on the decoding center upon binding. In case for TC007 it was demonstrated that PreTC read-through can be stimulated not only by binding in the decoding center.

The comparison of smFRET results with the obtained structural data allowed us to speculate on the mode of action of the studied aminoglycosides depening on their concentration. In case of paromomycin and TC007 increased concentrations shift ribosomal complex from one conformational state to another. The smFRET studies also showed the increasing rate of near cognate tRNA accommodation in the ribosomal A-site in the presence of selected aminoglycosides.

The nature of the observed aminoglycoside interactions with the eukaryotic ribosome hint at potentially multiple modes of action on the translation mechanism. These insights also provide an important framework for understanding the diversity of aminoglycoside interaction sites and drug-binding modes with the 80S ribosome. The combined perspectives afforded by X-ray crystallography and direct imaging of aminoglycoside impacts on functional ribosome complexes using smFRET has the potential to facilitate the design of new antibiotic derivatives and may be particularly suited for the identification of compounds capable of mediating efficient PTC read-through. Such efforts will be greatly aided by in-depth functional investigations of a diversity of functional ribosome complexes relevant to termination. In this regard, the present findings suggest that nonspecific impacts on decoding may be reduced by avoiding aminoglycoside scaffolds bearing a ring I 6′-OH moiety, which exhibit generally higher affinity for the h44 decoding site, and instead focusing on aminoglycosides, other compounds, or mixtures of compounds that give rise to stop codon-specific miscoding in the absence of dominant-negative downstream impacts.

Future structural investigations with lower concentration of aminoglycosides are required to prevent non-specific binding inside the ribosome that might lead to complete inhibition of protein synthesis *in vivo*. Soaking crystals with reduced concentration of aminoglycosides should reveal

specific binding sites that are likely responsible for modulating the affinity of the A-site of the ribosome to tRNAs.

The studies that were performed under the scope of the third project entitled “Structural studies of eukaryotic elongation complex” has obtained new crystal form of *S. cerevisiae* 80S ribosome bound with *S. cerevisiae* elongation factor 2, *S. cerevisiae* $tRNA^{phe}$ and mRNA. The optimization of the crystallization conditions and developed gentle crystal treatment significantly improved diffraction limit of the crystals, allowing us to collect complete datasets at 3.1 Å resoluiton. The quality of obtained density maps provided detailed conformation of not only the backbone of the molecules of the studied complex, but also a side chains and interaction between them. After finishing model building and refinement we obtained the first high-resolution structure of an eukaryotic ribosome 80S functional complex both in the presence and without translational inhibitors such as sordarin and hygromycin B. In a correspondence with the vitro complex formation the structure reveal ribosome in a pretranslocation state bound with eEF2•GDPCP, tRNA and mRNA.

Complete conformation of eEF2 in a functional state bound to the 80S ribosome was determined. Due to the presence of the eEF2 the P-stalk of the ribosome became more stabilized, in comparison to the vacant 80S ribosome, and we observe clear density for uL10 and uL11 proteins. The conformation of eEF2 that comes from our model together with previously published cryo-EM structures allowed us to suggest the mechanism by which His699 and diphthamide unhitch codon anticodon bases from the decoding center at the early stages of translocation.

For the first time the tRNA with mRNA bound inside eukaryotic 80S ribosome was observed at high resolution. Comparison with the low resolution *S. cerevisiae* 80S ribosome complex bound with two tRNAs in rotated and non-rotated state indicate that tRNA in our complex reside in P/E state. We could see the conformational changes inside the ribosome in order to accommodate mRNA and tRNA. In particular interaction of L1 stalk with tRNA and the movement of the head of small subunit towards the tRNA elbow.

The new developed crystal form provides a basis to study the effect of protein synthesis inhibitors on a ribosome in a functional state, as it was already demonstrated with hygromycin B. The obtained model with hygromycin B provided insight of its inhibition mechanism. Considering distant location to any intersubunit bridges suggests that translocation inhibition affect that hygromycin B possesses is be due to inducing additional restrains by binding to mRNA and

preventing it to move further on the ribosome. In perspective the model of hygromycin B will be fitted into the density that will allow analyzing interaction more precisely.

The work described in “Structural studies of eukaryotic elongation complex” project has already yielded four structures. Current crystal form together with the established treatment can be utilized for structural study of translational inhibitors on a functional eukaryotic pretranslocation complex at a high resolution. Nevertheless the project is still in development. The most near-term perspective is to obtain structure of elongation complex with two tRNAs inside the ribosome. To solve this issue we will use non-hydrolysable aminoacyl-tRNA analogs that are expected to prevent A-site tRNA from leaving the ribosome.

The resulting canonical complex with two tRNAs inside the ribosome will not only reveal the position of diphthamide and define its function, but could be also utilized to study decoding mechanism in eukaryotes. So far decoding mechanism has been studied structurally mostly on bacterial systems due to the lack of high resolution eukaryotic functional complexes. Even though decoding mechanism is considered to be consereved between prokaryotes and eukaryotes there are no structural evidence available.

Another interesting research direction based on the obtained crystal form is a study of the frameshifting or mRNA slippage mechanism. In general, protein biosynthesis on the ribosome is a very accurate process meaning that a newly synthesized protein is a mirrored polypeptide copy of the RNA transcript (mRNA). However, the ribosome does make mistakes while reading mRNA at a very low rate. Together with miscoding at the step of aminoacyl-tRNA recognition, slippage on mRNA or frameshifting contributes to translational errors. Frameshifting on the mRNA can happen ‘spontaneously’ on slippery tandems of codons encoding for one amino acid. It was estimated that in mammalian in vitro systems (-1) frameshifting occurs on slippery sequences at a rate of about 2%. Frameshifting can also be programmed by specific mRNA sequence elements such as internal Shine-Dalgarno, slippery sequences and structured hairpins or pseudoknots to regulate gene expression. Another case that contribute to the frameshifting in eukaryotes, as it was discussed previously, is a deletion of posttranslational modification diphthamide from eEF2.

Structural comparison of two identical complete (with two tRNAs) pretranslocation complexes with a native eEF2 and with eEF2 lacking diphthamide could shed light on not only on the function of diphthamide during translocation but also reveal the mechanism by which it prevents frameshifting. Further investigation of frameshifting caused by different mRNA sequence elements can also be performed based on the current crystal form by inducing different mRNA sequences with either slippery elements or structural motifs such as hairpins or pseudoknots.

The long-term perspective is to study intermediate or post-translocation state on the basis of current crystallization conditions. Post-translocation state can be formed by introducing GDP and sordarin instead of GDPCP, while for intermediate state inhibitors should be induced to lock the translocation. Preliminary trials showed that replacing GDPCP with GDP and sordarin did not interfere with crystal growth; however the established post crystallization treatment for the crystals with GDPCP complex turned out to be inefficient. Therefore a thorough research for new crystal treatment conditions is required.

Résumé en français

PROJETS DE RECHERCHE

Pendant mes études doctorales, j'ai travaillé sur trois projets différents. Tous ont été développés pour étudier l'aspect structural des machines de synthèse protéique des eucaryotes au moyen de la cristallographie aux rayons X. Tous les composants utilisés pour former différents états de traduction du ribosome 80S in vitro ont été purifiés à partir de *Saccharomyces cerevisiae*.

Liste des projets:

1. Étude structurale des complexes ribosomaux fonctionnels de *S. cerevisiae* 80S avec ARNm et ARNt.
2. Interactions des aminoglycosides et impacts sur le ribosome eucaryote *S. cerevisiae* 80S ribosome
3. Etudes structurales du complexe de la traduction eucaryote *S. cerevisiae* 80S

En raison de la taille limitée de ce résumé, je décrirai en détail uniquement le projet "Structural studies of eukaryotic S. cerevisiae 80S elongation complex".

Le ribosome

Dans tous les organismes vivants, la synthèse des protéines est un processus essentiel qui permet à chaque cellule de vivre et de se reproduire. Cette activité consomme la majeure partie de l'énergie produite par la cellule. Par conséquent, elle est étroitement régulée par de nombreux facteurs afin de s'assurer que seules les protéines nécessaires sont produites dans la quantité requise et au bon moment. L'information génétique, codée dans les gènes, est transcrite de l'ADN en ARN messager (ARNm) dans le processus appelé transcription. Ensuite, l'information contenue dans l'ARNm est traduite en protéine par une macromolécule spéciale appelée ribosome. Ce processus est appelé traduction puisque le substrat moléculaire contenant l'information est traduit du "langage" de l'acide nucléique en acide aminé.

Diversité du ribosome liée au noyau commun et au domaine.

Le ribosome est un assemblage cellulaire ribonucléoprotéiques géant qui catalyse et coordonne toutes les étapes nécessaires pour traduire les ARNm en protéines dans toutes les cellules vivantes. Bien que les aspects fondamentaux de la traduction soient très bien conservés chez les eucaryotes, les bactéries et les archaebactéries, il existe des différences structurales

importantes pour leurs ribosomes. L'étude de la première structure à haute résolution du ribosome eucaryote de *Saccharomyces cerevisiae* (Ben-Shem *et al.,* 2011) au moyen de la cristallographie aux rayons X combinée aux données génétiques et aux informations structurales des ribosomes procaryotes ont permis de mettre en évidence un noyau structural commun (Figure 1) pour les ribosomes eucaryotes et procaryotes, comprenant 34 protéines conservées (15 dans la petite sous-unité et 19 dans la grande sous-unité) et ~4 400 bases ARN, qui abritent les principaux centres fonctionnels des ribosomes, comme le centre de décodage, le centre peptidyltransférase et les sites de fixation des ARNt (Klinge *et al.* 2012 ; Melnikov *et al*. 2012).

Malgré la conservation universelle du noyau, la composition des ribosomes varie selon les domaines de la vie, les sous-groupes taxonomiques, les organites et même dans une moindre mesure au sein d'un même individu. Le ribosome bactérien (*Escherichia coli* ou *Thermus thermophilus*) contient 21 protéines spécifiques des bactéries, quelques extensions pour les protéines conservées et de l'ARN ribosomal. Le ribosome eucaryote de *S. cerevisiae* contient 46 protéines spécifiques des eucaryotes (800 kDa) et des extensions et insertions dans la plupart des protéines du cœur (200 kDa), et l'ARNr présentant plusieurs extensions au niveau de ses chaînes conservées (environ 800 nucléotides qui représentent 350 kDa) (Ben-Shem *et al.,* 2011 ; Melnikov *et al.,* 2012). Le poids moléculaire des ribosomes peut varier de 2,3 MDa chez les bactéries à 4,3 MDa chez les eucaryotes supérieurs (Figure 1).

Principaux sites fonctionnels

Le ribosome est une macromolécule asymétrique constituée d'une grosse (LSU) et d'une petite (SSU) sous-unité composée d'un ARN ribosomal (ARNr) et de protéines ayant un rapport moyen de 2:1 ARN:protéine (les exceptions sont les ribosomes mitochondriaux et chloroplastes qui ont un rapport 1:2 et 3:2 respectivement) (Sharma et Agrawal, 2012). Le poids moléculaire et la composition des sous-unités sont différents et chacune a un coefficient de sédimentation spécifique qui est utilisé pour caractériser et nommer les sous-unités isolées ou associées. Chez les eucaryotes, la grande sous-unité est 60S (50S chez les bactéries) et la petite sous-unité est 40S (30S chez les bactéries). Et lorsqu'il est associé dans un ribosome complet, il est de 80S (70S dans les bactéries) (Figure 2).

Les deux sous-unités contiennent des sites de liaison A-, P- et E-ARNt et chaque sous-unité apporte une contribution différente dans le processus de synthèse des protéines. SSU s'adapte et conduit l'ARNm pendant la traduction. Il est également responsable du processus de décodage où l'ARN-aminoacyl-ARNt (aa-ARNt) est sélectionné en fonction de la séquence d'ARNm (Figure 2).

La petite sous-unité ribosomique

La petite sous-unité est plus dynamique que la grande sous-unité, elle a une forme allongée et peut être divisée en trois domaines distincts : la tête, le corps et la plate-forme (Figure 3). Les sites fonctionnels sont situés dans le cou formé entre la tête et le corps/plateforme. Les trois sites de liaison de l'ARNt établissent des contacts avec la tige-boucle anticodon de l'ARNt. Le trajet de l'ARN messager s'étend tout le long du cou, du site A au site E (Yusupova *et al.,* 2001). En fait, le ribosome couvre environ 30 nucléotides de l'ARNm, comme l'ont révélé les premières expériences d'empreinte (Steitz, 1969). Pendant la translocation, la tête pivote par rapport au corps/plateforme pour faciliter la translocation d'ARNm et d'ARNt (Frank *et al.,* 2007 ; Ratje *et al.,* 2010).

La grande sous-unité ribosomique

La grande sous-unité catalyse la formation de la liaison peptidique, et sa structure est plus compacte que celle de la petite sous-unité et, en dehors de son corps, on peut observer trois caractéristiques distinctes : la tige L1, la tige P (tige L7/L12 dans les bactéries) et la protubérance centrale (PC) (Figure 4). La tige L1 est un élément dynamique qui participe à la libération de l'ARNt désacétylé tandis que la tige P est nécessaire pour la liaison et l'activité des facteurs de translation. La protubérance centrale contient l'ARNr 5S ainsi que quelques protéines. La protéine L41e sur le LSU forme le seul pont eB14 spécifique des eucaryotes et positionné au centre du ribosome. Les sites de liaison de l'ARNt interagissent avec la tige acceptrice des trois ARNt (Yusupov, 2001). Le centre de peptidyl transférase (CTP) est situé à la convergence de l'extrémité 3' des sites A-ARNt et P-ARNt et s'ouvre sur le tunnel de sortie peptidique qui traverse la majeure partie de la sous-unité et sort à l'arrière du côté solvant (bord du tunnel peptidique). Le tunnel peptidique a une longueur de 80-100 Å et un diamètre d'environ 10-20 Å. Avec les sites de liaison des facteurs, le bord du tunnel de sortie est la région la plus riche en protéines de la grande sous-unité. Le CTP est responsable de la formation des liaisons peptidiques, c'est une région conservée sur l'interface des LSU qui est principalement composée d'ARNr.

Pendant la synthèse protéique, l'aa-ARNt entre dans le ribosome par le site A, le site P contient l'ARNt portant la chaîne polypeptidique naissante (ARNt peptidylique), et le site E (sortie) est celui où l'ARNt désacylé se dissocie du ribosome. Pendant la traduction, après le transfert de la chaîne polypeptidique naissante de l'ARNt peptidyle du site P vers l'ARNt du site A, les ARNt sont transloqués du site A vers le site P et du site P vers le site E, étendant ainsi la chaîne naissante par un amino acide.

Synthèse de protéines

Les avancées récentes dans le domaine de la synthèse protéique sur le ribosome font l'objet d'analyses constantes et sont résumées dans de nombreuses revues actualisées. (Dever *et al.,* 2018 ; Rodnina 2018 ; Jobe *et al.,* 2018 ; Frank 2017 ; Ling *et al.,* 2016 ; Yusupova et Yusupov, 2014 ; Voorhees et Ramakrishnan, 2013).

Les progrès de la cristallographie aux rayons X et de la cryo-microscopie électronique ont apporté une quantité d'informations sans précédent en terme de structure du ribosome mais également fonctionnels. Cependant, malgré ces récentes évolutions, le mécanisme de traduction n'est pas encore complètement compris.

Dans ce chapitre, je vais faire un bref survol de toutes les principales étapes de la traduction, en me concentrant plus en profondeur sur le cycle de l'élongation.

On estime qu'une cellule de levure à division rapide se développant sur milieu riche synthétise près de 13 000 protéines par seconde (von der Haar 2008), limitée par la disponibilité des ribosomes (Shah *et al.,* 2013). La cellule moyenne contient près de 200 000 ribosomes (Warner 1999 ; Firczuk *et al.,* 2013) et 15 000 à 60 000 molécules d'ARNm (avec ~1/3 codant les protéines ribosomiques) (Warner 1999) (Zenklusen *et al.,* 2008). Avec des niveaux allant de 105 à 106 molécules par cellule, les facteurs d'élongation de la traduction sont parmi les protéines les plus abondantes dans la cellule (Firczuk *et al.,* 2013). Étant donné les vastes ressources que la cellule de levure consacre à la synthèse des protéines, une compréhension approfondie de la synthèse des protéines est essentielle pour comprendre la biologie des organismes vivants.

La synthèse ou traduction des protéines par le ribosome est un processus complexe, régulé par un certain nombre de facteurs protéiques. Il peut être divisé en quatre étapes principales :

- Initiation - assemblage de la petite et de la grande sous-unité du ribosome et positionnement du site P avec l'initiateur $ARNt^{met}$ sur le codon de départ ARNm (AUG).

- Elongation - cycle qui commence par la sélection d'aminoacyl-ARNt suivie de la catalyse du transfert peptidique du site P au site A et de la translocation de l'ARNm-ARNt. La plus longue phase de la traduction.

- Terminaison - terminaison de la synthèse protéique et libération de la protéine synthétisée, déclenchée par la présence d'un codon stop sur l'ARNm.

- Recyclage - dissociation des sous-unités ribosomiques et préparation de la prochaine itération traductionnelle.

Chacune de ces étapes est assistée par des facteurs protéiques appelés facteurs d'initiation (IFs pour les bactéries et eIFs pour les eucaryotes), les facteurs d'élongation (EFs ou eEFs), les facteurs de libération (RFs ou eRFs) et les facteurs de recyclage.

Elongation

Après l'initiation, le ribosome est prêt à entrer dans la phase d'élongation au cours de laquelle l'ARNm est traduit en protéine selon le cadre de lecture. Comme on l'a déjà mentionné, le cycle d'élongation est conservé, contrairement à l'initiation et à la terminaison, qui diffèrent considérablement entre les bactéries et les eucaryotes. L'élongation est un processus itéré composé de trois étapes principales : la sélection de l'ARNt-aminoacyle, la formation de liaisons peptidiques et la translocation de l'ARNm-ARNt. Chaque cycle dure de 0,1 à 1 seconde environ (Munro *et al.,* 2009) et correspond à l'incorporation d'un acide aminé dans la chaîne polypeptidique naissante. Il s'agit de l'étape la plus conservée qui comprend les éléments clés de la traduction : fidélité, catalyse et dynamique structurelle. Tout ceci est réalisé sous un contrôle serré des facteurs d'élongation.

ÉTUDES STRUCTURALES DU COMPLEXE D'ALLONGEMENT EUCARYOTE

Aperçu du projet

A ce jour, toutes les connaissances structurales sur le cycle d'élongation chez les eucaryotes sont fournies par des reconstructions par cryo-EM qui ont jeté les bases de la compréhension des principaux réarrangements conformationnels guidant la translocation des ARNt et ARNm. Cependant, ces reconstructions sont soit de faible résolution ou ne fournissent pas de détails suffisants permettant de détailler le mécanisme de translocation. La compréhension du processus chez les eucaryotes provient ainsi des reconstructions par cryo-EM disponibles et les structures obtenues en cristallographie aux rayons X à haute résolution de complexes analogues bactériens.

L'objectif du projet est de réduire l'écart dans la compréhension des caractéristiques spécifiques des eucaryotes du cycle d'élongation en obtenant des structures à haute résolution par cristallographie aux rayons X du ribosome eucaryote 80S piégé à différents stades de la traduction.

Au cours de la synthèse protéique, les ligands macromoléculaires du ribosome, c'est-à-dire l'ARNm, les ARNt et la chaîne peptidique naissante, se déplacent de façon précise et contrôlée dans le ribosome. Il s'agit d'un procédé en plusieurs étapes dans lequel les substrats se déplacent

par étapes de 10 à 30 Å, à travers des sites de liaison structuralement et spatialement distincts dans un canal accessible aux solvants formé par l'interface des petites et grandes sous-unités. Des mouvements à grande échelle du ribosome accompagnent la réaction de traduction. Au cours de cette étape, le ribosome passe de l'état pré-translocatif (PRE) à l'état post-translocatif (POST) lorsque les ARNt liés au site A- (accepteur) et P- (peptidyle) passent aux sites P et E (sortie), respectivement. La translocation est catalysée par le facteur d'élongation G (EFG) chez les procaryotes et le facteur d'élongation 2 (eEF-2) pour les eucaryotes et couplée à la rotation de la petite sous-unité par rapport à la grande sous-unité. Dans la vision classique de la translocation, EF-G/eEF-2 agit par un mécanisme de commutation GTPase similaire à une protéine G régulatrice (Figure 66). L'un des principaux facteurs contribuant à la précision de la synthèse protéique sur le ribosome est le maintien du cadre de lecture de l'ARNm. Ce dernier est essentiel et principalement réalisé par l'action du facteur d'élongation 2 chez les eucaryotes. Le décalage du cadre de lecture conduit à la traduction d'une protéine dont la séquence est incorrecte et potentiellement délétère pour la cellule pouvant entraîner des maladies graves.

L'objectif principal du projet était de résoudre les structures cristallines du ribosome 80S de la levure eucaryote (*Saccharomyces cerevisiae*) avec de l'ARNm, des ARNt eucaryote naturellement modifiés et le facteur eEF-2 de *S. cerevisiae* avec un analogue non hydrolysable du GTP mimant les états canoniques de l'élongation (complexe pré-traductionnel).

Résultats et discussion

Criblage des conditions de cristallisation

Les difficultés importantes de cristallisation des ribosomes sont dues à un manque absolu de kits de criblages commerciaux, qui sont en général développés pour la cristallisation de protéines. Par conséquent, la recherche d'une nouvelle forme cristalline d'une macromolécule aussi grosse que le ribosome eucaryote 80S avec une masse moléculaire de 3,3 MDa représente un processus long et complexe nécessitant des idées innovantes et une grande quantité d'échantillons.

Les réservoirs pour le criblage ont été préparés à l'aide d'un système robotisé Freedom EVO®. 200 nl de réservoir ont été mélangés à l'aide du système de cristallisation Mosquito® avec 200 nl de complexe ribosomique préparé sur la plaque MRC 96, 2 gouttes par puits. Les plaques ont été stockées à 4°C dans le système d'imagerie automatisé ROCK IMAGER®.

Parallèlement aux essais de cristallisation utilisant le système robotique Mosquito®, un criblage manuel a été réalisé dans des plaques VDX à 24 puits de grande géométrie pour des expériences de diffusion de vapeur à goutte suspendue et dans des plaques MRC à 48 puits.

Traitement des cristaux

Le traitement post-cristallisation est couramment utilisé en cristallographie par rayons X pour protéger les cristaux de la température cryogénique pendant la collecte des données radiographiques et pour les stabiliser en réduisant la teneur en solvant. Le traitement des cristaux permet d'introduire des agents cryoprotectants empêchant la formation de glace à l'intérieur du cristal. Cette protection permet donc d'éviter la cristallisation de l'eau au sein du cristal qui entraînerait sa destruction. Le rôle du cryoprotectant sera ici de changer la forme cristalline de la glace et éviter son expansion au sein du cristal d'intérêt. En effet, la collecte de données à basse température réduit les dommages causés par le rayonnement, ce qui permet de recueillir davantage de données pour chaque cristal.

Les cristaux stabilisés sont ensuite exposés à des rayons X au synchrotron. Les connaissances développées en cristallisation et étude structurale des ribosomes au sein de mon équipe d'accueil suggèrent que chaque forme cristalline a un traitement adapté spécifique qui, dans la plupart des cas, est développé expérimentalement et est rarement déduit en théorie. Par conséquent, pour surmonter cet obstacle, une recherche approfondie des conditions de traitement post-cristallisation doit être menée.

Le procédé de traitement des cristaux développé, qui comprend une procédure de déshydratation douce des cristaux pendant la nuit ainsi que l'ajout d'agents stabilisants et cryoprotectants, ont permis de collecter des jeux de données de complets de diffraction aux rayons X pour quatre complexes de ribosomes *S. cerevisiae* 80S piégés au stade de la translocation (Tableau 1). Tous ces complexes d'allongement (pré-translocation) de *S.cerevisiae* 80S ribosome/eEF2/GDPNP/ARNm/ARNts contenaient U9 comme construction d'ARNm, l'ARNt^{Phe} de *S.cerevisiae* et le facteur d'élongation de *S.cerevisiae* eEF2 en présence de GDPCP ou de GDP/- AlF4. Dans certains cas, de la sordarine ou de l'hygromycine B ont été ajoutées. Il s'agissait des mesures visant à assurer la stabilisation des "complexes intermédiaires de translocation" afin d'obtenir une diffraction à haute résolution.

Caractérisation des structures obtenues.

Actuellement, nous avons réussi à obtenir des jeux de données complets pour les complexes suivants

Number of complex*	Resolution	Hygromycin B	Sordarin	Nucleotide
1	3.1 Å	-	+	GDPCP
2	3.1 Å	+	+	GDPCP
3	3.2 Å	-	-	GDPCP
4	3.6 Å	-	+	GDP/AlF_4^-

*Tableau 1. Résumé des structures obtenues. *Le cœur de tous les complexes analysés contenait du ribosome S. cerevisiae 80S avec le facteur eEF2, un ARNm de type U9 et l'ARNt*^{Phe} de *S. cerevisiae fixés.*

Après l'étape de remplacement moléculaire, des densités claires pour l'ARNt, l'ARNm et le facteur eEF2 au sein du ribosome ont pu être identifiées. Les cartes à haute résolution ont ainsi permis de distinguer la position non seulement des chaînes principales mais aussi des chaînes latérales des molécules composant le complexe.

Quatre structures du ribosome 80S de *S. cerevisiae* liées au facteur eEF2 natif ont été obtenues avec une résolution de 3.1 à 3.6 Å. Tous les complexes ont été formés avec un ARNm de type U9 et d'ARNt^{Phe} de *S. cerevisiae*. Le complexe de la première structure a été formé en présence d'inhibiteurs de la traduction l'hygromycine B et la sordarine, empêchant la libération d'eEF2 du ribosome (Hygromycine B/Sordarin/GDPCP). Ensuite, l'accent a été mis sur la résolution de la structure du complexe de la traduction en absence d'hygromycine B (Sordarin/GPDCP) et ensuite en l'absence de sordarine (GDPCP). Pour observer l'état de traduction ultérieur dans le quatrième complexe, le GDPCP a été remplacé par GDP et AlF4- qui imite l'état de transition de l'hydrolyse du GTP avec le phosphate γ restant encore dans la poche (Sordarin/GDP- AlF4-).

Ce travail fournit la première structure d'un complexe fonctionnel à haute résolution du ribosome eucaryote 80S lié à eEF2, un ARNm et un ARNt dans un état hybride P/E (avec et sans inhibiteurs de la traduction). Les structures obtenues sont caractéristiques d'un état intermédiaire pré-traductionnel avec le facteur eEF2 lié au ribosome eucaryote avant l'hydrolyse GTP.

Les études réalisées dans le cadre de ce projet intitulé "Structural studies of eukaryotic elongation complex" ont permis d'obtenir une nouvelle forme cristalline du ribosome 80S de *S. cerevisiae* lié au facteur d'élongation 2 de *S. cerevisiae*, d'ARNt^{Phe} et d'un ARNm. L'optimisation des conditions de cristallisation et le traitement doux des cristaux ont considérablement amélioré la limite de diffraction des cristaux, ce qui nous a permis de recueillir des jeux de données complets à une résolution de 3.1 Å. La qualité des cartes de densité obtenues a fourni des informations détaillées non seulement sur la conformation des chaînes principales des molécules du complexe étudié, mais aussi des chaînes latérales et des interactions entre elles. Après avoir

la reconstruction et l'affinement du modèle, la première structure à haute résolution d'un complexe fonctionnel ribosomique eucaryote 80S en présence mais également en absence d'inhibiteurs de la traduction tels que la sordarine et l'hygromycine B ont été obtenu. La structure a révélé un ribosome dans un état pré-traductionnel lié au facteur eEF2-GDPCP, un ARNt et un ARNm.

La conformation complète du facteur eEF2 dans un état fonctionnel lié au ribosome 80S a pu être déterminée. En raison de la présence de l'eEF2, la tige P du ribosome est stabilisée par rapport au ribosome 80S vacant, et on observe une densité claire pour les protéines uL10 et uL11. La conformation de eEF2 issue de notre modèle ainsi que les structures cryo-EM publiées précédemment nous ont permis de suggérer le mécanisme par lequel l'His 699 et le diphtamide permettent lors de l'étape de translocation la dissociation au niveau du centre de décodage des bases codon-anticodon.

Pour la première fois, l'ARNt avec ARNm lié à l'intérieur du ribosome 80S eucaryote a été observé à haute résolution. La comparaison avec le complexe ribosomique de *S. cerevisiae* 80S à faible résolution lié à deux ARNt en rotation et non-rotation indique que l'ARNt dans notre complexe réside en état P/E. Nous avons pu voir les changements de conformation à l'intérieur du ribosome afin d'accommoder l'ARNm et l'ARNt. En particulier l'interaction de la tige L1 avec l'ARNt et le mouvement de la tête de la petite sous-unité vers le coude de l'ARNt.

La nouvelle forme cristalline développée permet d'étudier l'effet des inhibiteurs de la synthèse protéique sur un ribosome dans un état fonctionnel, comme cela a déjà été démontré avec l'hygromycine B. Le modèle obtenu avec l'hygromycine B a permis d'interpréter son mécanisme d'inhibition. Ainsi du fait de sa localisation éloignée des ponts inter sous-unités, il a été proposé que le mécanisme d'inhibition de l'hygromycine B reposait sur des contraintes lié aux interaction de ce dernier avec l'ARNm. Ainsi ces interactions entre l'hygromycine B, l'ARNm et l'ARNt empêcheraient leurs déplacements sur le ribosome.

Perspectives

Les travaux décrits dans le projet "Etudes structurales du complexe d'élongation eucaryote" ont déjà donné quatre structures. La forme cristalline actuelle ainsi que le traitement établi peuvent être utilisés pour l'étude structurale des inhibiteurs de traduction sur un complexe fonctionnel eucaryote de pré-translocation à haute résolution. Néanmoins, le projet est toujours en développement, la prochaine étape étant d'obtenir la structure du complexe d'élongation avec deux ARNt au sein du ribosome. Pour cela, des analogues non hydrolysable d'ARNt aminoacylés seront utilisés de manière à empêcher l'ARNt de quitter le site A du ribosome. L'obtention

d’informations structurales d’un tel complexe fonctionnel permettra non seulement de révéler de nouvelles informations sur la position et le rôle du diphtamide mais également d’enrichir les connaissances sur le mécanisme de traduction chez les eucaryotes. En effet, jusqu’à présent, ce mécanisme a été principalement étudié d’un point de vu structural pour des organismes bactériens en raison de l’absence de données à haute résolutions de ce complexe fonctionnel chez les eucaryotes. Bien que ce mécanisme soit considéré comme conservé chez les procaryotes et eucaryotes, il n’existe aucune preuve structurale à cela.

Une autre direction de recherche intéressante basée sur la nouvelle forme cristalline obtenue est l'étude du mécanisme de décalage du cadre de lecture ou de glissement de l'ARNm. Ces deux mécanismes sont à l’origine de l’apparition d’erreurs lors de l’étape de reconnaissance codon-anticodon par l’ARNt amino-acylé lors de la traduction. Le décalage du cadre de lecture est un événement pouvant se produire de façon spontanée au niveau de séquences dites glissantes ou de façon programmée dû à la présence d’éléments de séquence spécifiques tel que la séquence de type Shine-Dalgarno et/ou la présence de structures secondaires stables de type pseudonoeuds régulant l’expression génétique. A cela s’ajoute le rôle de la modification post-traductionnelle conservée, la diphthamide au niveau du facteur eEF2, qui jouerait elle aussi un rôle dans la fidélité de la traduction.

La perspective à long terme est d'étudier l'état intermédiaire et l’état post-traductionnel sur la base des conditions de cristallisation développées et présentées ici. L'état post-traductionnel peut être formé en introduisant le GDP et la sordarine au lieu du GDPCP, tandis que pour états intermédiaires l’utilisation d’inhibiteurs pourront être utilisé en vue de bloquer la traduction et verrouiller ainsi un état précis. Des essais préliminaires ont montré que le remplacement du GDPCP par le GDP et la sordarine n'entravait pas la croissance des cristaux ; cependant, le traitement post-cristallisation établi pour les cristaux avec le complexe GDPCP s'est révélé inefficace. C'est pourquoi une recherche approfondie de nouvelles conditions de traitement des cristaux est nécessaire.

REFERENCES

Abeyrathne, P.D., Koh, C.S., Grant, T., Grigorieff, N., and Korostelev, A.A. (2016). Ensemble cryo-EM uncovers inchworm-like translocation of a viral IRES through the ribosome. Elife *5*.

Adio, S., Senyushkina, T., Peske, F., Fischer, N., Wintermeyer, W., and Rodnina, M.V. (2015). Fluctuations between multiple EF-G-induced chimeric tRNA states during translocation on the ribosome. Nat Commun *6*, 7442.

Afonine, P.V., Moriarty, N.W., Mustyakimov, M., Sobolev, O.V., Terwilliger, T.C., Turk, D., Urzhumtsev, A., and Adams, P.D. (2015). FEM: feature-enhanced map. Acta Crystallogr D Biol Crystallogr *71*, 646–666.

Agirrezabala, X., Lei, J., Brunelle, J.L., Ortiz-Meoz, R.F., Green, R., and Frank, J. (2008). Visualization of the hybrid state of tRNA binding promoted by spontaneous ratcheting of the ribosome. Mol. Cell *32*, 190–197.

Agrawal, R.K., and Sharma, M.R. (2012). Structural aspects of mitochondrial translational apparatus. Curr. Opin. Struct. Biol. *22*, 797–803.

Andersen, C.B.F., Becker, T., Blau, M., Anand, M., Halic, M., Balar, B., Mielke, T., Boesen, T., Pedersen, J.S., Spahn, C.M.T., et al. (2006). Structure of eEF3 and the mechanism of transfer RNA release from the E-site. Nature *443*, 663–668.

Andersen, G.R., Valente, L., Pedersen, L., Kinzy, T.G., and Nyborg, J. (2001). Crystal structures of nucleotide exchange intermediates in the eEF1A-eEF1Balpha complex. Nat. Struct. Biol. *8*, 531–534.

Ashe, M.P., De Long, S.K., and Sachs, A.B. (2000). Glucose depletion rapidly inhibits translation initiation in yeast. Mol. Biol. Cell *11*, 833–848.

Badu-Nkansah, A., and Sello, J.K. (2010). Deletion of the elongation factor 4 gene (lepA) in Streptomyces coelicolor enhances the production of the calcium-dependent antibiotic. FEMS Microbiol. Lett. *311*, 147–151.

Behrmann, E., Loerke, J., Budkevich, T.V., Yamamoto, K., Schmidt, A., Penczek, P.A., Vos, M.R., Bürger, J., Mielke, T., Scheerer, P., et al. (2015). Structural snapshots of actively translating human ribosomes. Cell *161*, 845–857.

Belitsina, N.V., Tnalina, G.Z., and Spirin, A.S. (1981). Template-free ribosomal synthesis of polylysine from lysyl-tRNA. FEBS Lett. *131*, 289–292.

Ben-Shem, A., Jenner, L., Yusupova, G., and Yusupov, M. (2010). Crystal structure of the eukaryotic ribosome. Science *330*, 1203–1209.

Ben-Shem, A., Garreau de Loubresse, N., Melnikov, S., Jenner, L., Yusupova, G., and Yusupov, M. (2011). The structure of the eukaryotic ribosome at 3.0 Å resolution. Science *334*, 1524–1529.

Beringer, M., and Rodnina, M.V. (2007). The ribosomal peptidyl transferase. Mol. Cell *26*, 311–321.

Bidou, L., Allamand, V., Rousset, J.-P., and Namy, O. (2012). Sense from nonsense: therapies for premature stop codon diseases. Trends Mol Med *18*, 679–688.

Blaha, G., Stanley, R.E., and Steitz, T.A. (2009). Formation of the first peptide bond: the structure of EF-P bound to the 70S ribosome. Science *325*, 966–970.

Blanchard, S.C., Gonzalez, R.L., Kim, H.D., Chu, S., and Puglisi, J.D. (2004a). tRNA selection and kinetic proofreading in translation. Nat. Struct. Mol. Biol. *11*, 1008–1014.

Blanchard, S.C., Kim, H.D., Gonzalez, R.L., Puglisi, J.D., and Chu, S. (2004b). tRNA dynamics on the ribosome during translation. Proc. Natl. Acad. Sci. U.S.A. *101*, 12893–12898.

Borovinskaya, M.A., Shoji, S., Fredrick, K., and Cate, J.H.D. (2008). Structural basis for hygromycin B inhibition of protein biosynthesis. RNA *14*, 1590–1599.

Budkevich, T., Giesebrecht, J., Altman, R.B., Munro, J.B., Mielke, T., Nierhaus, K.H., Blanchard, S.C., and Spahn, C.M.T. (2011). Structure and dynamics of the mammalian ribosomal pre-translocation complex. Mol Cell *44*, 214–224.

Butcher, S.E., and Jan, E. (2016). tRNA-mimicry in IRES-mediated translation and recoding. RNA Biol *13*, 1068–1074.

Caldon, C.E., and March, P.E. (2003). Function of the universally conserved bacterial GTPases. Curr. Opin. Microbiol. *6*, 135–139.

Chen, C.-M., and Behringer, R.R. (2004). Ovca1 regulates cell proliferation, embryonic development, and tumorigenesis. Genes Dev *18*, 320–332.

Chen, C., Stevens, B., Kaur, J., Cabral, D., Liu, H., Wang, Y., Zhang, H., Rosenblum, G., Smilansky, Z., Goldman, Y.E., et al. (2011). Single-Molecule Fluorescence Measurements of Ribosomal Translocation Dynamics. Molecular Cell *42*, 367–377.

Chen, J., Petrov, A., Tsai, A., O'Leary, S.E., and Puglisi, J.D. (2013a). Coordinated conformational and compositional dynamics drive ribosome translocation. Nat. Struct. Mol. Biol. *20*, 718–727.

Chen, Y., Feng, S., Kumar, V., Ero, R., and Gao, Y.-G. (2013b). Structure of EF-G-ribosome complex in a pretranslocation state. Nat. Struct. Mol. Biol. *20*, 1077–1084.

Cherry, J.M., Hong, E.L., Amundsen, C., Balakrishnan, R., Binkley, G., Chan, E.T., Christie, K.R., Costanzo, M.C., Dwight, S.S., Engel, S.R., et al. (2012). Saccharomyces Genome Database: the genomics resource of budding yeast. Nucleic Acids Res. *40*, D700-705.

Colca, J.R., McDonald, W.G., Waldon, D.J., Thomasco, L.M., Gadwood, R.C., Lund, E.T., Cavey, G.S., Mathews, W.R., Adams, L.D., Cecil, E.T., et al. (2003). Cross-linking in the living cell locates the site of action of oxazolidinone antibiotics. J. Biol. Chem. *278*, 21972–21979.

Connell, S.R., Topf, M., Qin, Y., Wilson, D.N., Mielke, T., Fucini, P., Nierhaus, K.H., and Spahn, C.M.T. (2008). A new tRNA intermediate revealed on the ribosome during EF4-mediated back-translocation. Nat. Struct. Mol. Biol. *15*, 910–915.

Darnell, J.C., and Klann, E. (2013). The translation of translational control by FMRP: therapeutic targets for FXS. Nat. Neurosci. *16*, 1530–1536.

Davydova, E.K., and Ovchinnikov, L.P. (1990). ADP-ribosylated elongation factor 2 (ADP-ribosyl-EF-2) is unable to promote translocation within the ribosome. FEBS Lett. *261*, 350–352.

Demeshkina, N., Jenner, L., Westhof, E., Yusupov, M., and Yusupova, G. (2012). A new understanding of the decoding principle on the ribosome. Nature *484*, 256–259.

Dever, T.E., Kinzy, T.G., and Pavitt, G.D. (2016). Mechanism and Regulation of Protein Synthesis in Saccharomyces cerevisiae. Genetics *203*, 65–107.

Dever, T.E., Dinman, J.D., and Green, R. (2018). Translation Elongation and Recoding in Eukaryotes. Cold Spring Harb Perspect Biol *10*.

Dibb, N.J., and Wolfe, P.B. (1986). lep operon proximal gene is not required for growth or secretion by Escherichia coli. J. Bacteriol. *166*, 83–87.

Doerfel, L.K., Wohlgemuth, I., Kothe, C., Peske, F., Urlaub, H., and Rodnina, M.V. (2013). EF-P is essential for rapid synthesis of proteins containing consecutive proline residues. Science *339*, 85–88.

Drummond, D.A., and Wilke, C.O. (2008). Mistranslation-induced protein misfolding as a dominant constraint on coding-sequence evolution. Cell *134*, 341–352.

Ermolenko, D.N., and Noller, H.F. (2011). mRNA translocation occurs during the second step of ribosomal intersubunit rotation. Nat. Struct. Mol. Biol. *18*, 457–462.

Ermolenko, D.N., Majumdar, Z.K., Hickerson, R.P., Spiegel, P.C., Clegg, R.M., and Noller, H.F. (2007a). Observation of intersubunit movement of the ribosome in solution using FRET. J. Mol. Biol. *370*, 530–540.

Ermolenko, D.N., Spiegel, P.C., Majumdar, Z.K., Hickerson, R.P., Clegg, R.M., and Noller, H.F. (2007b). The antibiotic viomycin traps the ribosome in an intermediate state of translocation. Nat. Struct. Mol. Biol. *14*, 493–497.

Ferguson, A., Wang, L., Altman, R.B., Terry, D.S., Juette, M.F., Burnett, B.J., Alejo, J.L., Dass, R.A., Parks, M.M., Vincent, T.C., et al. (2015). Functional dynamics within the human ribosome regulate the rate of active protein synthesis. Mol Cell *60*, 475–486.

Firczuk, H., Kannambath, S., Pahle, J., Claydon, A., Beynon, R., Duncan, J., Westerhoff, H., Mendes, P., and McCarthy, J.E. (2013). An in vivo control map for the eukaryotic mRNA translation machinery. Mol Syst Biol *9*, 635.

Francklyn, C.S. (2008). DNA Polymerases and Aminoacyl-tRNA Synthetases: Shared Mechanisms for Ensuring the Fidelity of Gene Expression. Biochemistry *47*, 11695–11703.

Frank, J., and Agrawal, R.K. (2000). A ratchet-like inter-subunit reorganization of the ribosome during translocation. Nature *406*, 318–322.

Frank, J., Gao, H., Sengupta, J., Gao, N., and Taylor, D.J. (2007). The process of mRNA-tRNA translocation. Proc. Natl. Acad. Sci. U.S.A. *104*, 19671–19678.

Gao, Y.-G., Selmer, M., Dunham, C.M., Weixlbaumer, A., Kelley, A.C., and Ramakrishnan, V. (2009). The structure of the ribosome with elongation factor G trapped in the posttranslocational state. Science *326*, 694–699.

Garreau de Loubresse, N., Prokhorova, I., Holtkamp, W., Rodnina, M.V., Yusupova, G., and Yusupov, M. (2014). Structural basis for the inhibition of the eukaryotic ribosome. Nature *513*, 517–522.

Geggier, P., Dave, R., Feldman, M.B., Terry, D.S., Altman, R.B., Munro, J.B., and Blanchard, S.C. (2010). Conformational sampling of aminoacyl-tRNA during selection on the bacterial ribosome. J. Mol. Biol. *399*, 576–595.

Glick, B.R., and Ganoza, M.C. (1975). Identification of a soluble protein that stimulates peptide bond synthesis. Proc. Natl. Acad. Sci. U.S.A. *72*, 4257–4260.

Greenspan, L. (1977). Humidity fixed points of binary saturated aqueous solutions. Journal of Research of the National Bureau of Standards Section A: Physics and Chemistry *81A*, 89.

Gromadski, K.B., Schümmer, T., Strømgaard, A., Knudsen, C.R., Kinzy, T.G., and Rodnina, M.V. (2007). Kinetics of the interactions between yeast elongation factors 1A and 1Balpha, guanine nucleotides, and aminoacyl-tRNA. J. Biol. Chem. *282*, 35629–35637.

Guo, Z., and Noller, H.F. (2012). Rotation of the head of the 30S ribosomal subunit during mRNA translocation. Proc. Natl. Acad. Sci. U.S.A. *109*, 20391–20394.

Gutierrez, E., Shin, B.-S., Woolstenhulme, C.J., Kim, J.-R., Saini, P., Buskirk, A.R., and Dever, T.E. (2013). eIF5A promotes translation of polyproline motifs. Mol. Cell *51*, 35–45.

von der Haar, T. (2008). A quantitative estimation of the global translational activity in logarithmically growing yeast cells. BMC Syst Biol *2*, 87.

Heras, B., and Martin, J.L. (2005). Post-crystallization treatments for improving diffraction quality of protein crystals. Acta Crystallogr. D Biol. Crystallogr. *61*, 1173–1180.

Horan, L.H., and Noller, H.F. (2007). Intersubunit movement is required for ribosomal translocation. Proc. Natl. Acad. Sci. U.S.A. *104*, 4881–4885.

Inoue-Yokosawa, N., Ishikawa, C., and Kaziro, Y. (1974). The role of guanosine triphosphate in translocation reaction catalyzed by elongation factor G. J. Biol. Chem. *249*, 4321–4323.

Jenner, L.B., Demeshkina, N., Yusupova, G., and Yusupov, M. (2010). Structural aspects of messenger RNA reading frame maintenance by the ribosome. Nat. Struct. Mol. Biol. *17*, 555–560.

Jørgensen, R., Carr-Schmid, A., Ortiz, P.A., Kinzy, T.G., and Andersen, G.R. (2002). Purification and crystallization of the yeast elongation factor eEF2. Acta Crystallogr. D Biol. Crystallogr. *58*, 712–715.

Jørgensen, R., Ortiz, P.A., Carr-Schmid, A., Nissen, P., Kinzy, T.G., and Andersen, G.R. (2003a). Two crystal structures demonstrate large conformational changes in the eukaryotic ribosomal translocase. Nat. Struct. Biol. *10*, 379–385.

Jørgensen, R., Ortiz, P.A., Carr-Schmid, A., Nissen, P., Kinzy, T.G., and Andersen, G.R. (2003b). Two crystal structures demonstrate large conformational changes in the eukaryotic ribosomal translocase. Nat. Struct. Biol. *10*, 379–385.

Jørgensen, R., Yates, S.P., Teal, D.J., Nilsson, J., Prentice, G.A., Merrill, A.R., and Andersen, G.R. (2004). Crystal structure of ADP-ribosylated ribosomal translocase from Saccharomyces cerevisiae. J. Biol. Chem. *279*, 45919–45925.

Jørgensen, R., Merrill, A.R., and Andersen, G.R. (2006). The life and death of translation elongation factor 2. Biochem. Soc. Trans. *34*, 1–6.

Joseph, S., and Noller, H.F. (1998). EF-G-catalyzed translocation of anticodon stem-loop analogs of transfer RNA in the ribosome. EMBO J. *17*, 3478–3483.

Justice, M.C., Hsu, M.J., Tse, B., Ku, T., Balkovec, J., Schmatz, D., and Nielsen, J. (1998). Elongation factor 2 as a novel target for selective inhibition of fungal protein synthesis. J. Biol. Chem. *273*, 3148–3151.

Kemper, W., Berry, K., and Merrick, W. (1976). Purification and properties of rabbit reticulocyte protein synthesis initiation factors M2Bα and M2Bβ. J Biol Chem *251*.

Kimsey, I.J., Petzold, K., Sathyamoorthy, B., Stein, Z.W., and Al-Hashimi, H.M. (2015). Visualizing transient Watson-Crick-like mispairs in DNA and RNA duplexes. Nature *519*, 315–320.

Klinge, S., Voigts-Hoffmann, F., Leibundgut, M., and Ban, N. (2012). Atomic structures of the eukaryotic ribosome. Trends in Biochemical Sciences *37*, 189–198.

Kurland, C.G., Hughes, D., and Ehrenberg, M. (1996). Limitations of translational accuracy. In Escherichia coli and Salmonella. Cellular and Molecular Biology (Neidhardt, F. C., Ed.) 979–1004.

Laurberg, M., Kristensen, O., Martemyanov, K., Gudkov, A.T., Nagaev, I., Hughes, D., and Liljas, A. (2000). Structure of a mutant EF-G reveals domain III and possibly the fusidic acid binding site. J. Mol. Biol. *303*, 593–603.

Laursen, B.S., Sørensen, H.P., Mortensen, K.K., and Sperling-Petersen, H.U. (2005). Initiation of Protein Synthesis in Bacteria. Microbiol Mol Biol Rev *69*, 101–123.

Leipe, D.D., Wolf, Y.I., Koonin, E.V., and Aravind, L. (2002). Classification and evolution of P-loop GTPases and related ATPases. J. Mol. Biol. *317*, 41–72.

Lin, J., Gagnon, M.G., Bulkley, D., and Steitz, T.A. (2015). Conformational changes of elongation factor G on the ribosome during tRNA translocation. Cell *160*, 219–227.

Ling, C., and Ermolenko, D.N. (2016). Structural insights into ribosome translocation. Wiley Interdiscip Rev RNA *7*, 620–636.

Liu, S., Wiggins, J.F., Sreenath, T., Kulkarni, A.B., Ward, J.M., and Leppla, S.H. (2006). Dph3, a Small Protein Required for Diphthamide Biosynthesis, Is Essential in Mouse Development. Mol Cell Biol *26*, 3835–3841.

Liu, S., Bachran, C., Gupta, P., Miller-Randolph, S., Wang, H., Crown, D., Zhang, Y., Wein, A.N., Singh, R., Fattah, R., et al. (2012). Diphthamide modification on eukaryotic elongation factor 2 is needed to assure fidelity of mRNA translation and mouse development. Proc. Natl. Acad. Sci. U.S.A. *109*, 13817–13822.

Loveland, A.B., Demo, G., Grigorieff, N., and Korostelev, A.A. (2017). Ensemble cryo-EM elucidates the mechanism of translation fidelity. Nature *546*, 113–117.

Lu, W., Roongsawang, N., and Mahmud, T. (2011). Biosynthetic studies and genetic engineering of pactamycin analogs with improved selectivity toward malarial parasites. Chem. Biol. *18*, 425–431.

M Anger, A., Armache, J.-P., Berninghausen, O., Habeck, M., Subklewe, M., Wilson, D., and Beckmann, R. (2013). Structures of the human and Drosophila 80S ribosome. Nature *497*, 80–85.

Margus, T., Remm, M., and Tenson, T. (2007). Phylogenetic distribution of translational GTPases in bacteria. BMC Genomics *8*, 15.

Mateyak, M.K., and Kinzy, T.G. (2013). ADP-ribosylation of translation elongation factor 2 by diphtheria toxin in yeast inhibits translation and cell separation. J. Biol. Chem. *288*, 24647–24655.

Melnikov, S., Ben-Shem, A., Garreau de Loubresse, N., Jenner, L., Yusupova, G., and Yusupov, M. (2012). One core, two shells: bacterial and eukaryotic ribosomes. Nat. Struct. Mol. Biol. *19*, 560–567.

Melnikov, S., Mailliot, J., Rigger, L., Neuner, S., Shin, B.-S., Yusupova, G., Dever, T.E., Micura, R., and Yusupov, M. (2016a). Molecular insights into protein synthesis with proline residues. EMBO Rep. *17*, 1776–1784.

Melnikov, S., Mailliot, J., Shin, B.-S., Rigger, L., Yusupova, G., Micura, R., Dever, T.E., and Yusupov, M. (2016b). Crystal Structure of Hypusine-Containing Translation Factor eIF5A Bound to a Rotated Eukaryotic Ribosome. J. Mol. Biol. *428*, 3570–3576.

Moazed, D., and Noller, H.F. (1989). Intermediate states in the movement of transfer RNA in the ribosome. Nature *342*, 142–148.

Moazed, D., Robertson, J.M., and Noller, H.F. (1988). Interaction of elongation factors EF-G and EF-Tu with a conserved loop in 23S RNA. Nature *334*, 362–364.

Moore, P.B., and Steitz, T.A. (2011). The Roles of RNA in the Synthesis of Protein. Cold Spring Harb Perspect Biol *3*.

Munro, J.B., Sanbonmatsu, K.Y., Spahn, C.M.T., and Blanchard, S.C. (2009). Navigating the ribosome's metastable energy landscape. Trends Biochem. Sci. *34*, 390–400.

Murray, J., Savva, C.G., Shin, B.-S., Dever, T.E., Ramakrishnan, V., and Fernández, I.S. (2016). Structural characterization of ribosome recruitment and translocation by type IV IRES. Elife *5*.

Nygård, O., and Nilsson, L. (1990). Kinetic determination of the effects of ADP-ribosylation on the interaction of eukaryotic elongation factor 2 with ribosomes. J. Biol. Chem. *265*, 6030–6034.

Ogle, J.M., Brodersen, D.E., Clemons, W.M., Tarry, M.J., Carter, A.P., and Ramakrishnan, V. (2001). Recognition of cognate transfer RNA by the 30S ribosomal subunit. Science *292*, 897–902.

Ogle, J.M., Murphy, F.V., Tarry, M.J., and Ramakrishnan, V. (2002). Selection of tRNA by the Ribosome Requires a Transition from an Open to a Closed Form. Cell *111*, 721–732.

Ortiz, P.A., Ulloque, R., Kihara, G.K., Zheng, H., and Kinzy, T.G. (2006). Translation elongation factor 2 anticodon mimicry domain mutants affect fidelity and diphtheria toxin resistance. J. Biol. Chem. *281*, 32639–32648.

Pan, D., Kirillov, S.V., and Cooperman, B.S. (2007). Kinetically competent intermediates in the translocation step of protein synthesis. Mol. Cell *25*, 519–529.

Parmeggiani, A., and Sander, G. (1981). Properties and regulation of the GTPase activities of elongation factors Tu and G, and of initiation factor 2. Mol. Cell. Biochem. *35*, 129–158.

Pech, M., Karim, Z., Yamamoto, H., Kitakawa, M., Qin, Y., and Nierhaus, K.H. (2011). Elongation factor 4 (EF4/LepA) accelerates protein synthesis at increased Mg2+ concentrations. Proc. Natl. Acad. Sci. U.S.A. *108*, 3199–3203.

Pellegrino, S., Demeshkina, N., Mancera-Martinez, E., Melnikov, S., Simonetti, A., Myasnikov, A., Yusupov, M., Yusupova, G., and Hashem, Y. (2018a). Structural Insights into the Role of

Diphthamide on Elongation Factor 2 in mRNA Reading-Frame Maintenance. J. Mol. Biol. *430*, 2677–2687.

Pellegrino, S., Meyer, M., Zorbas, C., Bouchta, S.A., Saraf, K., Pelly, S.C., Yusupova, G., Evidente, A., Mathieu, V., Kornienko, A., et al. (2018b). The Amaryllidaceae Alkaloid Haemanthamine Binds the Eukaryotic Ribosome to Repress Cancer Cell Growth. Structure *26*, 416-425.e4.

Peske, F., Savelsbergh, A., Katunin, V.I., Rodnina, M.V., and Wintermeyer, W. (2004). Conformational changes of the small ribosomal subunit during elongation factor G-dependent tRNA-mRNA translocation. J. Mol. Biol. *343*, 1183–1194.

Proud, C.G. (2018). Phosphorylation and Signal Transduction Pathways in Translational Control. Cold Spring Harb Perspect Biol.

Qin, Y., Polacek, N., Vesper, O., Staub, E., Einfeldt, E., Wilson, D.N., and Nierhaus, K.H. (2006). The highly conserved LepA is a ribosomal elongation factor that back-translocates the ribosome. Cell *127*, 721–733.

Qu, X., Wen, J.-D., Lancaster, L., Noller, H.F., Bustamante, C., and Tinoco, I. (2011). The ribosome uses two active mechanisms to unwind messenger RNA during translation. Nature *475*, 118–121.

Ramakrishnan, V. (2002). Ribosome Structure and the Mechanism of Translation. Cell *108*, 557–572.

Ramrath, D.J.F., Lancaster, L., Sprink, T., Mielke, T., Loerke, J., Noller, H.F., and Spahn, C.M.T. (2013). Visualization of two transfer RNAs trapped in transit during elongation factor G-mediated translocation. PNAS *110*, 20964–20969.

Ratje, A.H., Loerke, J., Mikolajka, A., Brünner, M., Hildebrand, P.W., Starosta, A.L., Dönhöfer, A., Connell, S.R., Fucini, P., Mielke, T., et al. (2010). Head swivel on the ribosome facilitates translocation by means of intra-subunit tRNA hybrid sites. Nature *468*, 713–716.

Rodnina, M.V. (2012). Quality control of mRNA decoding on the bacterial ribosome. Adv Protein Chem Struct Biol *86*, 95–128.

Rodnina, M.V., and Wintermeyer, W. (2009). Recent mechanistic insights into eukaryotic ribosomes. Curr. Opin. Cell Biol. *21*, 435–443.

Rodnina, M.V., Beringer, M., and Wintermeyer, W. (2007). How ribosomes make peptide bonds. Trends Biochem. Sci. *32*, 20–26.

Rodnina, M.V., Fischer, N., Maracci, C., and Stark, H. (2017). Ribosome dynamics during decoding. Philos. Trans. R. Soc. Lond., B, Biol. Sci. *372*.

Rozov, A., Demeshkina, N., Westhof, E., Yusupov, M., and Yusupova, G. (2015). Structural insights into the translational infidelity mechanism. Nat Commun *6*.

Rozov, A., Demeshkina, N., Westhof, E., Yusupov, M., and Yusupova, G. (2016). New Structural Insights into Translational Miscoding. Trends in Biochemical Sciences *41*, 798–814.

Rozov, A., Wolff, P., Grosjean, H., Yusupov, M., Yusupova, G., and Westhof, E. (2018). Tautomeric G•U pairs within the molecular ribosomal grip and fidelity of decoding in bacteria. Nucleic Acids Res. *46*, 7425–7435.

Saini, P., Eyler, D.E., Green, R., and Dever, T.E. (2009). Hypusine-containing protein eIF5A promotes translation elongation. Nature *459*, 118–121.

Salsi, E., Farah, E., and Ermolenko, D.N. (2016). EF-G Activation by Phosphate Analogs. J. Mol. Biol. *428*, 2248–2258.

Santagata, S., Mendillo, M.L., Tang, Y., Subramanian, A., Perley, C.C., Roche, S.P., Wong, B., Narayan, R., Kwon, H., Koeva, M., et al. (2013). Tight coordination of protein translation and HSF1 activation supports the anabolic malignant state. Science *341*, 1238303.

Savelsbergh, A., Matassova, N.B., Rodnina, M.V., and Wintermeyer, W. (2000). Role of domains 4 and 5 in elongation factor G functions on the ribosome. J. Mol. Biol. *300*, 951–961.

Savelsbergh, A., Katunin, V.I., Mohr, D., Peske, F., Rodnina, M.V., and Wintermeyer, W. (2003). An elongation factor G-induced ribosome rearrangement precedes tRNA-mRNA translocation. Mol. Cell *11*, 1517–1523.

Schaffrath, R., Abdel-Fattah, W., Klassen, R., and Stark, M.J.R. (2014). The diphthamide modification pathway from Saccharomyces cerevisiae--revisited. Mol. Microbiol. *94*, 1213–1226.

Schmeing, T.M., and Ramakrishnan, V. (2009). What recent ribosome structures have revealed about the mechanism of translation. Nature *461*, 1234–1242.

Schmeing, T.M., Huang, K.S., Strobel, S.A., and Steitz, T.A. (2005). An induced-fit mechanism to promote peptide bond formation and exclude hydrolysis of peptidyl-tRNA. Nature *438*, 520–524.

Schmidt, C., Becker, T., Heuer, A., Braunger, K., Shanmuganathan, V., Pech, M., Berninghausen, O., Wilson, D.N., and Beckmann, R. (2016). Structure of the hypusinylated eukaryotic translation factor eIF-5A bound to the ribosome. Nucleic Acids Res. *44*, 1944–1951.

Schuller, A.P., Wu, C.C.-C., Dever, T.E., Buskirk, A.R., and Green, R. (2017). eIF5A Functions Globally in Translation Elongation and Termination. Mol. Cell *66*, 194-205.e5.

Sengupta, J., Nilsson, J., Gursky, R., Kjeldgaard, M., Nissen, P., and Frank, J. (2008). Visualization of the eEF2-80S ribosome transition-state complex by cryo-electron microscopy. J. Mol. Biol. *382*, 179–187.

Shah, P., Ding, Y., Niemczyk, M., Kudla, G., and Plotkin, J.B. (2013). Rate-Limiting Steps in Yeast Protein Translation. Cell *153*, 1589–1601.

Shin, B.-S., Katoh, T., Gutierrez, E., Kim, J.-R., Suga, H., and Dever, T.E. (2017). Amino acid substrates impose polyamine, eIF5A, or hypusine requirement for peptide synthesis. Nucleic Acids Res. *45*, 8392–8402.

Shoji, S., Walker, S.E., and Fredrick, K. (2009). Ribosomal translocation: one step closer to the molecular mechanism. ACS Chem. Biol. *4*, 93–107.

Shoji, S., Janssen, B.D., Hayes, C.S., and Fredrick, K. (2010). Translation factor LepA contributes to tellurite resistance in Escherichia coli but plays no apparent role in the fidelity of protein synthesis. Biochimie *92*, 157–163.

Skogerson, L., and Engelhardt, D. (1977). Dissimilarity in protein chain elongation factor requirements between yeast and rat liver ribosomes. J. Biol. Chem. *252*, 1471–1475.

Smith, T.F., Lee, J.C., Gutell, R.R., and Hartman, H. (2008). The origin and evolution of the ribosome. Biol. Direct *3*, 16.

Sousa, R. (1995). Use of glycerol, polyols and other protein structure stabilizing agents in protein crystallization. Acta Cryst D *51*, 271–277.

Spahn, C.M., Beckmann, R., Eswar, N., Penczek, P.A., Sali, A., Blobel, G., and Frank, J. (2001). Structure of the 80S ribosome from Saccharomyces cerevisiae--tRNA-ribosome and subunit-subunit interactions. Cell *107*, 373–386.

Spahn, C.M., Gomez-Lorenzo, M.G., Grassucci, R.A., Jørgensen, R., Andersen, G.R., Beckmann, R., Penczek, P.A., Ballesta, J.P., and Frank, J. (2004). Domain movements of elongation factor eEF2 and the eukaryotic 80S ribosome facilitate tRNA translocation. EMBO J *23*, 1008–1019.

Spiegel, P.C., Ermolenko, D.N., and Noller, H.F. (2007). Elongation factor G stabilizes the hybrid-state conformation of the 70S ribosome. RNA *13*, 1473–1482.

Stanley, R.E., Blaha, G., Grodzicki, R.L., Strickler, M.D., and Steitz, T.A. (2010). The structures of the anti-tuberculosis antibiotics viomycin and capreomycin bound to the 70S ribosome. Nat. Struct. Mol. Biol. *17*, 289–293.

Steitz, J.A. (1969). Polypeptide Chain Initiation: Nucleotide Sequences of the Three Ribosomal Binding Sites in Bacteriophage R17 RNA. Nature *224*, 957–964.

Steitz, T.A. (2008). A structural understanding of the dynamic ribosome machine. Nat. Rev. Mol. Cell Biol. *9*, 242–253.

Su, X., Lin, Z., and Lin, H. (2013). The biosynthesis and biological function of diphthamide. Crit. Rev. Biochem. Mol. Biol. *48*, 515–521.

Svidritskiy, E., Brilot, A.F., Koh, C.S., Grigorieff, N., and Korostelev, A.A. (2014). Structures of yeast 80S ribosome-tRNA complexes in the rotated and non-rotated conformations. Structure *22*, 1210–1218.

Szaflarski, W., Vesper, O., Teraoka, Y., Plitta, B., Wilson, D.N., and Nierhaus, K.H. (2008). New features of the ribosome and ribosomal inhibitors: non-enzymatic recycling, misreading and back-translocation. J. Mol. Biol. *380*, 193–205.

Taylor, D.J., Nilsson, J., Merrill, A.R., Andersen, G.R., Nissen, P., and Frank, J. (2007). Structures of modified eEF2 80S ribosome complexes reveal the role of GTP hydrolysis in translocation. EMBO J. *26*, 2421–2431.

Tourigny, D.S., Fernández, I.S., Kelley, A.C., and Ramakrishnan, V. (2013). Elongation factor G bound to the ribosome in an intermediate state of translocation. Science *340*, 1235490.

Triana-Alonso, F.J., Chakraburtty, K., and Nierhaus, K.H. (1995). The elongation factor 3 unique in higher fungi and essential for protein biosynthesis is an E site factor. J. Biol. Chem. *270*, 20473–20478.

Ude, S., Lassak, J., Starosta, A.L., Kraxenberger, T., Wilson, D.N., and Jung, K. (2013). Translation elongation factor EF-P alleviates ribosome stalling at polyproline stretches. Science *339*, 82–85.

Valle, M., Sengupta, J., Swami, N.K., Grassucci, R.A., Burkhardt, N., Nierhaus, K.H., Agrawal, R.K., and Frank, J. (2002). Cryo-EM reveals an active role for aminoacyl-tRNA in the accommodation process. EMBO J. *21*, 3557–3567.

Valle, M., Zavialov, A., Li, W., Stagg, S.M., Sengupta, J., Nielsen, R.C., Nissen, P., Harvey, S.C., Ehrenberg, M., and Frank, J. (2003). Incorporation of aminoacyl-tRNA into the ribosome as seen by cryo-electron microscopy. Nat. Struct. Biol. *10*, 899–906.

Vera, L., Czarny, B., Georgiadis, D., Dive, V., and Stura, E.A. (2011). Practical Use of Glycerol in Protein Crystallization. Crystal Growth & Design *11*, 2755–2762.

Voorhees, R.M., and Ramakrishnan, V. (2013). Structural basis of the translational elongation cycle. Annu. Rev. Biochem. *82*, 203–236.

Wang, L., Pulk, A., Wasserman, M.R., Feldman, M.B., Altman, R.B., Cate, J.H.D., and Blanchard, S.C. (2012). Allosteric control of the ribosome by small-molecule antibiotics. Nat. Struct. Mol. Biol. *19*, 957–963.

Warner, J.R. (1999). The economics of ribosome biosynthesis in yeast. Trends Biochem. Sci. *24*, 437–440.

Wasserman, M.R., Alejo, J.L., Altman, R.B., and Blanchard, S.C. (2016). Multiperspective smFRET reveals rate-determining late intermediates of ribosomal translocation. Nat. Struct. Mol. Biol. *23*, 333–341.

Webb, T.R., Cross, S.H., McKie, L., Edgar, R., Vizor, L., Harrison, J., Peters, J., and Jackson, I.J. (2008). Diphthamide modification of eEF2 requires a J-domain protein and is essential for normal development. J. Cell. Sci. *121*, 3140–3145.

Weinger, J.S., Parnell, K.M., Dorner, S., Green, R., and Strobel, S.A. (2004). Substrate-assisted catalysis of peptide bond formation by the ribosome. Nat. Struct. Mol. Biol. *11*, 1101–1106.

White-Gilbertson, S., Kurtz, D.T., and Voelkel-Johnson, C. (2009). The role of protein synthesis in cell cycling and cancer. Mol Oncol *3*, 402–408.

Wilson, D.N. (2009). The A-Z of bacterial translation inhibitors. Crit. Rev. Biochem. Mol. Biol. *44*, 393–433.

Wilson, D.N. (2014). Ribosome-targeting antibiotics and mechanisms of bacterial resistance. Nat. Rev. Microbiol. *12*, 35–48.

Wohlgemuth, I., Brenner, S., Beringer, M., and Rodnina, M.V. (2008). Modulation of the rate of peptidyl transfer on the ribosome by the nature of substrates. J. Biol. Chem. *283*, 32229–32235.

Yang, F., Li, Z., Hao, J., and Qin, Y. (2014). EF4 knockout E. coli cells exhibit lower levels of cellular biosynthesis under acidic stress. Protein Cell *5*, 563–567.

Youngman, E.M., Brunelle, J.L., Kochaniak, A.B., and Green, R. (2004). The active site of the ribosome is composed of two layers of conserved nucleotides with distinct roles in peptide bond formation and peptide release. Cell *117*, 589–599.

Yusupov, M.M., Yusupova, G.Z., Baucom, A., Lieberman, K., Earnest, T.N., Cate, J.H., and Noller, H.F. (2001). Crystal structure of the ribosome at 5.5 A resolution. Science *292*, 883–896.

Yusupova, G., and Yusupov, M. (2014). High-Resolution Structure of the Eukaryotic 80S Ribosome. Annu. Rev. Biochem. *83*, 467–486.

Yusupova, G.Z., Yusupov, M.M., Cate, J.H., and Noller, H.F. (2001). The path of messenger RNA through the ribosome. Cell *106*, 233–241.

Zaher, H.S., and Green, R. (2009). Fidelity at the molecular level: lessons from protein synthesis. Cell *136*, 746–762.

Zavialov, A.V., Hauryliuk, V.V., and Ehrenberg, M. (2005). Guanine-nucleotide exchange on ribosome-bound elongation factor G initiates the translocation of tRNAs. J. Biol. *4*, 9.

Zenklusen, D., Larson, D.R., and Singer, R.H. (2008). Single-RNA counting reveals alternative modes of gene expression in yeast. Nat Struct Mol Biol *15*, 1263–1271.

Zhou, J., Bhattacharjee, A., Chen, S., Chen, Y., Duffy, E., Farmer, J., Goldberg, J., Hanselmann, R., Ippolito, J.A., Lou, R., et al. (2008). Design at the atomic level: generation of novel hybrid biaryloxazolidinones as promising new antibiotics. Bioorg Med Chem Lett *18*, 6179–6183.

Zhou, J., Lancaster, L., Donohue, J.P., and Noller, H.F. (2013). Crystal structures of EF-G-ribosome complexes trapped in intermediate states of translocation. Science *340*, 1236086.

Zhou, J., Lancaster, L., Donohue, J.P., and Noller, H.F. (2014). How the ribosome hands the A-site tRNA to the P site during EF-G-catalyzed translocation. Science *345*, 1188–1191.

Muminjon DJUMAGULOV

Accuracy of gene expression through understanding structural basis of a translation cycle on the eukaryotic ribosomes

Résumé

Le ribosome est un complexe macromoléculaire impliqué dans la synthèse protéique de toutes les cellules vivantes. L'étape d'élongation de cette synthèse est un processus itératif débutant par la séléction au sein du ribosome d'un ARNt aminoacylé suivie par le transfert du peptide du site P- vers le site A- et de la translocation de l'ARNm et de l'ARNt. Le facteur d'élongation 2 (eEF2), qui catalyse la translocation, est l'un des acteurs majeur de cette étape d'élongation chez les eucaryotes. Cependant le mécanisme par lequel eEF2 induit ce processus est encore aujourd'hui inconnu.

Dans cette étude structurale, nous présentons la première structure à haute résolution (3.1 Å) du complexe de pré-translocation résolu par cristallographie aux rayons X.

La structure obtenue nous a permis d'identifier les différents composants du complexe de translocation et de proposer le rôle de l'His699 et celui de la diphtamide, modification post-traductionnelle d'eEF2, lors du stade de pré-translocation.

Mots clés: Ribosome, eucaryote, translocation, eEF2, cristallographie

Résumé en anglais

Elongation is the longest stage of protein synthesis that takes place on the ribosome and represents a cycle that begins with an aminoacyl-tRNA selection followed by the catalysis of peptide transfer from the P- to the A-site and mRNA-tRNA translocation. Elongation factor 2 (eEF2) is one of the key player of elongation cycle in eukaryotes that catalyzes translocation of mRNA and tRNA on the ribosome. However the mechanism how eEF2 induces translocation on the ribosome is unknown.

Current work investigates the structural aspect of protein synthesis machinery in eukaryotes. In particular we present first high resolution structure of functional pretranslocation complex solved at 3.1 A by X-ray crystallography.

The obtained structure allowed us to see several features of translocation complex and to propose the role of His699 and post translational modification of eEF2 diphthamide during at pretranslocation stage.

Keywords: Ribosome, eukaryote, translocation, eEF2, crystallography